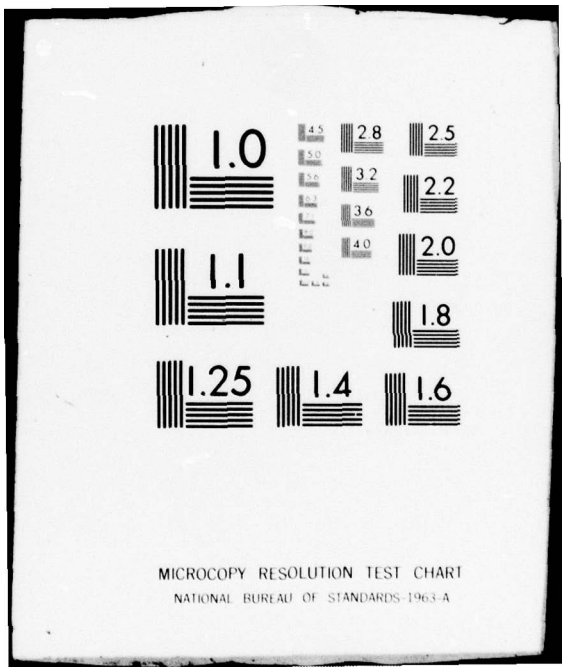
AD-A073 437 TRW DEFENSE AND SPACE SYSTEMS GROUP REDONDO BEACH CA F/G 22/1
9433 DESIGN POINTING ANOMALY. VOLUME I. TECHNICAL REPORT.(U)
JAN 76 P C WHEELER F04701-75-C-0257
UNCLASSIFIED TRW-28600-AR-010-01-VOL-1 SAMSO-TR-79-13-VOL-1 NL

1 OF 3
AD A073437




1.0
1.1
1.25
1.4
1.6
1.8
2.0
2.2
2.5
2.8
3.2
3.6
4.0
4.5
5.0
5.6
6.3
MICROCOPY RESOLUTION TEST CHART
NATIONAL BUREAU OF STANDARDS-1963-A

LEVEL II

FINAL REPORT

0433 DESPIN POINTING ANOMALY

DDC
REPRODUCTION
AUG 31

O. 28400-AR-010-01

30 JANUARY 1976

VOLUME I
TECHNICAL REPORT

APPROVED FOR PUBLIC RELEASE; DISTRIBUTION UNLIMITED.

UNDER CONTRACT NO. F04701-75-C-0257

SAMSO-TR-79-13

DDC
RECEIVED
AUG 30 1979
C

FINAL REPORT

9433 DESPIN POINTING ANOMALY

REPORT NO. 28600-AR-010-01

30 JANUARY 1976

VOLUME I
TECHNICAL REPORT

PREPARED:
P. C. Wheeler, Manager
Electromechanical Equipment Dept
Control & Sensor Systems Lab

APPROVED:
J. A. Durschinger
APM Satellite Engineering
DSCS II Project

APPROVED:
D. E. Kendall, Manager
DSCS II Project

Approved for public release; distribution unlimited.

UNDER CONTRACT NO. F04701-75-C-0257
CDRL ITEM SEQUENCE NO. A009

TRW
SYSTEMS GROUP

ONE SPACE PARK • REDONDO BEACH, CALIFORNIA 90278

This final report was submitted by TRW Defense and Space Systems Group, One Space Park, Redondo Beach, CA 90278; under Contract F04701-75-C-0257, with the Space and Missile Systems Organization, Deputy for Space Communications Systems, P.O. Box 92960, Worldway Postal Center, Los Angeles, CA 90009.

Captain G. D. Nordley, SAMSO/SKD, was the Project Officer for Space Communications Systems.

This report has been reviewed by the Information Office (OI) and is releasable to the National Technical Information Service (NTIS). At NTIS, it will be available to the general public, including foreign nations.

This technical report has been reviewed and is approved for publication. Publication of this report does not constitute Air Force approval of the report's findings or conclusions. It is published only for the exchange and stimulation of ideas.

Gerald D. Nordley

GERALD D. NORDLEY, Capt, USAF
Project Officer,
Deputy for Space Comm Systems

Lawrence A. Barlock

LAWRENCE A. BARLOCK, Lt Col, USAF
Director of Engineering, DSCS II
Deputy for Space Comm Systems

FOR THE COMMANDER

James E. Freytag

JAMES E. FREYTAG, Col, USAF
System Program Director, DSCS
Deputy for Space Comm Systems

Accession For
NTIS GRA&I ☑
DDC TAB ☐
Unannounced ☐
Justification
By
Distribution/
Availability Codes
Dist | Avail and/or special
A

UNCLASSIFIED

SECURITY CLASSIFICATION OF THIS PAGE (When Data Entered)

(12) (19) REPORT DOCUMENTATION PAGE

READ INSTRUCTIONS BEFORE COMPLETING FORM

1. REPORT NUMBER	2. GOVT ACCESSION NO.	3. RECIPIENT'S CATALOG NUMBER
SAMSO-TR-79-13-VOL-1		

4. TITLE (and Subtitle)
9433 DESPIN POINTING ANOMALY, VOL I, AND APPENDICES, VOL II

(10)

5. TYPE OF REPORT & PERIOD COVERED (9)
Final Report,

6. PERFORMING ORG. REPORT NUMBER
TRW TR-28600-AR-010-01

7. AUTHOR(s)
P.C. Wheeler

8. CONTRACT OR GRANT NUMBER(s) (15)
F04701-75-C-0257

9. PERFORMING ORGANIZATION NAME AND ADDRESS
TRW Defense and Space Systems Group
One Space Park
Redondo Beach, CA 90278

10. PROGRAM ELEMENT, PROJECT, TASK AREA & WORK UNIT NUMBERS

11. CONTROLLING OFFICE NAME AND ADDRESS (11)
Space and Missile Systems Organization
Air Force Systems Command
Los Angeles, CA 90009

12. REPORT DATE
30 January 1976

13. NUMBER OF PAGES
Vol I - 263 & Vol II - 354

14. MONITORING AGENCY NAME & ADDRESS (if different from Controlling Office) (14)
TRW-28600-AR-010-01-VOL-1

15. SECURITY CLASS. (of this report)
Unclassified

15a. DECLASSIFICATION/DOWNGRADING SCHEDULE

16. DISTRIBUTION STATEMENT (of this Report)
Approved for public release; distribution unlimited.

(12) 271 p.

17. DISTRIBUTION STATEMENT (of the abstract entered in Block 20, if different from Report)
(6) 9433 Despin Pointing Anomaly. Volume I. Technical Report.

18. SUPPLEMENTARY NOTES

19. KEY WORDS (Continue on reverse side if necessary and identify by block number)
Satellite
Despin Mechanical Assembly

20. ABSTRACT (Continue on reverse side if necessary and identify by block number)
This report presents the 9433 Despin Control anomaly investigations, resulting conclusions and recommendations. General recommendations are identified in two categories; design changes and process changes. First category includes a retainer design, increase of DEA current limit to increase motor capability of DMA. Secondary design considerations are positive lubrication system, a flexure payload mechanism for the bearing race and a controller rate loop redesign to make the system insensitive to torque perturbations. Second category relates to the processing of metal parts, non-metal parts, bearing screening, lubricants, assembly and test procedures, and DMA handling and storage.

DD FORM 1473 (FACSIMILE)

UNCLASSIFIED 409 637

SECURITY CLASSIFICATION OF THIS PAGE (When Data Entered)

ACKNOWLEDGEMENT

This report presents the results of work accomplished by numerous TRW staff members, with support from Ball Brothers Research Corporation and consultants. The helpful suggestions and data from SAMSO and Aerospace personnel are also acknowledged.

PREFACE

This report presents the 9433 Despin Control anomaly investigations, and the resulting conclusions and recommendations. The 9433 spacecraft is still in operation and orbital data is being received and reviewed on a continuing basis. For this reason, these results and conclusions should be viewed as provisional, inasmuch as new data (after 16 January 1976) could provide fresh insight into the spacecraft's status. It should be noted that the character of orbital behavior in the past months has been highly variable; therefore, no attempt is made to predict its future behavior. Measures taken to maintain operational status of 9433 have thus far been highly successful.

CONTENTS

		Page
1.	INTRODUCTION	1-1
	1.1 Summary Evaluation of 9433 Anomaly	1-3
	1.1.1 Anomaly Characterization	1-3
	1.1.2 Cause of Anomalous Performance	1-4
	1.2 Despin Controller Description	1-5
	1.2.1 Despin Mechanical Assembly	1-5
	1.2.2 Despin Electronics Assembly	1-9
2.	ORBITAL CHRONOMOGY	2-1
	2.1 DSCS-II Flight History	2-1
	2.2 9433 Chronology	2-4
	2.3 Comparative Data (9431, 9432, 9434)	2-14
3.	ANALYSIS OF SLECTED ORBITAL DATA	3-1
	3.1 Sumary of Orbital Data	3-1
	3.2 Operational Data	3-4
	3.3 Unplanned Events	3-25
	3.4 Friction Tests	3-47
	3.5 Recovery Data	3-56
	3.6 Orbital Dynamic Tests	3-66
4.	FAILURE MODES AND EFFECTS	4-1
5.	THERMAL/DIMENSIONAL ANALYSES	5-1
	5.1 Thermal Analyses	5-1
	5.2 Dimensional Analyses	5-17
6.	SYSTEM, ASSEMBLY, AND COMPONENT TESTS	6-1
	6.1 System Tests	6-1
	6.2 DMA Assembly Level Tests	6-4
	6.3 Bearing and Slip Ring Tests	6-9
	6.4 Snubber Tests	6-16
	6.5 Motor Tests	6-20
7.	DMA DISASSEMBLY AND INSPECTION	7-1
	7.1 Approach	7-1
	7.2 Disassembly and Inspection Results	7-8
	7.3 Conclusions	7-14

CONTENTS (Continued)

		Page
8.	DMA ASSEMBLY, TEST AND STORAGE HISTORY	8-1
	8.1 General Data	8-1
	8.2 9433 DMA (S/N 3-2)	8-1
9.	SYSTEM SIMULATION AND ANALYSIS	9-1
	9.1 Simulation Results	9-1
	9.2 Spectral Analysis	9-17
10.	CONSULTANT EVALUATIONS	10-1
	10.1 Donald H. Buckley (NASA/LeRC)	10-1
	10.2 Delco Electronics	10-1
	10.3 Draper Labs	10-2
	10.4 Thomas Barish (Independent Consultant)	10-3
	10.5 Chet Pentlicki (ComSat Labs)	10-3
11.	CORRELATION OF FAILURE MODES WITH DATA	11-1
	11.1 Review of Data	11-1
	11.2 Discussion of Failure Modes	11-5
	11.3 Conclusions	11-10
12.	RECOMMENDED ACTION	12-1
	12.1 Design Changes	12-2
	12.2 Process Changes	12-7

1. INTRODUCTION

This report presents results of the 9433 despin control anomaly investigation and summarizes pertinent data available from other activities reported, or to be reported, elsewhere (for example, the DMA life test anomaly evaluation). In addition, general recommendations for remedial action are presented; the detailed definition of these actions are still under study and will be reported when complete. The primary focus of this document is assessment of the 9433 anomaly.

When confronted with multiple anomalies (the short-term pointing perturbations seen in several spacecraft, the high friction torques of 9433, and the lead deposits found in the life test DMA), it is natural to conjecture a relationship between these events; indeed, the possibility of such connections must be pursued to the extent permitted by the available data. However, it is essential that a strict account be kept of which conclusions are factual and which are conjectural.

It is characteristic of the DSCS-II orbital anomalies that almost all conclusions drawn will be somewhat less than conclusive. A lack of absolute certainty in assessing the 9433 orbital anomaly is of practical concern only if the decisions made in response are affected. In this case, due to design changes already made within the replenishment DMA, the redesign action recommended can safely focus upon the most probable cause of the anomaly.

During the course of the anomaly investigation, a variety of activities have been pursued (see matrix of Figure 1-1). Although some of these tasks have not shed light on the anomaly itself, all have contributed to a better understanding of the despin control system, the DMA and DEA, and the various components of the DMA. Moreover, a number of the process studies and tests completed and in progress are providing important insight into the more subtle aspects of bearing processing and lubrication.

The next part of this introductory section presents a summary evaluation of the 9433 anomaly. Remaining introductory subsections provide brief descriptions of the despin control system, the despin mechanical assembly (DMA), and the despin electronics assembly (DEA).

FAILURE MECHANISM	DIMENSIONAL ANALYSES	THERMAL ANALYSES	ORBITAL TESTS	LAB SYSTEM TESTS	LUBRICATION ANALYSES	COMPUTER SIMULATION	MOTOR/ELECTRONIC ANALYSES	BEARING TESTS	RECOVERY DATA ANALYSIS	DMA DISASSEMBLY AND INSPECTION	CONSULTANTS
	ACTIVITIES										
MECHANICAL INTERFERENCE ("RUBBING")	X	X							X		
LUBRICATION SYSTEM		X	X		X	X				X	X
DEBRIS IN BEARINGS			X			X	X	X	X	X	X
MOTOR/RSVR/ELECTRONICS			X	X		X	X				X
BEARING LOADING	X	X		X				X			X

Figure 1-1. Failure Mechanism Identification

1.1 Summary Evaluation of 9433 Anomaly

1.1.1 Anomaly Characterization

The 9433 orbital anomaly is characterized by an elevated constant running friction ($\tilde{\gamma}$100 in-oz) across the rotor-platform rotating interface, accompanied by occasional torque transients. The highest level of running friction observed to date is 575 in-oz, with smaller perturbations (25-50 in-oz) more common. The average friction torque and the amplitude of the torque perturbations appear to be correlated with spacecraft ambient temperatures; however, this correlation has not been conclusively and quantitatively established.

By contrast, the anomalies observed in previous DSCS-II satellites (and at early stages of 9433 operation) showed no increase in the average running friction. These anomalies, occasional attitude perturbations in the 0.2-0.4 degree range, were consistent with small torque transients (e.g., 5 in-oz) and have generally been attributed to the "retainer whirl" phenomenon observed in the laboratory and in other synchronous dual-spin satellites.

In the case of 9433, small transient perturbations were observed to occur shortly after launch and on other occasions during the first 18 months of operation. The growth of average running torque, as evidenced by a rise in the "torque voltage" telemetry data, was first observed in July 1975; during August and September, this growth became pronounced, leading to loss of operational status on 13 September 1975.

Operational status was re-established in October, with occasional partial spin-ups due to extreme torque transients. Throughout this period, the average running torque has persisted at a level in the neighborhood of 100 in-oz; however, occasional periods of near-normal friction (30-40 in-oz) have been observed since late November.

During operational periods, the running friction has been estimated from the torque voltage telemetry, an indirect measurement. This indirect estimate has been corroborated by direct dynamic measurements taken during non-operational periods (partial spin-ups, total spin-ups, friction tests), thus verifying a high level of mechanical friction, rather than an electronic (DEA) anomaly.

1.1.2 Cause of Anomalous Performance

In order to assess the cause of the observed increase in running friction, a variety of test, analysis, and simulation activities were initiated; in addition, a number of recognized bearing and lubrication experts were consulted.

The conclusions reached by these activities are:

- The anomaly is due to a mechanical effect rather than an electronic failure in the DEA
- No possible source of friction torque external to the DMA appears consistent with the observed orbital data
- The most likely failure mechanism is a bearing degradation due to poor lubrication (e.g., inadequate lubricant supply or deterioration of lubrication quality)
- The lubrication supply system is the least understood and weakest aspect of the DMA design.

The last two conclusions are supported by the majority of the consultants, and are given further credibility by evidence of lubricant degradation within the four-year life-test DMA.*

Other possible, but less likely, failure mechanisms have not been ruled out. Most prominent among these is possible mechanical interference ("rubbing") at the power module snubber. This could occur only with an extreme buildup of mechanical tolerances, accompanied by thermally-induced material creep. Disassembly of the life test and flight spare DMA's has not supported this theory; nor have the time-history of orbital data and the results of laboratory tests.

Other potential friction sources include: the slip ring assembly bearings; delamination of the motor or the resolvers; mechanical interference at the labyrinth seal of the DMA; rotation of the inner race of the top main bearing on its journal; and, a fracture of the motor's hypernik ring. Again, the orbital data, analyses, and tests conducted do not support these candidates.

In summary, a main bearing degradation due to inadequate lubrication is the most likely explanation of the 9433 anomaly, both for the rise in

---

* It should be noted that the life test DMA, despite the evidence of lubricant degradation, did not exhibit the anomalous performance seen on 9433 after only 19 months in orbit.

running friction and the torque perturbations observed. However, this conclusion must be viewed as a probability rather than a certainty. Such a bearing degradation could lead to a variety of additional mechanical problems and symptoms (e.g., debris due to bearing wear, retainer rubbing and jamming), resulting in the observed erratic behavior.

1.2 Despin Controller Description

The platform despin controller is a sampled-data servo which controls the speed and orientation of the platform relative to the local vertical. Its functional block diagram is shown in Figure 1-2.

The magnetic pipper which generates the platform reference pulse is aligned with the earth-coverage horns and indicates the earth-pointing reference of the platform. In the rate mode, the platform reference pulse is compared to clock pulses to form the error signal that is applied to the despin motor.

Search mode is entered by ground command, and the clock pulses are replaced by reference pulses formed at the center of the earth image signal. The up/down counter increases between the earth centroid pulse and the next platform pulse, is held steady until the next earth centroid pulse, and is counted down to the subsequent platform pulse. This leaves a measure of earth-referenced platform rate which is compared to a 0.5°/sec command search rate to form the error signal that is applied to the motor driver. The search rate, rotating the platform opposite to rotor spin, eventually brings platform and earth centroid pulses into coincidence, automatically switching the control to normal mode.

Normal mode pointing errors are derived in the up/down counter beginning at the leading edge of the earth-image signal. The count decreases from that time until the instant the platform reference pulse is received, after which it is increased until terminated by the earth-image signal trialing edge. The residual count is proportional to the pointing error, indicating that the reference pulse is not centered in the earth's apparent chord. Lead-lag and integral compensation is achieved by analog circuity after A/D conversion of the residual count. The integrator is used in the Rate and Search modes as well as in Normal mode.

1.2.1 Despin Mechanical Assembly

The despin mechanical assembly (DMA) is the mechanical and electrical link between the spinning and despun section of the spacecraft. It supports

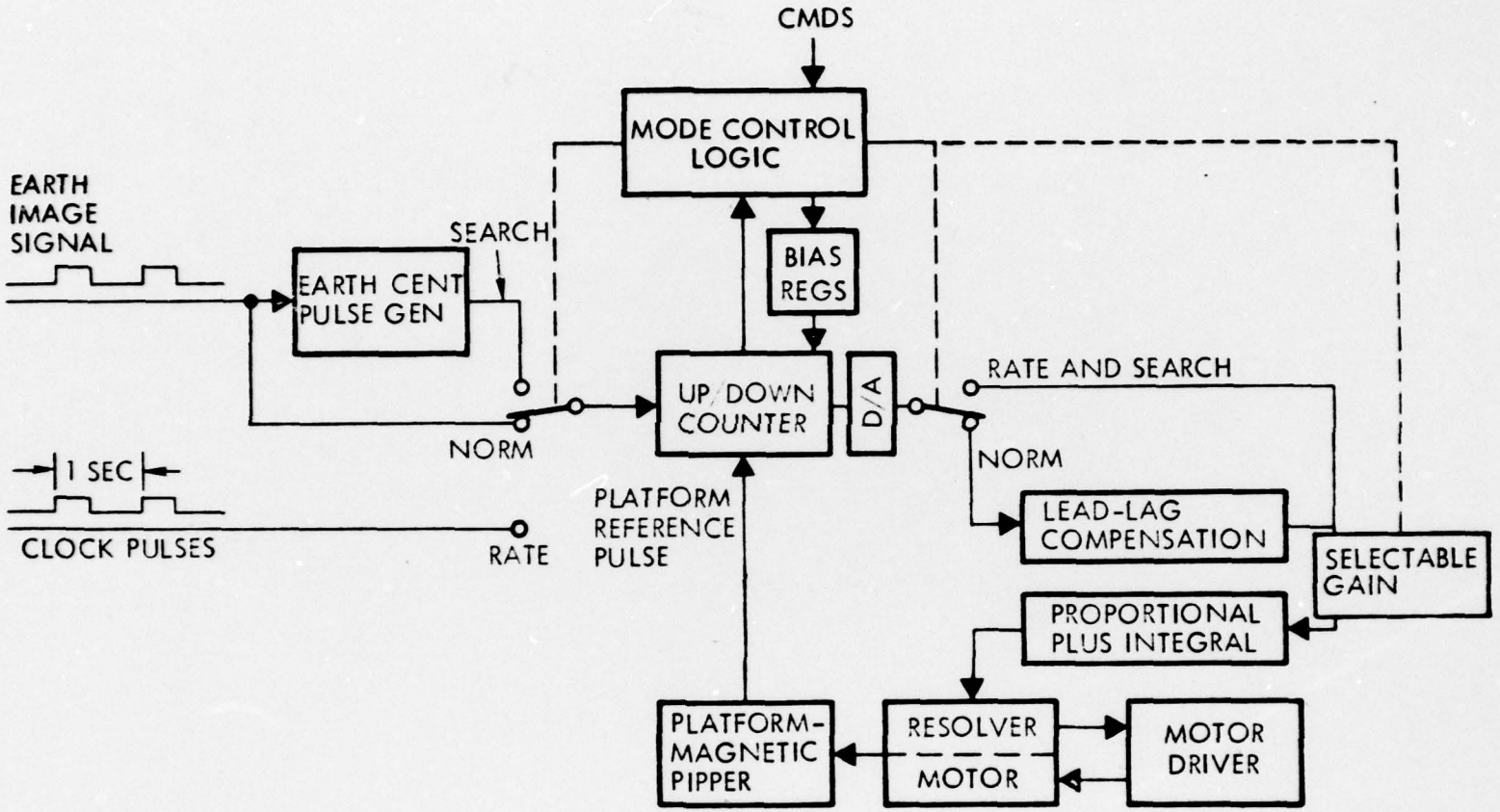


Figure 1-2. Simplified Functional Diagram of Despin Controller

the despun platform and provides the necessary torque to despin the platform. It provides the electrical power and signal paths between the platform and the spinning rotor. The design of the despin mechanical assembly is strongly influenced by launch-load environments and the long-life requirements in vacuum.

The unit consists of two principal subassemblies, a drive subassembly and a slip ring subassembly (Figure 1-3). The drive subassembly includes the main housing, the spinning shaft, a motor with redundant windings, redundant magnetic pickups that generate once-per-revolution platform reference and interference window pulses, lubricant reservoirs, temperature sensors, alignment mirrors, and appropriate electrical leads and electrical connectors. The slip ring subassembly contains the required power and signal rings, brush blocks, brushes, lubricant reservoirs, cover enclosures, and the electrical leads and connectors. The slip rings are completely redundant and in addition contain redundant brushes for every slip ring.

The DMA motor is an inside-out, two-phase synchronous motor. The rotating magnetic field in the motor is supplied by exciting the motor based on the output from a two-phase resolver with the same number of poles as the motor. As the resolver and motor are mounted on the same shaft, the motor is in synchronism and runs at the speed at which the output torque balances the shaft load. This combination has characteristics similar to those of a dc motor. Redundant motor-resolver combinations are supplied to ensure the high reliability required.

The magnetic pickups are of the permanent-magnet driven, flux-circuit type. When the reluctance of the circuit between the pole tip and shell is interrupted by driving an iron tooth past the pickup, the changing flux in the circuit produces a voltage in the output winding. This interruption occurs once per shaft revolution and is used to provide shaft position information.

The shaft bearings are deep groove radial ball bearings. They support the rotating shaft which in turn attaches to the spinning section of the spacecraft. Bearing lubrication is obtained by treating the bearings with the Ball Brothers Research Corporation's VacKote process and by using lubricant reservoirs adjacent to the bearings, sized by analysis to contain lubricant for many times the 7-year required life.

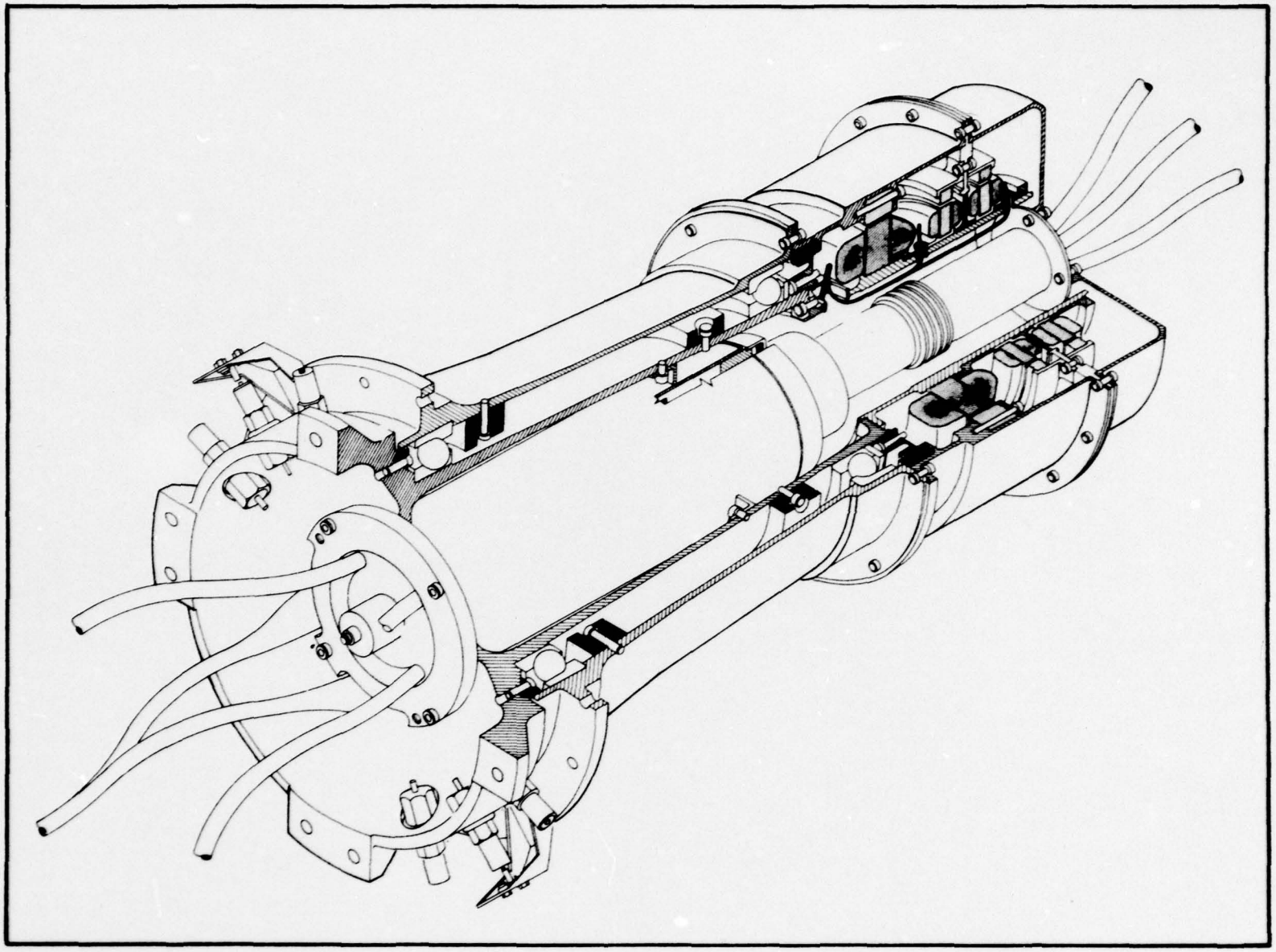


Figure 1-3. DSCS-II Despin Mechanical Assembly (Flights 1-6)

The slip ring assembly uses soft gold rings overplated with hard gold on a ceramic-filled epoxy drum. The brushes are flat wire brushes of 75 percent gold, 22 percent silver, and 3 percent nickel alloy. The slip ring assembly is also lubricated by the VacKote process.

1.2.2 Despin Electronics Assembly

A simplified block diagram of the despin electronics assembly (DEA) is given in Figure 1-4. The primary functions of this assembly are:

- Acquisition Error Computation. In rate and search, the time between platform reference pulses is compared to the time between clock or earth centroid pulses using an up/down counter, and the controller acts to align the platform reference pulse with the clock or earth centroid pulse.

- Normal Mode Error Computation. The up/down counter begins counting up with the rising edge of the quantized earth signal signal. The direction of count is reversed at the rising edge of the platform reference pulse. The counter is always stopped with the following edge of the earth image signal. The final count in the up/down counter is proportional to the platform earth pointing error.

- Bias Registers. Bias registers are provided to command maneuver rates in the rate and search modes and to command position offsets for use with either north or south earth sensor during normal mode.

- Digital to Analog Conversion. A D/A converter is provided to convert the error into an equivalent dc analog signal to feed the despin driver.

- Analog Compensation. Integral plus lead compensation, along with lead-lag filtering needed for stability, is implemented with passive components and operational amplifiers. Eight selectable gains are included.

- Motor Controller. The shaped signal is applied to the motor resolver to obtain sine/cosine commutation. The motor Controller modulates bus voltage with the outputs of the resolver and applies the result to the corresponding motor windings so that the motor drive signal is proportional to platform error. Gain compensation is achieved by motor voltage feedback. Current limiting is also incorporated.

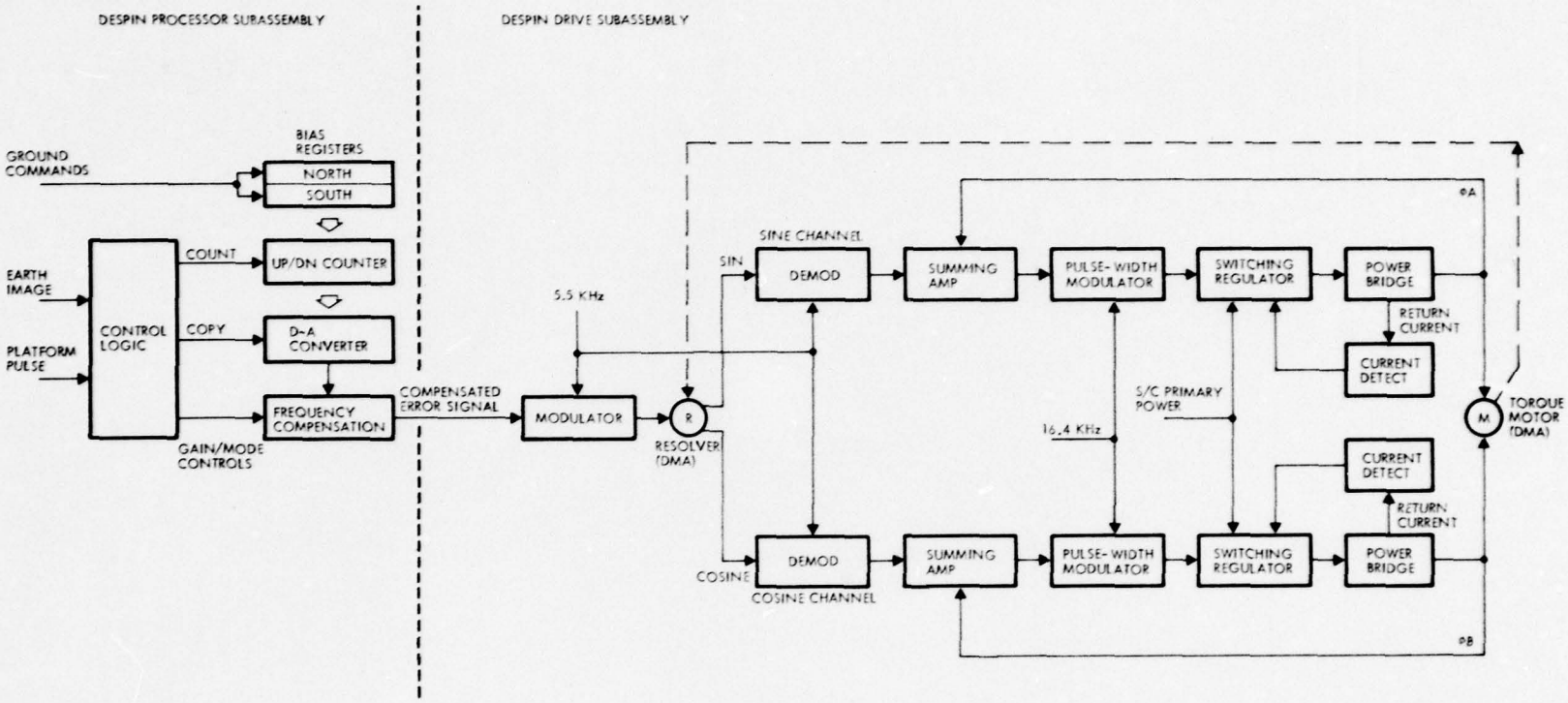


Figure 1-4. Functional Block Diagram, Despin Electronics Assembly

2. ORBITAL CHRONOLOGY

2.1 DSCS-II Flight History

The chronology of the DSCS-II program is presented for review in Table 2.1. Pertinent dates for all influencing events on despin pointing are listed.

Two launches have provided four spacecraft for operational communications usage for various lengths of time. Both spacecraft of the Launch I configuration (9431 and 9432) are no longer usable for communications. The prime and redundant ACS subsystems on 9431 are capable of supporting normal mode despin pointing at the present time. The ACS status of 9432 at the time of the 8 September 1972 failure was "operational" (normal mode pointing) on the primary units. A possible failure of the redundant DEA resulted in the December 1971 spin-up (reference 9670-REP-040-01).

The Launch II spacecraft have provided the normal mode pointing required for communications usage without the failure of any ACS functions. However, 9433 has experienced a degradation in its performance of despin pointing (reference Section 2.2) to a much greater degree than any previously observed.

Table 2.1. DSCS II History

SPACECRAFT	LAUNCH DATE	NORMAL MODE		ANOMALIES	REMARKS
		DURATION	PERFORMANCE		
9431	11/3/71	11/6/71-12/12/71	Pointing ≤.1° Constant running torque (30 in-oz friction)	Command EXEXUTE Anomaly caused spin-up which resulted in omni antenna fold back during recovery	Due to degraded TLM and CMD capability, operational usage was not attempted until 1/72
		1/28/72-6/2/73	Pointing ≤.1°* Constant running torque *After 6/2/72, limited pointing excursions experienced during eclipse seasons	Thermal anomaly observed 6/2/72 caused deviations in predicted temperatures	After the thermal anomaly of 6/2/72, pointing variations were observed >.15° during eclipse seasons. However, no torque drive increases were observed.
		6/2/73 to Present	Periodic Normal Mode pointing tests	Loss of power to the despin platform renders S/C useless for Comm.	Despin pointing data as a function of temperature being collected. Satellite is in rate mode except during special normal mode tests.
9432	11/3/71	11/5/71-12/2/71	Pointing variations of ±.25° observed at constant running torque (30in-oz friction)	DEA No. 2 failure caused spin-up, loss of lock	Dynamics problem prevented recovery from spun-up condition.
		6/8/72-9/8/72	Initial variations of ±.4° decreasing to ±.2° at thermal equilibrium. No increase in drive torque from previous normal mode operating period.	Loss of secondary power to spinning section caused permanent S/C spin-up	

Table 2.1. DSCS II History (Continued)

SPACECRAFT	LAUNCH DATE	NORMAL MODE		ANOMALIES	REMARKS
		DURATION	PERFORMANCE		
9433	12/14/73	12/15/73-12/27/73	Pointing $\leq .3°$ running torque decreased $\approx$ 10 in-oz (friction torque $\approx$ 25 in-0z)		
		12/28/73-4/30/75	Pointing $\leq .1°$ except for occasional $\pm .2°$ variations during last half of eclipse season (4/74)		No noticeable increase in drive torque during the period when pointing variations were being experienced (Spring eclipse season of 74)
		5/9/75-Present	Very large variations at times. $\pm 6.5°$ resulting in loss of lock etc.	Excessive friction torque, with major transient variations.	Drive torque began to increase in late March 75. Pointing variations grew continually in August-Sept. until first spin-up occurred on 9/13/75
9434	12/14/75	12/15/73-Present	Pointing $\leq .1°$ Constant torque drive throughout life time ($\approx$35 in-oz friction)		No observed pointing problems since launch

2.2 9433 Chronology

The characterization of 9433 in a historical sense would be described as follows. Spacecraft 9433 was placed in Normal Mode on 15 December 1973 on the No. 1 units followed by the Controls Redundancy Test on 18 December. Final post redundancy test normal mode operation was configured using the N1, S1 earth sensors with CTA-2 and DEA-2 units. However, performance of 9433 indicated pointing variations of $\pm$.3 deg worst case, with numerous occurrences between $\pm$.2 deg from 15 December through 27 December. Since during this time span the DMA bearing temperatures varied only $\pm$2 deg around 70°, it was assumed that no thermal disturbances were in evidence. However, there did seem to be a gradual decrease in the DMA drive torque of approximately 10 in-oz over this time period. The cause of this decrease in drive torque was later attributed to a friction decrease since the spin-rate of the spacecraft was constant during this time interval. Once the lower drive level was reached on 27 December, despin pointing did not exceed $\pm$.09 deg until the latter part of the first eclipse season.

During the latter half of the eclipse season (March 20 through 20 April) a limited number of pointing variations were observed. The eclipse period presented the first opportunity for observance of performance under large thermal variations. Telemetry data disclosed that both a slight increase in torque voltage (-.91 volts to -.94 to -.98 volts)* and a corresponding change in despin pointing error variations were evident. Due to eclipse support requirements for monitoring battery operation, telemetry pass times during that time period were consistently made at the same time each day. Despin pointing variations in excess of $\pm$.1 deg were observed during supports covering the portion of the day where the DMA temperatures were increasing towards or had reached their peak values (approximately satellite local noon). Most support times were 15 to 30 minutes in duration. Under these conditions, one to three variations of from .12 to .21 deg were observed. The average value observed was .17° with the maximum frequency occurring during the time span of 7 April through 19 April. With the completion of the eclipse

---

* The "torque voltage" is the compensated error signal and is a measure of drive torque under steady-state conditions (see Appendix F).

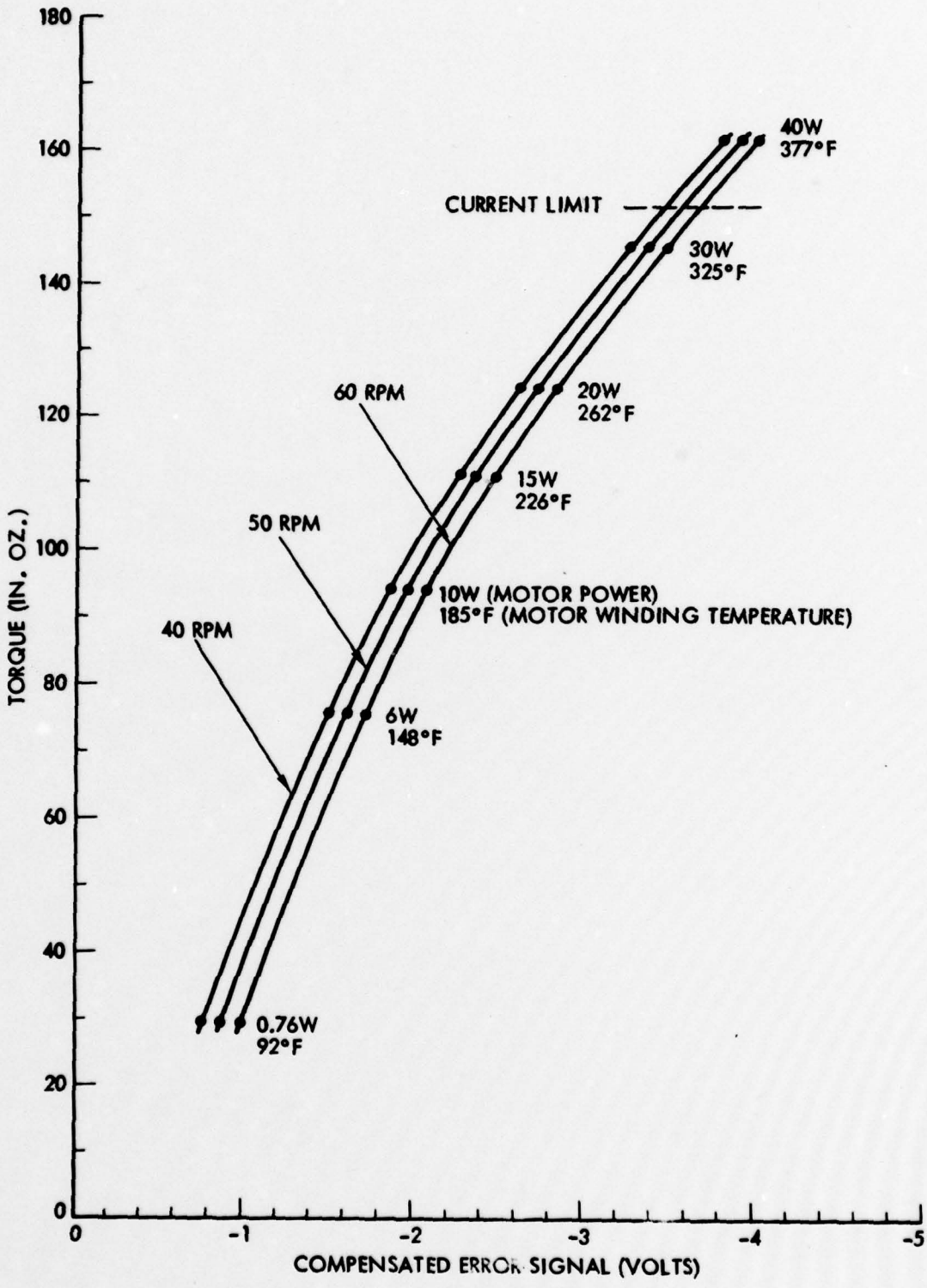


Figure 2-1. Motor Torque as a Function of Torque Voltage Telemetry with Steady-State Thermal Conditions

season, 9433 did not exhibit observable pointing variations until the following eclipse season (March of 1975). The temperature profile during this time span was a duplicate of that experienced in the year previous. A review of the telemetry data plots of the despin torque values indicated that beginning in mid-March, 9433 showed a small increase in the average torque voltage reaching a value of -1.06 volts during May (Figure 2-1 shows the correspondence Y torque voltage and torque for steady-state operation). The maximum observed transients of 0.5° occurred on May 9, June 26 and 27. However, numerous occurrences of pointing variations above 0.2° were in evidence during the intervening period. During the period of approximately one and a half months between the end of June and 12 August, pointing variations were less than .15°.

Beginning on 12 August, large values of despin pointing error again became evident as the average despin torque voltage started to rise. The initial pointing excursions were approximately 0.5 deg at torque voltage levels of -1.2 volts. By 4 September, excursions in excess of 1.0 deg were being experienced with average torque voltage levels of -1.8 to 2.0 volts. Table 2.2 lists the sequence of events on 9433 starting in September. Initial attempts at altering performance consisted of gain state changes and unit switchings. By 8 September, it had been determined that gain state and the DEA unit providing drive to the DMA did not seem to change observed performance characteristics.

The second attempt to improve pointing error was instituted on 8 September. The low level DMA heaters were commanded On. After approximately 18.5 hours, the heaters were commanded Off (9 September, 1830Z) since a slight degradation in pointing had been observed. It was then felt that a reduction in the satellite spin speed might possibly increase the life of the spacecraft if the problem was bearing related. Therefore, on 12 September, the spacecraft was spun down to 50 rpm from the previous 60 rpm operating point.

Approximately 12 hours later, despin control was lost and the spacecraft subsequently switched to Standby Mode. A number of attempts were made on 13 September to despin the platform (reference Table 2.2). DMA motor, spin thrusters, and a combination of both were unsuccessful. By unsuccessful it is meant that a total despin did not occur; however, a measure of relative motion was achieved during at least two of the attempts.

A second recovery attempt was initiated in late September. Data analysis of the initial recovery attempt indicated the apparent existence of high friction levels in the DMA bearing interface. The second recovery attempt was designed to develop the maximum despin torque possible. Three discreet methods of accomplishing this were postulated and assigned an order of attempt. Prior to the recovery itself, a spin-down of the spacecraft was accomplished to a point at which the narrow coverage antennas (NCA's) could be moved to the opposite of the cross-eyed stops. The movement of the NCA's favorably alters the mass properties of the platform to reduce sideloads on the DMA.

On 26 September, the recovery was initiated. The second attempt was successful. After the ensuing increase in spin rate, several normal mode evaluations at various spin rates were performed in an attempt to establish an optimum operating point. At the completion of the 26 September recovery pass, the spacecraft was commanded back to Rate Mode control. On 30 September, a series of friction tests was performed in an attempt to establish net drive torque and friction levels. A repeat of this test was begun on 10/4; however, a spin-up resulted from a DEA current overload torque requiring a repeat of the 9/26 recovery sequence. On 10/7, Normal mode was reestablished utilizing continuous SCF monitoring, attempting to prevent future spin-ups. Between 10/7 and 10/20, normal mode pointing was lost, then reestablished ten times without a total spin-up occurring. The third total spin-up occurred on 10/20, due to excessive friction torques, requiring a spin-down of the spacecraft for recovery. Since the recovery from spin-up No. 3, numerous other partial spin-ups have occurred; all have been recovered by using contingency procedures at the SCF.

On 11 December, the first occurrence of a new type of partial spin-up was observed. On this date, rate control was reestablished using SCF block command recovery sequences. However, when normal mode earth lock was attempted, it could not be maintained. For a period of approximately 12 hours, each normal mode attempt resulted in an ensuing switch to Standby mode. Performance in Rate mode indicated frequent torque transients

were being experienced. The magnitudes were such that normal mode pointing could not be maintained. These symptoms were experienced again on 12/18 and 12/27 for approximately 17 hours on each occasion.

In each of the three lengthy losses of Normal mode during December, the frequency and magnitude of torque transients has been sufficient to prevent a lasting reestablishment of earth pointing. The magnitude characterization of these transients is discussed in Section 3.3. It should be noted that prior to the 12/11 performance, a loss of Normal mode pointing was typically reestablished within 30 minutes with no ensuing loss experienced for several hours.

Table 2.2. 9433 Anomaly Chronology

DATE	EVENT	REMARKS
9/4/75	GAIN STATE EVALUATION	Evaluated despin controller performance under increased loop gain conditions (G.S. 7-8-7-8) in Normal mode.
9/5/75	SELECT DEA 1	Determine effect of a redundant DEA electronics unit under G.S. 7 and 8 conditions on despin pointing in Normal mode.
9/8-9/75	DMA HEATER EVALUATION	Utilize low level DMA heaters to alter thermal environment of DMA and determine effect on Normal mode despin pointing.
9/12/75	DECREASE S/C SPIN RATE	Evaluate spin rate effect on despin pointing at 50 RPM.
9/13/75	LOSS OF DESPIN CONTROL AND SPIN-UP #1	
9/13/75	INITIAL RECOVERY ATTEMPTS	DESPIN ATTEMPTS USING: 1. DEA 2 and motor only, 3 times 2. DEA 1 and motor only, 1 time 3. Repeat of motor only attempts after DMA heaters used to warm DMA with each DEA. 4. DEA 2, motor and spin-up thruster pulse. 5. DEA 2, motor and spin-down, spin-up thruster pulse (spin-jerk). None of the above were successful, however relative motion during two attempts was observed.
9/24/75	SECOND RECOVERY ATTEMPT PREPARATIONS	1. Normalizing $\Delta\emptyset$ maneuver. 2. S/C spin down to speed at which the NCA's can be moved to the opposite of 'X' eyed stops and held. 3. Determine earth sensor operability at 20 RPM for attitude data measurements (spin rate and earth chord).

Table 2.2. 9433 Anomaly Chronology (Continued)

DATE	EVENT	REMARKS
9/26/75	SECOND RECOVERY ATTEMPTS	1. DEA 2, motor and spin-down, spin-up thruster pulses (spin-jerk) - slight relative motion only. 2. DEA 2, 2 sec spin-down, spin-up thruster pulses ending with motor on and a 10 sec spin-up pulse (rotor jiggle) - successful despin accomplished.
9/26/75	SPIN-UP OF SPACECRAFT OPERATING SPEED	Evaluation of normal mode despin pointing at different spin rates after initial spin-up with the spin-up thrusters.
9/30/75	FRICTION TEST SEQUENCE #1	Evaluation of net drive torque and friction levels with DEA 2 and DEA 1.
10/4/75	FRICTION TEST SEQUENCE #2, SPIN-UP #2	Friction test, spin-up, switch to DEA-2, Recovery block at 52 rpm - 1/2 rev relative motion. Change spin rate to 20 rpm, slew NCA's, recovery block -de-spin initiated. Change spin rate to 46 rpm
10/7/75	ESTABLISH OPERATIONAL SUPPORT	Normal mode, start full time SCF support and DCA utilization.
10/8/75	COMMUNICATIONS CONFIGURATION	No comm turned on.

Table 2.2. 9433 Anomaly Chronology (Continued)

DATE	EVENT	REMARKS
10/8	**Loss of Normal Mode**	Partial spin-up
		Rate mode plus 15 sec spin-up thruster pulse resulted in de-spin
		Normal mode (spin rate 50 rpm)
10/11	"	Partial spin up (standby mode)
		Rate mode
		Change spin rate to 44 rpm
		Normal mode
10/11	"	Partial spin up (standby mode)
		Rate mode → normal mode
10/12	"	Partial spin up (standby mode)
		Rate mode → normal mode
10/13	"	Partial spin up (standby mode)
		Rate mode → normal mode
10/13	"	Partial spin up (standby mode)
		Rate mode plus 15 sec spin up thruster resulted in de-spin
		Normal mode (spin rate 47 rpm)
10/14	"	Partial spin up (standby mode)
		Rate mode → normal mode
10/14	"	Partial spin up (standby mode)
		Rate mode → normal mode
10/14	"	Partial spin up (standby mode)
		Rate mode → normal mode
10/14	"	Partial spin up (standby mode)
		Rate mode → normal mode
10/20	**SPIN-UP #3**	Spin up
		De-spin attempts at 42 and 31 rpm were unsuccessful
		NCA slew and axial thruster recovery block at 20 rpm initiated de-spin
		Increased spin rate to 45 rpm
10/21	**Loss of Normal Mode**	Partial spin-up (standby mode)

Table 2.2. 9433 Anomaly Chronology (Continued)

DATE	EVENT	REMARKS
10/21	Loss of Normal Mode	Partial spin-up (standby mode) Rate mode plus 2 sec. spin-up thruster pulse
10/23	"	Partial spin-up (standby mode) Change spin rate to 40.7 rpm
10/23	"	Partial spin-up (standby mode)
10/24	"	Partial spin-up (standby mode)
10/25	"	Partial spin-up (standby mode)
10/26	"	Partial spin-up (standby mode)
10/28	"	Partial spin-up (standby mode)
10/30	Rate Mode	No continuous RTS coverage available
12/11	Loss of Normal Mode for extended time (1210-2342)	Partial spin-up (standby mode) Five reacquisitions in normal mode all went to standby. Changed spin-rate to 35 rpm Executed RB-9956. Spin rate 36.2 rpm Two additional reacquisitions in normal mode went to standby. Normal mode after 45 minutes of good search mode performance.
12/18, 12/19	Loss of Normal Mode for extended time (0740-0033)	Partial spin-up (standby mode) Seven reacquisitions in normal mode all went to standby. Executed RB-9956. Spin rate 37.4 rpm Reacquisition in normal mode went to standby Reacquisition in normal mode (GS-4) went to standby. Normal mode.

Table 2.2. 9433 Anomaly Chronology (Continued)

DATE	EVENT	REMARKS
12/22	Loss of Normal Mode	Partial spin-up (standby mode)
	"	Three partial spin-ups (last one in GS-2)
	"	Partial spin-up (standby mode) with GS-6)
12/23	Loss of Normal Mode	Partial spin-up (standby mode)
12/23	Loss of Normal Mode	Partial spin-up (standby mode)
12/27, 12/28	Loss of Normal Mode for extended time (1119-1134)	Partial spin-up (standby mode) Six reacquisitions of normal mode resulted in automatic switch to standby mode)
12/30	Loss of Normal Mode	Partial spin-up (standby mode)

2.3 Comparative Data (9431, 9432, 9434)

A characterization of 9433 performance in a chronological sense has been provided above. A comparison of Launch I (9431 and 9432) and Launch II (9433 and 9434) can be made as follows: until the thermal anomaly of June 1972 (Table 2.1), 9431 and 9434 were identical to each other, pointing$\approx$.07° with no abnormal variations as a function of the normal thermal extremes which occurred during eclipse seasons. 9431 pointing following the thermal anomaly has shown a degradation (evaluated during Normal Mode passes) which seems to follow a thermal cycle. Very low (<34°) bearing temperatures are being experienced during eclipse seasons. These low bearing temperatures are also resulting in higher drive torque requirements during these times. 9432 and 9434 each exhibited 0.25° attitude variations immediately following launch. Due to the 9432 DEA failure on 2 December 1971, a comparison of post-launch performance with that of 9433 cannot be made. With the ensuing recovery (8 June 1972), 9432 continued to exhibit pointing variations in excess of 0.2° although an increase in drive torque was not evident. It should be noted that initial attitude variations after recovery were 0.4°, decreasing to typical 0.2° level prior to the final failure on 8 September 1972 (not an ACS failure).

In comparing the pointing performance of 9433 prior to September 1975 versus 9431, 9432, and 9434, a critical point should be made. No short term increases in average drive torque levels have been evident during relatively active pointing variation time intervals (9431 and 9432). As noted above, 9431 has shown a long term increase in average drive torque which seems to have resulted from a thermal enclosure degradation, beginning in June of 1972. The torque increase does not follow the characteristics of 9433. An additional data point of comparison exists for each launch in the thermal area, especially for Launch II. The thermal environment for 9433 and 9434 were initially identical while drive torque requirements did not drastically differ. The use of the DMA heaters (Table 2-2 and Section 3.2) appeared to alter the thermal environment of 9433 so that a direct comparison with 9434 is no longer possible.

During periods of performance comparisons, thermal environment, launch and operating configurations, etc., have been similar. These similarities have provided valid data to evaluate pointing performance. In these comparisons, an increase in average drive torque has not been observed on 9431, 9432, and 9434.

3. ANALYSIS OF SELECTED ORBITAL DATA

Characterization of the on-orbit performance of 9433 requires analysis of selected orbital data. Although the quantity and quality (e.g., readout frequency) of telemetry data are limited, this information is the primary factor in identifying the possible and probable causes of the 9433 anomaly. Of particular interest are the magnitude of the rotor-to-platform friction torque (as indicated by various measurement data) and the dependence of this torque on other variables (for example, time and temperature).

3.1 Summary of Orbital Data

Several types of orbital data are available and discussed in following sections:

- Operational Data: Primary data of interest while the spacecraft is in its operational configuration ("Normal Mode") is the pointing error, the compensated error signal, and the three DMA temperature measurements.

- Unplanned Events: Unplanned events put the spacecraft out of Normal mode (into Standby, Search, or Rate mode). In any of these modes, the rate data provided a direct indication of torque. Temperature data is also of interest.

- Friction Tests: Systematic tests were performed on 30 October 1975 to provide direct measurements of friction torque. The data taken was similar to that from many unplanned events 'most of which occurred after the friction tests). Similar data (referred to as "Orbital Dynamic Tests") was obtained on 15-16 January 1976.

- Recovery Data: Data taken during various attempted and successful recoveries from full spin give indications of the character of friction at low relative rates (and its dependence upon the side loads produced by platform unbalance while spun up).

The first indication of anomalous performance came from a growth in the compensated error signal during normal operation, showing an increase in the running friction. Beginning in August 1975, this increase became significant, leading to loss of normal operation on 13 September.

This increase in friction torque was accompanied by increased thermal gradients along the DMA shaft, apparently due to the rise in motor power dissipation. Since that time, the running friction has been in the neighborhood of 100 in-oz most of the time (compared to a pre-anomaly value of 30 in-oz).

Immediately following the switch to Standby on 13 September, and the resulting platform spin-up, several unsuccessful recovery attempts occurred. The data from these attempts provided estimates of the running and static friction. This data was augmented by that from the successful recovery operations of 27 September and by subsequent recovery attempts on 20 October (following a platform spin-up due to excessive running friction). The main conclusion from recovery data is that the success of recovery depends upon spin rate, with lower spin rates (e.g., 20 rpm) improving recovery probability.

Shortly after the successful recovery of 27 September, a series of orbital friction tests were conducted by accelerating the platform by use of the motor and then allowing friction-only spin-up by disabling the DEA power amplifier. These tests provided the first direct friction measurement at operating speeds and showed an unexpected torque saturation. These results, described in Section 3.4, indicated a rise in running friction during the tests.

Between 27 September and end of 1975, numerous unplanned events occurred, including:

- partial spin-ups due to loss of earth lock
- a full spin-up due to a DEA current trip
- A full spin-up due to excessive friction
- a short period (2-3 hours) during which the running friction dropped to its pre-anomaly level
- several periods of extreme torque transients preventing sustained normal operation.

Since many of these unplanned events occur in Rate (or Search) mode, they provide excellent measurements of the running torque - as indicated by the slope of the rate data. However, since this data, for the most part,

relates to abnormal periods of friction transient activity, it must be viewed as representing extreme circumstances.* Indeed, the highest running friction transient observed (in excess of 500 in-oz) occurred during a partial spin-up on 13 October. Furthermore, the correlation of partial spin-up (due to friction caused losses of earth lock) - or lack of correlation - with time and temperature, has diagnostic value.

On 28 November, 9433 exhibited a new performance characteristic: the running torque dropped to a very low level (near the normal value of 35 in-oz) and remained there for approximately 3 hours. Such drops in torque were observed during several periods during the remainder of 1975, generally resulting in extended losses of operational status. Indeed, it appears that the overall character of the friction torques changed on 28 November from that of the previous period - suggesting a change in the phenomenon (or phenomena) giving rise to the orbital anomaly.

Most of the time since the successful recovery of 27 September has been spent in Normal mode, yielding operational data (pointing error, compensated error signal, DMA temperatures). For the most part, friction levels in the neighborhood of 100 in-oz have been observed from compensated error data.

---

* An exception is the full spin-up due to the DEA shut-down, apparently due to a current transient in DEA #1.

3.2 Operational Data

3.2.1 General

Figures 3.2-1 through 3.2-3 depict despin pointing error plots for three types of observed performance. Figure 3.2-1 demonstrates what a typical despin controller error signal looks like under normal on-orbit pointing conditions ($\leq .1°$). Figures 3.2-2 and 3.2-3 depict how the pointing error degraded through the August-September time span.

The general chronology presented in Section 2.2 describes the scenario of events related to the 9433 despin control anomaly. The review of comparative data for all DSCS II spacecraft indicates that except for 9434, all spacecraft have exhibited some periods of pointing wander. The following section describes how the performance of 9433 has differed from previously experienced despin pointing behavior. The attempts to alleviate the pointing abnormalities through on-board mode and configuration changes are described in detail with their ensuing results presented. Operational data will be covering four time spans: 1 May through 2 August; September; 3 October through 10 December; and 11 to 31 December.

3.2.2 May-August Time Span

Initial pointing disturbances during this time span appeared to be larger magnitude variations than previously observed in December of 75. On May 9, the initial observation of a 0.4" pointing transient occurred. Subsequent 0.3° excursions occurred on 5/12 through 5/16, then again on 6/24, 6/26, and 6/27. During each of these observed pointing perturbations, an increase in the despin torque was noted. Figures 3.2-4 and 3.2-5 present the daily drive torque and DMA temperatures for this time span. The torque drive increases in the May and June excursion periods amounted to approximately 5 to 10 in-oz. A comparison of temperatures in the DMA with 9434 during this time frame did not indicate thermal deviations were occurring in 9433 which could explain the higher drive torque.

Performance between the dates noted above was the typical $\leq 0.1°$ pointing being previously experienced as characteristic of 9433. With the cessation of pointing perturbations on 27 June, this characteristic

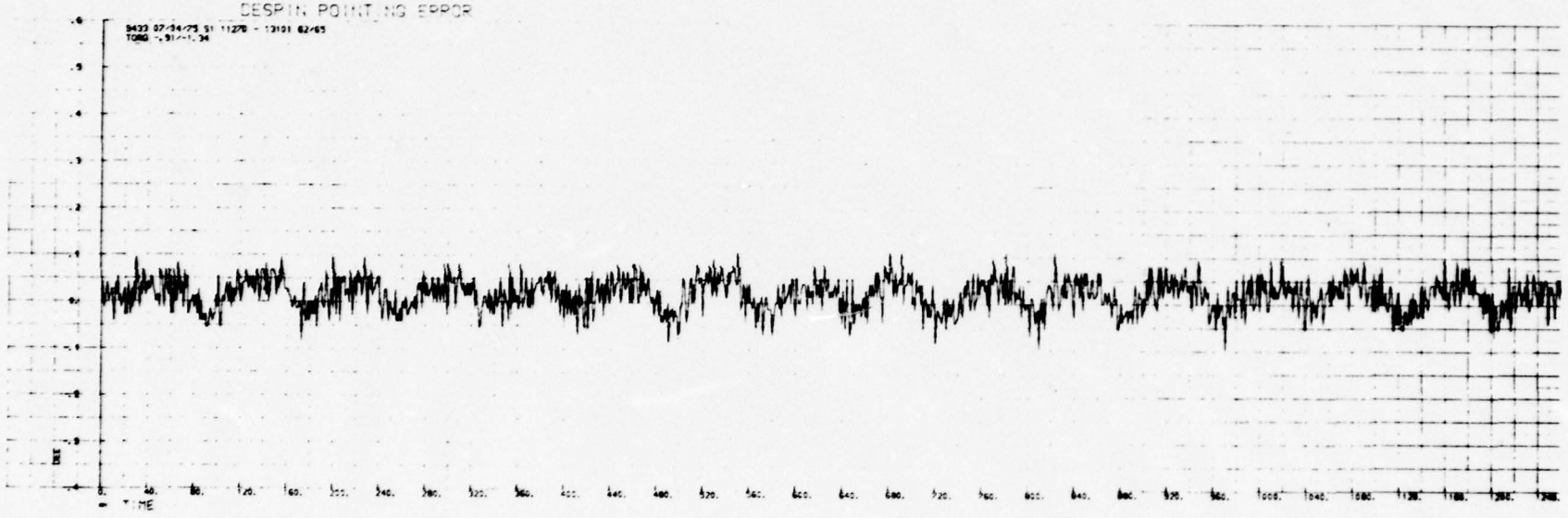


Figure 3.2-1. Nominal Despin Controller Pointing Error

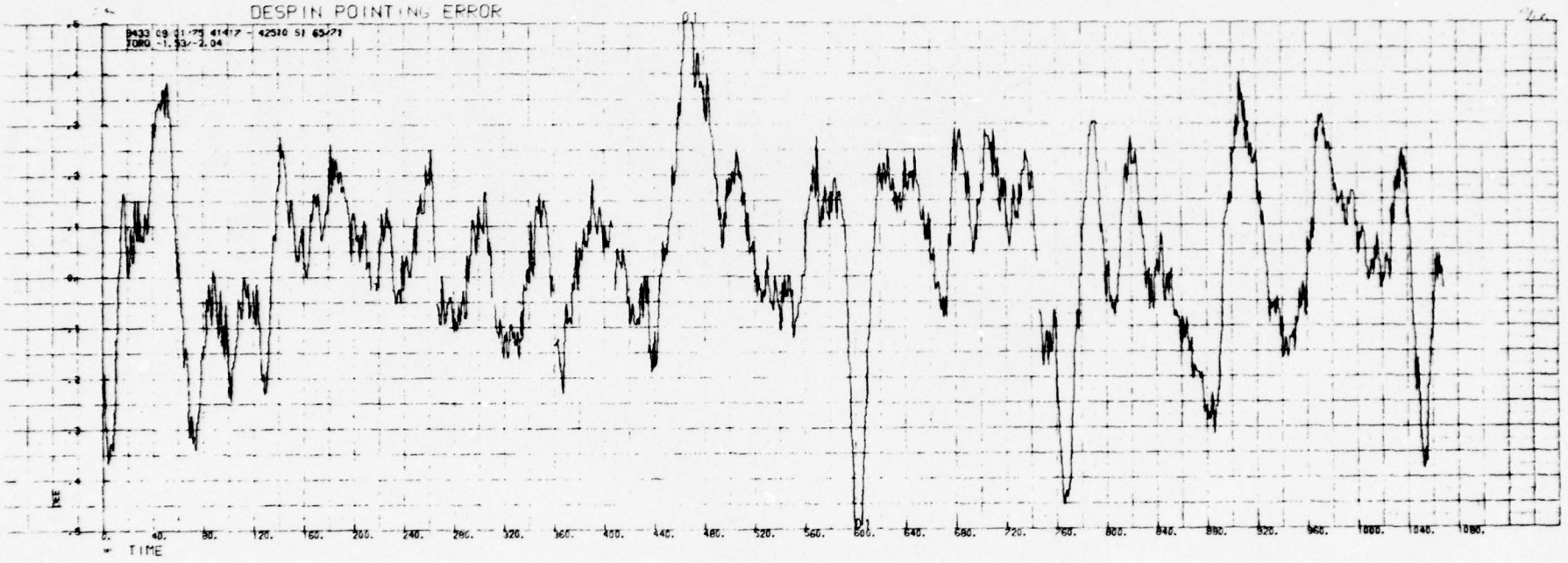


Figure 3.2-2. Typical .5° Pointing Error Transient

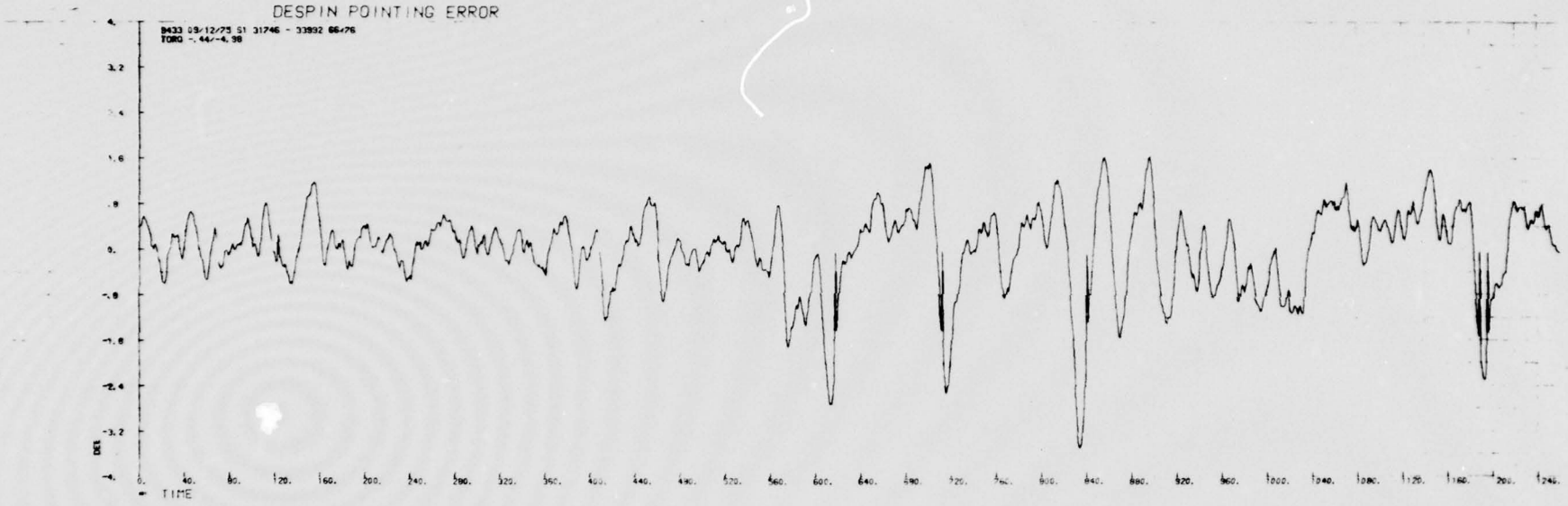


Figure 3.2-3. ≥1.0^{o} Pointing Error Transient

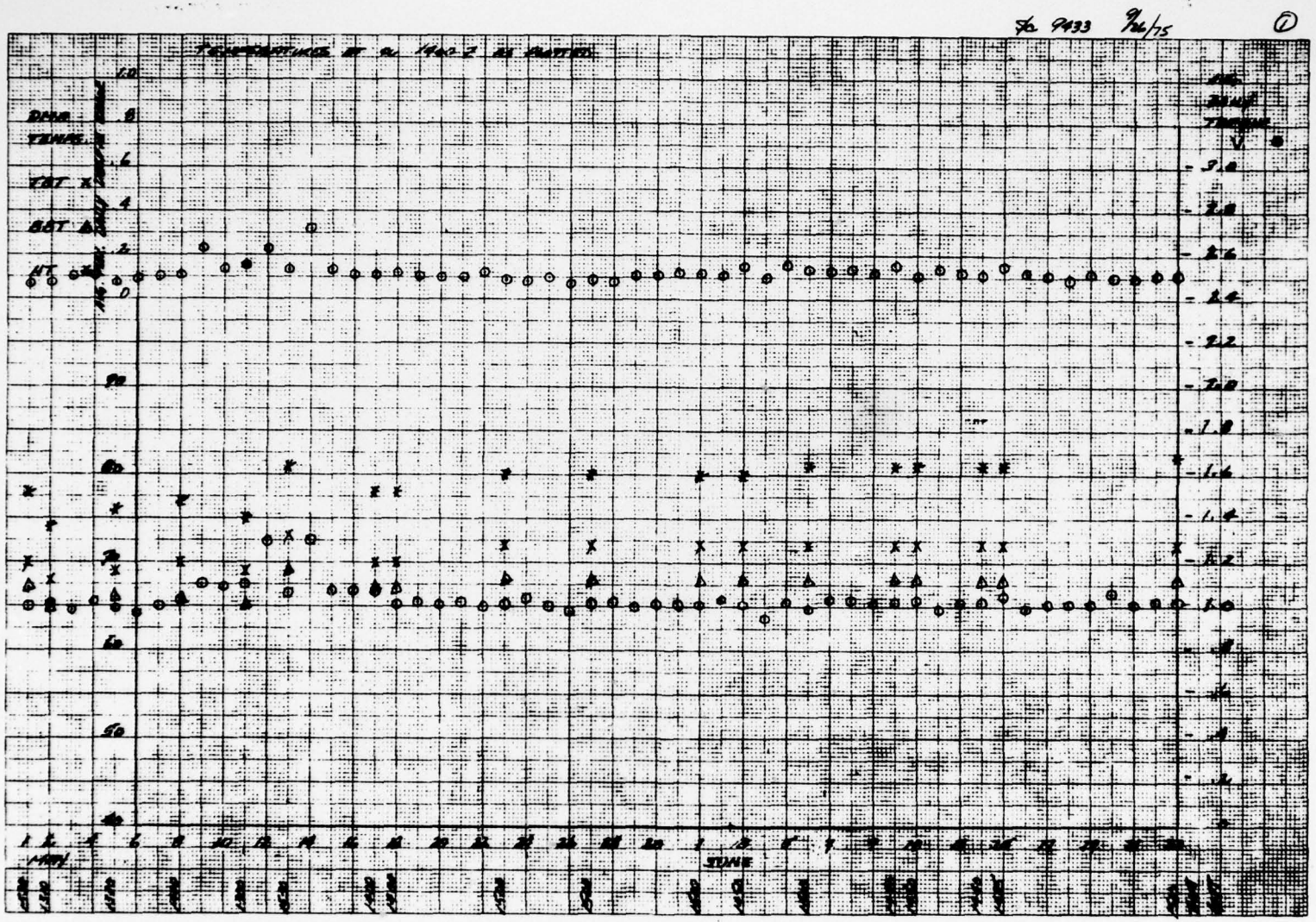


Figure 3.2-4. Daily Drive Torque, Despin Error, and DMA Temperature (1 May Through 23 June)

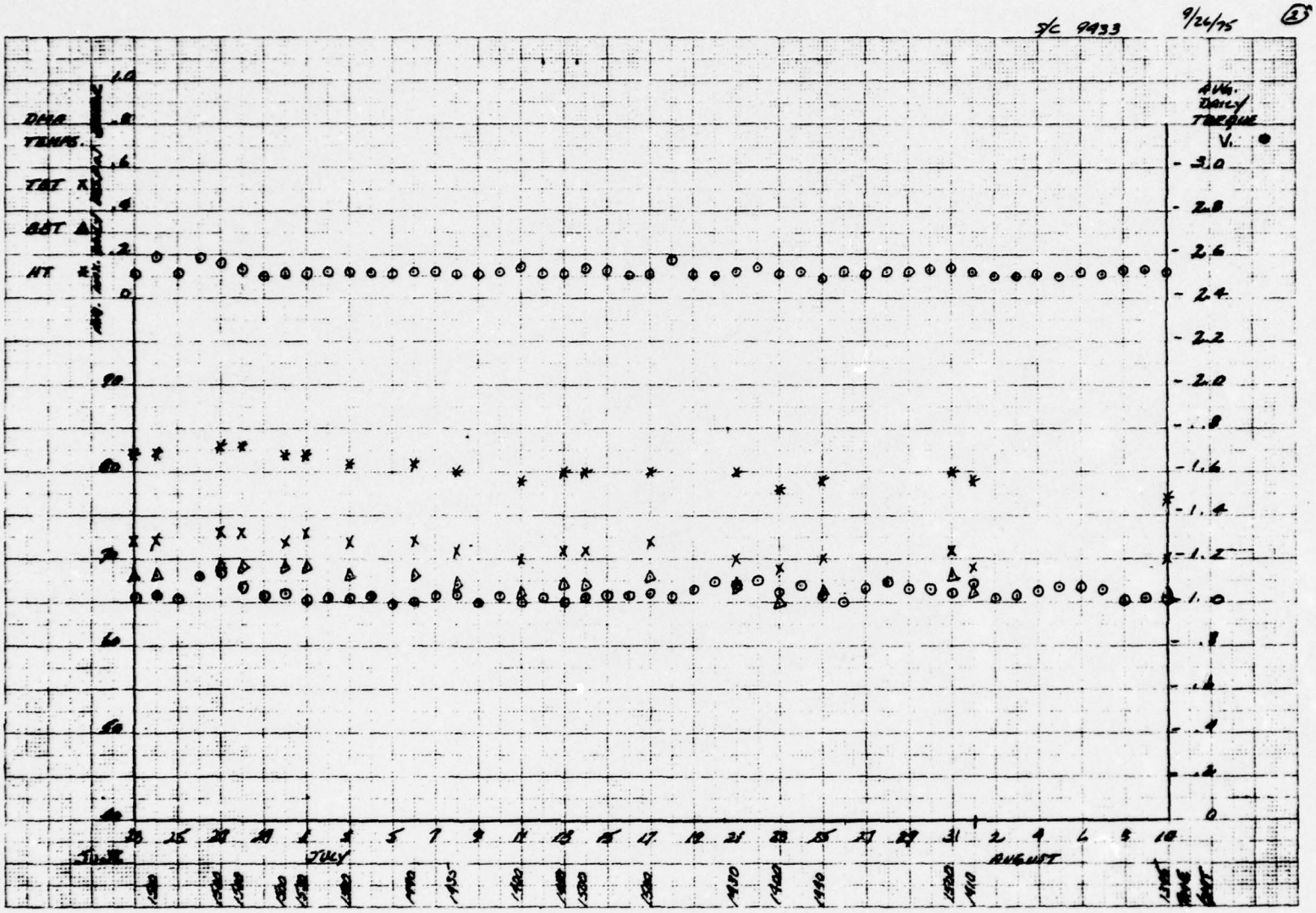


Figure 3.2-5. Daily Drive Torque, Despin Error, and DMA Temperature (23 June Through 10 August)

pointing was experienced until August 12. At this time, desping pointing variations began being observed as the average despin drive torque began to increase once again.

By the end of August, average drive torque increases of 60 to 80% (50 to 65 in-oz) were in evidence with despin pointing variations of 0.2° being commonplace.

3.2.3 September Time Span

Figure 3.2-6 contains the average daily temperature and torque voltage plots for most of August and early September. It is very apparent that a rapid degradation in pointing and required drive torque began at the end of August. The sequence of events for early September is contained in Table 2-2.

Evaluations of pointing performance with an increase in the despin controller forward loop gain (Gain State #8 vs #7), alternate electronics units providing despin drive torque, and decreased spacecraft spin rate were undertaken during early September (Table 2-2). In each case, no sustained improvement was attained. Pointing variations of 0.5° were becoming commonplace with increases in drive torque of 80 to 100% observed by 8 September.

Because there appeared to be a correlation of performance with time-of-day, it was thought that thermal gradients might be a driving influence. Therefore, an attempt was made to alter the thermal environment on 9 September by using the low level DMA heaters. However, the result was a further degradation in despin pointing as the required drive torque continued to increase. Typical pointing variations of 0.5° with large excursions of 1.0° were observed during the time of heater operation.

Turn-off of the DMA heaters did not result in a return of the DMA to its earlier thermal environment, apparently due to the increased drive torque causing higher power dissipation in the DMA motor. Pointing performance from heater turn-off until 9 September (when the spacecraft spin rate was reduced) continued at 0.7° at a friction torque level of 90 in-oz (pre- May 9 levels of $\pm$.09° at friction levels of 30 in-oz were typical).

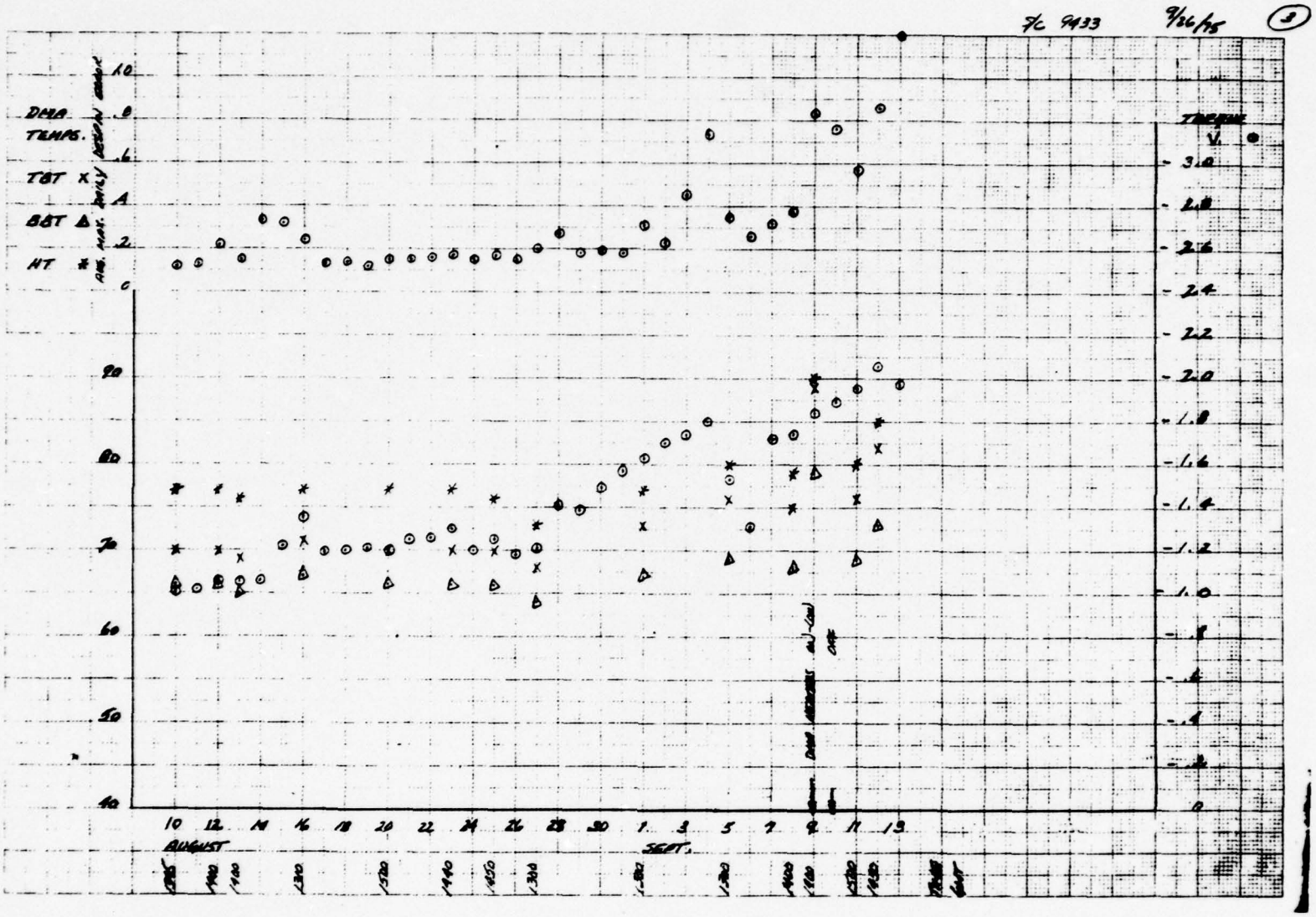


Figure 3.2-6. Daily Drive Torque, Despin Error, and DMA Temperature (10 August Through 13 September)

Several hours prior to reducing the spacecraft spin-rate, a 5.8° pointing transient had been observed (Figure 3.2-3). Since transients in excess of 6.0° would result in a loss of earth lock (normal mode), it was decided to reduce the spacecraft spin rate in an effort to possibly prevent this occurrence. A spin rate reduction to 50 RPM (from 60 RPM) was accomplished at 2000Z on 12 September.

This change in operating environment did not seem to affect either despin pointing or required drive torque level. Approximately 12 more hours of despin pointing were realized before a full spin-up occurred.

The details of friction levels at spin-up, recovery attempts, and special post-recovery tests are presented in Sections 3.3 through 3.5 which follow. These recovery efforts and special tests occupied the remainder of September (see Table 2-2 for chronology of events following 13 September spin-up).

3.2.4 October-December Time Span

The development of a successful recovery technique coupled with achieved results of several normal mode passes for special DC usage fostered the development of a high level of confidence for the reestablishment of normal mode on 7 October. To eliminate the time and fuel consuming recoveries from a fully spun-up condition, full time SCF monitoring was also instituted on 7 October. The use of Block Commands to re-initiate rate mode despin control as quickly as possible was instituted. In the time span of 7 to 20 October, ten (10) partial spin-ups (loss of earth pointing) occurred. The use of block commanding prevented a total spin-up from occurring in each of these cases.

Spin-up No. 3 occurred on 20 October followed by eight (8) additional partial spin-ups, the last of which occurred on October 28. Calculations of friction levels relative to these unplanned events is described in Section 3.3. Observations made from telemetry data during this time span indicate levels of running friction of approximately 100 in-oz. At the time of a partial spin-up, torque transients of 30 to 60 in-oz, in addition to the 100 in-oz of friction torque, are being

experienced for short periods of time, resulting in the loss of earth pointing. During the normal pointing periods, variations are typically less than $\pm 1.0°$ at levels of about 100 in-oz of friction torque.

Figure 3.2-7 presents a map of the spin-up times (partial and total spin-ups) for the period up to 15 November. This plot and the corresponding chronology of Table 2-2 provides the details of events on 9433 since its initial recovery. Figure 3.2-7 discloses that losses of earth pointing have a thermal cycle correlation.

Figures 3.2-8 through 3.2-17 present the average DMA temperatures and torque values for most of October and November. It appears that the required drive torque has decreased with the end of losses in earth pointing. However, reference to Table 2-2 indicates that the spacecraft spin rate has been reduced several times since the initial recovery on 26 September. The reduction in spin-rate reduces the motor back; therefore, for a given friction level, the torque voltage decreases. It is concluded that the average friction torque of 90 to 100 in-oz was still present; however, the large torque variations ceased.

On 28 November, a more pronounced change in behavior occurred. There was a drop in torque voltage to the level of $\approx$1.0 volts experienced in pre-May. This drop occurred over approximately 16 seconds. For a period of almost three hours, despin pointing variations remained below 0.1 deg once again. Coincident with the return to the level of higher drive torque, large variations ($\geq$1.0 deg) in pointing error were again experienced. These "quiet" periods have been experienced several times since 28 November.

3.2.5 11 to 31 December Time Span

The completion of approximately 40 days of continuous normal mode operation came to an end on 11 December. Initially, the loss of normal mode appeared to exhibit the behavior previously experienced, large torque transient, high average torque, and rising top bearing temperatures. The attempts to reestablish normal mode, however, indicated a change in the characteristics of the anomalies was present. Transients were present over long periods of time. Transient magnitudes were such that normal mode could not be acquired and maintained during these long periods of

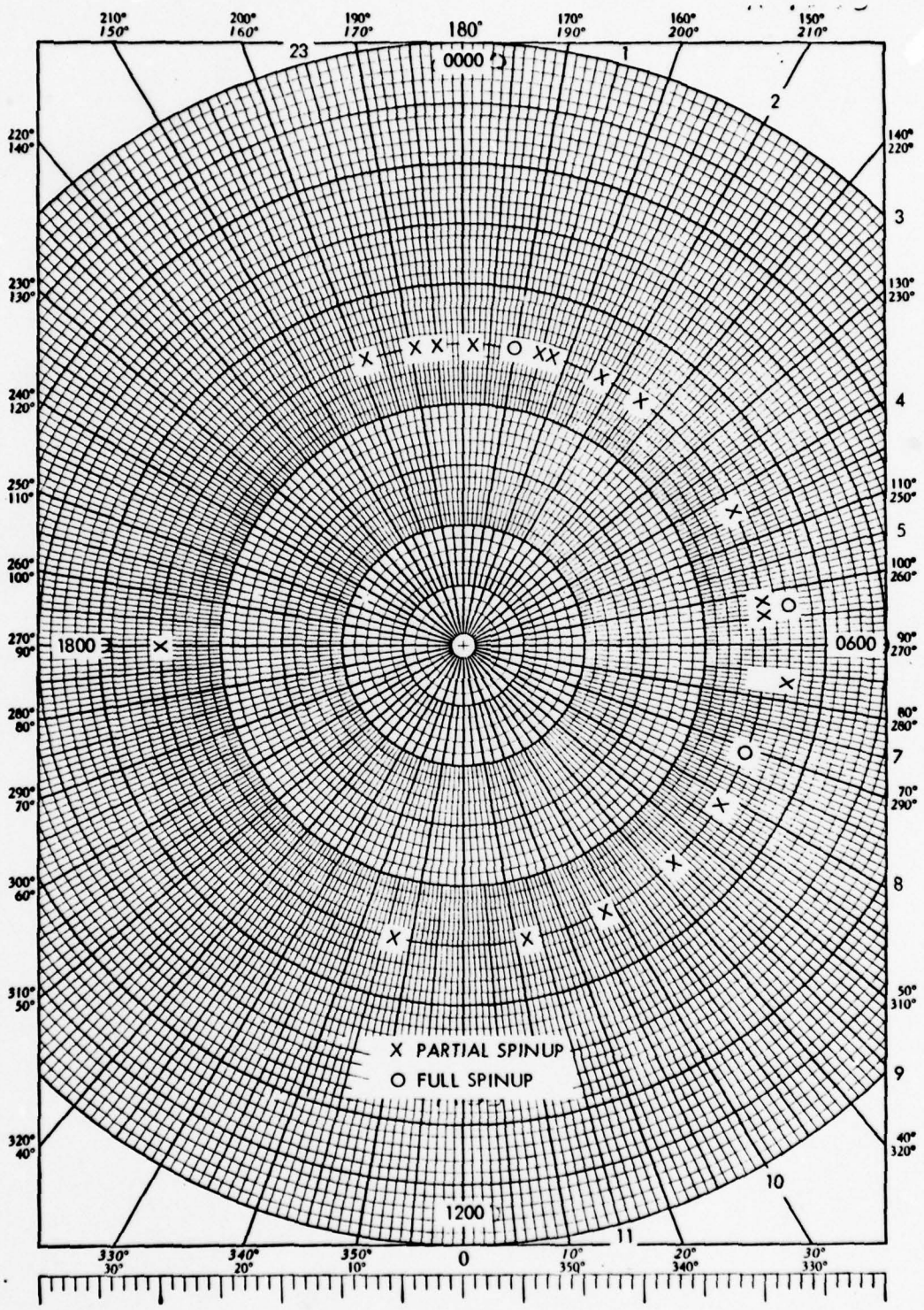


Figure 3.2-7. Loss of Earth Pointing Versus Time
(Through 28 Oct 1975)

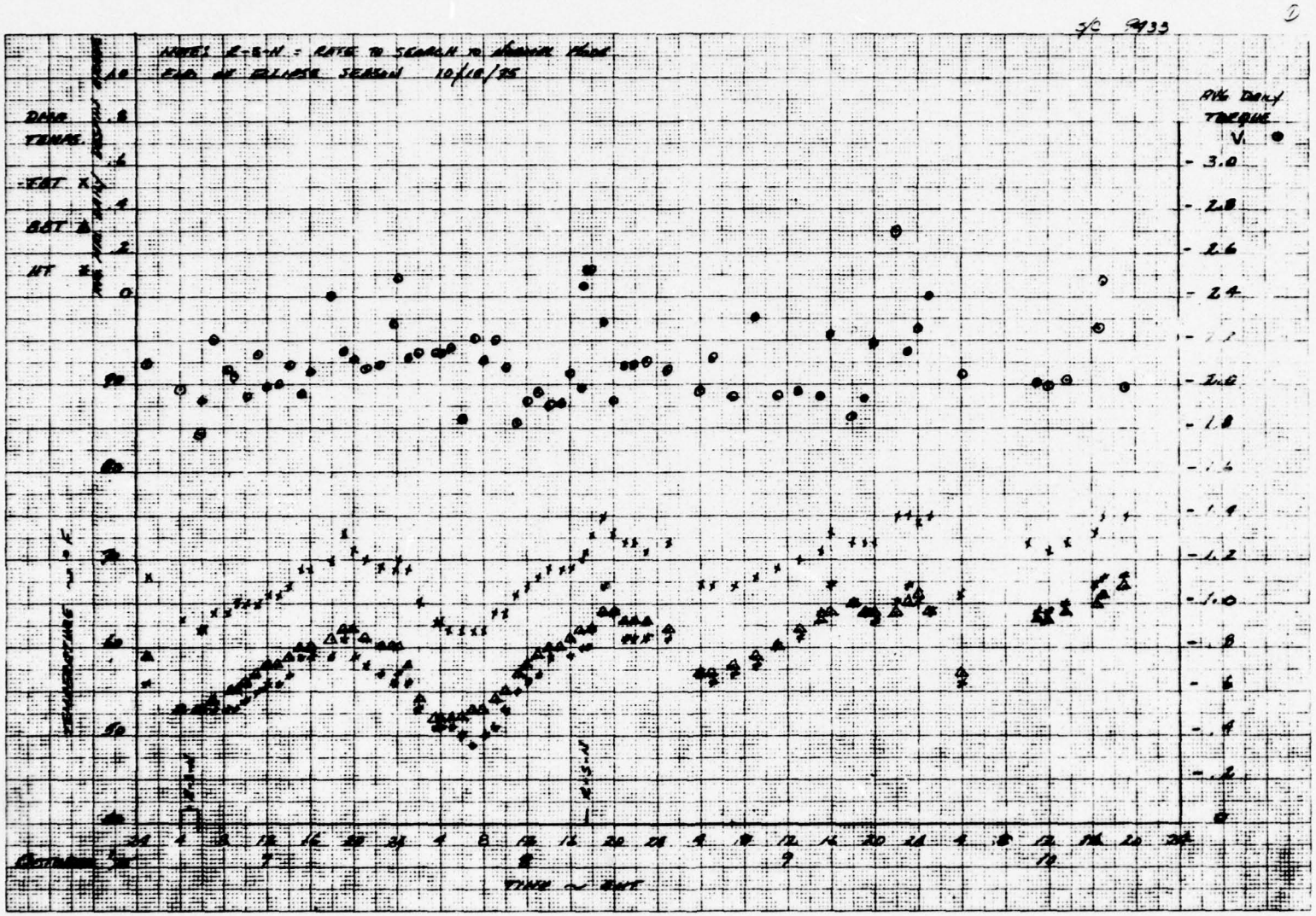


Figure 3.2-8. Daily Drive Torque, Despin Error, and DMA Temperature (7 Through 10 October)

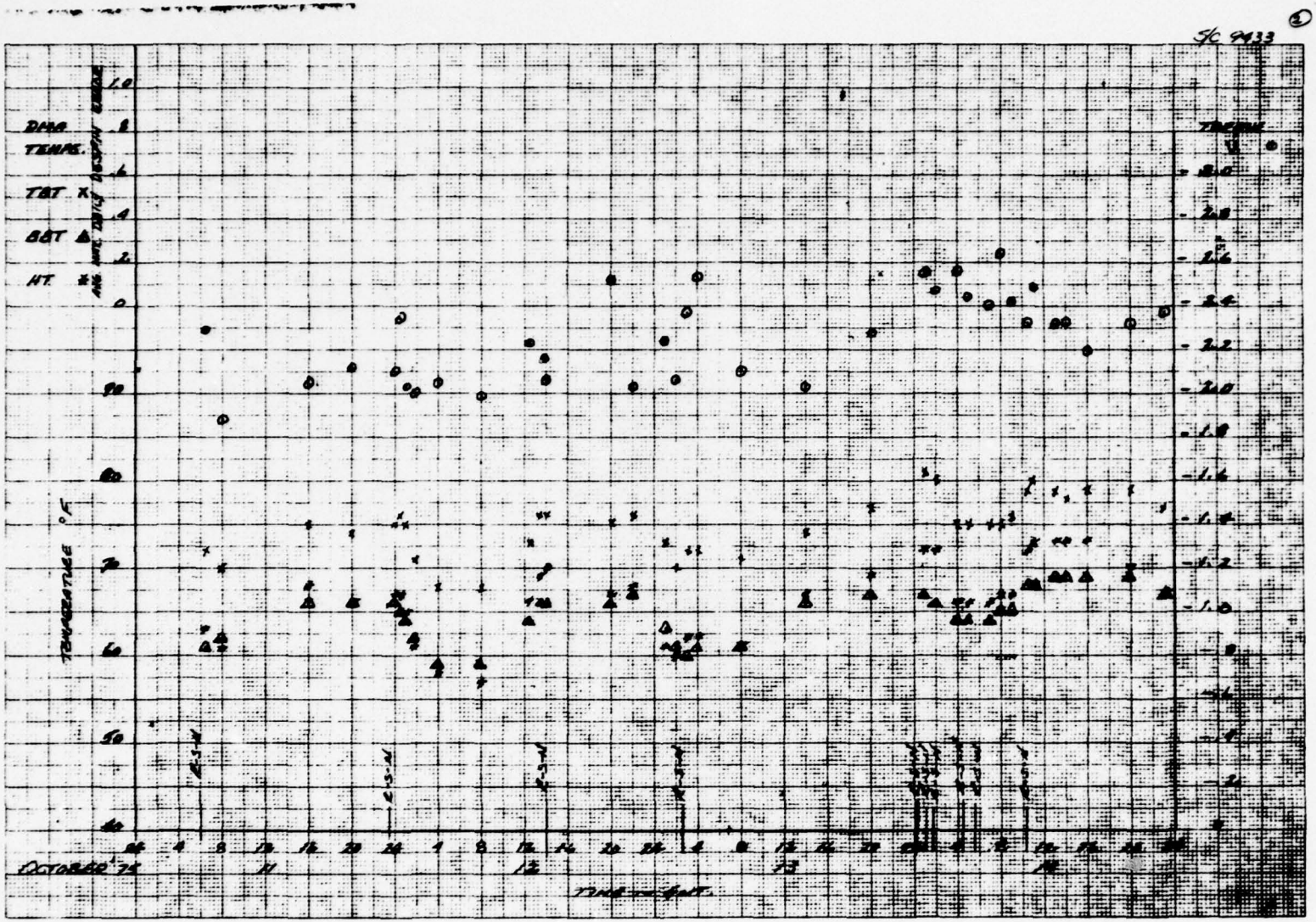


Figure 3.2-9. Daily Drive Torque, Despin Error, and DMA Temperature (11 Through 14 October)

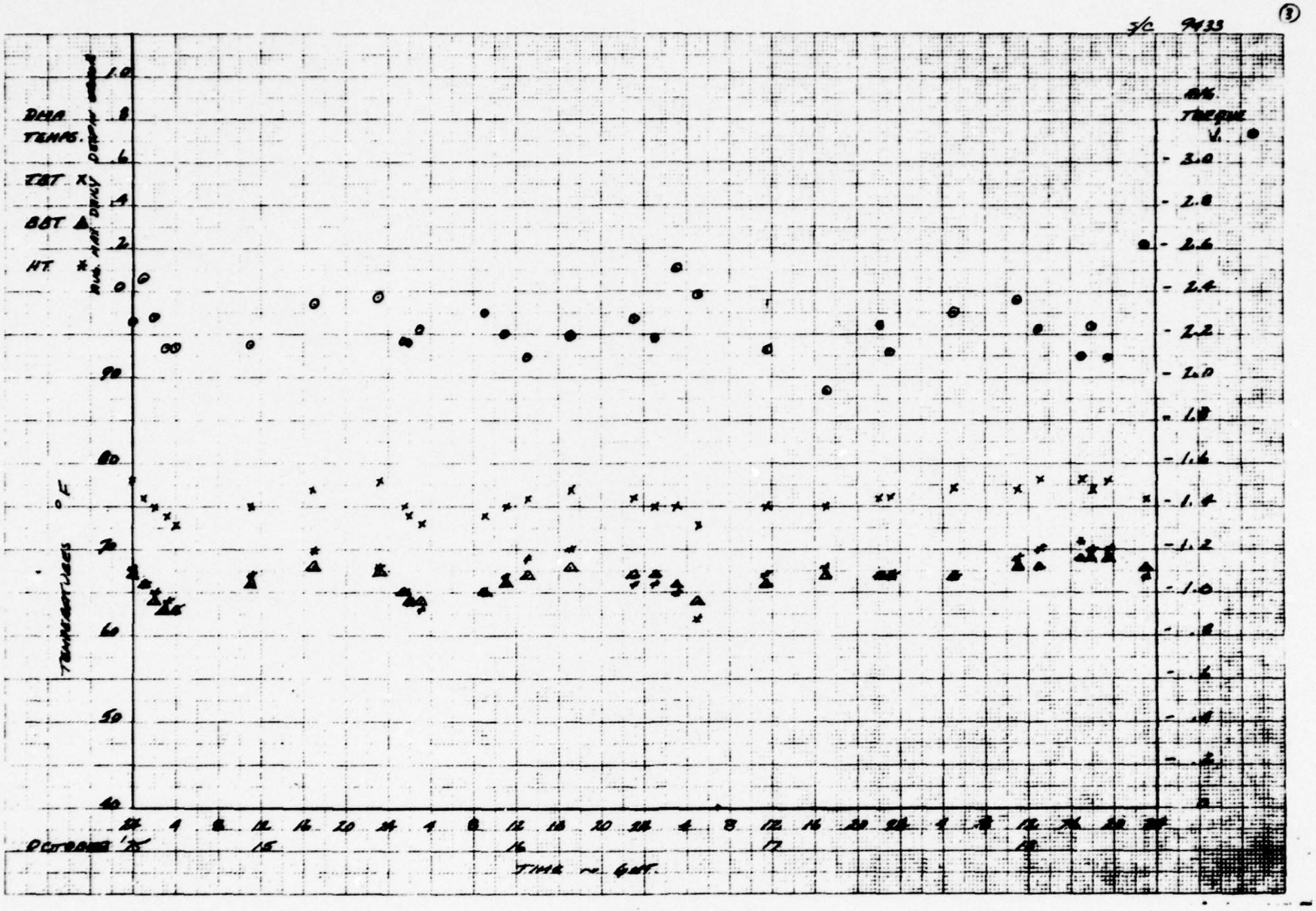


Figure 3.2-10. Daily Drive Torque, Despin Error, and DMA Temperature (15 Through 18 October)

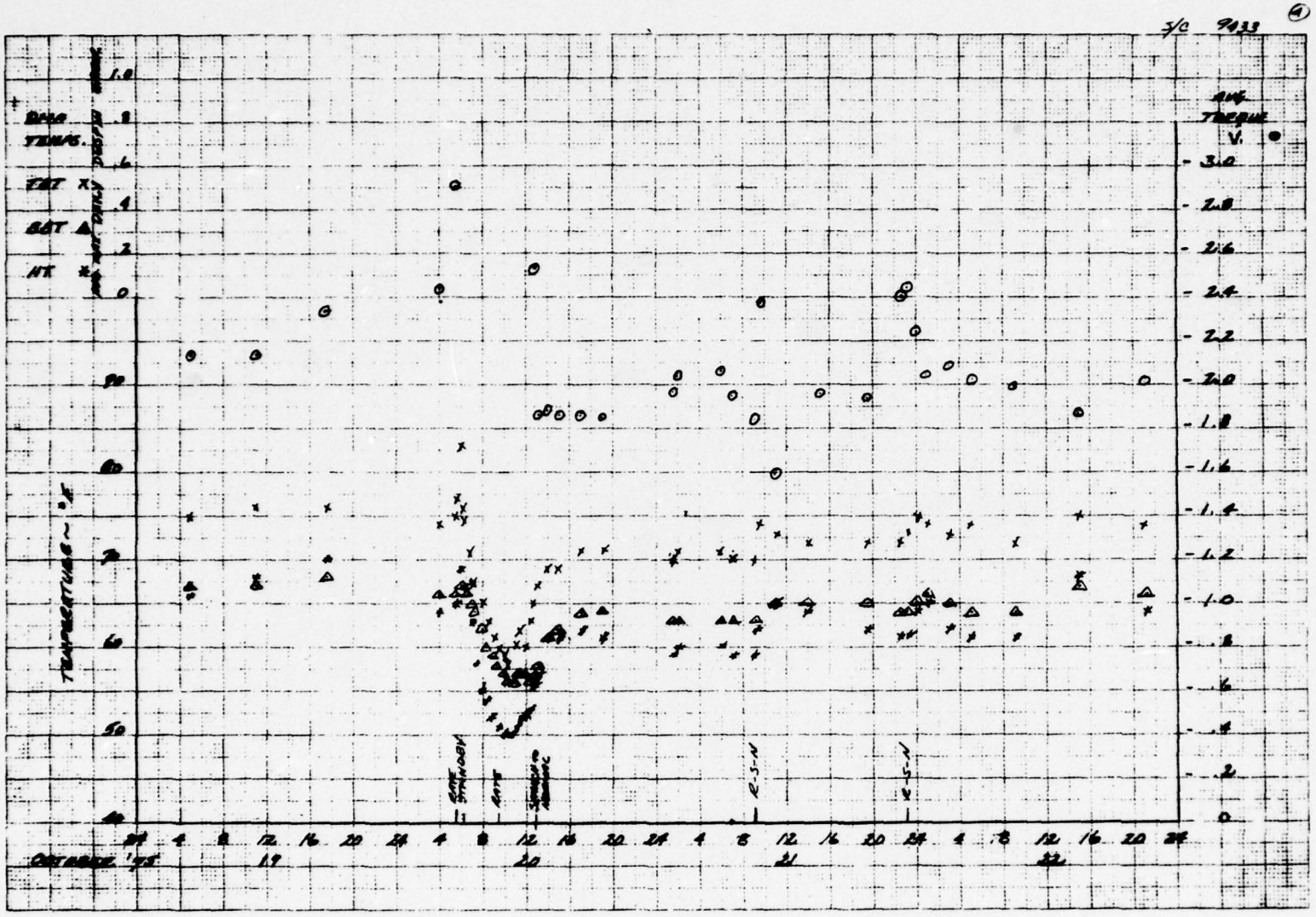


Figure 3.2-11. Daily Drive Torque, Despin Error, and DMA Temperature (19 Through 22 October)

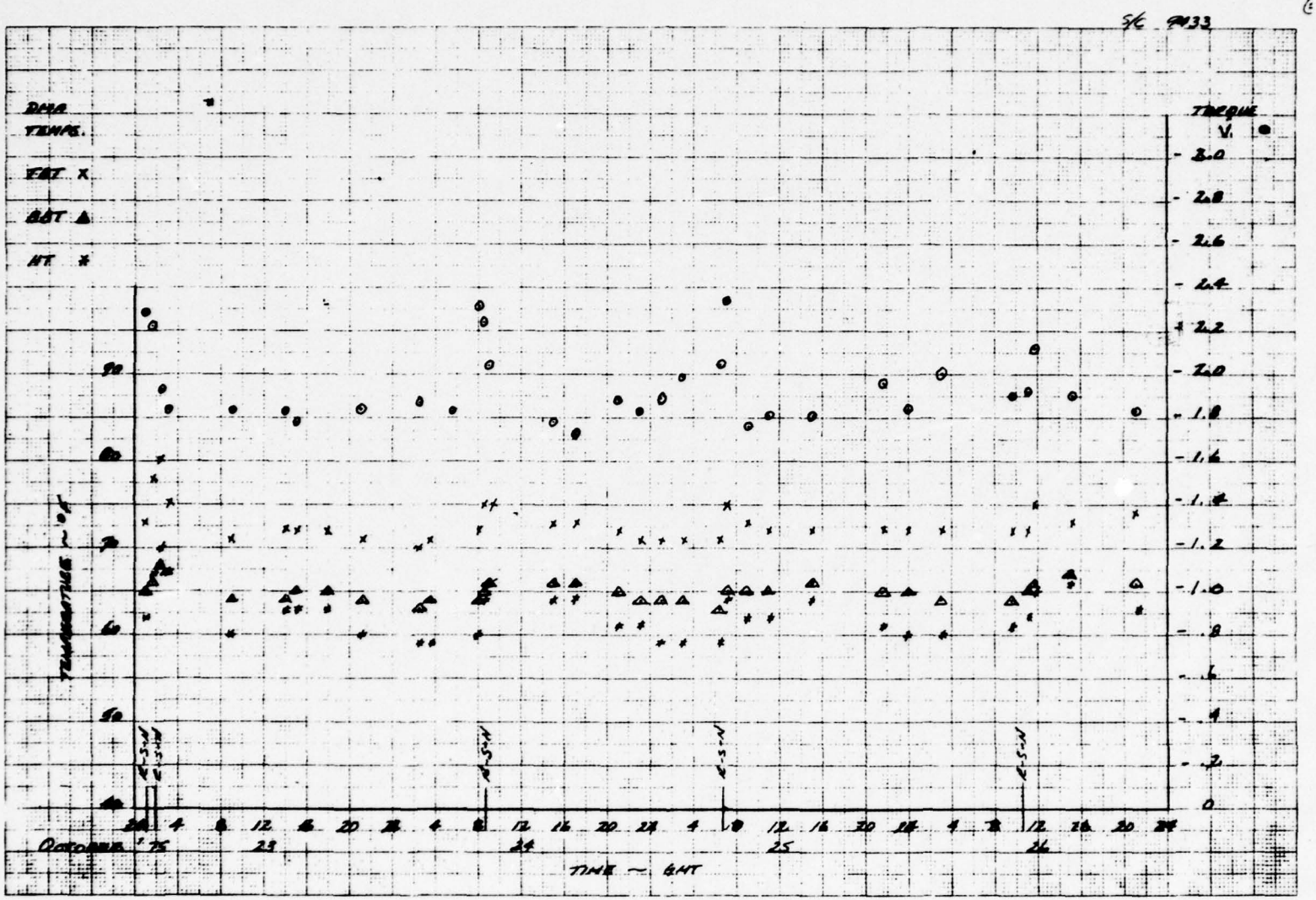


Figure 3.2-12. Daily Drive Torque, Despin Error, and DMA Temperature (23 Through 26 October)

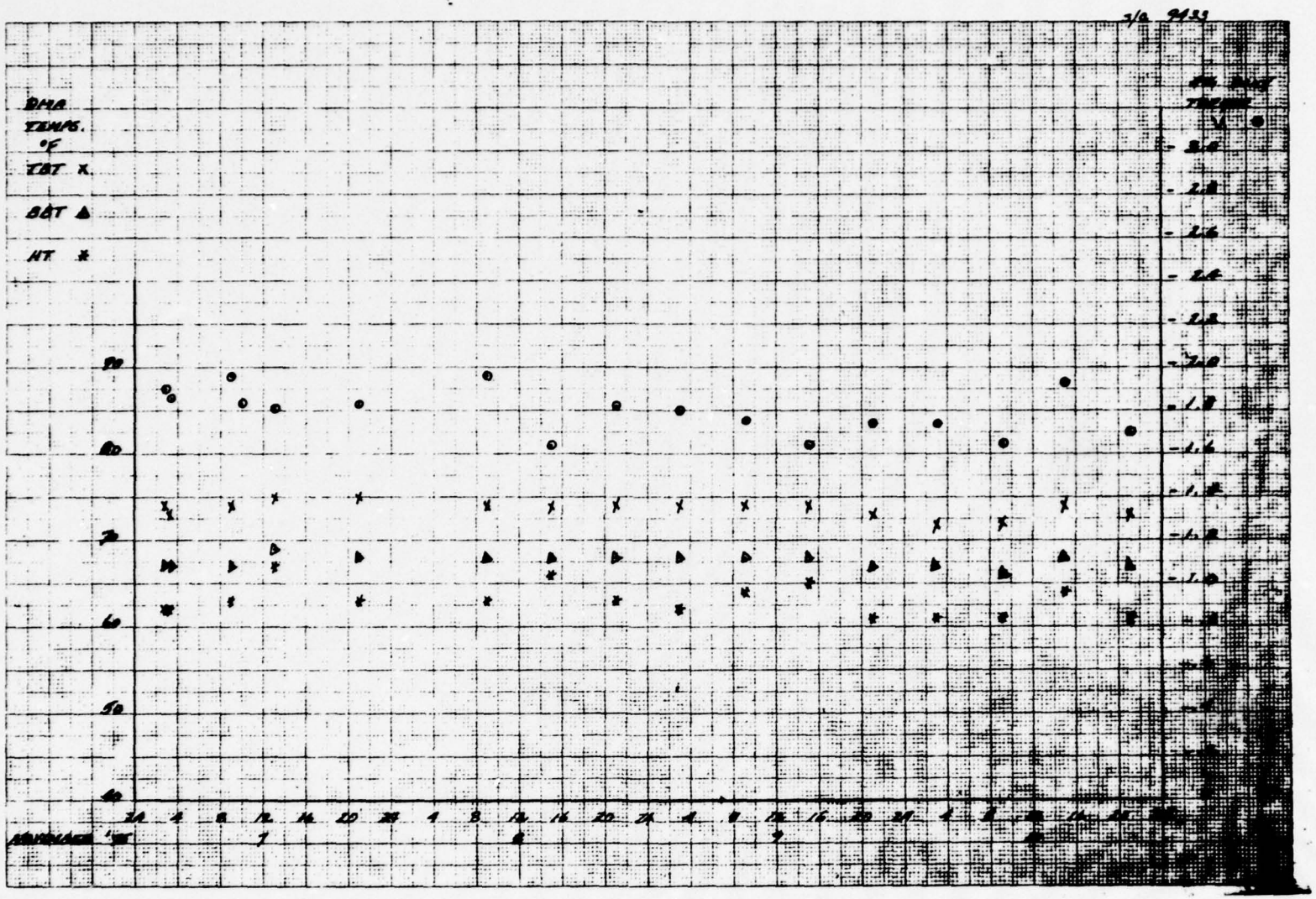


Figure 3.2-13. Daily Drive Torque, Despin Error, and DMA Temperature (7 Through 10 November)

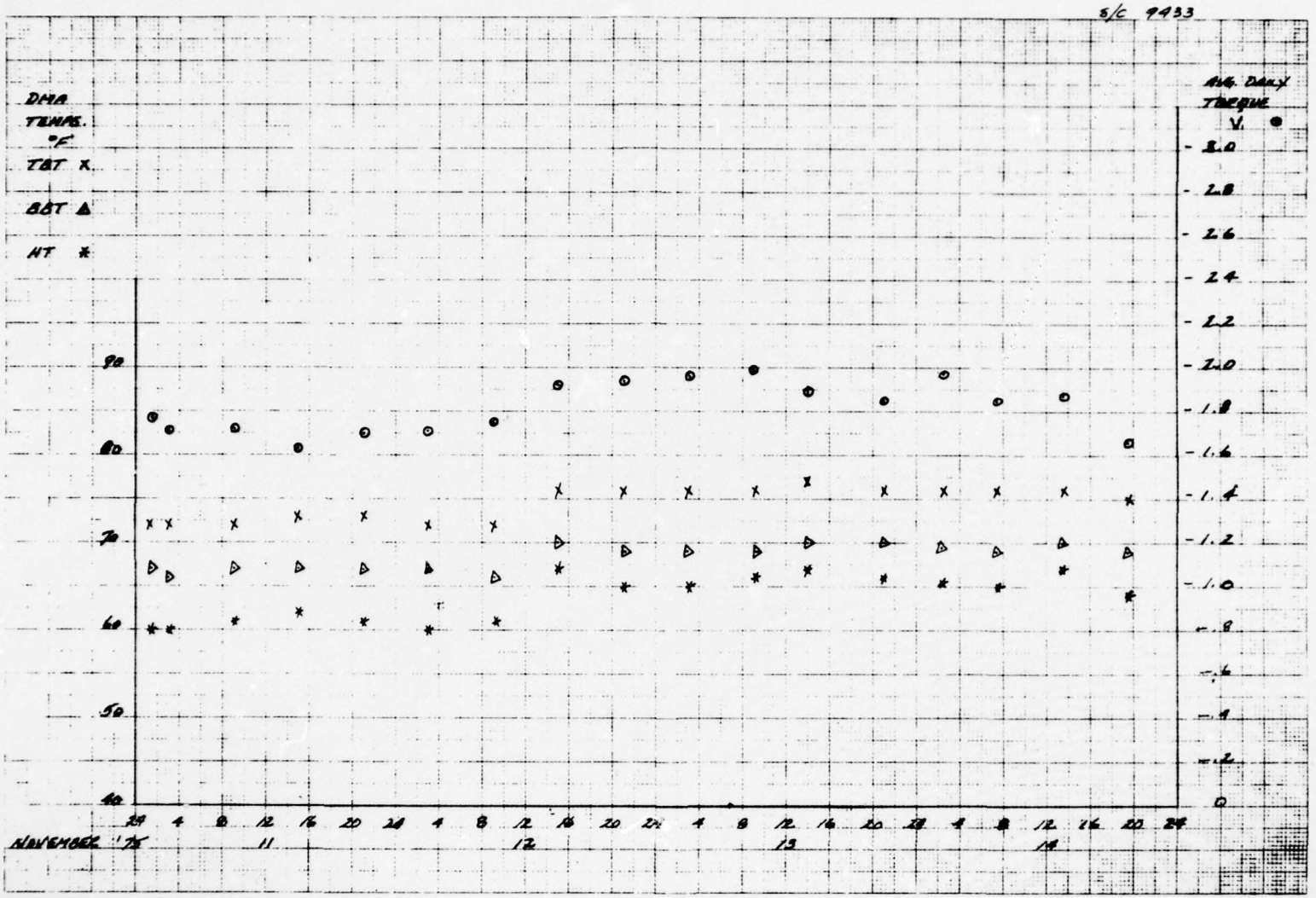


Figure 3.2-14. Daily Drive Torque, Despin Error, and DMA Temperature (11 Through 14 November)

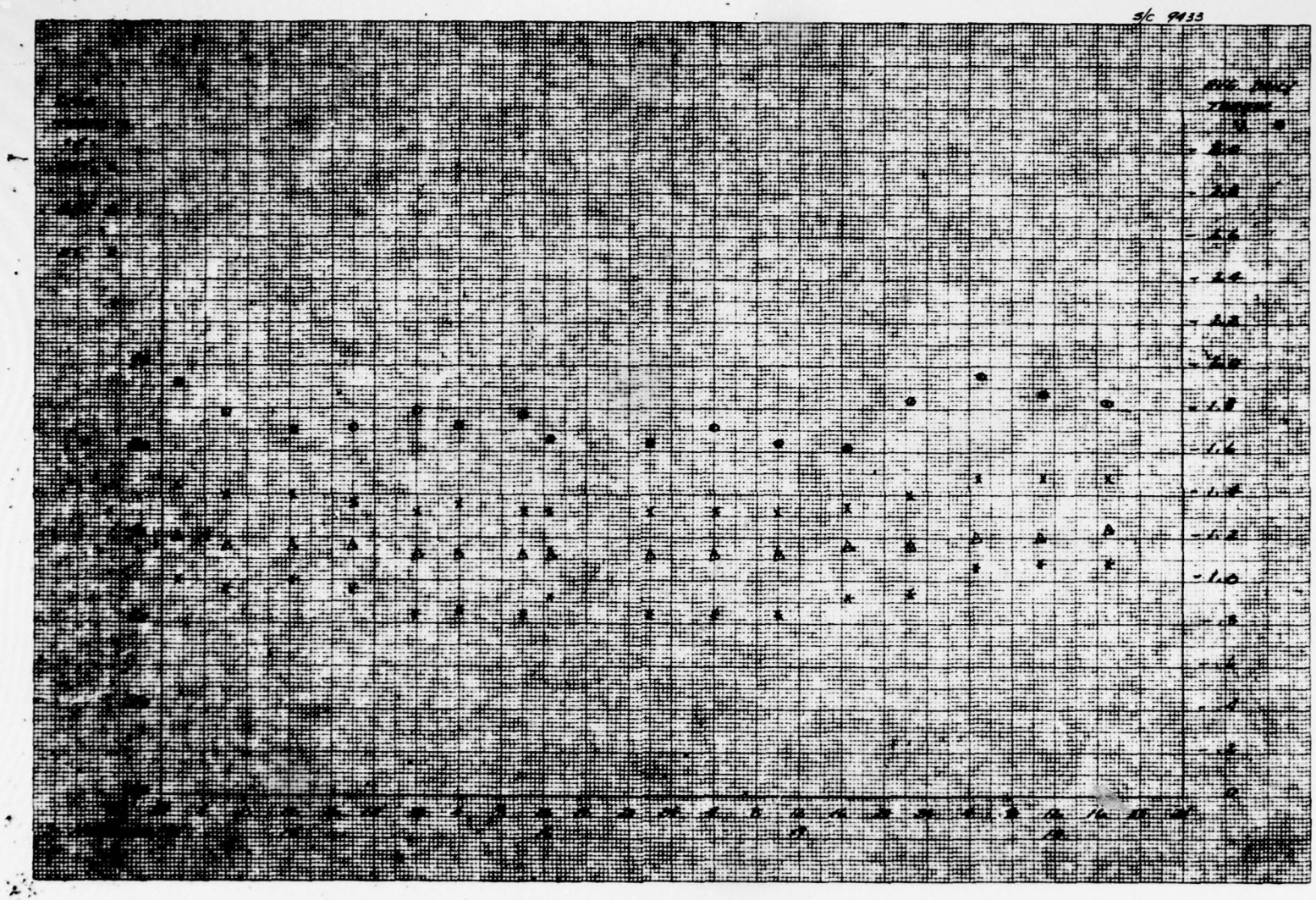


Figure 3.2-15. Daily Drive Torque, Despin Error, and DMA Temperature (15 Through 18 November)

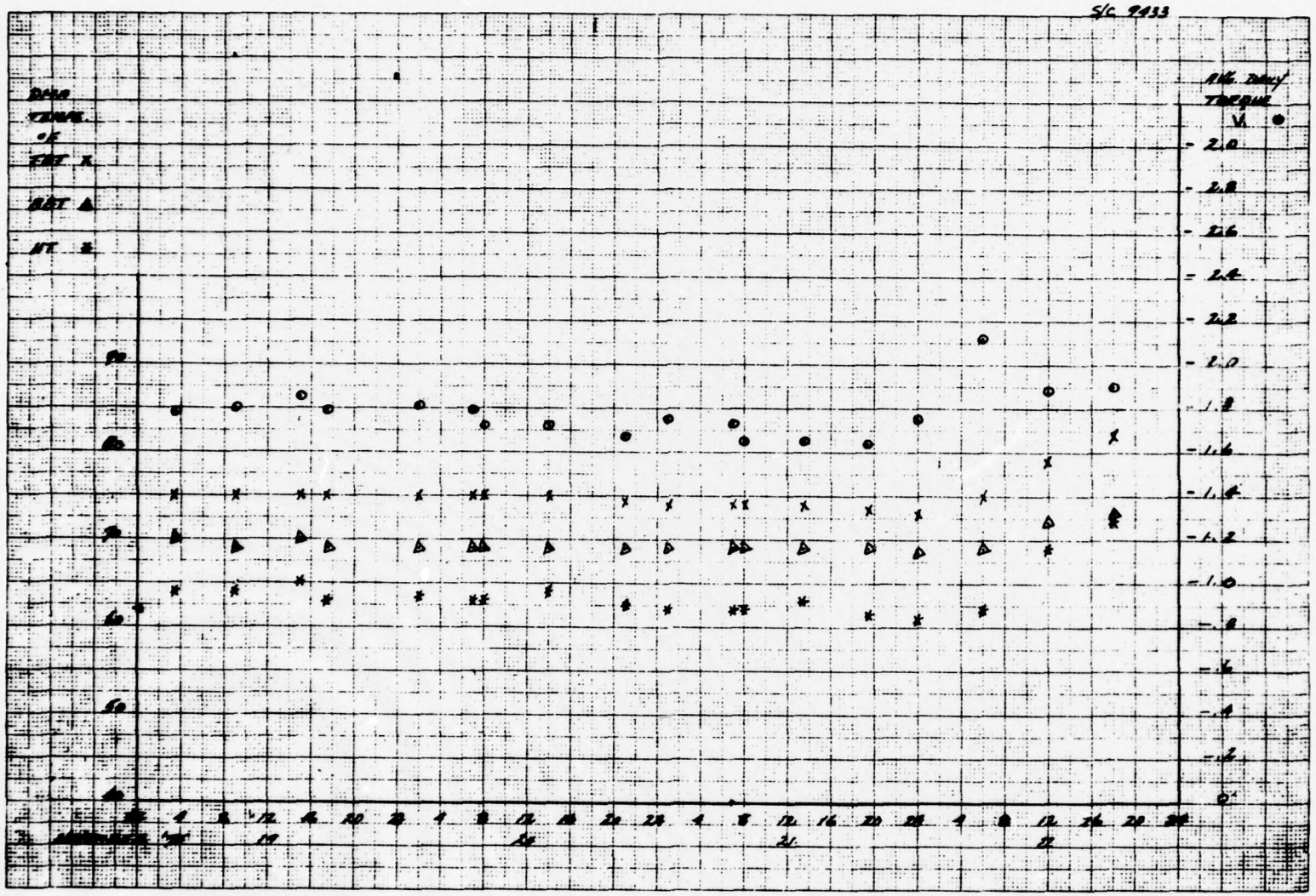


Figure 3.2-16. Daily Drive Torque, Despin Error, and DMA Temperature (19 Through 22 November)

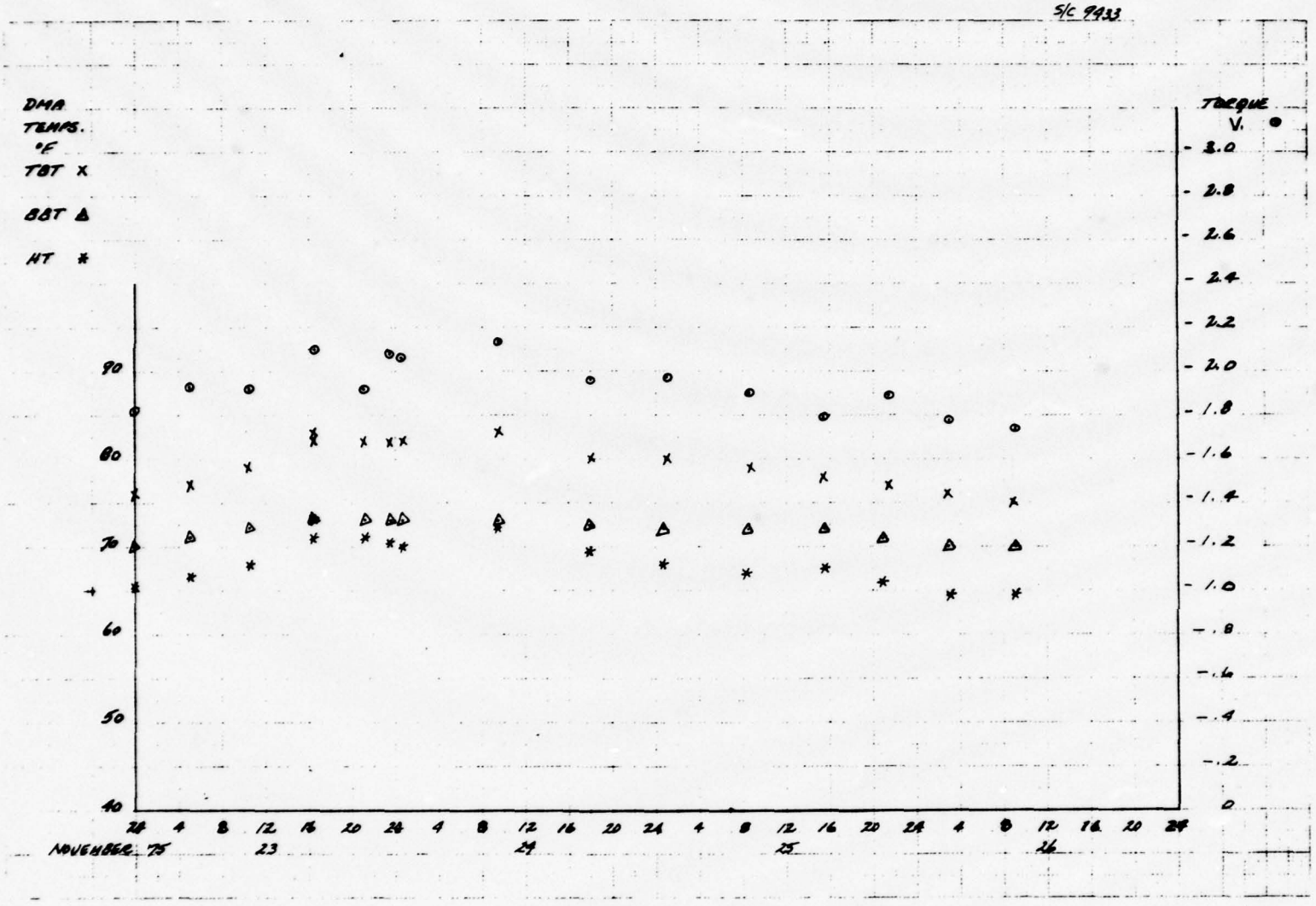


Figure 3.2-17. Daily Drive Torque, Despin Error, and DMA Temperature (23 Through 26 November)

of time. During the 20 days described in this time span, this condition was experienced three discreet times (11, 17, and 27 December). The reestablishment of normal mode seems to occur only after a period of lower average torque, followed by a subsequent decrease in bearing temperature differentials. Prior to this occurrence, each normal mode acquisition is followed almost immediately by an automatic switch to standby mode, the result of a large torque transient; both increasing and decreasing torque transients were observed as causes of loss of normal mode operation. Typical transients during this period are analyzed in Section 3.3.

3.3 Unplanned Events

During the past 24 months unplanned events have affected the pointing performance of the despin control system of S/C 9433. These events have either resulted in large platform pointing transients or large platform pointing transients, resulting in loss of earth lock followed by a spin-up (complete or partial) of the platform. Representative set of the data which illustrates both types of events are examined and discussed in the following paragraphs.

3.3.1 Platform Pointing Transients

Platform pointing transients or "wander" on S/C 9433 have been observed shortly after launch, but these transients have occurred most frequently during the last few months. However, an examination of the data shows that these transients have occurred under rather different circumstances. For example, with the running friction being nominal, platform transients occurred which have been attributed to retainer whirl with low amplitude disturbance torque pulses of short duration. A second type of transient was observed which occurred in the presence of nigh running friction torque; however, the magnitude of the pulses was typically 4 to 5 times greater than those attributed to "retainer instability" pulses. Finally, in late November 1975, a platform pointing transient was caused by a sudden increase in the running friction level in the absence of short duration torque pulses. Examples of each type of transient are discussed below.

3.3.1.1 Pointing Wander: December 15/16, 1973

Typical platform pointing transients which have been attributed to retainer instability were observed on S/C 9433 shortly after launch. With the running friction around 30 to 40 in-oz, platform transients were induced by torque pulses whose magnitude is on the order of 5 in-oz and lasting for a period of 10 to 15 seconds. An example of platform pointing error due to this effect is shown in Figure 3.3-1; the data shows that the platform error allocation of 0.15 deg was exceeded by as much as a factor of 2. Until recent 9433 operation, these platform point transients have exhibited similar characteristics on all satellites where present.

3.3.1.2 Sequence of Large Torque Pulses

During the last several months, a number of large platform pointing transients caused by large torque pulses in the presence of high (90 to 100 in-oz) running friction torque (as implied from the telemetered torque voltage) have been observed. These torque pulses are probably no longer attributable to retainer instability since their magnitudes are much greater.

- September 10 (Figure 3.3-2). A large platform pointing transient of -.15 deg is shown in Figure 3.3-2. Analysis of this transient via simulation shows that a torque pulse of 15-second duration and 20 in-oz amplitude in the presence of high running friction (-2.12 volts torque voltage - nominal is around -1.0 volt) will cause such a transient. An examination of other similar transients shows that the despin control system is being disturbed by a sequence of torque pulses whose amplitude and duration varies from pulse to pulse.

- September 27 (Figure 3.3-3). The data of Figure 3.3-2 did not give a direct measure of the characteristic of the torque pulses since the system was operating in Normal mode; a simulation of the system was required to "back-out" the torque pulse characteristics. However, on 27 September the despin control system was operating in the Rate mode. A direct measure of the net torque acting on the platform could be deduced from the despin rate error data. Platform rate error can be directly related to net torque; further, if the motor current is saturated

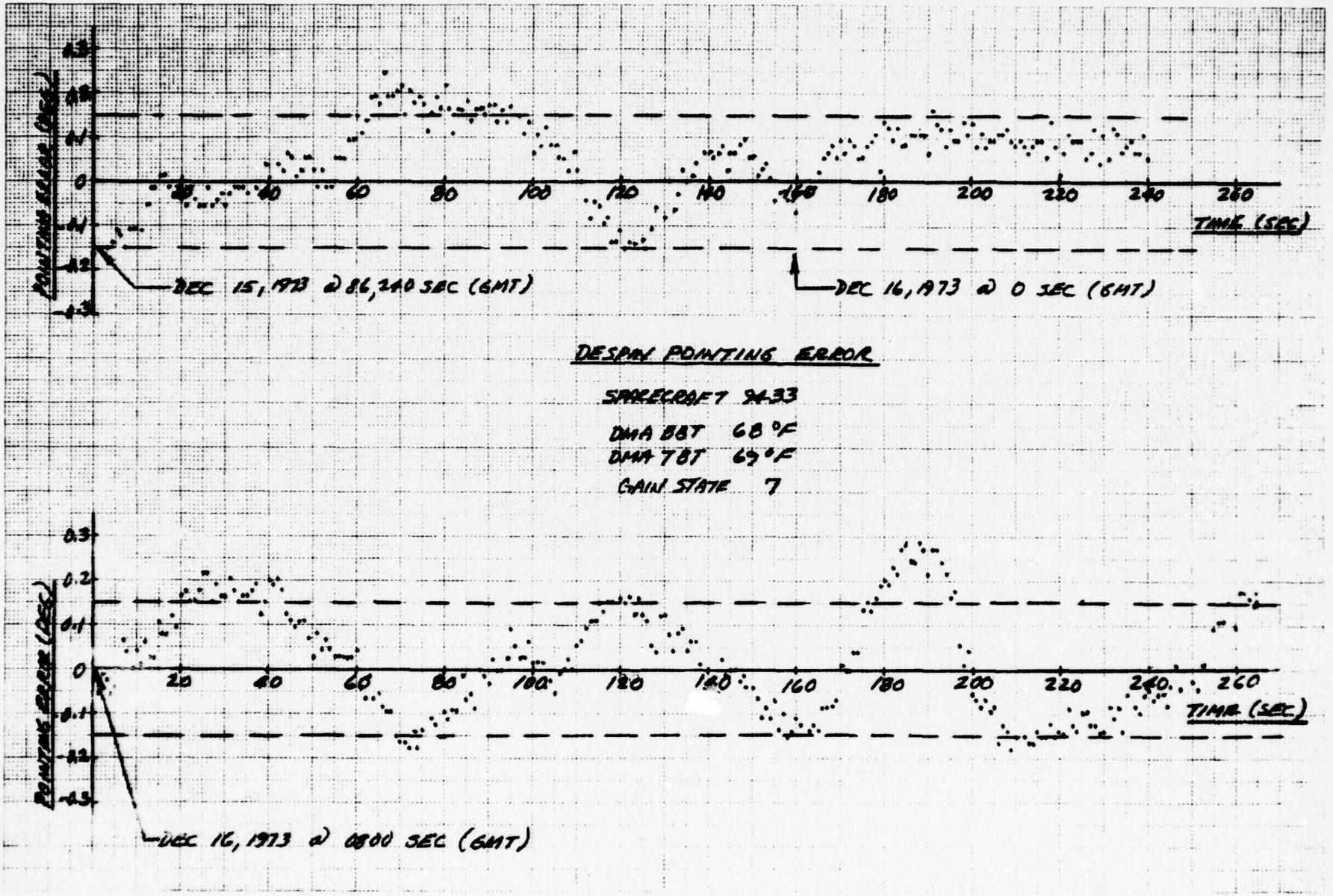


Figure 3.3-1. Despin Pointing Error, Spacecraft 9433

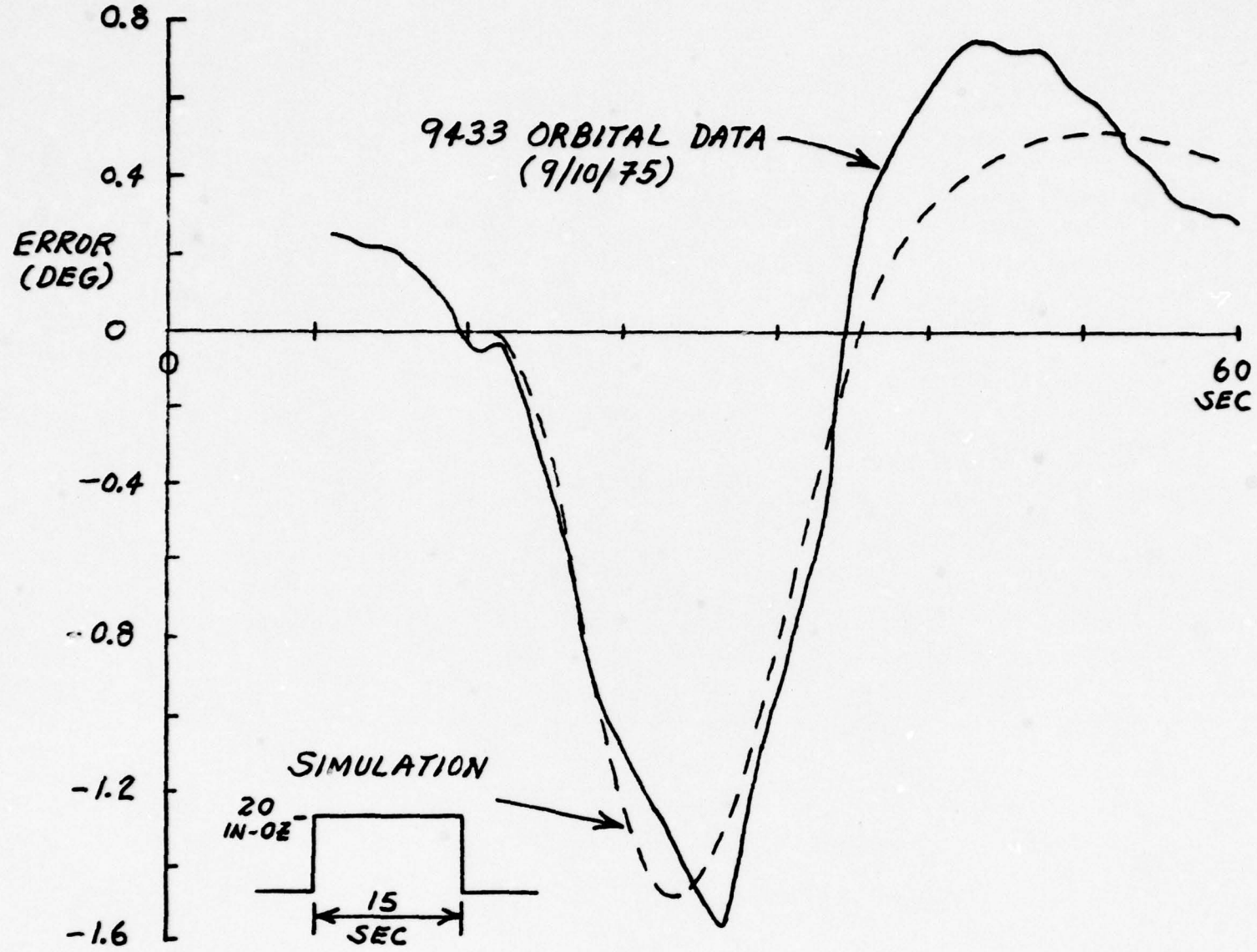


Figure 3.2-2. Normal Mode Data

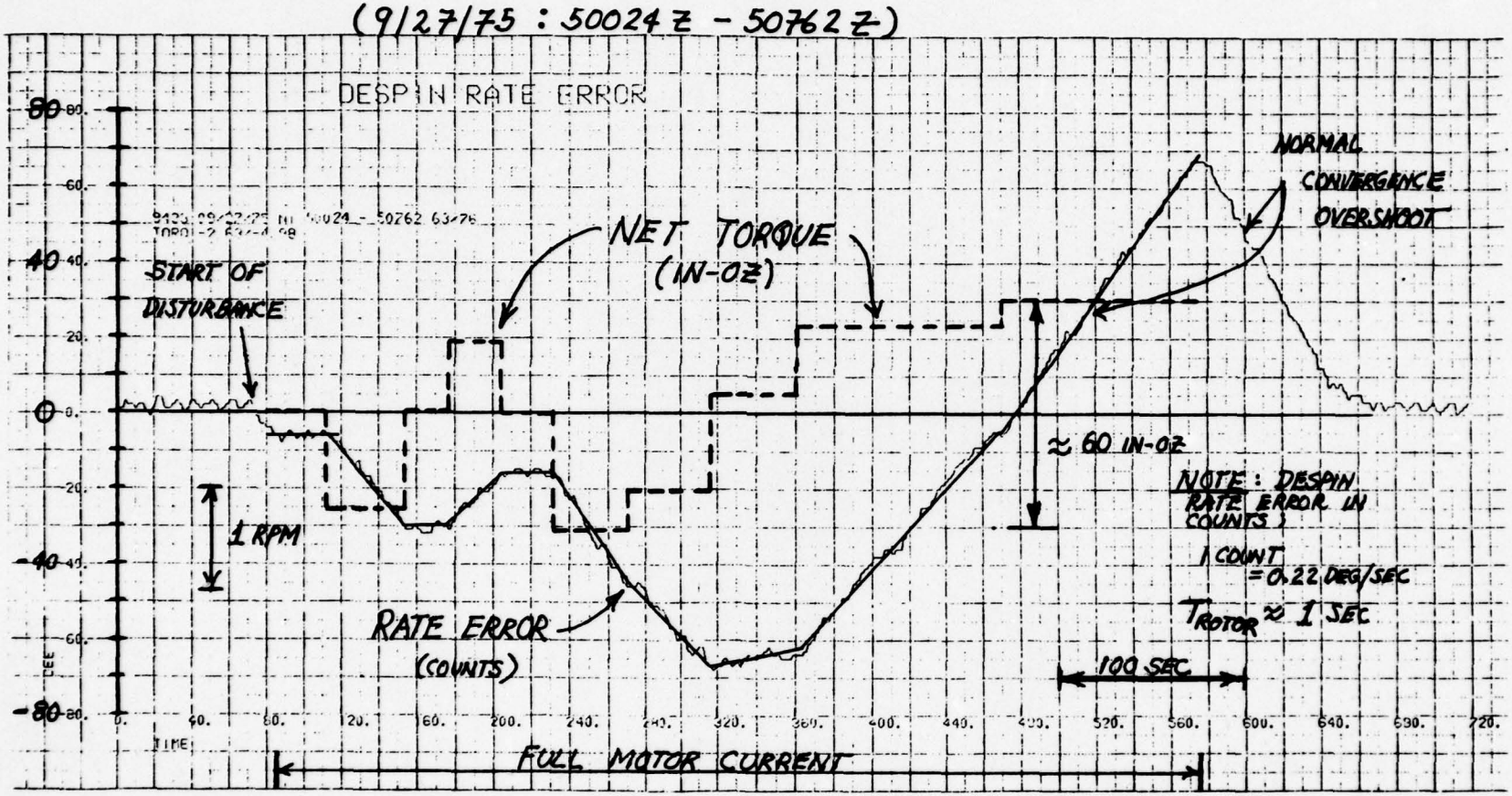


Figure 3.3-3. Analysis of Rate Mode Torque Transient

(this was the case between 90 and 580 seconds), friction torque variations can be deduced. An analysis of the data in Figure 3.3-3 shows that a sequence of torque pulses with amplitudes as large as 30 in-oz of varying duration disturbed the system. These results are consistent with those deduced from an analyses of recent Normal Mode pointing error data. Unlike the small pointing transients observed shortly after launch, the pointing error transients of recent months are being generated by torque pulses which are significantly larger than the 5 in-oz that has been heretofore attributed to retainer instability.

3.3.1.3 Sudden Decrease in Running Friction (Figure 3.3-4)

On 28 November, a new type of transient occurred. The despin control system was operating in Normal Mode with the telemetered torque voltage reading a high value (-1.7 to -1.8 volts); at 65630 seconds, a positive going platform transient of 2.8 deg was induced by a sudden decrease in running friction torque (Figure 3.3-4a). At the same time, the main bus current dropped from 11.2 amps down to 10.75 amps, and the torque voltage dropped to -1.26 volts (Figure 3.3-4b). From 65900 seconds to 75700 seconds, the torque voltage remained around -1.0 volt (which is nominal). Thereafter, the torque voltage again resumed its recent typical level (-1.8 volts). In the past, as noted earlier, pointing error transients have been attributed to torque pulses in the presence of a constant friction torque. This transient occurs because of a shift in the running torque level, but there appears to be no concurrent sequence of torque pulses. The reduction of friction implied by the torque voltage decrease is 50 in-oz (from 90 in-oz to 40 in-oz).

3.3.2 Platform Spin-ups

From 13 September through 31 December, 9433 has experienced three complete platform spin-ups along with a number of partial platform spin-ups. In most cases, the despin control system was put into Standby automatically because earth lock was lost for three rotor revolutions. The large pointing transients were accompanied by the presence of unusually high running friction torques as deduced from the telemetered torque voltage. The data for the three complete spin-ups and several respresentative partial spin-ups are discussed below.

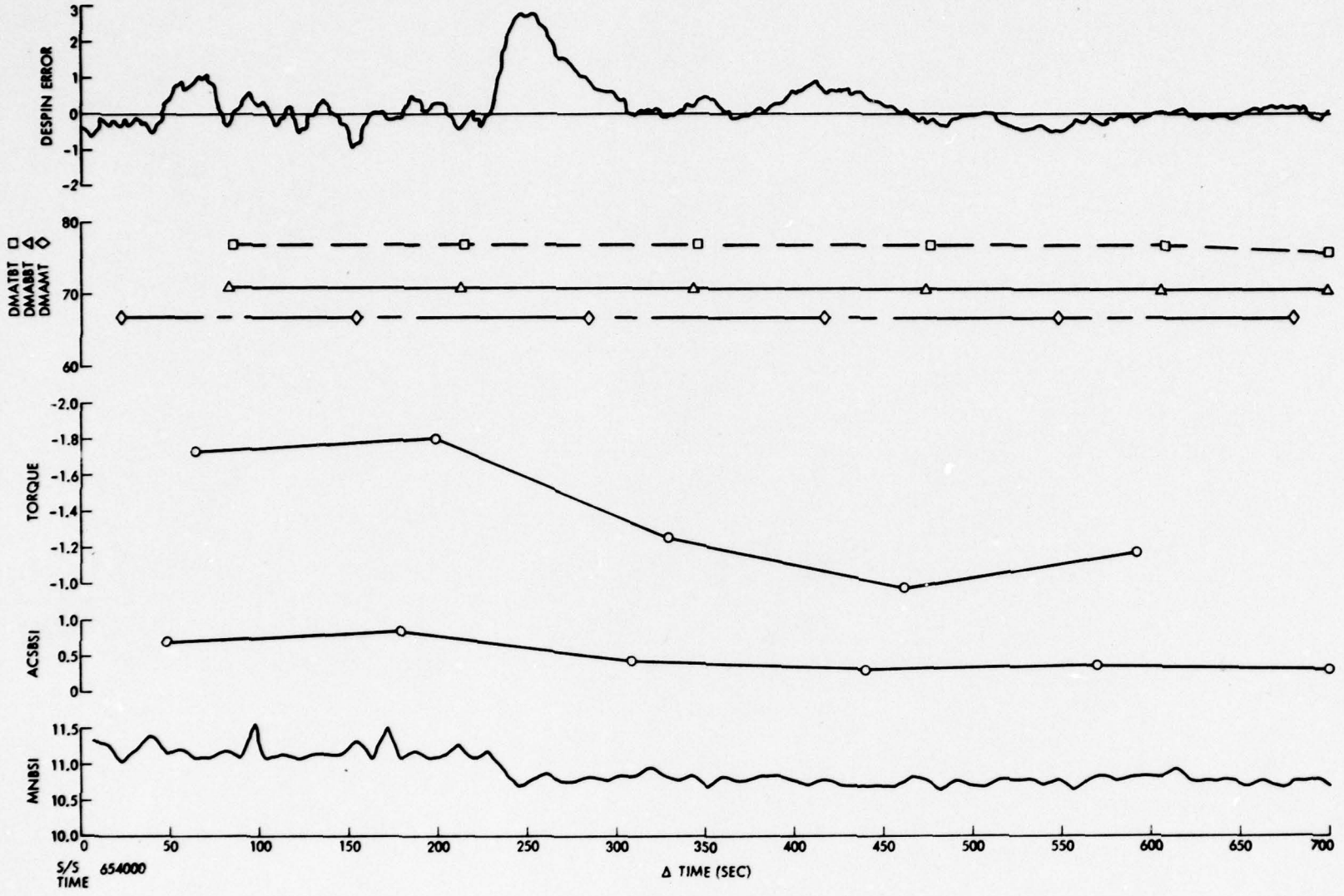


Figure 3.3-4. Quiet Period (11/28/75)

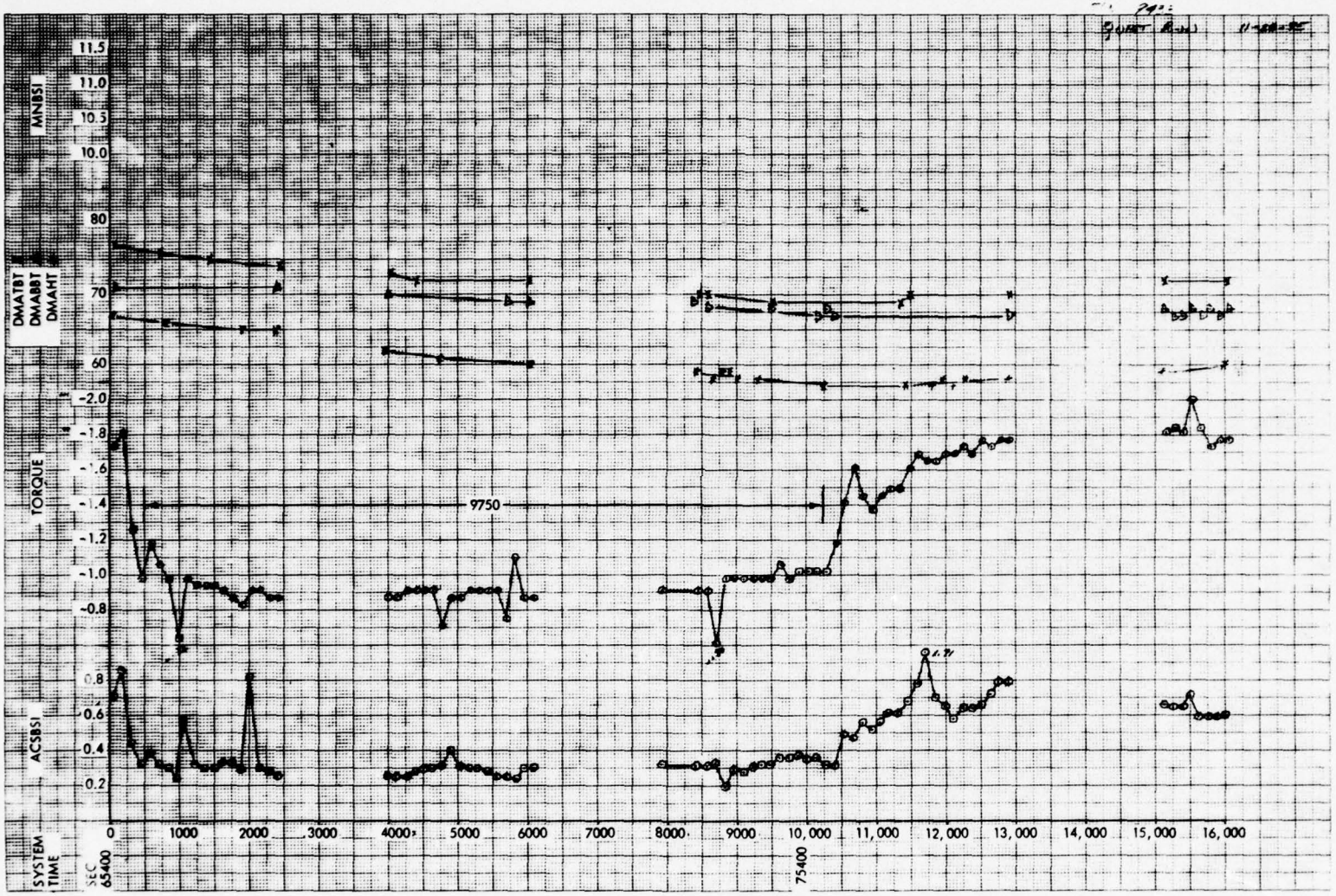


Figure 3.3-4. Quiet Period (11/28/75) (Continued)

3.3.2.1 Complete Spin-ups

• 13 September (Figure 3.3-5). On September 13, S/C 9433 went into Standby and subsequent unsuccessful attempts to recover it during that day showed that the friction torque exceeded motor torque capability. Best estimates by Orbital Operations personnel indicate that spin-up took about 5 minutes, implying a friction torque on the order of 200 in-oz.

The variation in the chord width at the end of the spin-up (Figure 3.3-5) indicates that the spacecraft was wobbling while the platform was slowing down until it stalled. The constant chord width after the stalled condition was achieved shows that the platform had stalled in such a way that the plane containing the platform mass unbalance was aligned virtually normal to the plane containing the earth sensor axis. Thus, the spacecraft tilt due to the platform unbalance is not discernible in the chord width data. See Section 3.5 for additional comments on this data.

• 4 October (Figure 3.3-6). The platform completely spun-up due to a DEA current overload try on October 4, 1975. The relative rate data is presented in Figure 3.3-6. At the time, the motor was driving the platform from 60 rpm toward 70 rpm. An overcurrent detector put DEA #1 into Standby and the platform spun-up due to friction. This data shows that the friction is on the order of 115 in-oz and is virtually independent of relative rate.

• October 20 (Figure 3.3-7). The third complete platform spin-up occurred on October 20, 1975, as shown in Figure 3.3-7. The despin control system went into Standby at 19937 seconds. The pointing error prior to this time was wandering ± 3 deg and the torque voltage was reading -2.9 volts at 19850 seconds, indicating a high value of friction torque. Shortly thereafter, a torque (pulse or pulses) induced a large transient (6.2 deg), putting the system into Standby. Because full-time support was provided to S/C 9433 since October 7, 1975 (0600Z), the commands of Rate Mode, Power Amp On, and Rate Bias were issued shortly thereafter. It is clear from the data that in spite of these commands, the platform was still slowly spinning up. At about 500 seconds, a two-second spin jet pulse was fired. This was followed 300 seconds later with a fifteen-second spin-jet pulse. After each spin jet firing, the platform continued to spin-up and eventually the PRP signal was lost.

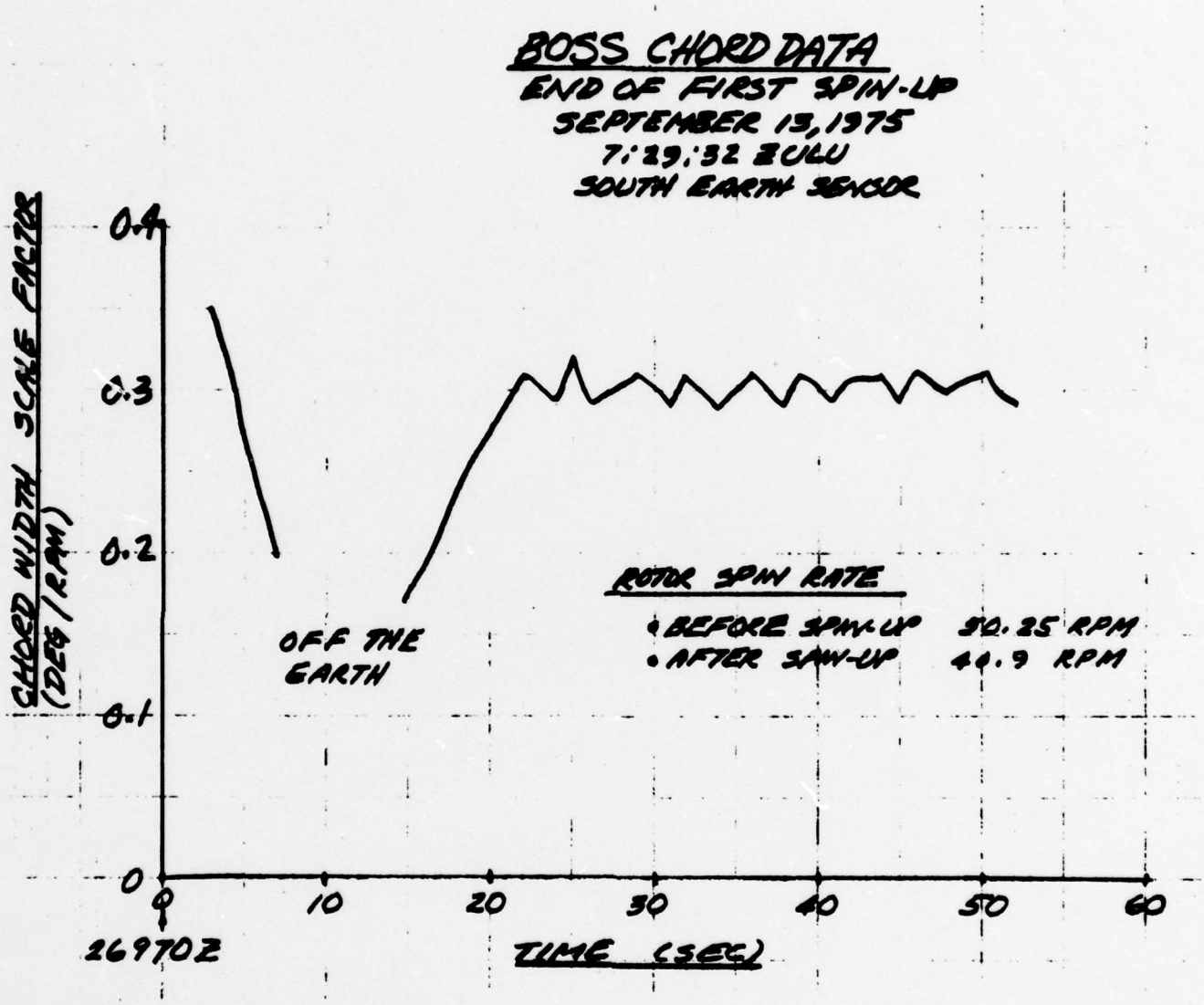


Figure 3.3-5. Boss Chord Data

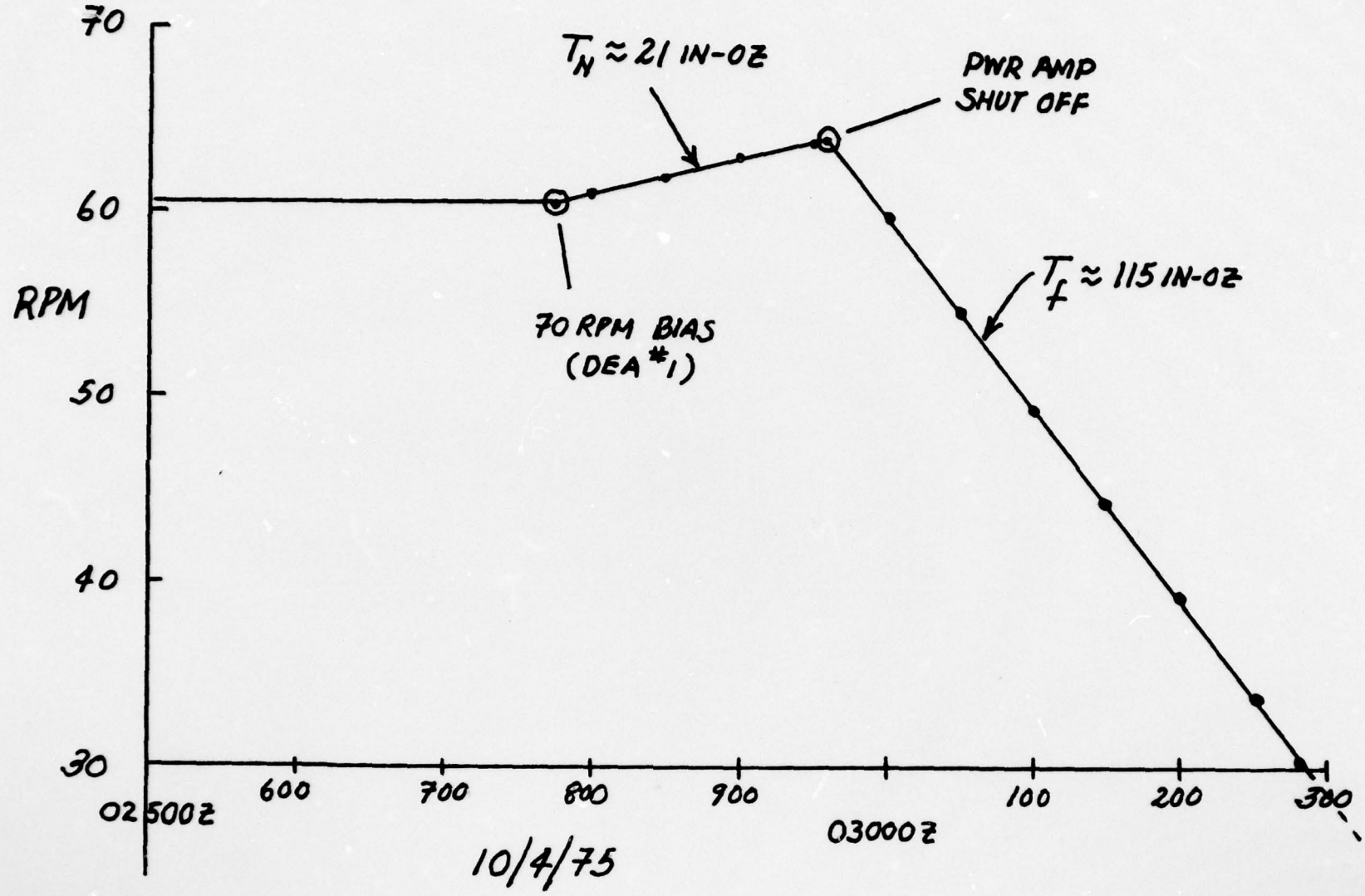
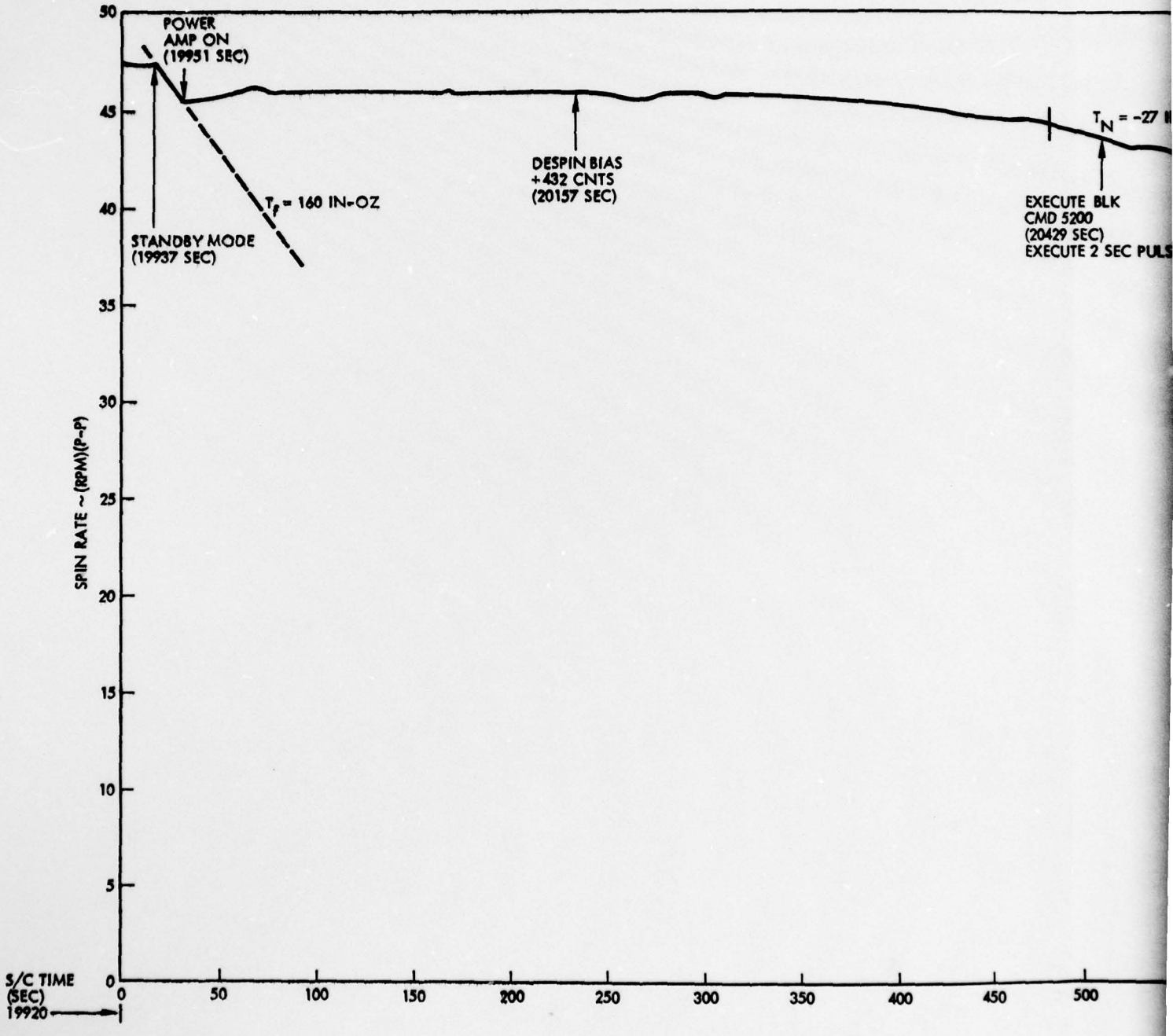
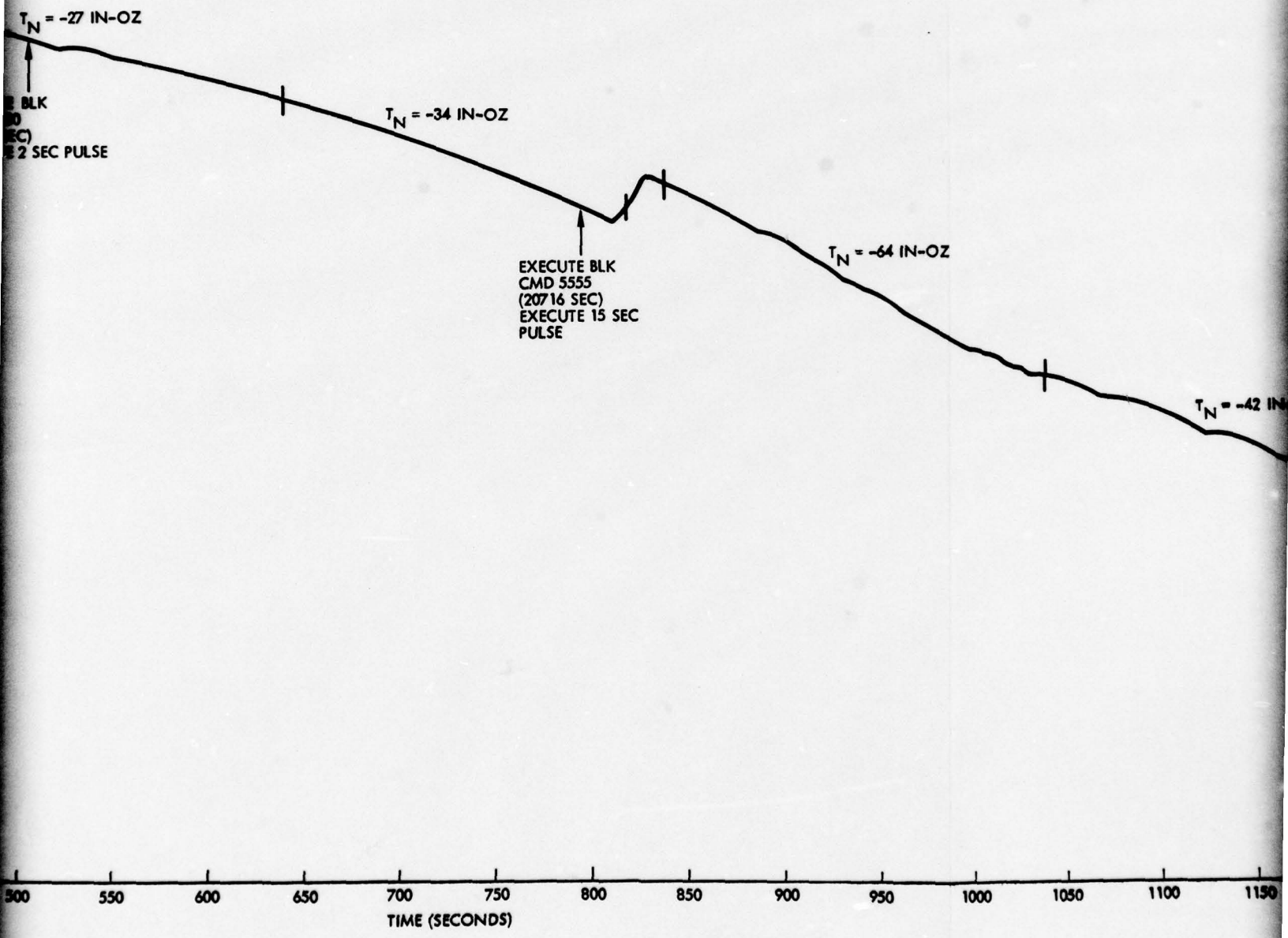


Figure 3.3-6. Platform Rate During Spin-Up


POWER
AMP ON
(19951 SEC)
STANDBY MODE
(19937 SEC)
T_f = 160 IN-OZ
DESPIN BIAS
+432 CNTS
(20157 SEC)
T_N = -27
EXECUTE BLK
CMD 5200
(20429 SEC)
EXECUTE 2 SEC PULS
SPIN RATE ~ (RPM)(P-P)
50
45
40
35
30
25
20
15
10
5
0
S/C TIME
(SEC)
19920
0
50
100
150
200
250
300
350
400
450
500

2


T_N = -27 IN-OZ
BLK
2 SEC PULSE
T_N = -34 IN-OZ
EXECUTE BLK
CMD 5555
(20716 SEC)
EXECUTE 15 SEC
PULSE
T_N = -64 IN-OZ
T_N = -42 IN
500
550
600
650
700
750
800
850
900
950
1000
1050
1100
1150
TIME (SECONDS)

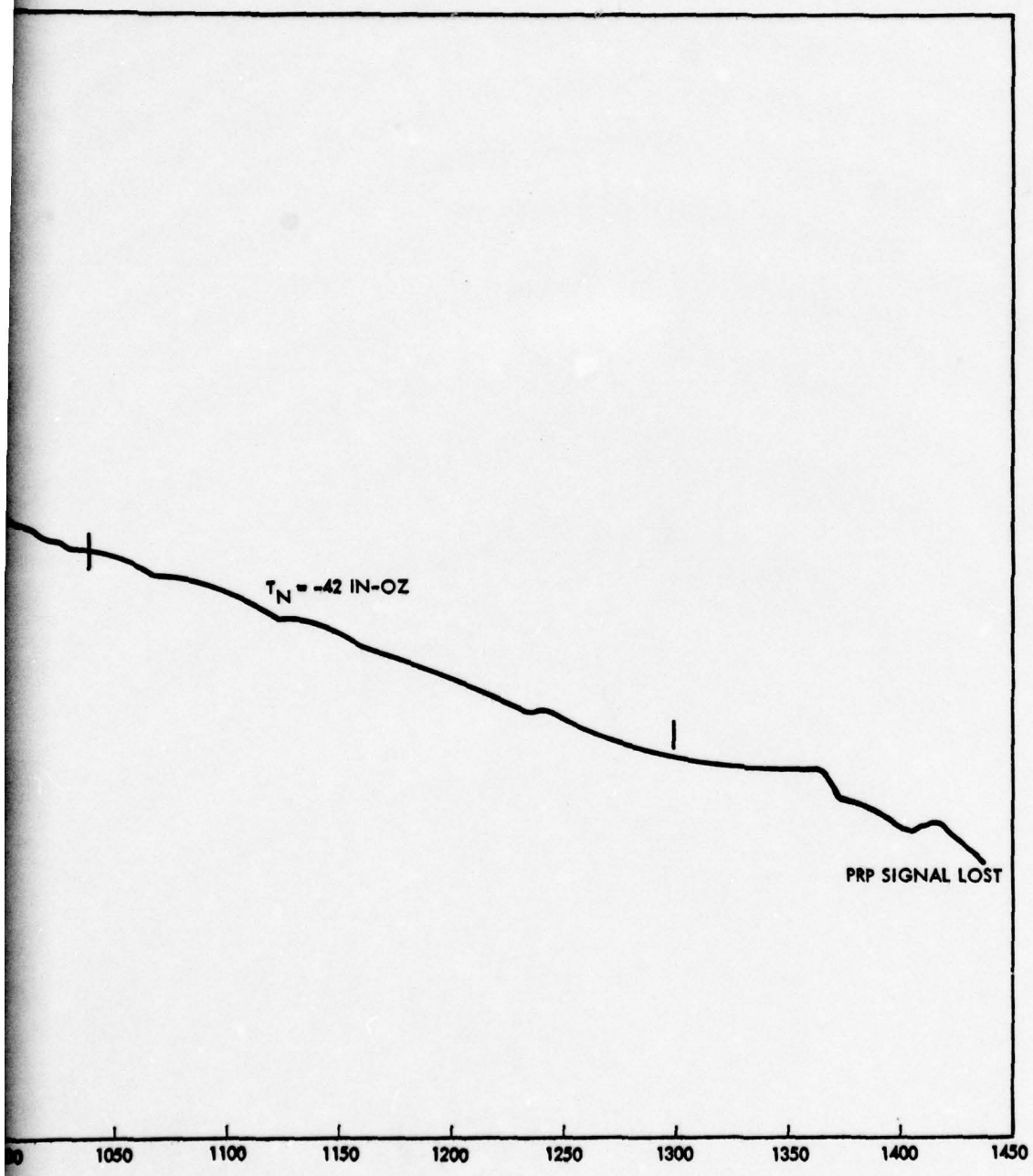


Figure 3.3-7. Spin-Up No. 3

During this whole sequence, it can be seen that the friction torque takes on several values. Initially, when the system was in Standby, the short piece of data indicates a friction torque on the order of 160 in-oz. Following the issuance of Rate Mode, Power On, and Rate Bias commands, the net torques (T_n) indicated by the data over several segments of time were 27, 34, 61, 42 in-oz. Assuming that the saturated motor torque is 178 in-oz, these data imply friction torques (T_f) respectively of 205, 212, 239, and 220 in-oz.

3.3.2.2 Partial Spin-ups (October 1975)

During the month of October 1975, 9433 went into Standby at various times and the platform spun-up partially before the spacecraft was commanded into Rate Mode and subsequently returned to Normal Mode. It some cases, thrusters were fired to augment the motor torque to recover the spacecraft. A few of the more interesting partial spin-up cases are discussed below. These data can be used to deduce function level by noting that the full motor torque (approximately 170 in-oz) was applied throughout recovery, until the time of peak overshoot characteristic of Rate Mode. Thus, friction torque equals peak motor torque minus the net torque (T_N).

- 8 October (Figure 3.3-8). The initial decay of the platform spin rate indicates a friction torque of 170 in-oz. Recovery was possible but very slow. 270 seconds following the Power On command, the spin rate was holding around 32-33 rpm. A 15-second firing of the spin jet was used to augment the motor torque. The platform then proceeded to be despun with a net torque of 46 in-oz. This implies that the friction torque was on the order of 125 in-oz. This apparent reduction in friction due to the dynamics induced by thruster firings has been observed on several occasions.

- 11 October (Figure 3.3-9). This Standby was preceded by large pointing error excursions of ± 5 to 6 degrees and the telemetry on the torque voltage saturated at -4.98 volts. However, about 540 seconds prior to Standby (19434 seconds), the pointing excursion was ± 0.7 deg and the torque voltage was -1.81 volts, again indicating a high running friction torque. The spin rate decay following Standby shows that a friction level of 171 in-oz was present. With the Power Amp On, it was expected that a

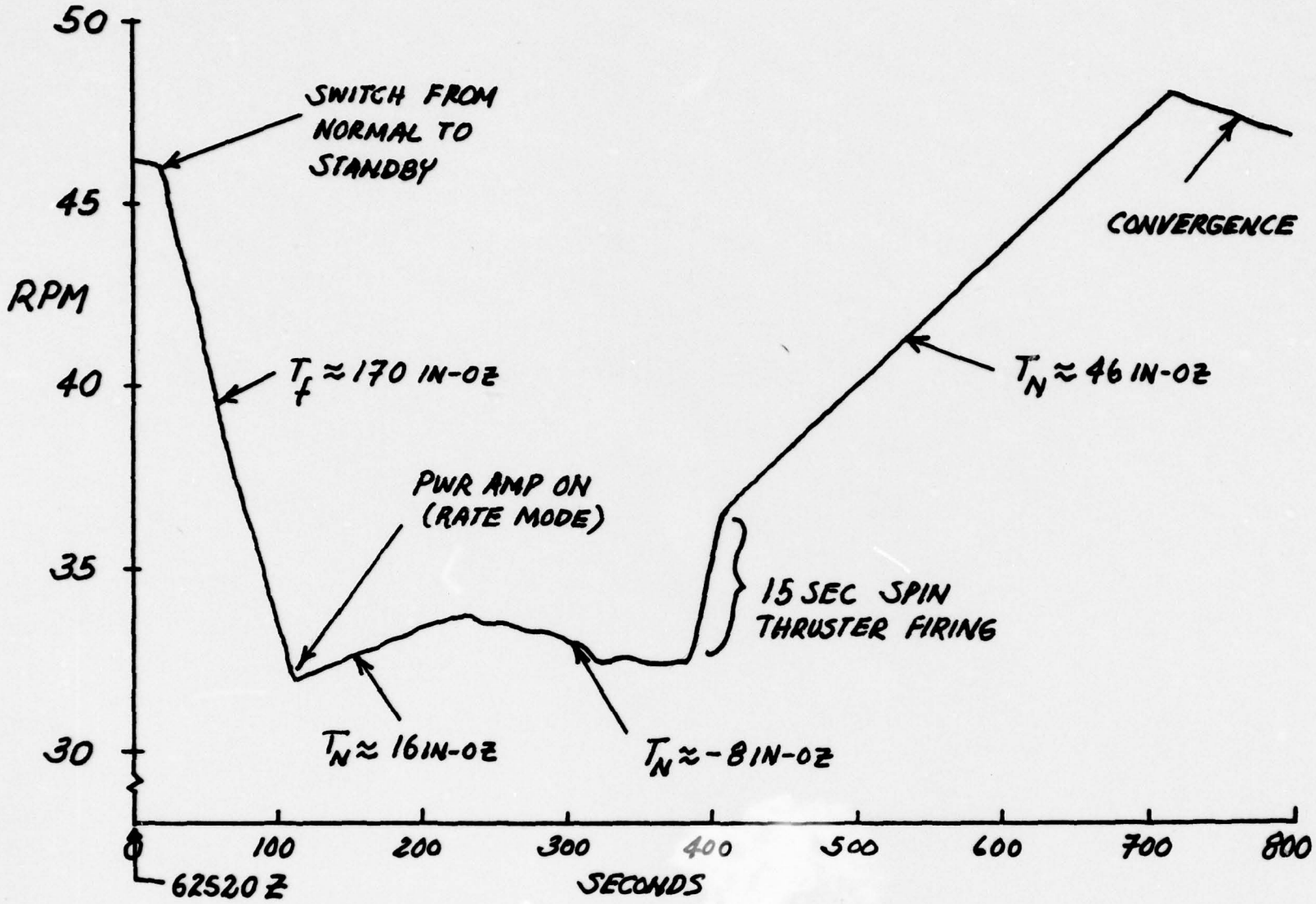


Figure 3.3-8. Platform Spin-Up and Recovery: 10/8/75

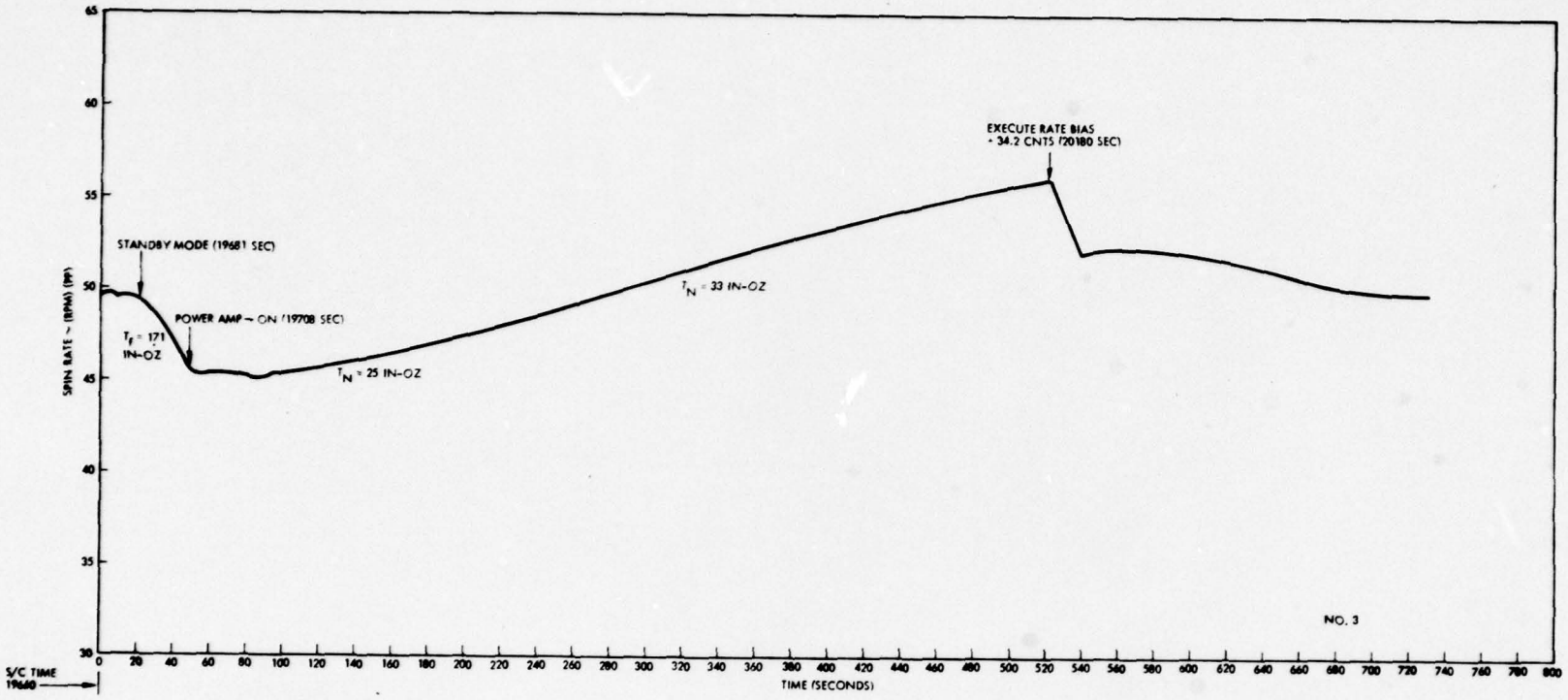


Figure 3.3-9. Partial Spin-Up

slow despinning of the platform was possible. After 30 seconds of a constant spin rate following Power Amp On, the platform proceeded to despin with a net torque of 25 in-oz (or friction of at least 140 in-oz) over the next seconds. For the next 230 seconds thereafter, a net torque of about 33 in-oz existed as the platform continued to despin. At about 520 seconds, the rate bias command of 342 counts (49.6 rpm) was issued and the system converged to the bias value.

- 13 October (Figure 3.3-10). The partial spin-up and recovery on October 13 is a case where a recovery began successfully but deteriorated. At around 580 seconds the friction torque suddenly increased and overwhelmed the motor. At 680 seconds a 15 second spin-up jet pulse was executed to augment the motor torque. About 1300 seconds later, after a slow convergent, the despin maneuver by the Rate Mode is completed and the bias rate of 45.8 rpm was achieved. Again, in a short period (0.5 hour), the friction level varied significantly, from a level of below 150 in-oz to a level of almost 600 in-oz ($T_f \tilde{\sim} 170 + 415$ in-oz).

3.3.2.3 Partial Spin-ups (December 1975)

Although partial spin-ups did not occur during the month of November, 9433 was plagued by a number of partial spin-ups during the month of December 1975 which resulted in the despin control system going into Standby, requiring many reacquisition attempts before achieving Normal Mode. Several of the more interesting of these events are discussed below; specifically, segments of data from December 11, 18, and 27 are discussed.

- 11 December (Figure 3.3-11). Two segments of the data of 11 December presented in Figure 3.3-11, show the system operating in the Search Mode during the many attempts to reacquire the system back to Normal Mode. Search Mode provided spin rate data from which an estimate of the net torque acting on the platform could be deduced. The net torque (T_N) acting on the system at various times in the transient is noted. It is apparent that the friction torque was roughly "bi-stable" with jumps of about 200 in-oz. At the lower level, the friction was no more than 70 in-oz. This data contrasts with transients prior to 28 November in that low levels of friction are present.

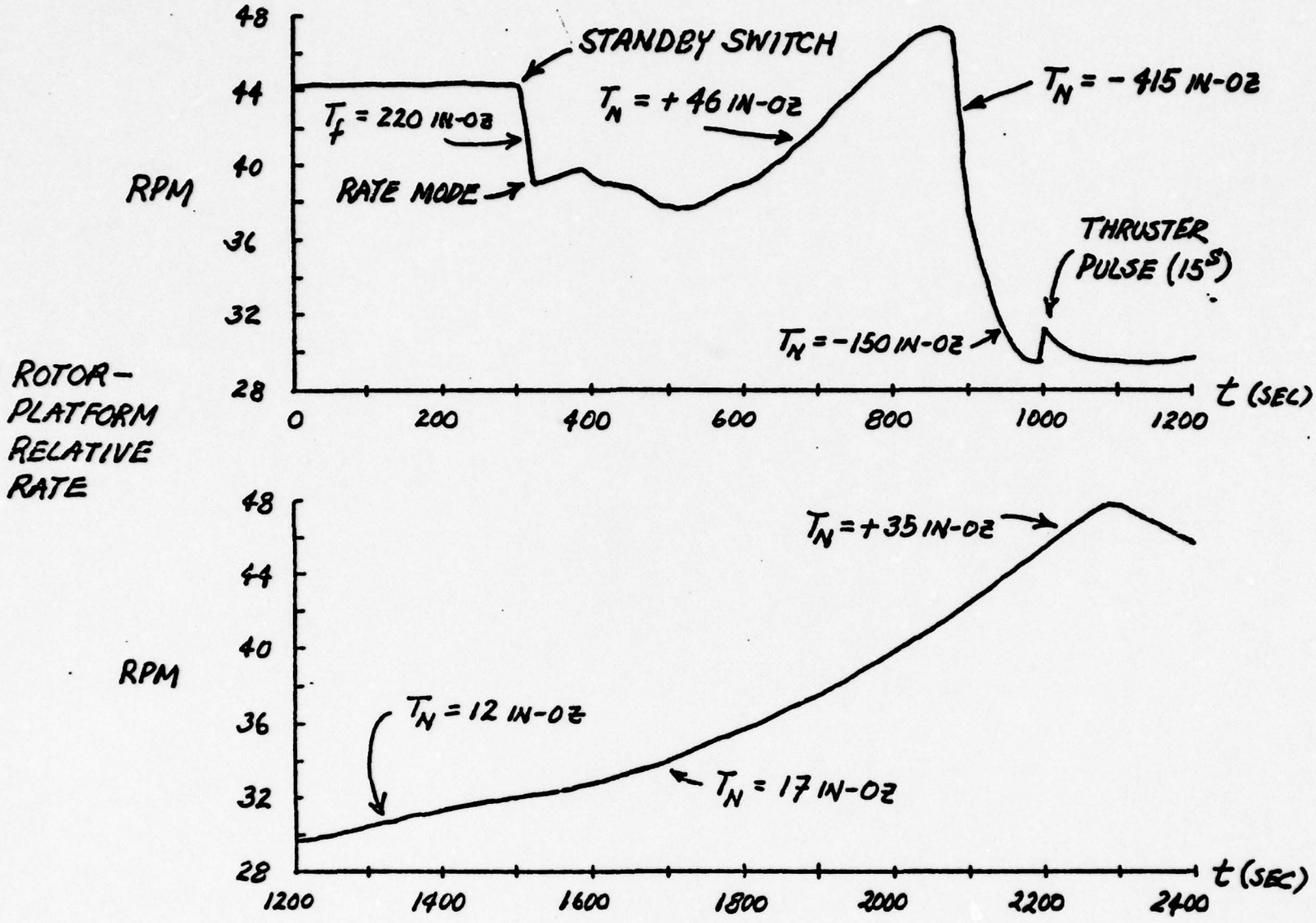


Figure 3.3-10. Partial Spin-Up: 85300Z, 10/13/75

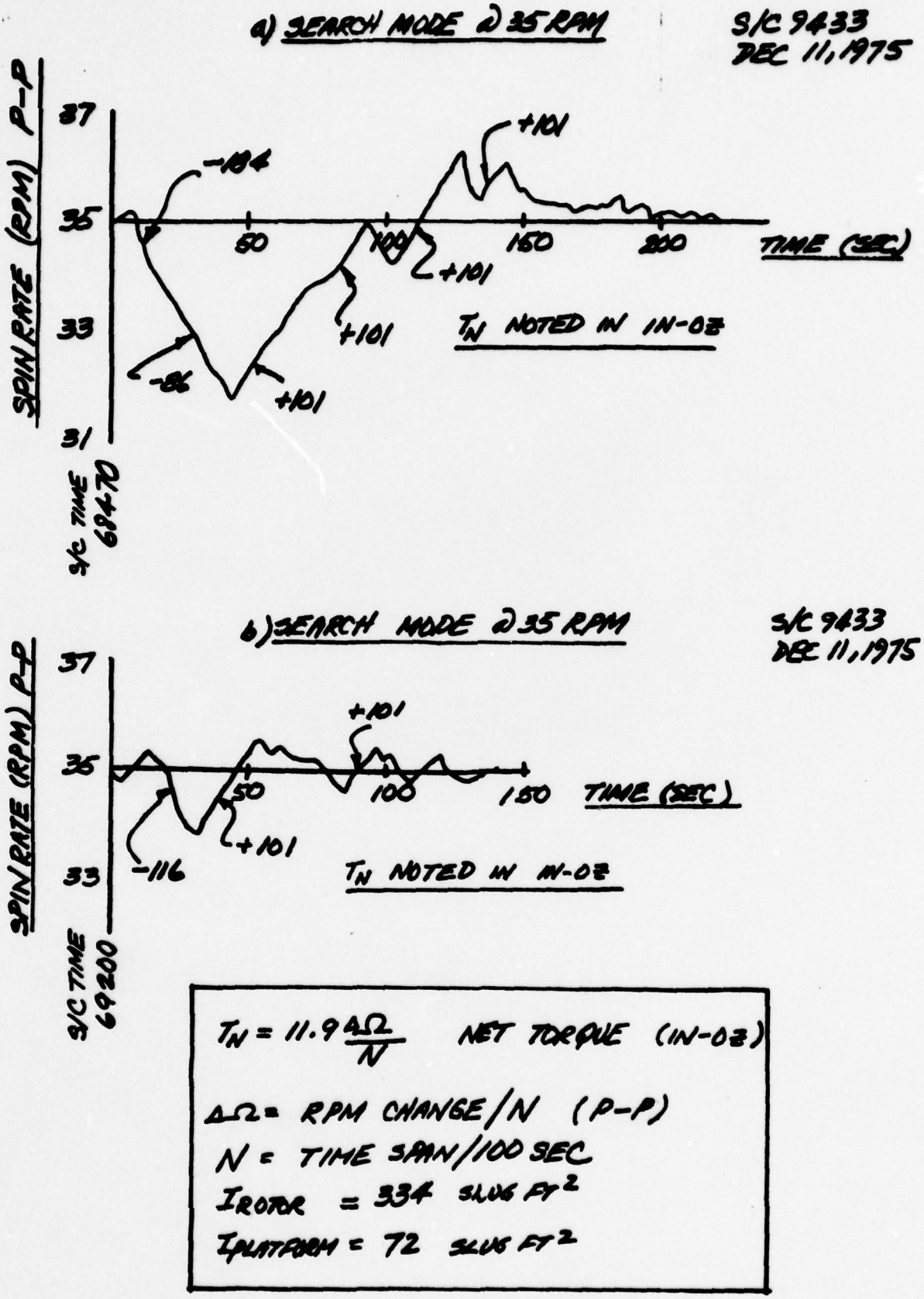


Figure 3.3-11. Search Mode

• 18 December (Figure 3.3-12). The data of Figure 3.3-12 shows a typical segment of the data of 18 December. During this day, a large number of reacquisition attempts were made, but the system ended up in Standby. This data shows that prior to going into Standby at 27599 seconds, the platform pointing error was exhibiting large excursions of +2 deg to -4.7 deg.

While in Standby, the platform was spinning up due to a friction level of 223 in-oz. Subsequently, during the time segments when the main bus current is high (+12 amps), it can be assumed that the motor is being commanded fall-on and that the net torque readings can be used to deduce friction levels. Assuming a conservative (optimistic) value of 170 in-oz for saturated motor torque, it can be seen from the spin rate data that the friction level is greater than 240 in-oz for the negative sloped segments of the data and in on the order of 45 to 100 in-oz for the positive sloped segment of the data. This data is similar to that of 11 December.

• December 27, 1975 (Figure 3.3-13). The data of Figure 3.3-13 shows the system initially operating in Normal Mode but at System Time 03660 a large platform pointing error of -4.2 deg is induced. Fifty-five seconds later the pointing error is so large the system ends up in Standby at 65 seconds the system is placed on Search Mode; during this 10-second interval, friction of 238 in-oz is spinning up the platform. After Search Mode is entered, the despin control system is struggling to establish the pre-Standby relative rate of 37.3 rpm. As can be seen from the data, the net torque (T_N) takes on a sequence of both positive and negative values.

The data shows that the friction is on the order of 200 to 223 in-oz in Search Mode when friction overwhelms the motor (negative slope segments) and drops off to 74 to 111 in-oz when the motor overwhelms the friction (positive slope segments). At 340 seconds there appears to be a dramatic reduction of friction level (down to 46 in-oz) and for the first time the motor is able to drive the relative rate past the 37.3 rpm value. At 400 seconds the main bus current level drops off from an average of 12.4 amps to 11.0 amps, which indicates a decrease in motor current. At 490 seconds, the P-P transient along

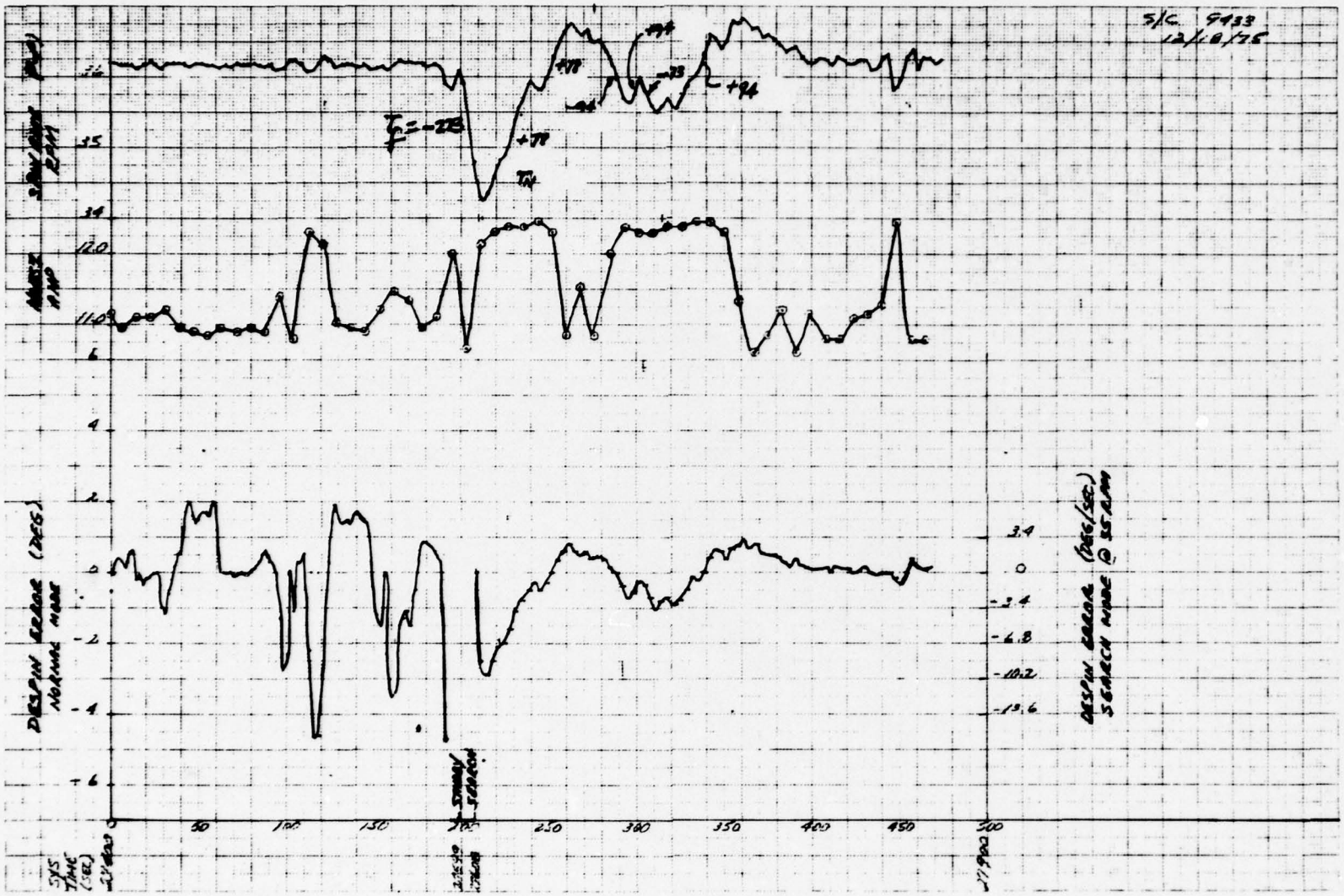


Figure 3.3-12. Typical Segment of Data for 18 December

with the increase in main bus current back to 12.3 amps again shows a demand on the motor but as was the case at 340 seconds, the friction level is still down near 49 in-oz. Thus, this data shows that for the first 300 seconds after Standby, the friction level seemed to vascillate between 100 to 200 in-oz, then suddenly to a low level of 49 in-oz.

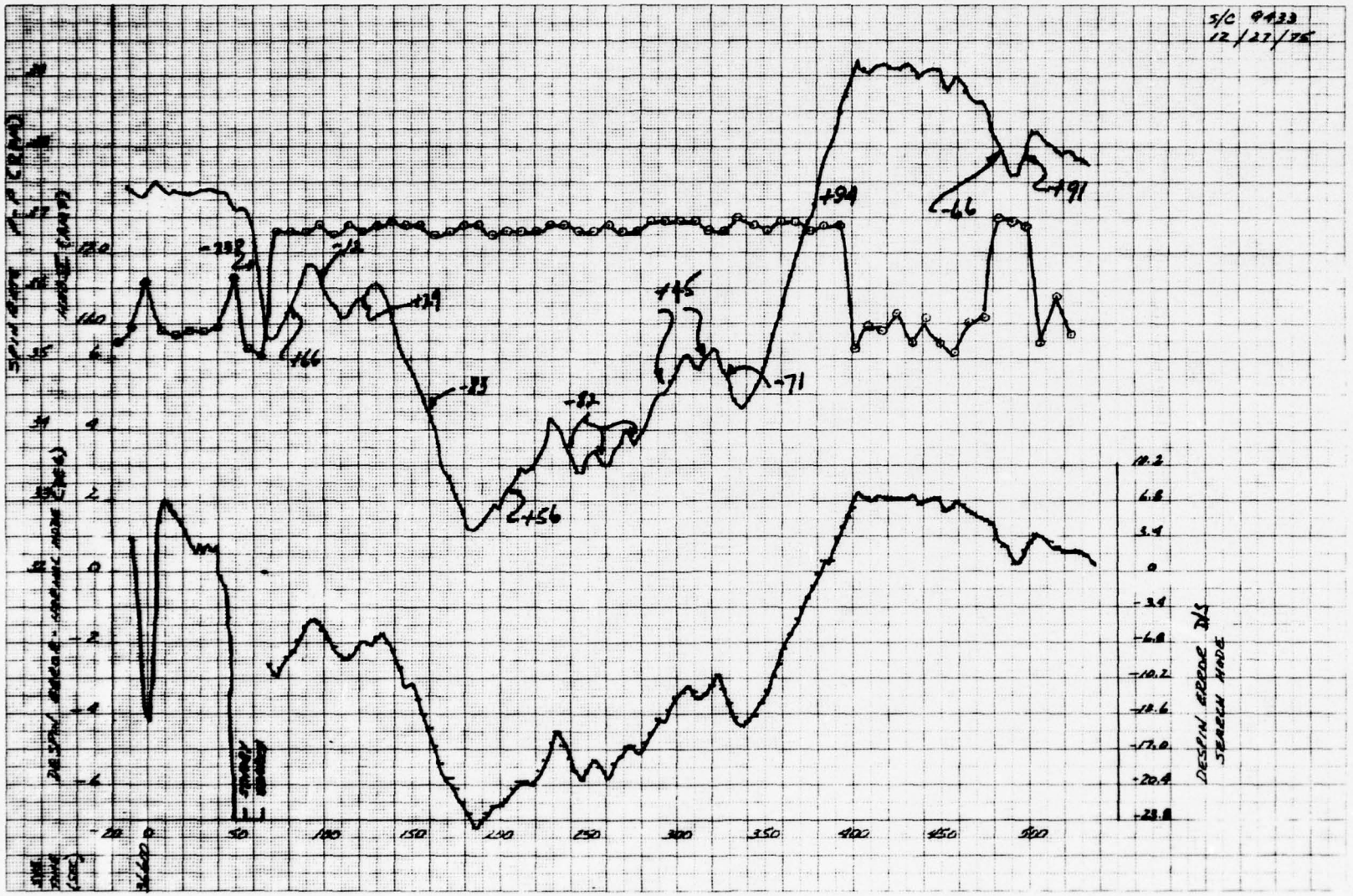


Figure 3.3-13. Normal Mode

3.4 Friction Tests

Shortly after the successful recovery of 9433 on 27 September, a series of on-orbit friction tests was planned. Primary objectives were to:

- provide direct dynamic friction measurements
- determine friction dependence upon speed
- compare performance of redundant drives.

These friction tests were performed on 30 September, prior to return of 9433 to operational status. Friction was successfully measured and exhibited no major speed dependence. However, the level of friction varied markedly between measurement runs. In addition, an unexpected "torque saturation" phenomenon (described below) was observed, and occurred with both drive channels. Motor test data (see Section 6.5) and analysis of the friction test orbital data have indicated this saturation effect to be due to a rise in mechanical friction during the test and a decrease in motor torque output (due to DEA phase shifts) with increased rotor-platform relative rates.

The friction tests were initiated at 1421Z on 30 September, with the rotor spinning at approximately 60 rpm and the platform approximately despun - that is, with a bias (relative) rate of 60 rpm. The plan was to:

(1) command a rate bias of 80 rpm

(2) allow the controller to converge at the new rate bias

(3) measure all rate parameters for calibration purposes

(4) disable the DEA power amplifier, allowing the relative rate to decrease due to running friction

(5) re-enable the power amplifier when the relative rate reaches 45 rpm, with a 45 rpm bias

(6) measure all rate parameters for calibration purposes

(7) repeat steps (1)-(6)

(8) switch to the alternate drive channel and again repeat steps (1)-(6).

Figure 3.4-1 shows the results of attempting the above sequence of operations. The initial run-up to 80 rpm was unsuccessful, even though maximum motor current (as indicated by the main bus current) was drawn

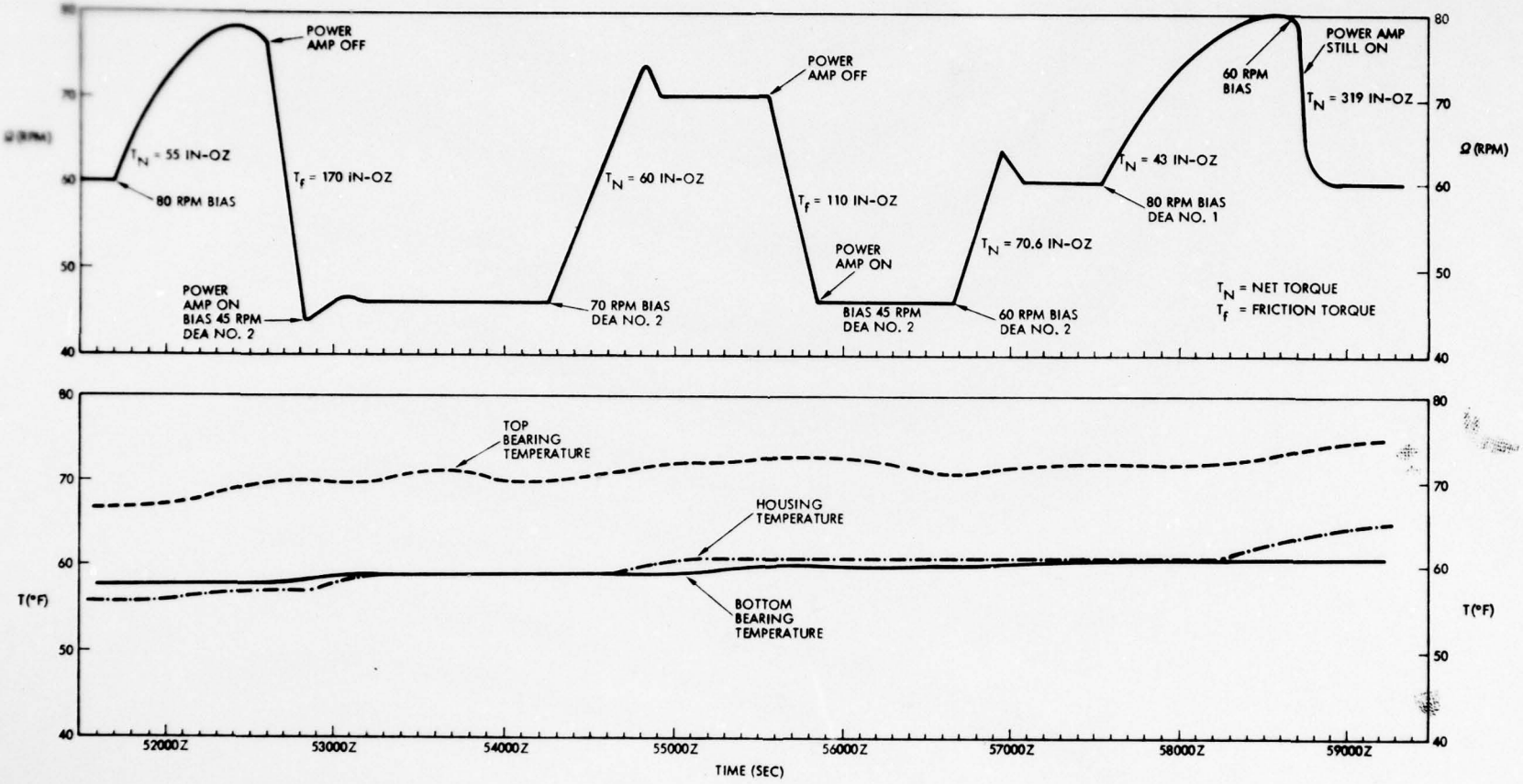


Figure 3.4-1. 9433 Friction Test Summary

throughout the period of the attempted run-up. Inspection of the initial run-up/run-down cycle (system time from 51700Z to 52800Z) yields the following observations (Figure 3.4-2):

- At the start of run-up, a torque margin of 52 in-oz existed, suggesting a friction torque in the neighborhood of 100 in-oz (and certainly no greater than 120 in-oz).*
- As the run-up progressed, the net torque decreased, becoming zero at 52400Z and then going negative, even with full motor current.
- Shut-down of the DEA power amp resulted in a run-down acceleration equivalent to an average friction level of approximately 170 in-oz, showing a definite and sizeable increase above the initial value.

The foldover in rate due to a change in sign of the net torque at 52400Z could be explained by a decrease in motor torque capability as a function of speed and termperature; indeed, motor test data reported in Section 6.5 shows such a characteristic to occur due to phase shifts in the DEA during the saturated regime. However, the change in friction level indicated by the run-down data suggests an increase in the mechanical friction, perhaps accompanied during run-up by a speed-dependent decrease in motor torquing capability.

Because the initial attempt to establish a relative rate of 80 rpm was unsuccessful, the target rate was reduced to 70 rpm for the next cycle of the test (Figure 3.4-4). This rate was reached successfully, with the normal overshoot which occurs due to the integration in the controller; moreover, the friction torque during the unpowered run-down differed little from that during run-up, and was considerably less than the friction level during the first run-down period.

In order to evaluate differences in performance between the two available drive channels, the alternate DEA (No. 1) was employed to repeat the first attempt to run up from 60 rpm to 80 rpm (Figure 3.4-5). The results during run-up were similar to those observed with DEA #2; although the 80 rpm bias level was reached, the controller did not settle out (since no

---

* See equations and parameters of Figure 3.4-3.

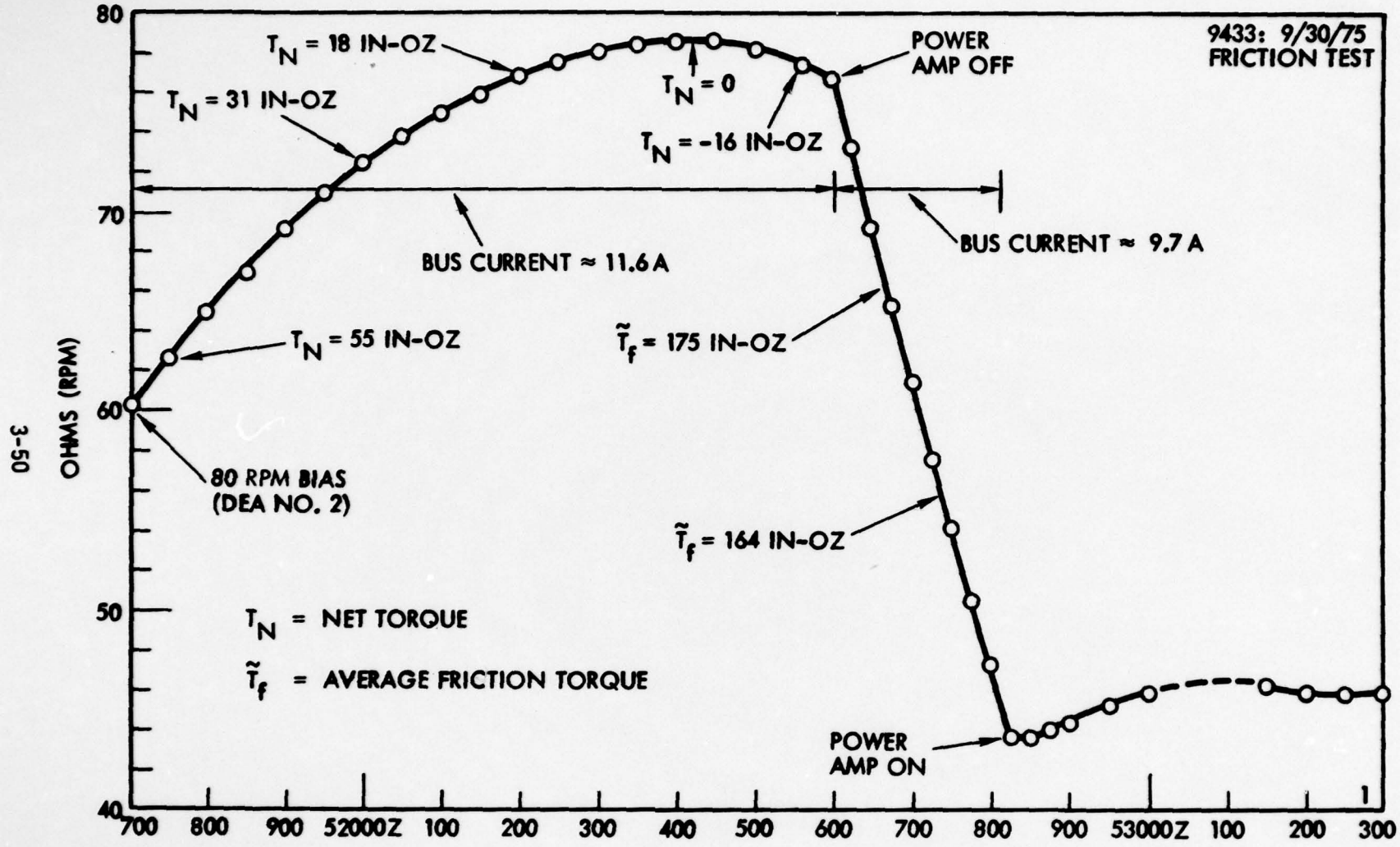


Figure 3.4-2. Friction Test Data (Case 1): 9/30/75

$$\text{NET TORQUE} = T_N = \frac{192\, I_P\, I_R}{954.93\,(I_P + I_R)} \cdot \Delta\Omega$$

- $\Delta\Omega$ = CHANGE IN RELATIVE RATE IN RPM PER 100 SECONDS
- I_P = 69.1 SLUG-FT^2
- I_R = 338.8 SLUG-FT^2

\}*

- T_N = NET TORQUE IN INCH-OUNCE

$T_N = 11.54\,\Delta$ INCH-OUNCE

- T_N = $-T_f$ WITH MOTOR DISABLED
- T_N = $T_M - T_f$ WITH MOTOR ACTIVE

*NOTE THAT I_R IS DETERMINED BY KNOWLEDGE OF THE INITIAL ROTOR MASS PROPERTIES AND THE AMOUNT OF HYDRAZINE EXPENDED; I_P IS A FUNCTION OF ANTENNA POSITION, AND WAS DETERMINED FROM THE CALIBRATION DATA TAKEN DURING THE TESTS

Figure 3.4-3. Calculation of Net Torque from Rate Data

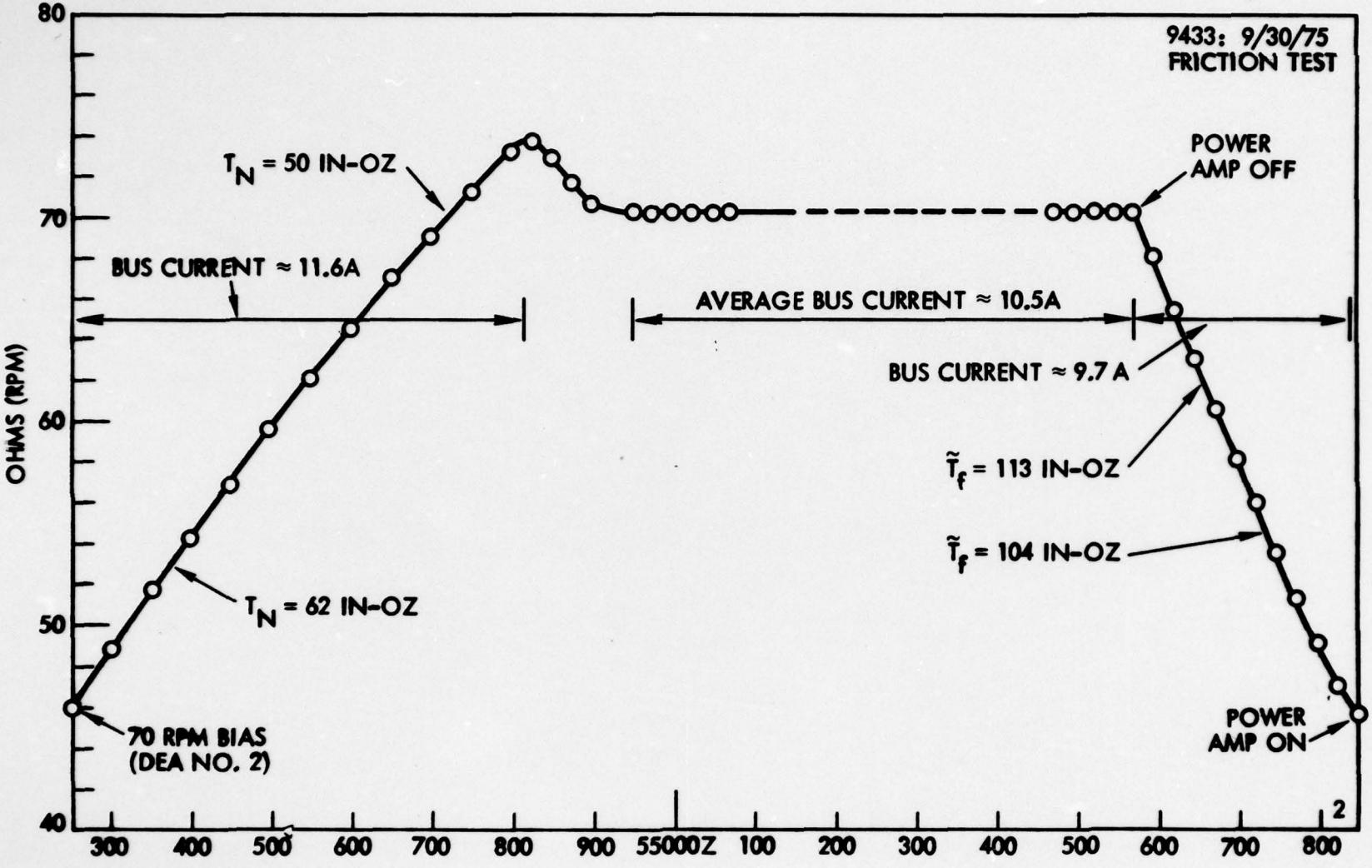


Figure 3.4-4. Friction Test Data (Case 2): 9/30/75

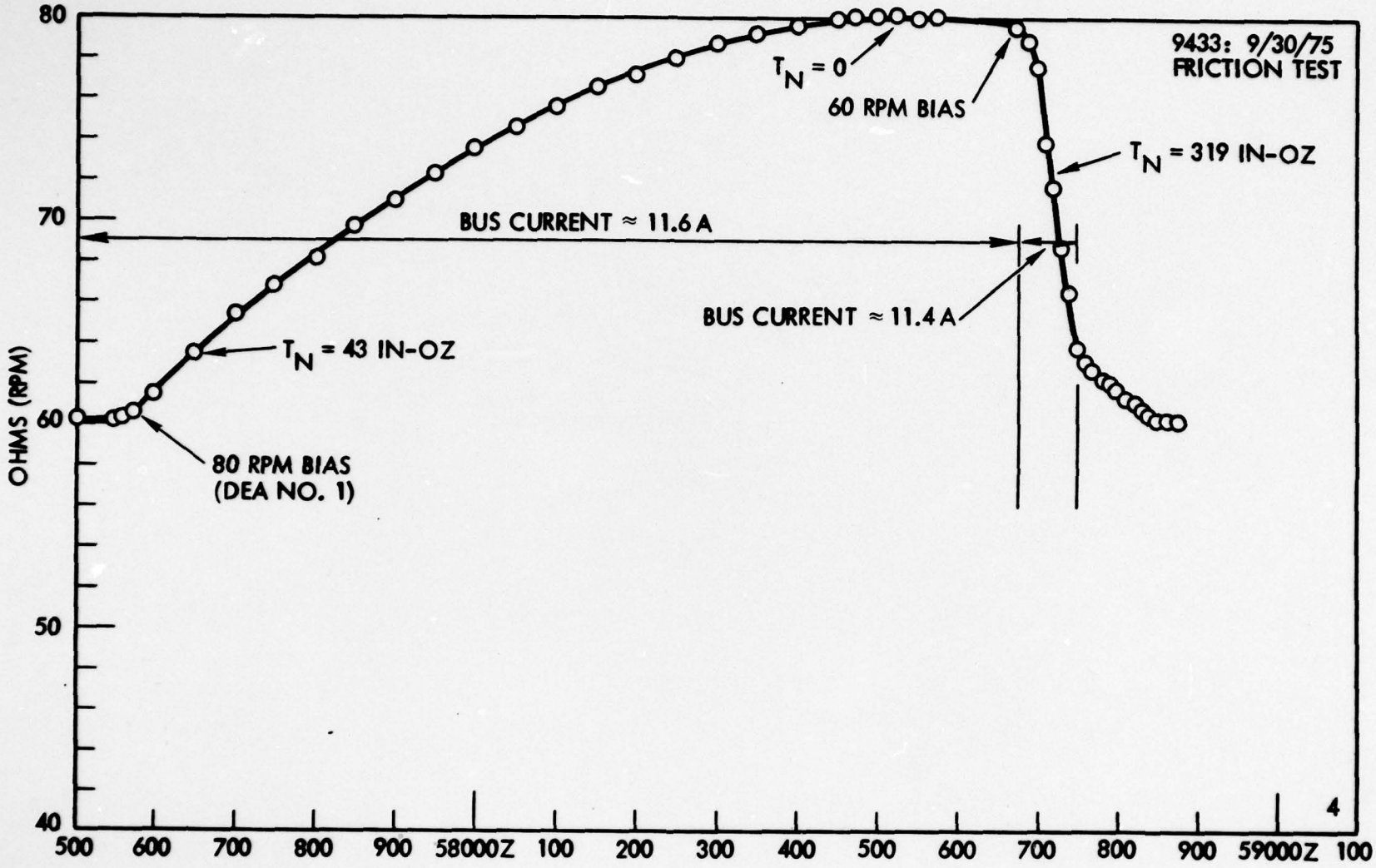


Figure 3.4-5. Friction Test Data (Case 3): 9/30/75

overshoot, required for convergence, occurred). Unfortunately, friction-only run-down was not permitted; instead, the bias command was changed to 60 rpm and the run-down was driven by both the DMA motor and friction. However, assuming a motor torque of 170 in-oz, the friction level was 150 in-oz — clearly higher than the apparent friction torque at the beginning of this third cycle. It is concluded that the two DEA-DMA drive channels produced similar results, with the differences attributable to normal tolerance variations between the two drive channels.

The friction tests indicated an apparent growth in friction during attempts to run-up to a relative rate of 80 rpm, accompanied by a decrease in motor torque capability. The reduction in motor torque output is consistent with lab test data (Section 6.5). The increase in friction torque has not yet been explained. However, it is probably due to thermal effects. It is worth noting that an attempt to reproduce this data in laboratory system tests was unsuccessful (see Section 6.1); nor have thermal simulation results provided any insight into this phenomenon (Appendix A).

Further friction tests were planned, to verify the results of Figure 3.4-1 and to study time-dependence of the drag torque. During the initial phase of these tests, a DEA current trip occurred, putting the system into the Standby mode and resulting in full spin-up of the platform. No further friction tests were performed in 1975.

The friction tests of 30 September yielded the following significant results:

(i) The first direct measurements of friction torque were obtained. These measurements verified the conclusion that the friction increase is mechanical (as opposed to a DEA-motor torque degradation). Subsequent "unplanned events" (e.g., partial spin-ups) add further support to this conclusion.

(ii) Motor torque capability in the saturated regime appears to be speed-dependent. This phenomenon has been verified by subsequent motor tests.

(iii) At least two distinct levels of friction torque were observed during periods when the DMA motor was not activated, indicating non-constant friction over the period of the tests.

(iv) No abrupt changes in friction were observed and no significant dependence of friction on speed was observed during run-down.

If, as this data indicates, there was a growth in mechanical friction during the attempts to run-up to 80 rpm, no clear explanation has been revealed by thermal simulations (Appendix A and Section 5); that is, the thermal simulations have not shown any critical thermal gradient (e.g., across the snubber gap in the power module - see Section 4 - or across the main bearings) to have reached extreme values during periods of friction growth). Nor has it been possible to duplicate these results in laboratory system tests (Section 6.1). The true explanation may be subtle (for example, a speed-temperature effect involving the retainer of the DMA top-main bearings). Finally, these on-orbit tests were not repeated in 1975 due to the desirability of maintaining operational status for 9433. The results may have been due to a non-repeatable transient condition.

Subsequent to these tests, orbital dynamic tests were conducted which were similar to the friction tests. Results were considerably different (Section 3.6), due partially to the decrease in average friction torque in the interim (approximately 3.5 months).

3.5 Recovery Data

Several unsuccessful recovery attempts were made, in which despin of the platform was initiated but ceased after a partial revolution in some cases and after a couple of revolutions in other cases. Evaluation of the earth sensor data (either earth chordwidth or rotor spin rate) provides some measure of the resistance torques encountered during these despin attempts.

3.5.1 Interpretation of Earth Sensor Data

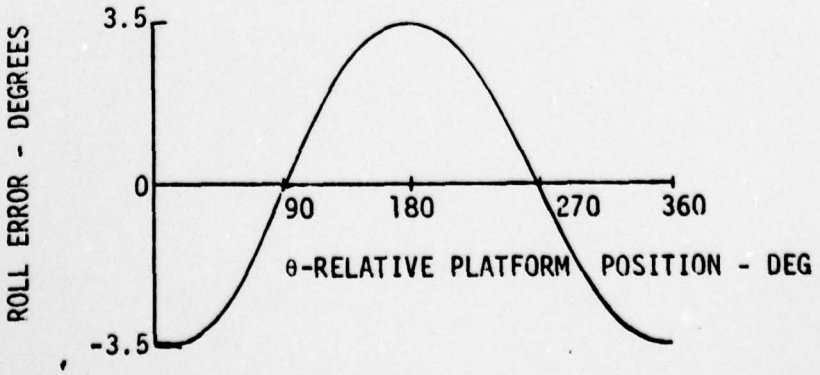
The earth sensors can be used to measure either the earth's chordwidth or the spacecraft spin rate. From these measurements, the despun platform position and/or relative rate may be determined, from which friction torque magnitudes can be deduced.

3.5.1.1 Chordwidth Data

The relatioship between the chordwidth scanned by the earth sensors and the spacecraft attitude in the direction towards the earth (Roll) is shown in Figure 3.5-1. The earth sensors nominally point $\pm 6°$ from the equator.

When the despun platform is completely spun up, the dynamic imbalance of the platform ($\tilde{\sim}8$ sl-ft^2) causes the spin axis to tilt approximately 3.5 deg relative to the spacecraft centerline. This will cause the earth sensors to read a roll error of between -3.5 and +3.5 deg depending on the relative position of the rotor (containing the earth sensors) and the platform (unbalanced by the narrow coverage antennas) at the time the chordwidth measurements are taken. The relationship is expressed as follows, where at $\theta = 0$ degrees, the rotor and platform +Z axes are aligned.

$$\theta = \sin^{-1}\left(\frac{\text{ROLL ERROR}}{3.5}\right) + 90°$$



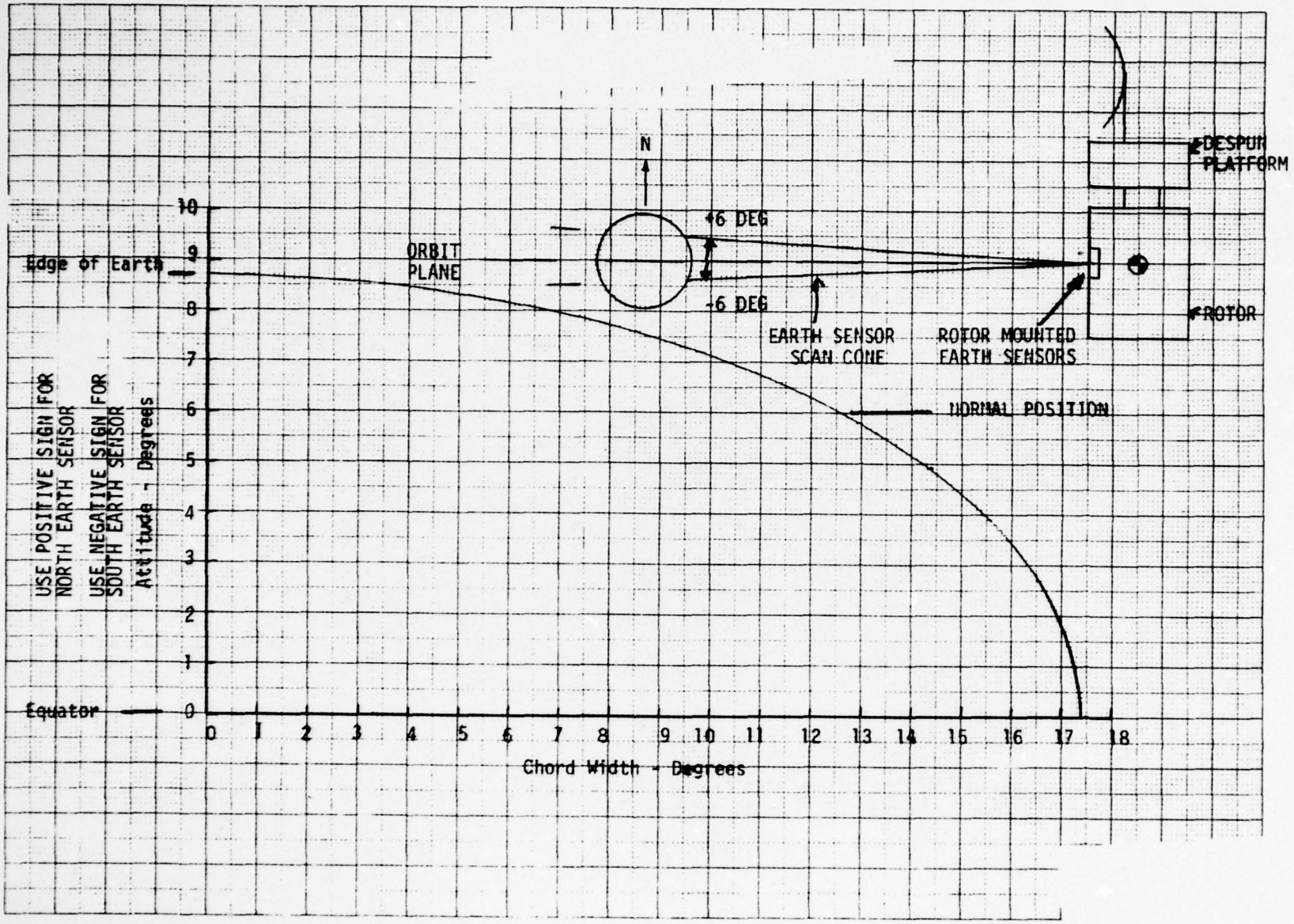


Figure 3.5-1. Cordwidth Versus Spacecraft Attitude

3.5.1.2 Spin Rate Data

The changes in the rotor spin rate data can be used to determine the friction torques between the rotor and platform according to the following expression

$$T_f = T_s + T_m - I_R \frac{\Delta\omega}{\Delta t}$$

where T_f = friction torque

T_s = spin thruster torque

T_m = DMA motor torque

I_R = spin moment of inertia of the rotor

$\Delta\omega$ = change in rotor spin rate

Δt = time interval

For the initial recovery attempts, this expression was:

$$T_f = 9.4 - 35.6 \frac{\Delta s}{\Delta t} \text{ (ft lb)}$$

where Δs = spin rate change in RPM

Δt = time interval in seconds

T_s = 8.5 ft lb

T_m = 0.9 ft lb

I_R = 340 sl ft^2

The values of spin thruster torque and rotor moment of inertia change as fuel is expended, thereby requiring an update of these numbers for later periods.

The realtive spin rate is related to the rotor spin rate by the following expression when no thruster torques are being applied (i.e., only DMA motor and/or friction torques are changing the relative rate)

$$\dot{\theta}_{REL} = \frac{I_R + I_P}{I_P} \left(\omega_o - \omega_{ROTOR}\right)$$

where
- $\dot{\theta}_{REL}$ = relative rate between platform and rotor
- I_R = spin axis moment of inertia of rotor
- I_P = spin axis moment of inertia of platform
- ω_o = spin rate of completely spun up spacecraft
- ω_{ROTOR} = spin rate of rotor

For the initial recovery attempts, this expression was

$$\dot{\theta}_{REL} = 5.5 \left(\omega_o - \omega_{ROTOR}\right)$$

Friction torque can also be calculated from the relative spin rate as follows.

$$T_f = T_m - \frac{\Delta\dot{\theta}_{REL}}{\Delta t} \times \frac{I_R I_P}{I_R + I_P}$$

3.5.2 Initial Recovery Attempts (13 September 1975)

After the platform spun-up on 13 September, an attempt to despin the platform was made by turning on the motor. The spacecraft spin rate was approximately 41 rpm at this time. Despin motion was initiated; however, relative motion ceased after slightly over one-half a revolution. The relative position, as deduced from earth chordwidth and spin rate data, is plotted vs time in Figure 3.5-2. DMA friction ranging from 130 to 240 in-oz are deduced from these data.

A second recovery attempt was then made utilizing the spin-up thruster to augment the DMA motor torque. A fifteen second firing of the thruster was performed while the motor was also turned on. This added an effective DMA torque of approximately 300 in-oz to the motor stall torque of approximately 170 in-oz. Again, relative motion was initiated, but ceased after approximately three-quarters of a revolution. Rotor spin rate measured during this attempt is shown in Figure 3.5-3. These data indicate that the resistance torque was approximately 500 in-oz at the end of relative motion, however, it was initially less than 470 in-oz in order for the relative motion to start. Another attempt was made in the same manner producing no relative motion, thereby implying that the resistance torque was still in excess of 470 in-oz.

3.5.3 Thirty RPM Recovery Attempts (20 October 1975)

On 20 October two recovery attempts were made with the spacecraft spinning at slightly over 30 rpm. The first attempt utilized the axial thrusters to induce nutation and the spin thrusters to augment the DMA motor torque. Despin was initiated during this attempt; however, relative motion ceased after slightly over two and one-half revolutions.

A second attempt was then made utilizing the DMA motor and both the spin-down and spin-up thrusters in a pulsing mode. Again despin was initiated but ceased after slightly over two revolutions of relative motion.

The spacecraft attitude data and deduced relative spin rate and position for these two attempts are shown in Figures 3.5-4 and 3.5-5.

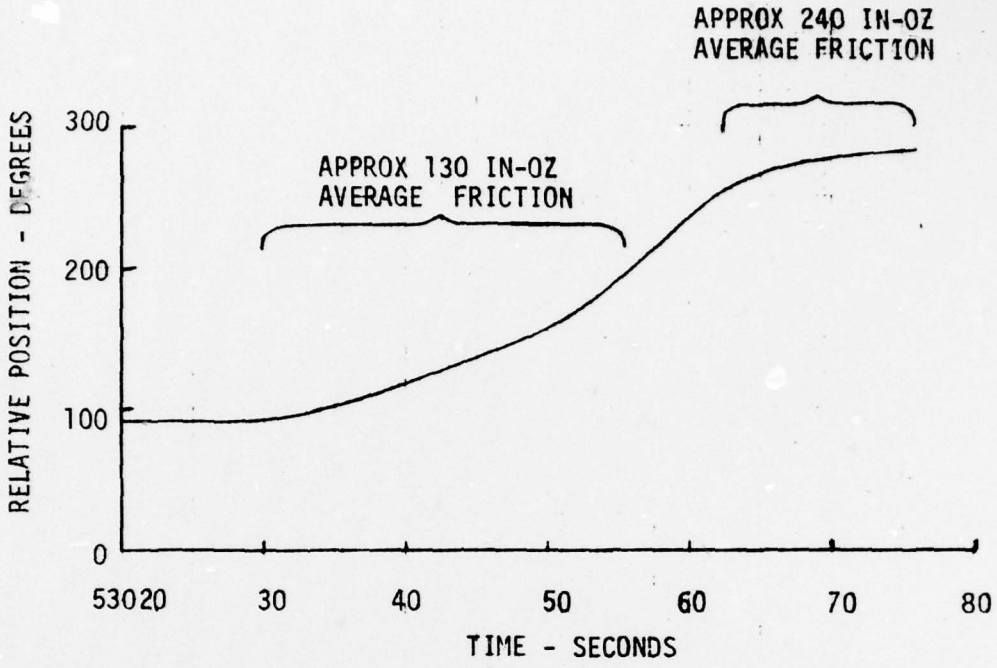


Figure 3.5-2. Relative Platform Position Versus Time, DMA Motor Only - September 13, 1975

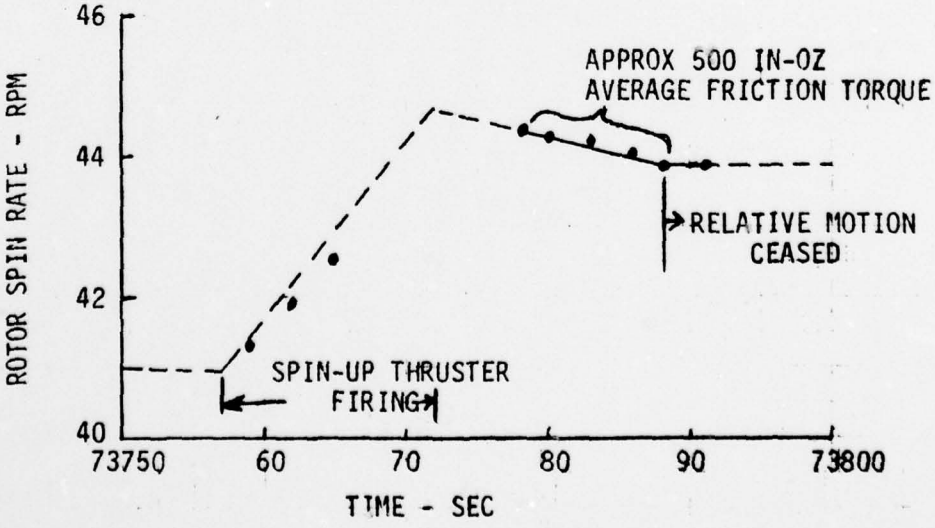
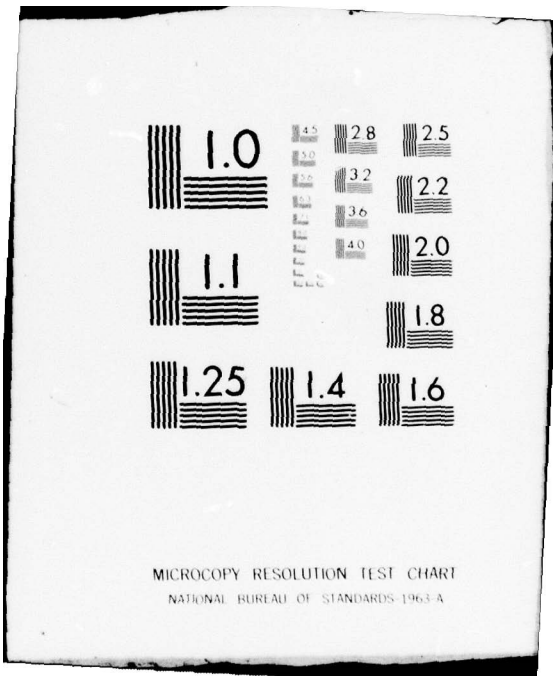


Figure 3.5-3. Rotor Spin Rate Versus Time During Spin-Jerk Recovery Attempt

AD-A073 437 TRW DEFENSE AND SPACE SYSTEMS GROUP REDONDO BEACH CA F/G 22/1
9433 DESIGN POINTING ANOMALY. VOLUME I. TECHNICAL REPORT.(U)
JAN 76 P C WHEELER F04701-75-C-0257
UNCLASSIFIED TRW-28600-AR-010-01-VOL-1 SAMSO-TR-79-13-VOL-1 NL

2 OF 3
AD A073437




1.0
1.1
1.25
1.4
1.6
2.0
2.2
2.5
2.8
3.2
3.6
4.0
4.5
5.0
MICROCOPY RESOLUTION TEST CHART
NATIONAL BUREAU OF STANDARDS-1963-A

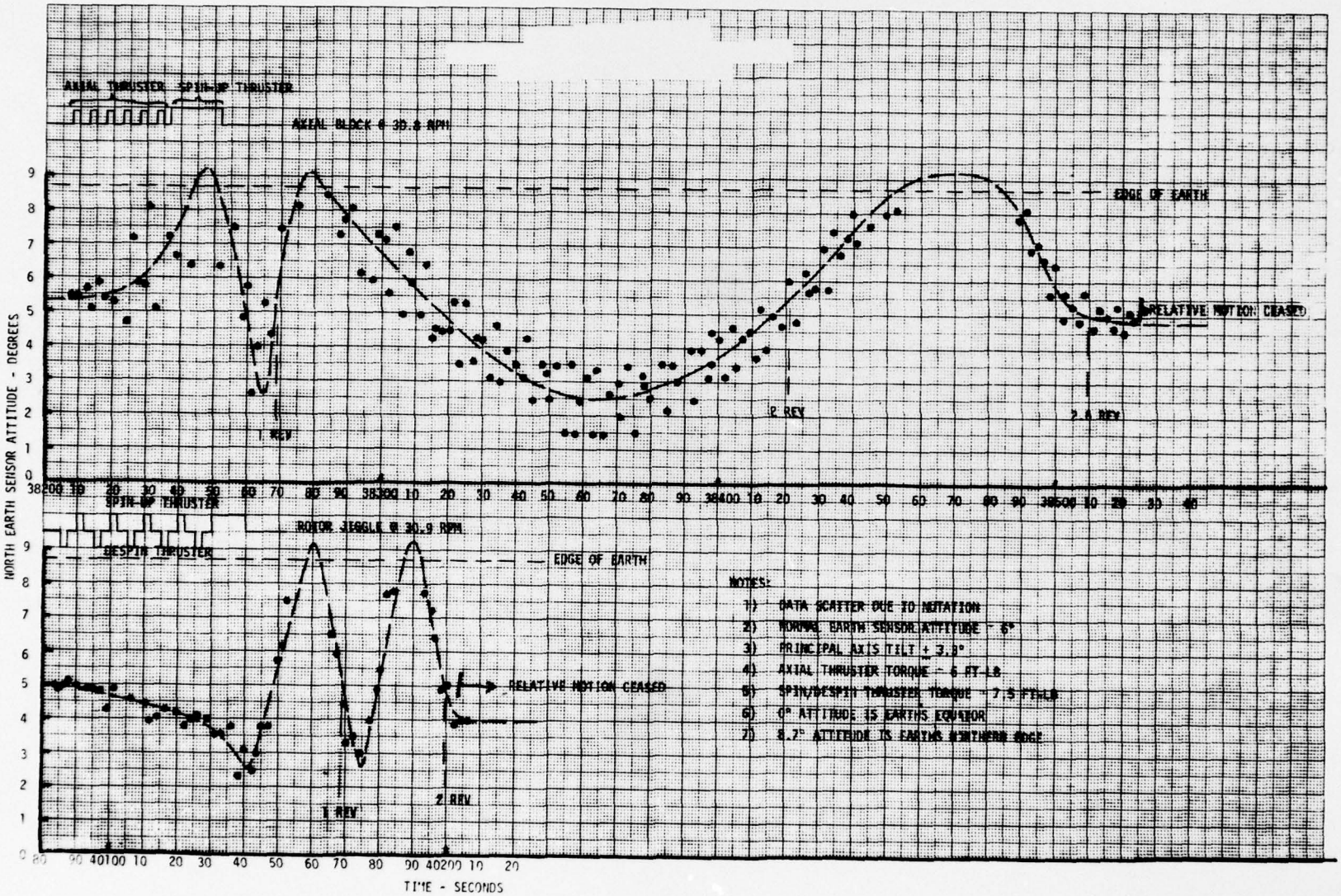


Figure 3.5-4. 777 F3 Recovery Attempts at 30 RPM 10-20-75 Earth Sensor Attitude Data

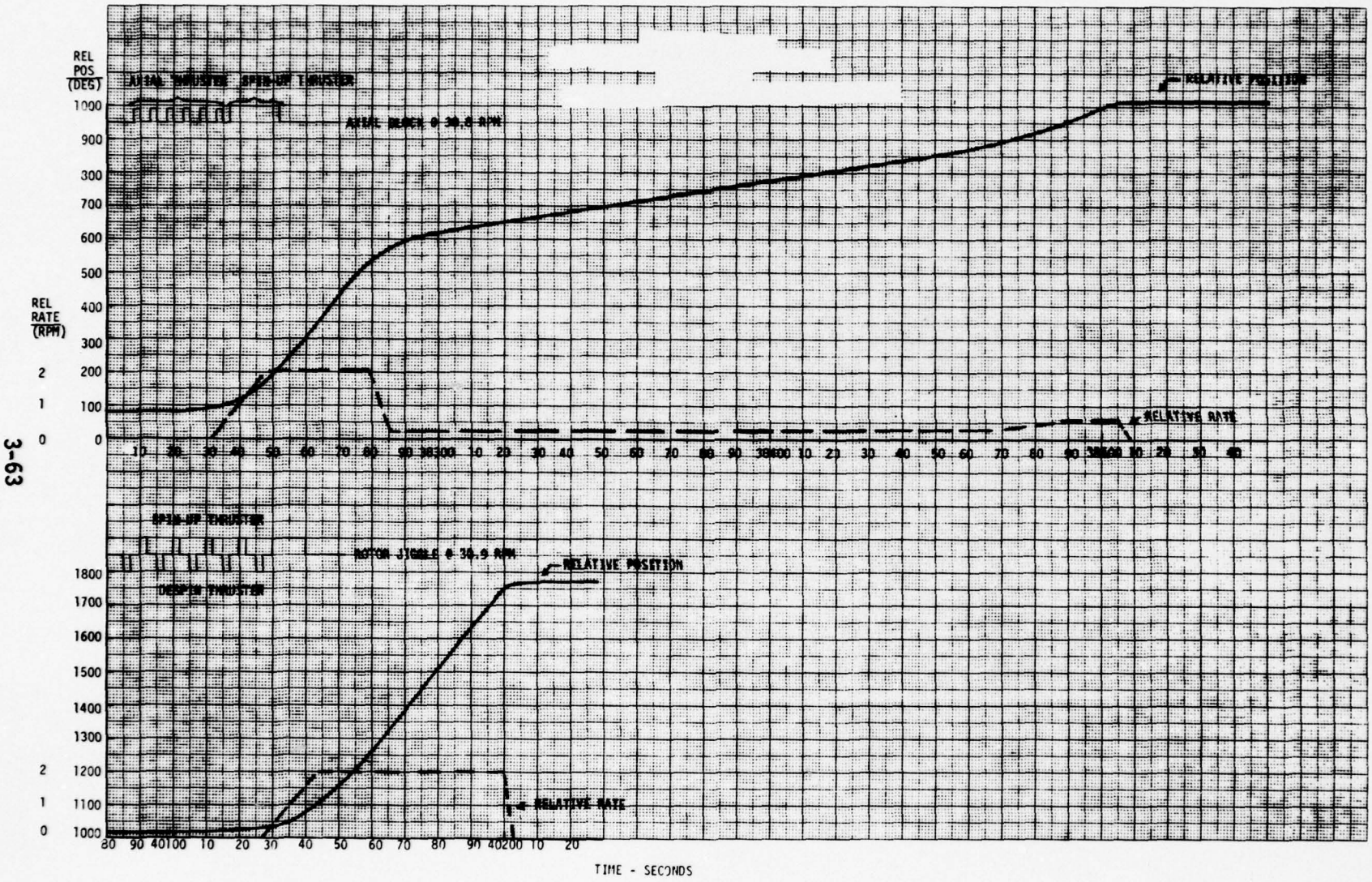


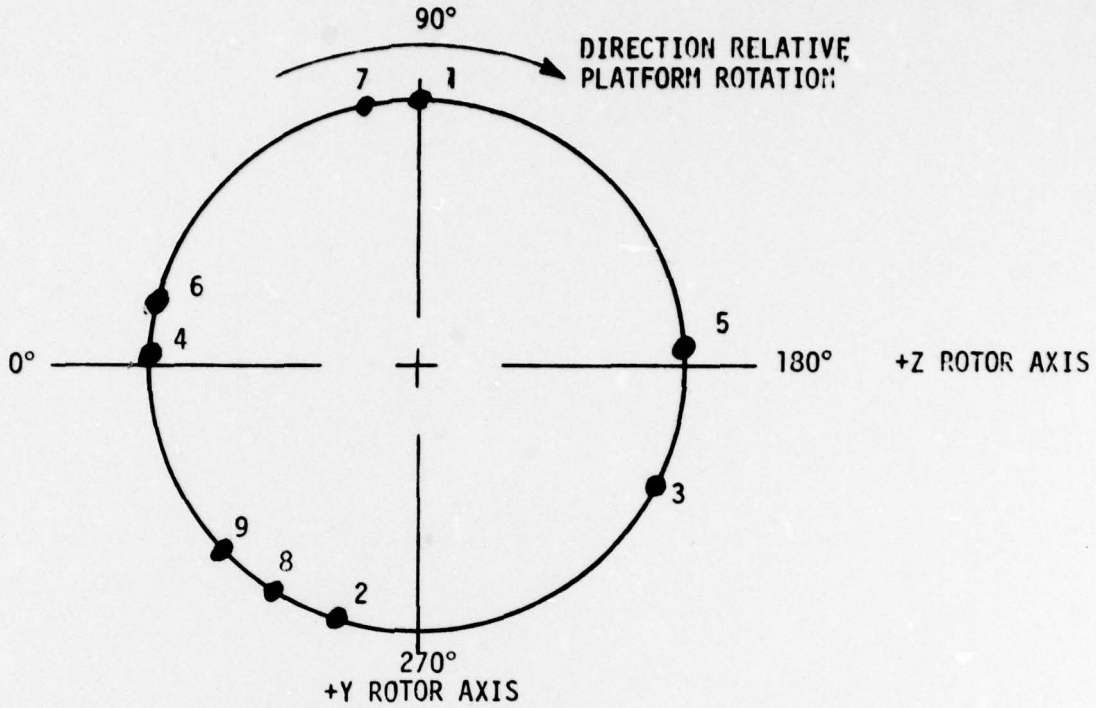
Figure 3.5-5. 777 F3 Recovery Attempts at 30 RPM 10-20-75 Platform Relative Position and Rates

The data seems to indicate that the spin-up thruster firing was most influential in initiating the motion. The periods of constant relative rate implies that the friction torque was essentially equal to the motor torque, i.e., 170 in-oz. Higher values of torque spikes apparently occurred for short periods to produce sudden changes in relative rate. A slight increase of relative rate was noted just prior to the stoppage of relative motion on the first attempt.

A subsequent reduction of spacecraft spin rate to 20 rpm and repositioning of the narrow coverage antennas to reduce the spin axis tilt from 3.5° to less than 1° allowed a successful recovery. Both the spin rate change and antenna repositioning reduced the DMA bearing side loads, apparently thereby alleviating the friction torques sufficiently for the DMA motor to complete the despin maneuver.

3.5.3 Platform Stopping Positions

The relative positions between the platform and rotor after the various spin-up events and unsuccessful recovery events are shown in Figure 3.5-6. These positions do not indicate any preferential position.



• DESIGNATES -Z PLATFORM AXIS POSITION, i.e., N.C. ANTENNA POSITION

NO	DATE	TIME	EVENT	COMMENTS
1	9-13-75	53000	INITIAL SPUN UP POSITION	
2	9-13-75	53174	AFTER RECOVERY ATTEMPT USING DMA MOTOR ONLY	SLIGHTLY OVER 1/2 REVOLUTION
3	9-13-75	73800	AFTER RECOVERY ATTEMPT USING SPIN JERK	APPROXIMATELY 3/4 REVOLUTION
4	10-3-75		INITIAL SPUN UP POSITION	
5	10-3-75	8350	AFTER ROTOR JIGGLE @ 50 RPM	APPROX 1/2 REVOLUTION
6	10-20-75	32700	AFTER SPIN UP, BEFORE 40 RPM RECOVERY ATTEMPT	APPROX 1/4 REVOLUTION
7	10-20-75	38200	BEFORE 30.8 RPM AXIAL RECOVERY ATTEMPT	APPROX 2.5 REVOLUTION
8	10-20-75	40080	BEFORE 30.9 RPM SPIN THRUSTER RECOVERY ATTEMPT	APPROX 2.1 REVOLUTION
9	10-20-75	40220	AFTER 30.9 RPM SPIN THRUSTER RECOVERY ATTEMPT	

Figure 3.5-6. Approximate Position of Despun Platform and Rotor During Various Spun-Up Conditions - F3 Spacecraft

3.6 Orbital Dynamic Tests

During early January (1976), 9433 performance became erratic due to relatively large and frequent torque transients. Performance was similar to that observed on December 11, 18-19, and 27-28. However, the loss of normal control was sustained for a much longer period.* On 14 January, a series of orbital dynamic tests were conceived to:

- Exercise the spacecraft in an attempt to modify its behavior in a favorable manner
- Obtain additional data pertaining to the friction characteristics.

Tests were initiated on 15 January in Search Mode at a rotor (and platform) rate of 35.5 rpm. The plan was to run-up the platform, in the rate mode, to an inertial rate of approximately 20 rpm and then to return it to the starting rate by an unpowered rundown (providing a direct friction measurement). Steady-state despun performance in Search Mode was then observed for a period of time to determine if any improvement in performance had been achieved. If so, Normal Mode was attempted; if not, the spin rate of the rotor was increased and the above procedure was repeated. Table 3.6-1 presents the chronology of the tests conducted on 15-16 January 1976.

The first runup/rundown cycle (steps 1, 2 of Table 3.6-1) was uneventful. It was noted that rate control in the overspun condition seemed much smoother than while despun. The rotor rate was subsequently increased to 47.5 rpm by spin thruster firings (step 3).

Runup of the relative rate from 47.5 rpm to 72.1 rpm (step 4) was similar to the previous runup, as was the rundown (step 5) similar to the previous rundown. This data is plotted in Figure 3.6-1. Note that the torque applied between the rotor and platform can be computed from the change in rate:

---

* As of this writing (1/22/76), Normal Mode operational periods are generally less than one hour. However, availabilities as high as 80% are being maintained by STC personnel.

Table 3.6-1. Summary of Dynamic Tests: 15-16 Jan 1976

1. 66191 - 66765Z: RUNUP OF P-P FROM 35.5 RPM TO 60 RPM; E-E = 39.8 RPM AT END; VERY SMOOTH CONTROL WHILE OVERSPUN.

2. 67164 - 67538Z: RUNDOWN TO 35.5 RPM. NOISY CONTROL WHILE DESPUN.

3. 68536 - 69700Z: SPINUP OF E-E FROM 35.5 RPM TO 47.5 RPM. NOISY CONTROL WHILE DESPUN.

4. 70885 - 71395Z: RUNUP P-P FROM 47.5 RPM TO 72.1 RPM; E-E = 51.8 RPM AT END; VERY SMOOTH CONTROL WHILE OVERSPUN

5. 72117 - 72501Z: RUNDOWN TO 47.5 RPM; NOISY CONTROL WHILE DESPUN.

6. 74444 - 74554Z: NORMAL MODE ATTEMPT

7. 75248 - 76350Z: RUNUP P-P FROM 47.5 RPM TO 72.1 RPM; VERY DIFFICULT RUNUP AT TIMES; SMOOTH CONTROL WHILE OVERSPUN.

8. 80816 - 89990Z: RUNDOWN P-P DOWN TO 60.2 RPM. SMOOTH CONTROL; CONTROL GENERALLY ROUGHER THAN AT 72.1 RPM.

9. 82618 - 82713Z: RUNDOWN P-P TO 53.7 RPM. CONTROL ROUGHER THAN AT 60.2 RPM.

10. 84066 - 84168Z: RUNDOWN P-P TO 47.5 RPM; E-E = 47.6 RPM; NOISY CONTROL WHILE DESPUN (WORSE THAN AT 53.7 RPM, BUT NOT MUCH WORSE)

11. 84883 - 85811Z: SPINUP E-E FROM 47.6 RPM TO 59.9 RPM. CONTROL WHILE DESPUN INITIALLY SMOOTH, LATER NOISIER. P-P = 59.9 RPM. SMOOTH CONTROL IN SEARCH MODE UNTIL TRANSIENT AT 00725+ (~22 MINUTES); THIS TRANSIENT DROVE P-P DOWN TO 57.8 RPM

Table 3.6-1. Summary of Dynamic Tests: 15-16 Jan 1976 (Continued)

12. 01002 - 01538Z: RUNUP OF P-P FROM 59.9 RPM TO 84.8 RPM. SMOOTH CONTROL WHILE OVERSPUN. E-E = 64.3 RPM.

13. 01826 - 02643Z: RUNDOWN TO 35.4 RPM; IMMEDIATE TURNAROUND VIA "PWR AMP ON".

14. 02643 - 03952Z: RUNUP OF P-P FROM 35.4 RPM TO 84.8 RPM. PROGRESS SLOW AT TIMES.

NOTES:

- PERIODS MARKED BY ASTERICKS (*) ARE PLOTTED IN SUBSEQUENT FIGURES.
- P-P IS MEASURE OF ROTOR-PLATFORM RELATIVE RATE FROM MAGNETIC PIPPER.
- E-E IS MEASURE OF ROTOR RATE FROM EARTH SENSOR PULSES.
- TIME INTERVALS ARE SYSTEM TIME IN SECONDS (ZULU).

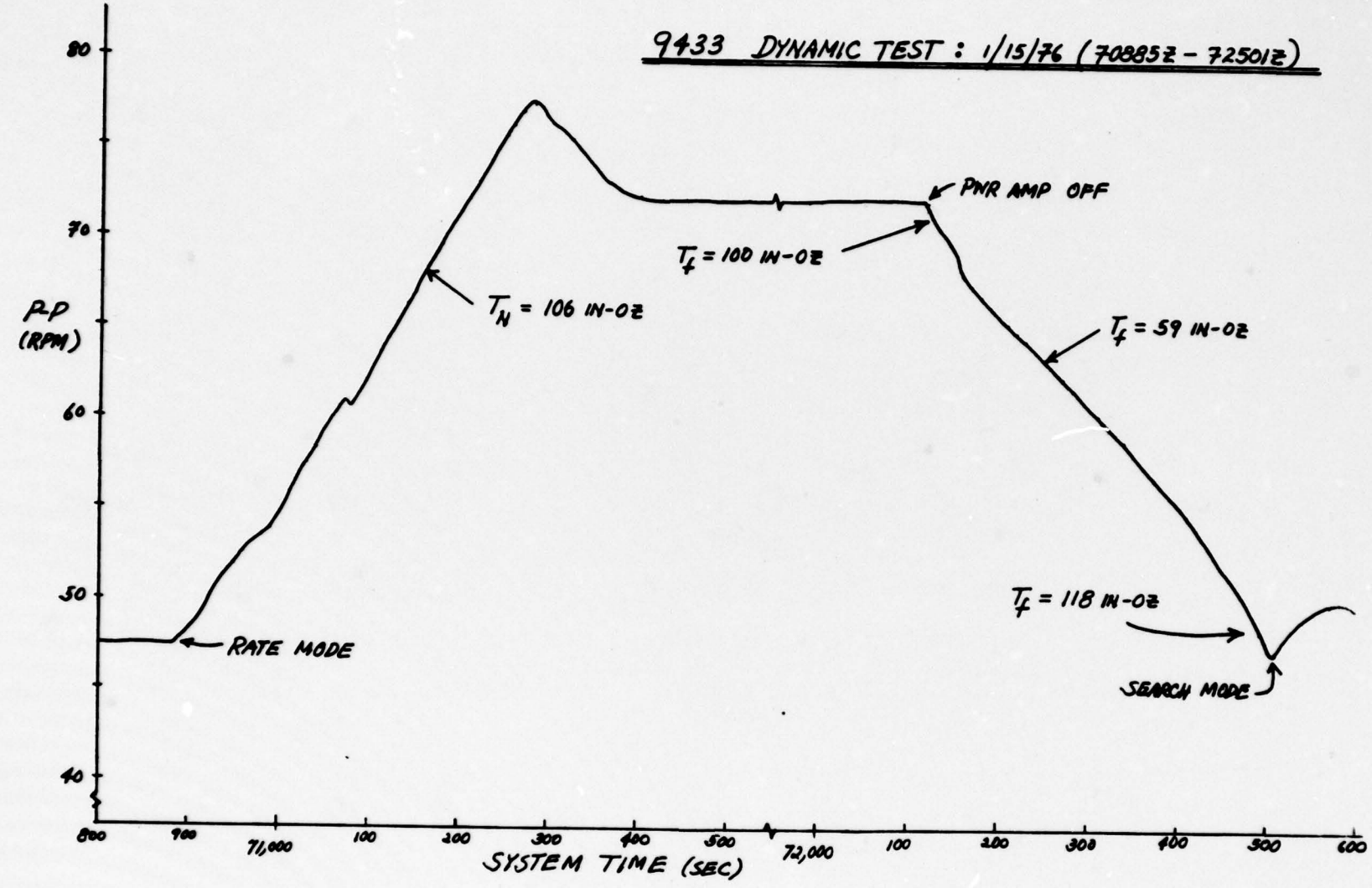


Figure 3.6-1. 9433 Dynamic Test: 1/15/76 (70885Z-72501Z)

$$T_N = \frac{192 I_R I_P}{954.93(I_R + I_P)} \cdot \Delta\Omega = 11.8\Delta\Omega \text{ in-oz}$$

where I_R = 333 slug-ft^2, I_p = 71 slug-ft^2, and $\Delta\Omega$ is the change in relative rate (P-P) in rpm during a 100 second interval. Again steady-state control while overspun was smooth and the bearing temperatures were seen to decrease. Rundown showed torque variations, with the largest torque occurring when the despun condition was approached. This data is generally comparable to the friction test data of 30 September 1975 shown in Figure 3.4-4.* By comparison, the friction level was generally lower in these more recent tests but showed greater variations (a characteristic noted at various times since 28 November 1975).

Following this runup/rundown cycle, Normal Mode operation was attempted and sustained for approximately two minutes (step 6). A second runup to 72.1 rpm was then executed (step 7, Figure 3.6-2). Notice the striking difference between the runup periods of Figure 3.6-1 and 3.6-2 which (given no change in friction characteristics) should have been identical. The apparent decrease in friction as overspin increases is also of interest.

At this stage, it was apparent that friction level (or at least friction transients) are decreased by introducing a platform inertial rate (which, due to the platform mass unbalance, causes sideloads on the DMA). In order to examine this phenomenon further, the platform was spun down in stages (from an inertial rate of about 20 rpm, to 10 rpm, to 5 rpm, and then despun) as noted in steps 8, 9, and 10. A general decrease in the quality of rate control was noted as the platform inertial rate was decreased. However, no abrupt transition at a particular speed was observed; rather, the change in performance quality appeared to be gradual.

The rotor rate was next increased to 59.9 rpm (step 11), closely approximating its despun value at the time of the friction tests of

---

* However, in those tests, the despun rate was, at all times, 60 rpm.

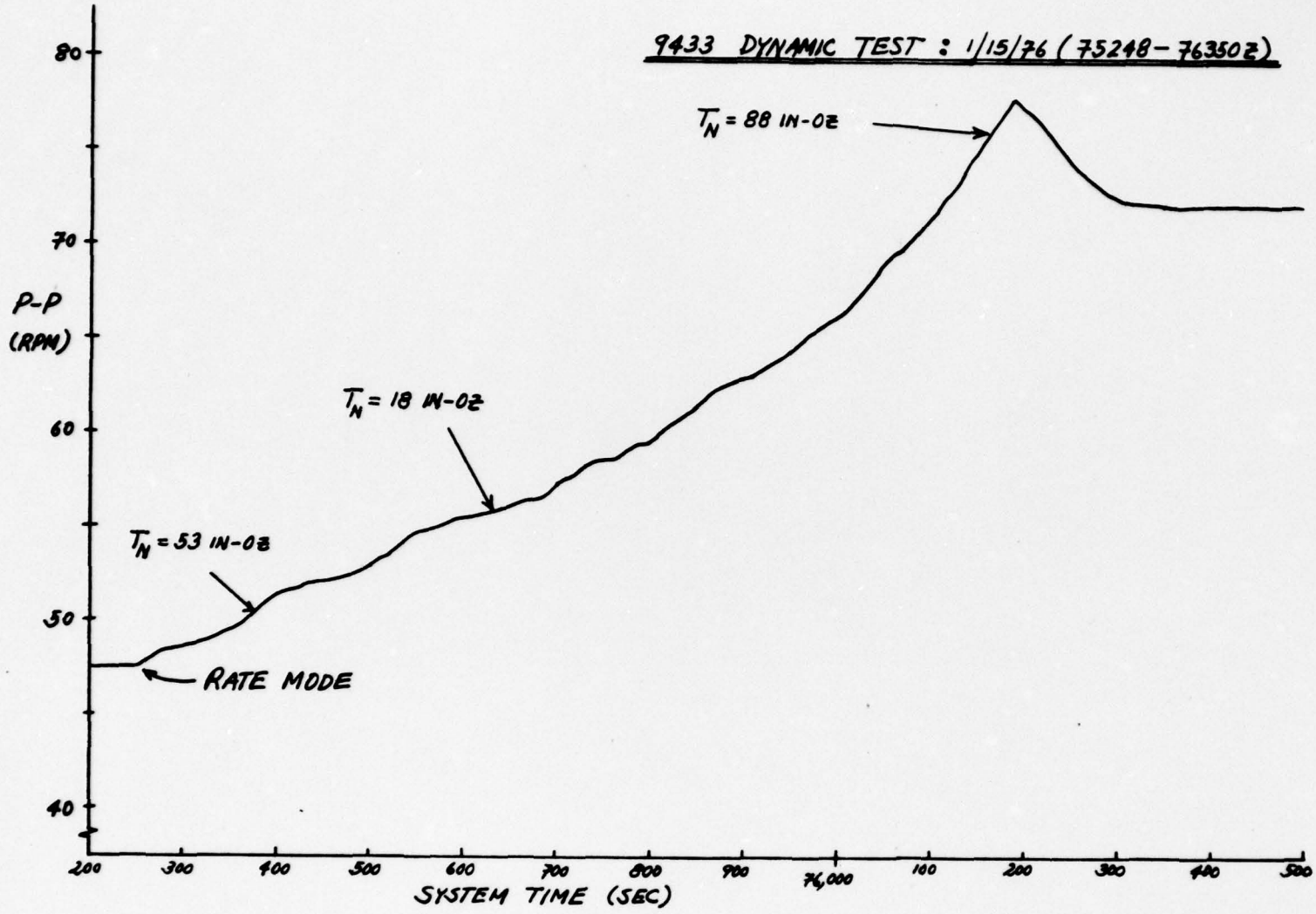


Figure 3.6-2. 9433 Dynamic Test: 1/15/76 (75248-76350Z)

30 September 1975. The platform was then overspun to 84.8 rpm and then allowed to despin to 35.4 rpm by turning off the DEA power amplifier (steps 12 and 13, Figure 3.6-3). Notice that the overspin rate was easily reached (compared to Figure 3.4-2 where the same equipment was in use), with net torques higher than before (and, therefore, lower friction torques). Rundown also showed lower friction torques than in Figure 3.4-2. Note also that the friction torque was highest (but not markedly so) near the despun condition (60 rpm).

As the final step, the platform was driven back up to a relative rate of 84.8 rpm by re-activating the DEA power amplifier. This operation is shown in Figure 3.6-4, which shows a performance characteristic which contrasts markedly with the data of Figure 3.6-3, while showing a similarity of the data of Figure 3.6-2. Note that maximum friction again occurs near the despun condition.

A review of the orbital dynamic test results yields the following conclusions:

- Overspin of the platform results in quieter rate control. This is (apparently) a monotonic function of the overspeed bias. Underspin may give the same result but was not tested as a steady-state condition.
- The reduction in rate errors while overspun is probably due to a reduction in the amplitude and/or frequency of torque transients. Average torques are still higher than nominal (torque voltage $\sim$-1.0 volt to -2.0 volts in the period from 76350Z to 80816Z).
- Runup and rundown data are not repeatable. Based on limited data, a bistable situation may exist (i.e., Figure 3.6-1 compares well with Figure 3.6-3, while Figure 3.6-2 compares well with that portion of Figure 3.6-4 above the 60 rpm level).
- The runup and rundown data also tends to indicate higher friction torques at despun speeds than while overspun or underspun.
- Sideloads due to platform unbalance are probably the factor causing the speed dependence of friction.

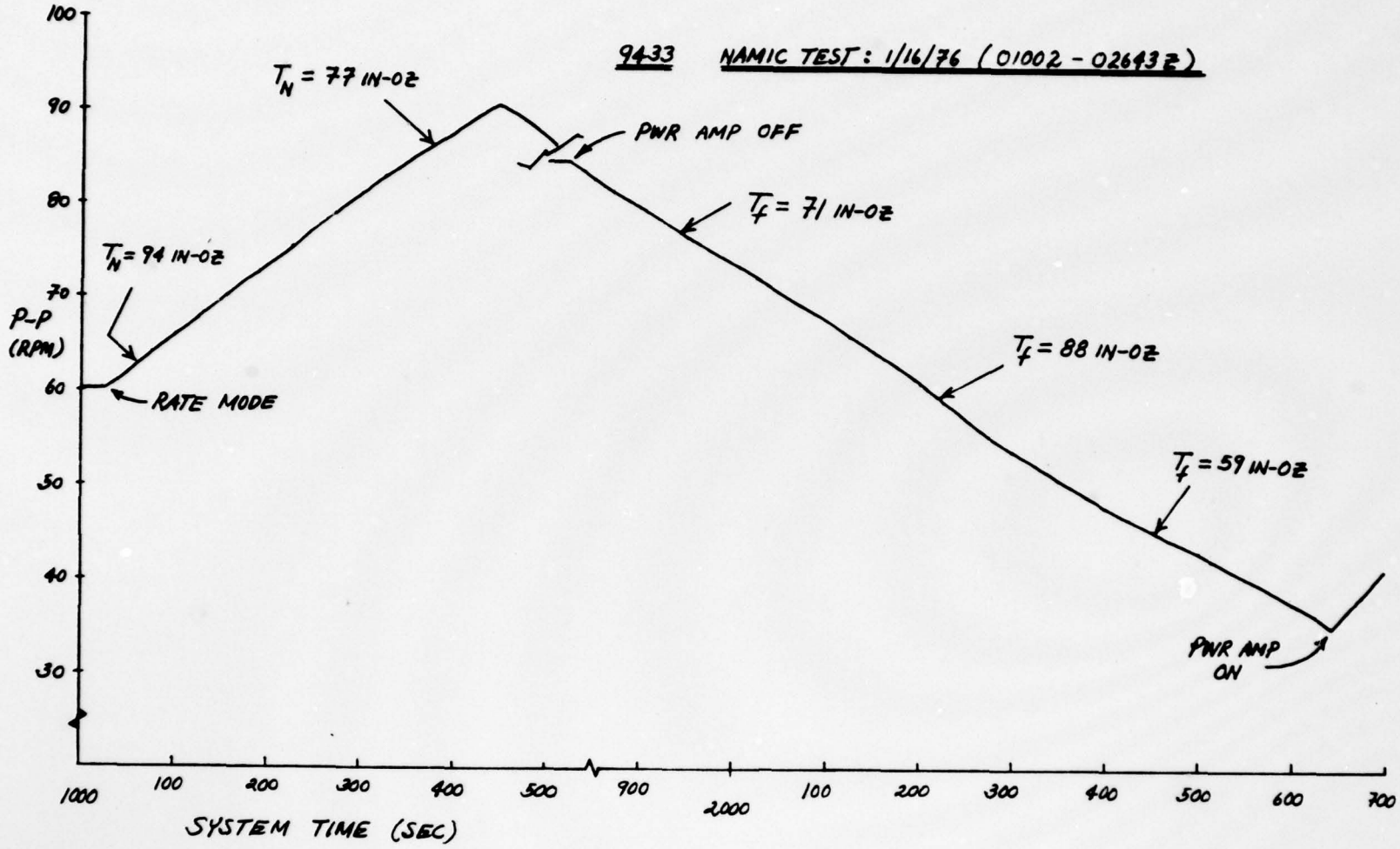


Figure 3.6-3. 9433 Dynamic Test: 1/16/76 (01002-02643Z)

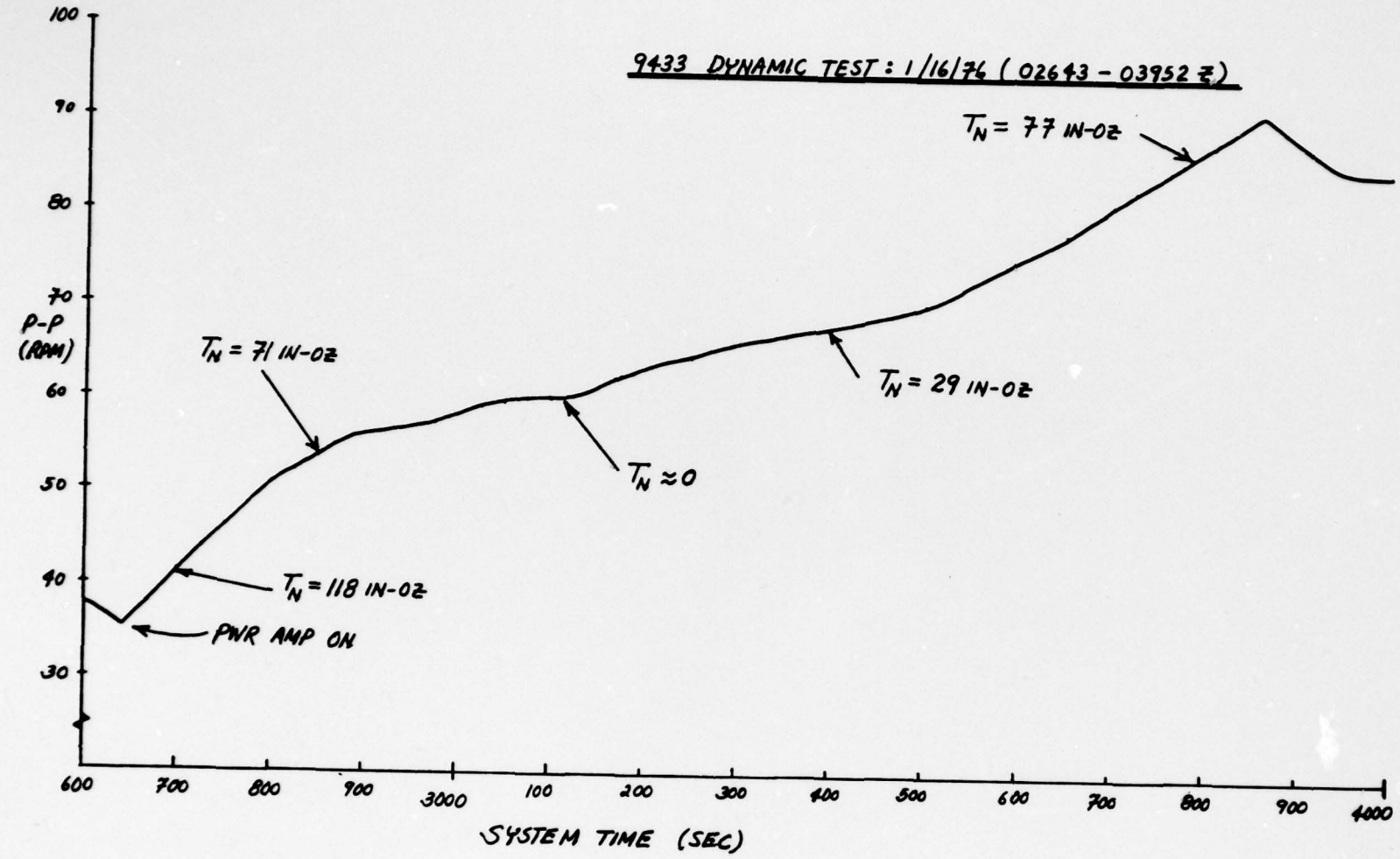


Figure 3.6-4. 9433 Dynamic Test: 1/16/76 (02643-03952Z)

4. FAILURE MODES AND EFFECTS

Table 4-1 delineates potential failure modes related to the 9433 despin control anomaly. These failure mechanisms are grouped according to location, considering the three modules of the DMA and factors external to the DMA. For each failure mode, the anticipated performance characteristics are described. A final column indicates the basis of the performance characterization. These bases are analyses, tests, consultant experience (Appendix G), and inference (i.e., engineering judgment).

These failure modes are presented without reference to their likelihood of occurrence nor their consistency with orbital data. Section 11 discusses the correlation of these failure modes with orbital data, drawing conclusions regarding their relationship to the 9433 despin control anomaly.

TABLE 4-1. 9433 FAILURE MODES AND EFFECTS

Failure Mode	Anticipated Performance Characteristics	Basis
1. STRUCTURAL MODULE		
1.1 Axial restriction of preload mechanism due to debris, galled shaft, structural distortions,etc	Moderate (e.g., 20 in-oz) increase in torque above nominal value (30 in-oz), correlated with temperature; no significant torque transients.	Analysis (Appendix B, Section 5); Test data (Section 6).
1.2 Degradation of lubrication (depletion, polymerization, etc.)	Rise in running torque; large torque transients, with possible return to near nominal level at times; eventual bearing failure.	Consultant data based on bearing tests to failure (Section 10, Appendix G).
1.3 Structural distortions causing loss of dimensional clearances, change in bearing contact angle, bearing tilt, etc.	Similar to Item 1.1.	See Item 1.1.
1.4 Metallic debris in bearings (from assembly defects, motion of bearing inner race on shaft, etc.)	Short-term torque transients; lubricant degradation due to debris piercing film, leading to results of Item 1.2.	Consultant data (Appendix G); test data (Section 6).
1.5 Retainer whirl due to classical retainer instability	Short-term torque transients of 5-15 in-oz amplitude (assuming normal lubrication, etc); no increase in average torque; no long-term degradation.	Previous studies (1973); open literature on retainer dynamics and effects.

TABLE 4-1. 9433 FAILURE MODES AND EFFECTS, CONTINUED

Failure Mode	Anticipated Performance Characteristics	Basis
1.6 Excessive lubricant in bearings or bridging gap at labyrinth seal.	Increase in torque level with significant speed and thermal dependence.	Inference based on viscous friction model.
1.7 Main bearing jammed by wear debris, fractured retainer, etc.	Bearing balls slide in raceway and/or bearings rotate as journals; torque increase of several hundred in-oz.	Analysis (Appendix B); test data (Section 6).
1.8 Mechanical interference at magnetic pipper (MPU)	Once per revolution torque pulse until material is worn away; MPU performance should be affected; repeatable stopping position.	Inference based on DMA design.
2. POWER MODULE		
2.1 Mechanical interference at snubber, motor, or resolver due to tolerance build-up assembly errors, dimensional instability.	Gradual onset of increased running torque (if due to material instability); interference could be increased or eliminated by wear/build-up effects in vacuum; significant torque transients possible.	Inference (Appendix B); test data (Section 6).
2.2 Debris in gap(s) due to foreign particles, fracture of motor or resolver lamination, etc.	Torque transients which should be eliminated by rejection of debris; no increase in average torque.	Inference.
2.3 Fracture and loosening of motor hypernik ring.	Jamming and lock-up of motor; permanent stall condition.	Test data (Section 6).

TABLE 4-1. 9433 FAILURE MODES AND EFFECTS, CONTINUED

Failure Mode	Anticipated Performance Characteristics	Basis
2.4 Breakdown in motor winding insulation resulting in shorted windings	Increase in power consumption, decrease torque capability, decrease in back emf for affected motor; speed-dependent increase in drag torque during unpowered run-down.	Inference based on motor and DMA design; test data (Section 6).
2.5 Open motor or resolver winding (or electronics failure)	Little or no torque from affected drive channel (significant performance reduction)	Inference based on DMA design.
3. SLIP RING MODULE		
3.1 Bearing related effects as noted under Items 1.2, 1.3, 1.4, 1.6	Effects similar to those noted under Structural Module entries; torques of much lower amplitude due to smaller bearing diameters.	See Structural Module entries.
3.2 Bearing jammed by wear debris, fractured retainer, etc.	Relatively large friction torques possible as bearings rotate as journals; sustained torquer unlikely due to wear effects; performance on slip rings adjacent to bearings should be affected.	Test data (Section 6); inference based on metered properties and mechanical configuration.
3.3 Deterioration of slip ring/brush mechanical interface due to excessive wear or change in mechanical configuration	Slight increase in average torque level; significant deterioration in performance of affected circuits.	Inference based on design.

TABLE 4-1. 9433 FAILURE MODES AND EFFECTS, CONTINUED

Failure Mode	Anticipated Performance Characteristics	Basis
4. NON-DMA EFFECTS		
4.1 Interference produced by thermal insulation material which has loosened from platform or rotor	Potentially large torque transient; persistent torques unlikely due to clearing effect as relatively flimsy material is "chewed up" or pushed away by mechanical action; should be anomalous spacecraft thermal signature, correlated to specific insulation degradation.	Inference based on spacecraft design, material properties, and dynamics (Appendix H).
4.2 Interference produced by HLTWT heater control harness peeling loose and catching on gas balance lines or spun beams	Similar to Item 4.1, except for absence of thermal signature.	See Item 4.1.
4.3 Interference at platform-caging pin-puller due to incomplete retraction	Once-per-revolution torque pulses, persisting until mechanical wear clears the interference; repeatable stopping positions in fully spun-up condition.	See Item 4.1.

5. THERMAL/DIMENSIONAL ANALYSES

5.1 Thermal Analyses

The thermal analysis activities consisted of:

1) To simulate the detailed temperature profile behavior using telemetry data for boundary conditions and check points.

2) Modification of the Ball Brothers thermal model of the DMA to provide an analytical tool to simulate the S/C 9433 DMA thermal behavior

3) Utilization of the DMA thermal model to assist mechanical designers in their investigation of possible failure mechanisms.

To establish a credible thermal model for simulating the DMA thermal behavior in orbit, an existing Ball Brothers Research Corporation thermal model was modified by TRW to accommodate actual S/C 9433 boundary conditions and torque motor thermal characteristics. This modified DMA thermal model was further refined into a second model which closely examined the motor shaft.

A. Thermal Model Verification. The DMA heater on activity of 8-9 September was selected for simulation since it offered a long transient heating duration with continuous temperature and error voltage (torque motor power) telemetry. This activity also offered long term data on the response of heater thermostats.

The results of the heater activity simulation showed good correlation with the flight telemetry as shown in Figure 5.1-1. In this simulation, all the friction increase (81 in-oz) was placed in the top bearing, distributed equally between its inner and outer rings. The slow DMA transient response implied that most of the DMA induced heating is quickly absorbed by the spacecraft compartments and may therefore mask any local heating effect. The heater thermostat's response was 90°F open and 89°F close.

B. Steady State Thermal Simulation. The DMA temperature telemetry for the 1974 year is comparable to that of 1975 prior to September 1. After this date, the telemetry showed an increased temperature gradient from a previous 4°F level to 7°F between the upper and lower main bearings which would indicate an increase in energy dissipation in the upper portion

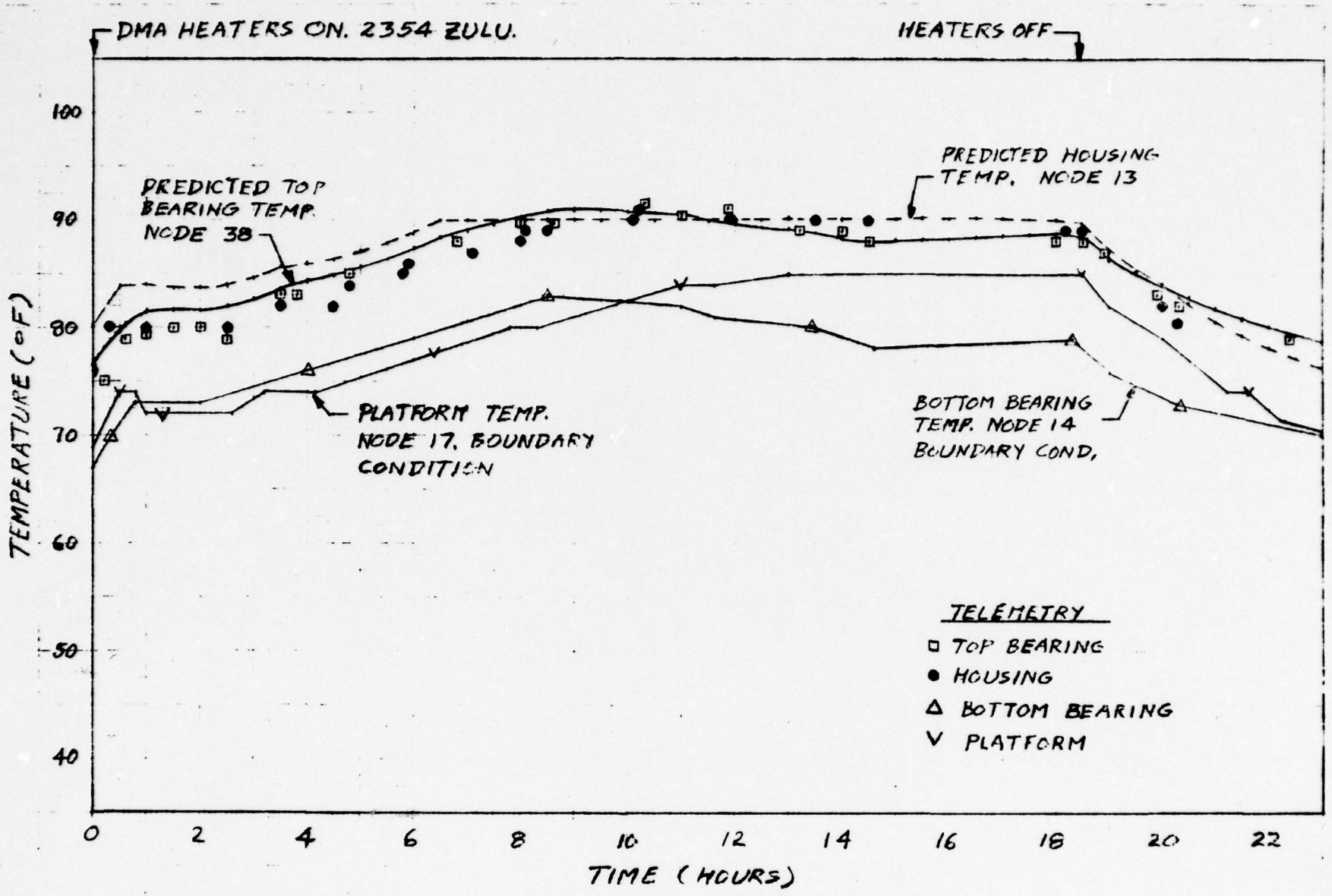


Figure 5.1-1. Temperature Simulation DMA Heater Test
September 8, 1975
Top Main Bearing Drag 96 oz-in.

of the DMA. This gradient increased still further during the heater-on activities of September 8-9, but it returned to the pre-heater-on level after the termination of the heater activity.

In order to gain some insight to the DMA anomaly and thermal behavior, several postulated failure mechanisms were introduced into the thermal model, and their outputs (modal temperatures) are compared with the telemetered data. The telemetry information of 13 November 1975 was selected for this case because of the relatively stable state of the DMA. Figure 5.1-2 shows the location of nodes in the thermal model. Table 5.1-1 lists the boundary conditions, check points, and the predicted temperatures based on 9 postulated cases.

It can be seen from Table 5.1-1 that Case 6 (for example) correlates well to the telemetry data and that the temperature gradient between top and bottom bearing thermistors agrees with the 7°F telemetry data. It must be pointed out, however, because of the limited telemetry data and the small temperature differences among all the postulated cases, the simulation results can be considered only consistent rather than conclusive. Table 5.1-2 lists the ciritical temperature gradients in the DMA, for consideration, in dimensional analysis.

A second steady-state simulation was performed using higher boundary conditions from 13 September telemetry data: platform interface temperature of 85°F; 60 rpm; and 116 in-oz total torque. The outputs are tabulated in Table 5.1-3 and the critical temperature gradients are listed in Table 5.1-4.

One important observation derived from these two simulations is that the motor power increase due to higher friction load has a more dominant thermal effect that the bearing friction itself. Temperature gradients remained insignificant in the structure module regardless of bearing friction value or location; larger gradients are developed in the power module due to motor power dissipation. This conclusion is further substantiated by the DMA temperature predictions based on motor power dissipation as tabulated in Table 5.1-5.

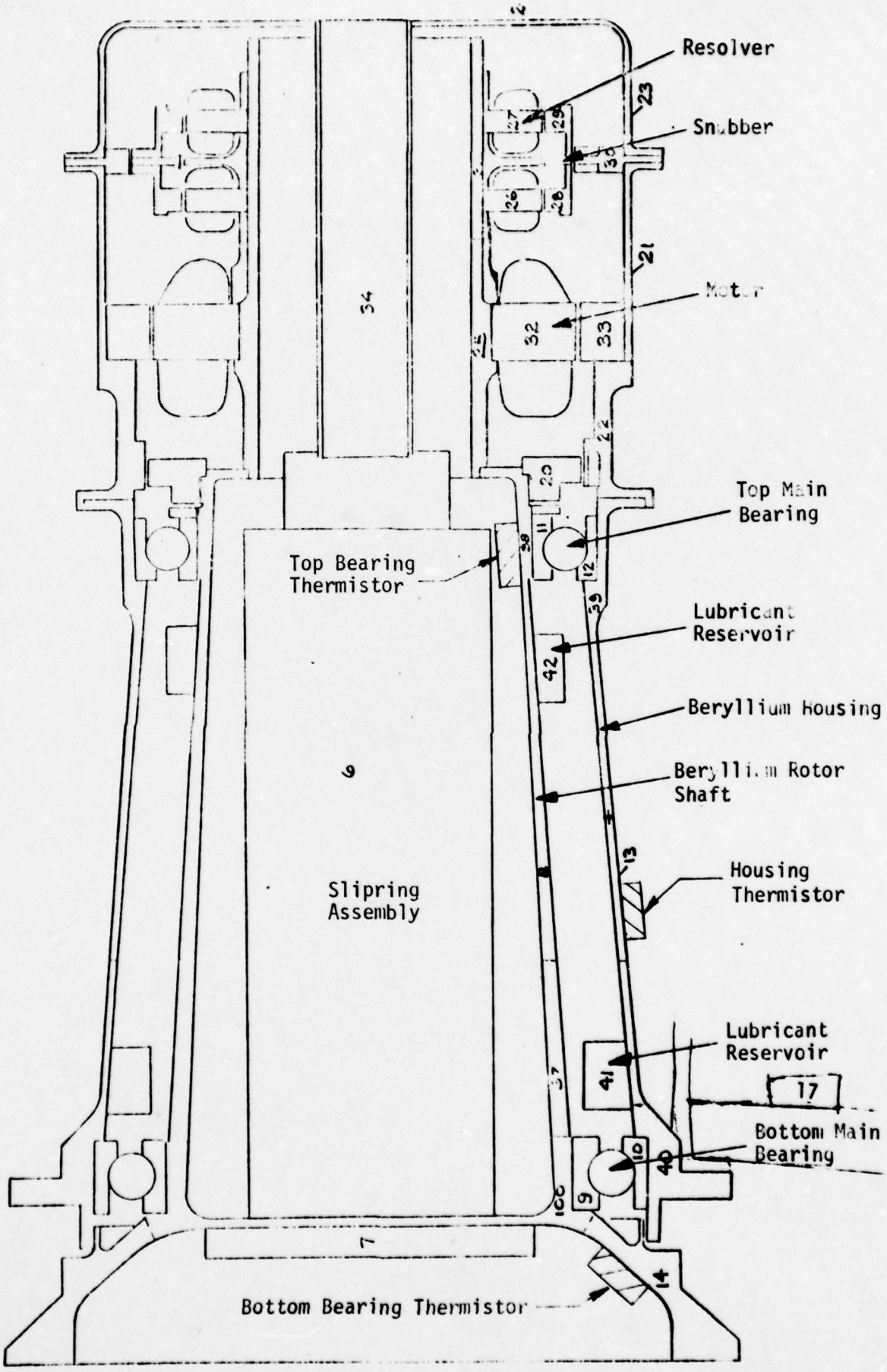


Figure 5.1-2. 38 Node Thermal Model, DMA

Table 5.1-1. Steady State Simulation Outputs (Nov. 13, 1975 Telemetry Boundary Condition)

BOUNDARY CONDITIONS:

SPIN RATE - 40 RPM
TOTAL TORQUE - 100 IN-OZ
PLATFORM TEMPERATURE - 61°F (NODE 17)
BOTTOM BEARING THERMISTOR - 69°F (NODE 14)

CHECK POINTS:

TOP BEARING THERMISTOR - 76°F (NODE 38)
HOUSING THERMISTOR - 66°F (NODE 13)

DMA Item	Thermal Model Node Number	Predicted Temperature (°F)									
		Case 1 Nominal Operation. Total Drag 29.2 oz-in	Case 2 Oil Loss at Bottom Bearing/Shaft Interface Total Drag 29.2 oz-in	Case 3 Increase Drag to 80 oz-in in Bottom Bearing	Case 4 80 oz-in Drag + Preload Washer Contact	Case 5 Oil Loss at Top Bearing/Shaft Interface Total Drag 29.2 oz-in	Case 6 Increase Drag to 80 oz-in in Top Bearing	Case 7 80 oz-in Drag + Preload Washer Contact	Case 8 80 oz-in Drag in Top Bearing. Oil Loss Race/Bore	Case 9 71 oz-in Drag at Snubber	
Top Main Bearing											
Inner Race	11	67.8	67.9	74.7	74.9	65.3	76.4	76.5	81.0	75.[illegible]	
Outer Race	12	65.2	65.0	73.7	73.7	64.5	75.3	75.3	76.5	[illegible].5	
Oil Reservoir	42	67.2	67.1	73.5	73.5	67.3	74.7	74.7	74.3	74.4	
Thermistor	38	68.2	68.2	74.7	74.7	68.6	76.0	76.0	75.0	[illegible]	
Bottom Main Bearing											
Inner Race	9	68.5	62.9	69.8	69.8	68.5	69.7	69.7	69.6	[illegible].7	
Outer Race	10	62.6	62.0	64.6	64.6	62.5	64.4	64.4	64.6	64.5	
Oil Reservoir	41	68.1	68.1	70.3	70.3	68.2	70.5	70.5	70.3	70.4	
Thermistor *	14	69.0	69.0	69.0	69.0	69.0	69.0	69.0	69.0	69.0	
Housing											
Upper	34	65.0	64.8	73.6	73.6	64.4	74.9	75.0	75.9	75.5	
Middle (corrected)	13	63.3	63.0	67.5	67.5	63.1	67.9	67.9	68.4	68.2	
Lower	40	62.3	61.9	64.2	64.2	62.2	64.2	64.2	64.3	64.3	
Rotor Shaft											
Upper	38	68.0	68.2	74.7	74.7	68.6	76.0	76.0	75.0	75.4	
Middle	8	68.2	68.4	72.2	72.2	68.5	72.8	72.8	72.2	72.5	
Lower	37	68.4	68.7	70.5	70.5	68.6	70.7	70.7	70.5	70.6	
Motor											
Winding	32	76.1	76.0	184.7	184.6	76.0	185.7	185.6	185.9	191.1	
Rotor	33	66.0	65.8	80.3	80.3	65.5	81.6	81.6	82.5	83.8	
Snubber											
Inner Ring	31	72.3	72.2	130.0	130.1	72.1	131.2	131.1	131.6	146.2	
Outer Ring	30	66.3	66.1	81.0	81.0	65.8	82.2	82.3	83.1	85.2	
Platform *	17	61.0	61.0	61.0	61.0	61.0	61.0	61.0	61.0	61.0	

NOTE: THE LUBRICANT RESERVOIR (NODE 41) WAS MISTAKENLY ATTACHED TO THE SHAFT (NODE 37) IN THE COMPUTER INPUT; THEREFORE DISREGARD THEIR ΔT.

Table 5.1-2. Critical Temperature Gradients from Steady-State Simulation (November 13, 1975, Telemetry)

	CASE NO.								
	1	2	3	4	5	6	7	8	9
Top bearing thermistor	68.2	68.2	74.7	74.7	68.6	76.0	76.0	75.0	75.4
Housing thermistor	63.3	63.0	67.5	67.5	63.1	67.9	67.9	68.4	68.2
ΔT's:									
Top-bottom thermistors (38-14)	-.8	-.8	5.7	5.7	-.4	7.0	7.0	6.0	6.4
Bottom bearing ID-OD (9-10)	5.9	.9	5.2	5.2	6.0	5.3	5.3	5.0	5.2
Top bearing ID-OD (11-12)	2.6	2.9	1.0	1.2	.8	1.1	1.2	4.5	-0-
Motor winding - stator (32-33)	10.1	10.2	104.4	104.3	10.5	104.1	104.0	103.4	107.3
Snubber inner-outer (31-30)	6.0	6.1	49.0	49.1	6.3	49.0	48.8	48.5	61.0
Housing - shaft (8-13)	4.9	5.4	4.7	4.7	5.4	4.9	4.9	3.8	4.3

Table 5.1-3. Steady State Outputs (Sept 13, 1975 Telemetry Boundary Conditions Telemetry Boundary Conditions

BOUNDARY CONDITIONS:

SPIN RATE - 60 RPM
TOTAL TORQUE - 116 OZ-IN
PLATFORM TEMPERATURE - 85°F
BOTTOM BEARING THERMISTOR - 80°F

DMA Item	Thermal Model Node Number	Predicted Temperature (°F) Case 1 Nominal Operation. Total Drag 29.2 oz-in	Case 2 Oil Loss at Bottom Bearing/ Shaft Total Drag 29.2 oz-in	Case 3 Increase Drag to 96 oz-in in Bottom Bearing	Case 4 96 oz-in Drag + Preload Washer Contact	Case 5 Oil Loss at Top Bearing/ Shaft Total Drag 29.2 oz-in	Case 6 Increase Drag to 96 oz-in in Top Bearing	Case 7 96 oz-in Drag + Preload Washer Contact	Case 8 96 oz-in Drag in Top Bearing. Oil Loss Race/Bore		
Top Main Bearing											
Inner Race	11	82.4	82.3	91.6	92.5	83.7	94.7	95.5	110.8		
Outer Race	12	84.3	84.5	95.9	96.8	85.2	98.7	99.7	103.7		
Oil Reservoir	42	82.7	82.7	91.5	92.1	82.5	93.5	94.2	92.9		
Thermistor	38	82.1	82.0	91.1	91.7	81.4	93.4	93.9	90.7		
Bottom Main Bearing											
Inner Race	9	80.8	85.8	82.7	82.8	80.7	82.6	82.7	82.2		
Outer Race	10	84.5	85.1	87.4	87.6	84.6	87.2	87.3	87.8		
Oil Reservoir	41	81.2	81.2	84.3	84.5	81.1	84.6	84.8	84.2		
Thermistor	14	80.0	80.0	80.0	80.0	80.0	80.0	80.0	80.0		
Housing											
Upper	39	84.4	84.6	96.1	97.0	85.1	98.5	99.4	102.7		
Middle (corrected)	13	84.5	84.7	90.5	90.9	84.8	91.3	91.8	93.3		
Lower	40	84.6	84.9	87.3	87.5	84.8	87.3	87.5	88.0		
Rotor Shaft											
Upper	38	82.1	82.0	91.1	91.7	81.4	93.4	93.9	90.7		
Middle	8	81.4	81.3	86.8	87.1	81.1	87.9	88.3	86.5		
Lower	37	80.9	80.7	83.8	83.9	80.7	84.1	84.3	83.5		
Motor											
Winding	32	92.3	92.4	226.1	234.5	92.4	227.9	236.3	236.9		
Rotor	33	84.6	84.8	104.0	105.6	85.2	106.3	107.9	111.9		
Snubber											
Inner Ring	31	89.1	89.2	159.1	163.5	89.4	160.9	165.3	166.7		
Outer Ring	30	84.5	84.7	104.4	106.0	85.2	106.7	108.3	111.2		
Platform	17	85.0	85.0	85.0	85.0	85.0	85.0	85.0	85.0		

NOTE: THE LUBRICANT RESERVOIR (NODE 41) WAS MISTAKENLY ATTACHED TO THE SHAFT (NODE 37) IN THE COMPUTER INPUT; THEREFORE DISREGARD THEIR ΔT.

Table 5.1-4. Critical Temperature Gradients From Steady State Simulation (September 13, 1975 Telemetry)

ΔT, °F	CASE NO. 1	2	3	4	5	6	7	8	9
Top-Bottom Thermistors (38-14)	2.1	2.0	11.1	11.7	1.4	13.4	13.9	10.7	
Bottom Bearing ID-OD (9-10)	-3.7	.7	-4.7	-4.8	-3.9	-4.6	-4.6	-5.6	
Top Bearing ID-OD (11-12)	-1.9	-2.2	-4.3	-4.3	.5	-4.0	-4.2	7.1	
Motor Winding - Stator (32-33)	7.7	7.6	122.1	128.9	7.2	121.6	128.4	126.0	
Snubber - Inner-Outer (31-30)	4.6	4.5	54.7	57.5	4.2	54.2	57.0	55.5	
Housing - Shaft (8-13)	-3.1	-3.4	-3.7	-3.8	-3.7	-3.4	-3.5	-6.8	

Table 5.1-5. Effect of Motor Power Dissipation on DMA Steady State Steady State Temperature Prediction

DMA Item	Thermal Model Node Number	Nominal Operating Torque - 29.2 oz-in, 60 rpm						96 oz-in Drag in Upper Main Bearing; 116 oz-in Total DMA Torque, 60 rpm					
		Case 1 6 Watts Motor Dissipation	Case 2 10 Watts Motor Dissipation	Case 3 15 Watts Motor Dissipation	Case 4 20 Watts Motor Dissipation	Case 5 30 Watts Motor Dissipation	Case 6 40 Watts Motor Dissipation	Case 7 6 Watts Motor Dissipation	Case 8 10 Watts Motor Dissipation	Case 9 15 Watts Motor Dissipation	Case 10 20 Watts Motor Dissipation	Case 11 30 Watts Motor Dissipation	Case 12 40 Watts Motor Dissipation
Top Main Bearing													
Inner Race	11	85.7	88.2	91.2	94.2	99.9	105.7	89.2	91.7	94.7	97.6	103.4	109.1
Outer Race	12	88.3	91.5	95.4	99.4	107.4	115.4	91.7	94.8	98.7	102.7	110.7	118.6
Oil Reservoir	42	85.8	88.2	91.0	93.9	99.5	105.0	88.3	90.7	93.5	96.4	101.9	107.4
Thermistor	38	85.4	87.8	90.7	93.5	99.1	104.5	88.1	90.4	93.3	96.2	101.7	107.2
Bottom Main Bearing													
Inner Race	9	81.3	81.7	82.1	82.6	83.5	84.4	81.7	82.1	82.6	83.0	83.9	84.8
Outer Race	10	85.3	85.9	86.6	87.4	88.9	90.4	85.8	86.4	87.2	87.9	89.4	90.9
Oil Reservoir	41	82.2	82.9	83.8	84.7	86.5	88.2	83.0	83.7	84.6	85.5	87.3	89.0
Thermistor *	14	80.0	80.0	80.0	80.0	80.0	80.0	80.0	80.0	80.0	80.0	80.0	80.0
Housing													
Upper	39	88.5	91.6	95.6	99.7	107.8	115.9	91.3	94.4	98.4	102.5	110.6	118.7
Middle (corrected)	13	86.5	88.0	90.0	91.9	95.9	99.8	87.9	89.4	91.3	93.3	97.2	101.1
Lower	40	85.4	86.9	86.8	87.5	89.1	90.6	86.0	86.6	87.3	88.1	89.6	91.2
Rotor Shaft													
Upper	38	85.4	87.8	90.7	93.5	99.1	104.5	88.1	90.4	93.3	96.2	101.7	107.2
Middle	8	83.3	84.7	86.4	88.0	91.2	94.4	84.8	86.2	87.9	89.5	92.7	95.9
Lower	37	81.8	82.5	83.4	84.2	85.8	87.4	82.6	83.3	84.1	85.0	86.6	88.1
Motor													
Winding	32	148.2	168.1	225.9	262.1	324.5	377.3	150.4	187.0	227.6	263.7	325.9	378.5
Rotor	33	91.4	96.8	103.6	110.4	124.3	138.3	94.1	99.5	106.3	113.1	127.0	141.0
Snubber													
Inner Ring	31	118.4	137.6	158.9	177.8	210.6	238.7	120.7	139.8	160.8	179.6	212.3	240.3
Outer Ring	30	91.6	97.1	104.0	110.9	125.0	139.1	94.2	99.7	106.6	113.6	127.6	141.6
Platform *	17	85.0	85.0	85.0	85.0	85.0	85.0	85.0	85.0	85.0	85.0	85.0	85.0

*Fixed boundary condition from 13 September 1975 telemetry data.

C. Steady State Shaft Temperature Gradient Analysis. A more refined thermal model was used to map the circumferential thermal gradients of both motor and main bearing shafts. The results are shown in Figure 5.1-3. Because of the asymmetric motor winding configuration and heat distribution, circumferential gradient at the motor stack was 27°F. This shaft gradient dropped to 3°F at the snubber ring and 5°F at the interface of the motor and main bearing shafts. Due to the superior thermal conductivity of beryllium (bearing shaft) over titanium (motor shaft), no gradient appeared at the top bearing mounting diameter. This is indicative of no therma. distortion at the bearing/shaft interface.

D. Transient Simulation of Orbital Data. In addition to the simulation of September 8-9 heater-on activity, two other transient simulations were attempted.

- An on-orbit friction test was simulated and its predicted results are compared with the September 30, 1975, telemetry data, as plotted in Figure 5.1-4. (A 96 in-oz friction in the top bearing was used to simulate the orbital data.) The two main bearing temperatures correlate closely with the telemetry data, but the 2° to 3°F discrepancy between the telemetered and predicted housing temperatures could be caused by two factors:

  1) the platform thermistors might not establish an accurate boundary condition for the DMA; and
  2) the platform thermistor reading might be at its high end of tolerance.

  As a reference for dimensional analysis, the temperature gradients across the two main bearings and the snubber rings are plotted in Figure 5.1-5.

- The major friction transient occurring on 13 October was also simulated, and the comparative data was plotted in Figure 5.1-6. The key temperature gradients are recorded in Figure 5.1-7. The predicted temperatures are all within the tolerance range of telemetry data; note, however, that the simulation again predicted housing temperatures higher than observed in orbital data.

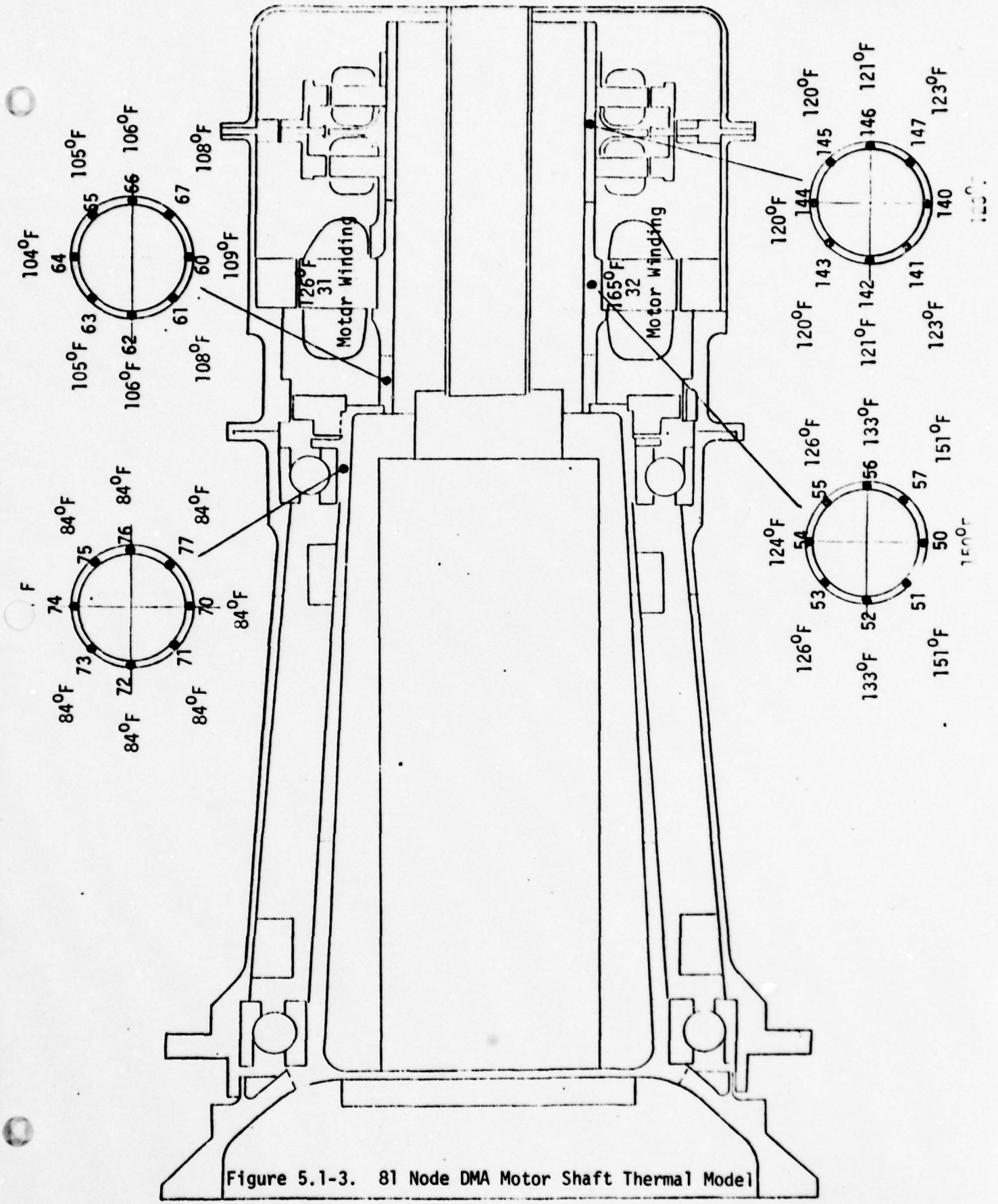


Figure 5.1-3. 81 Node DMA Motor Shaft Thermal Model

NO. 340-20 DIETZGEN GRAPH PAPER
20 X 20 PER INCH

EUGENE DIETZGEN CO.
MADE IN U. S. A.

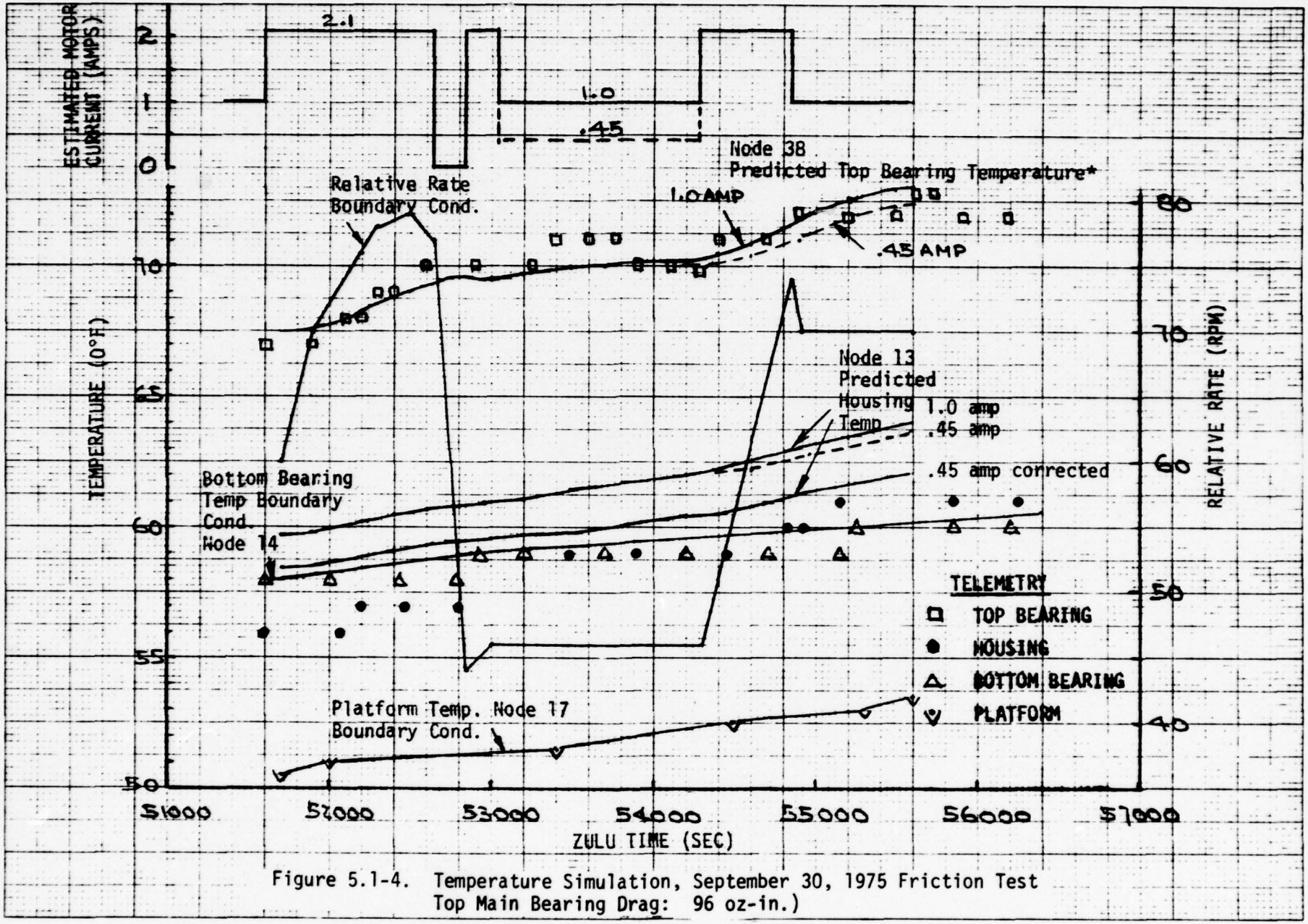


Figure 5.1-4. Temperature Simulation, September 30, 1975 Friction Test
Top Main Bearing Drag: 96 oz-in.)

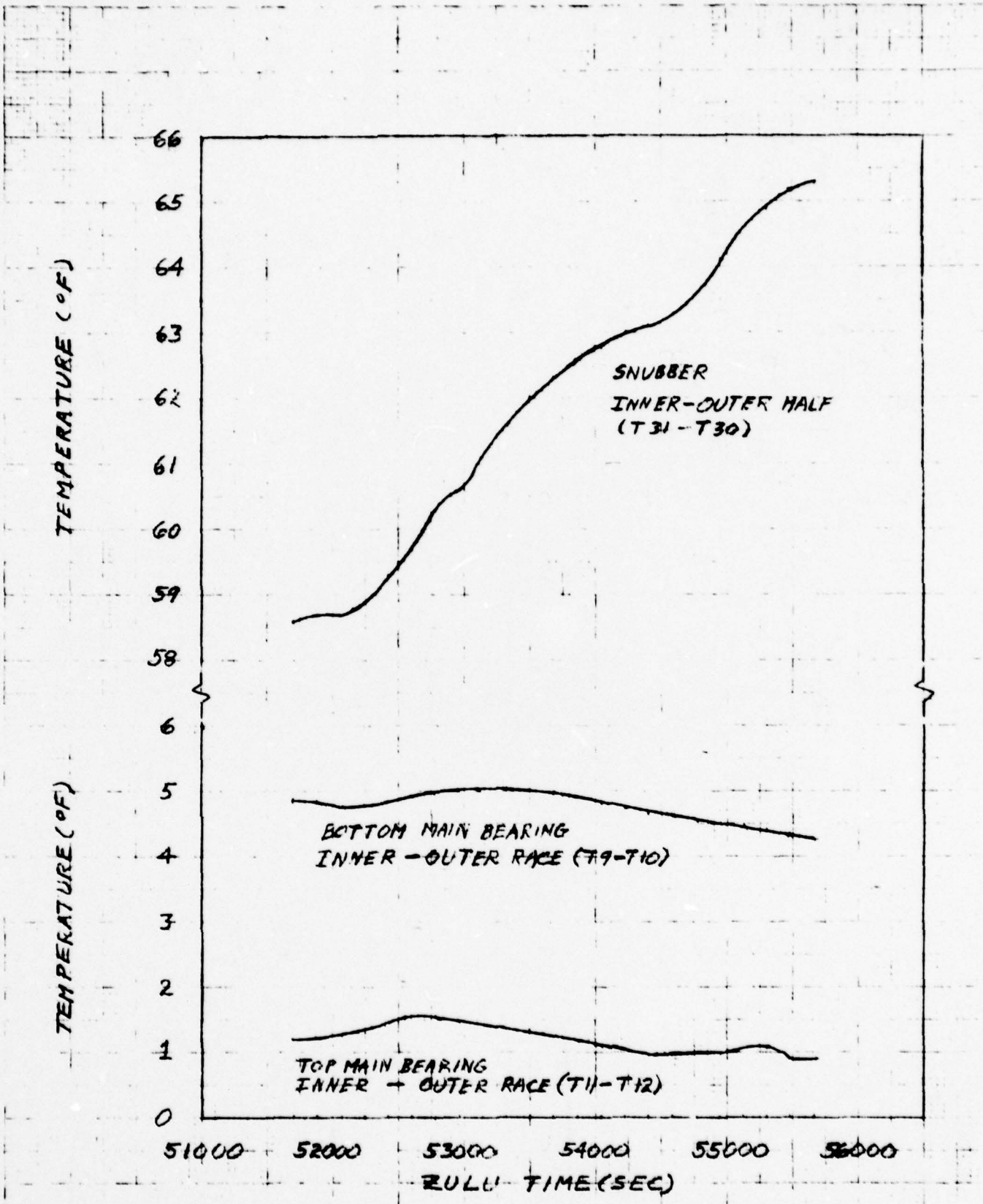


Figure 5.1-5. Thermal Gradients Temperature Simulation of September 30, 1975 Friction Test

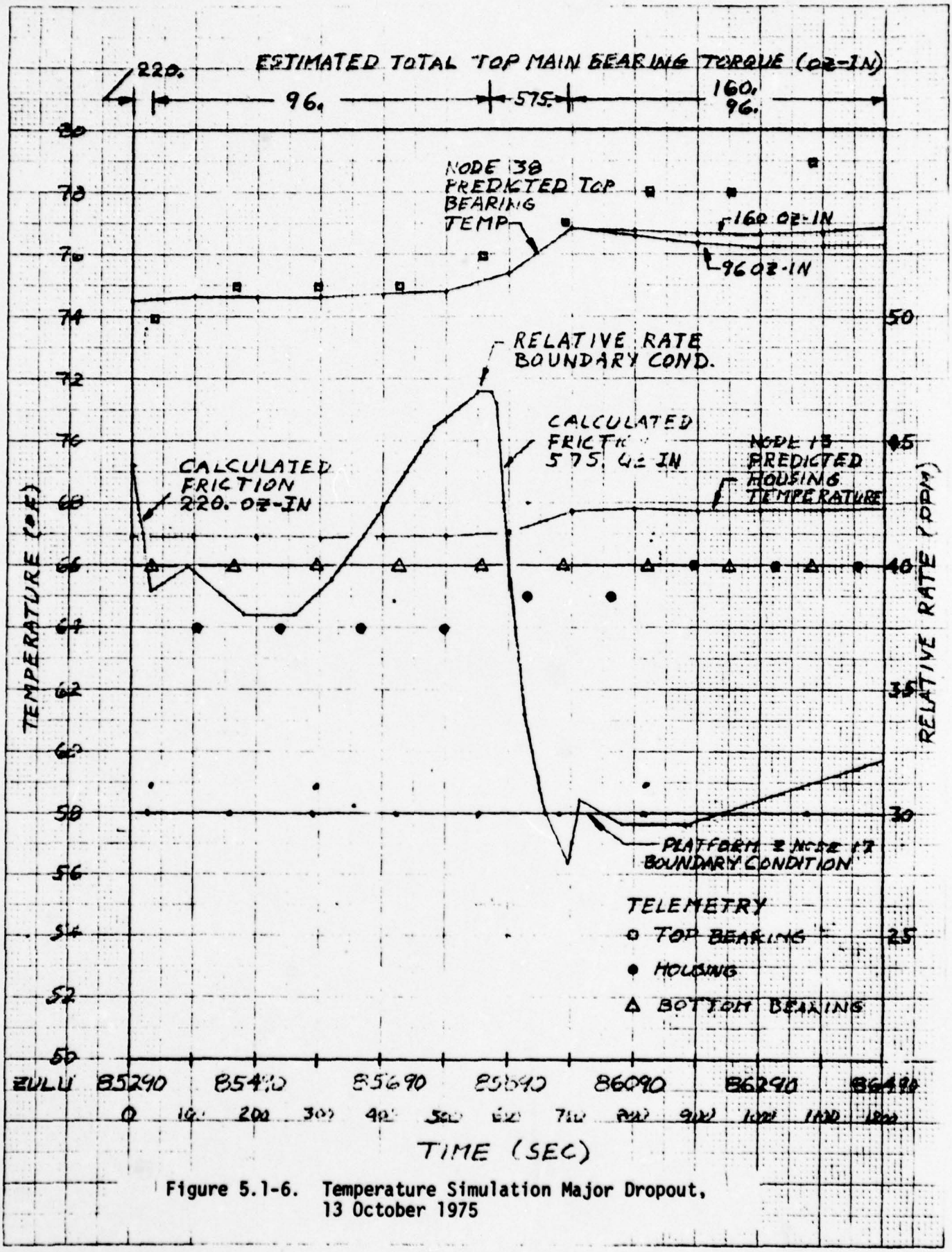


Figure 5.1-6. Temperature Simulation Major Dropout, 13 October 1975

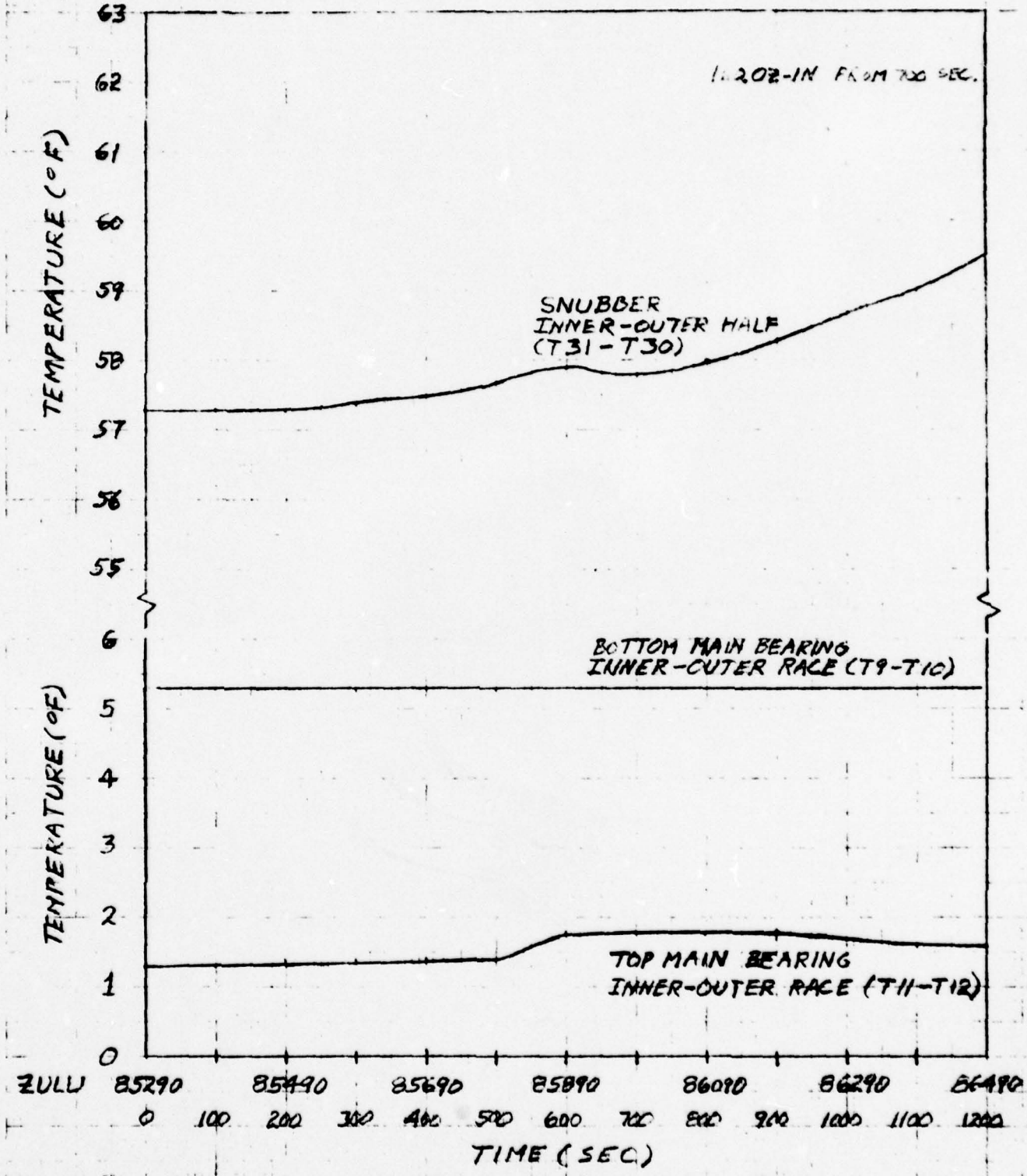


Figure 5.1-7. Thermal Gradients Temperature Simulation of 13 October 1975 Major Dropout

These runs were generated in an attempt to correlate periods of high friction torque with extreme values of critical thermal gradients (i.e., at the bearings and at the power module snubber). In the friction test data (Figure 5.1-4), the peak torque period is 52400Z to 53000Z; the only significant correlation is with the top bearing gradient (Figure 5.1-5), which is too small in magnitude to be of concern. The same conclusion can be applied to the second case (Figures 5.1-6 and 5.1-7). The thermal gradient at the snubber gap continues to grow (and, therefore, reduce the gap) throughout each run, well beyond the period of extreme torque. This data tends to suggest that interference at the snubber is not responsible for either the increase in average torque or the occasional large torque transients.

5.2 Dimensional Analyses

5.2.1 Introduction and Scope

The dimensional analyses represent an attempt to identify a design-dependent (i.e., predictable) malfunction mechanism, explaining the steady-state friction torque increase exhibited by the Despun Mechanical Assembly (DMA) of 9433. The anomaly is characterized by a steady-state torque demand from the DMA motor of approximately 90-100 in-oz and the random increases of that torque demand lasting for time periods of 60 ms or greater. The noted steady-state is a 55-65 in-oz demand increase with respect to the nominal level of 35 in-oz. This torque increment is the principal factor to which the malfunction mechanism will equate if indeed it is a true model of the observed anomaly.

The basic approach characterizing the analyses is: (1) hypothesize a likely mechanism of malfunction; (2) test the hypothesis by analysis and available orbital data; and (3) reject or accept the hypothesis. The analyses itself is keyed to evaluating the dimensional sufficiency of the major elements in the structural and power modules by subjecting them to variations of the temperature environment, temperature induced loading, and the platform induced loads during spun-up conditions. The specific dimensional changes considered were those of the bearings, their installation fit-ups, and their preload mechanism; also considered were the critical dimensional suitability of the bearing ball retainers with their associated race and ball. The possibility of bearing inner race rotation was also examined. A summarizing discussion of the significant study aspects associated with the anomaly and the related conclusions are given in the paragraphs that follow. The details of this work are assembled in Appendix B.

5.2.2 DMA Characteristics

A general description of the DMA is given in Section 1.2.1 (see Figure 1-3). Figure 5.2-A is a sectional view showing the primary elements of the structural module: main bearings (90 MM and 110 MM); lubricant reservoirs; thermistors (for telemetry); mounting flanges; and preload mechanism. Tables 5.2-A and 5.2-B summarize the principal characteristics of the main bearing elements.

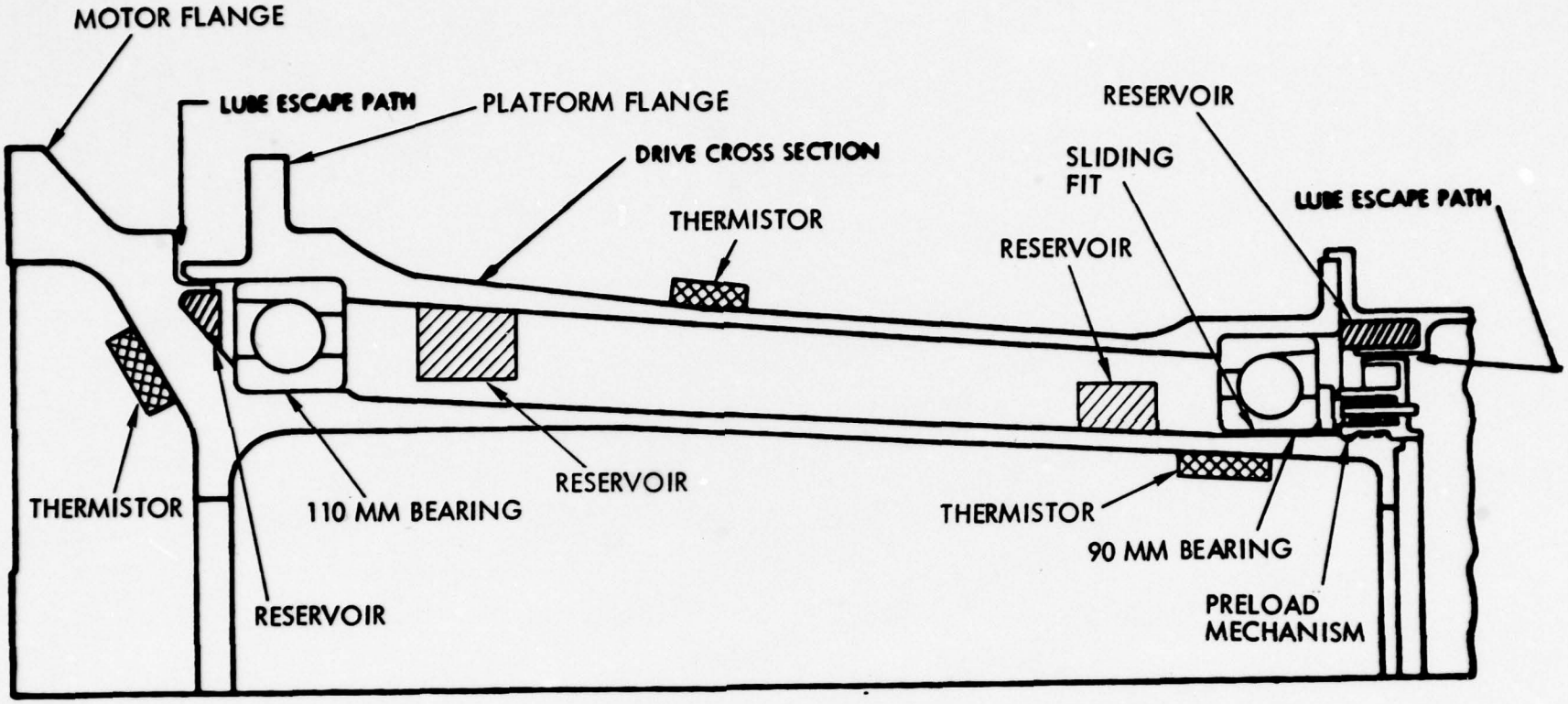
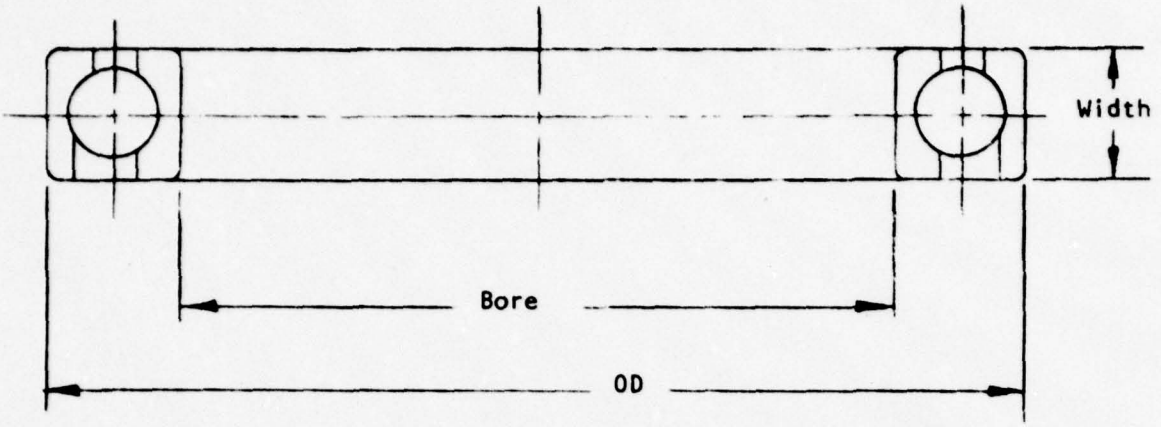


Figure 5.2-A. DMA Structural Module

Table 4.2-A. Bal Bearing Dimensions



Reference: BBRC Source Control Drawing 32709

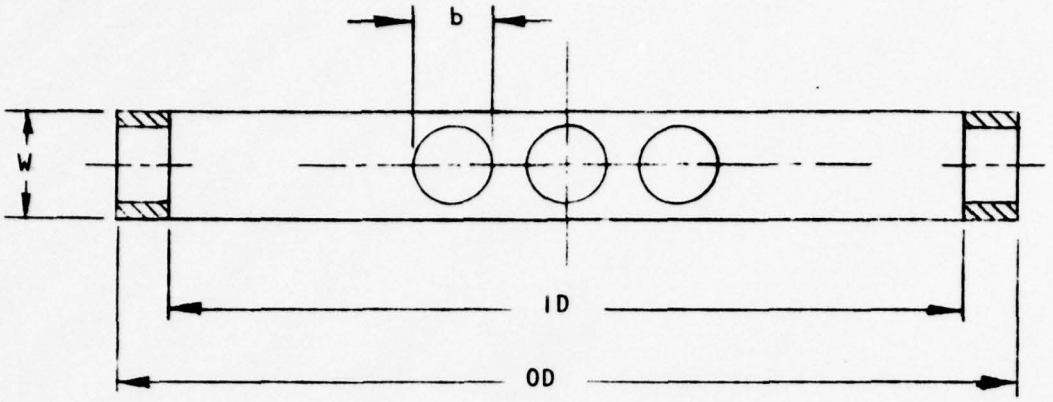
Dimensions	Bearing Size	
	110 mm Bore	90 mm Bore
* Bore, Inch	$\frac{4.33070}{4.33045}$ (110 mm)	$\frac{3.54330}{3.54305}$ (90 mm)
* OD, Inch	$\frac{5.9055}{5.9051}$ (150 mm)	$\frac{4.9213}{4.9209}$ (125 mm)
Width, Inch	$\frac{.7874}{.7824}$ (20 mm)	$\frac{.7087}{.7037}$ (18 mm)
No. of Balls	23	21
** Ball Diameter, Inch	$\frac{1}{2}$	$\frac{15}{32}$
*** Shaft Diameter, Inch	$\frac{4.3304}{4.3301}$	$\frac{3.5426}{3.5423}$
*** Housing Bore, Inch	$\frac{5.9047}{5.9051}$	$\frac{4.9205}{4.9209}$

* AFBMA ABEC-7 bearing tolerances.

** AFBMA Standard Grade Ten (10) ball size variation.

*** From BBRC drawings - 32703 shaft and 32713 housing.

Table 5.2-B. Bearing Retainer Dimensions



Material: NEMA Grade LE Phenolic

Retainer Dimension	Bearing Size	
	110 mm Bore	90 mm Bore
OD	$\frac{5.278}{5.268}$	$\frac{4.359}{4.349}$
ID	$\frac{4.883}{4.891}$	$\frac{4.002}{4.010}$
Width (W)	$\frac{0.700}{0.695}$	$\frac{0.685}{0.680}$
Ball Pocket (b)	$\frac{0.514}{0.520}$	$\frac{0.482}{0.488}$
Outer Race Land Bearing, Dia.	$\frac{5.436}{5.440}$	$\frac{4.518}{5.522}$
Inner Race Land Bearing, Dia.	$\frac{4.843}{4.841}$	$\frac{3.962}{3.960}$

5.2.3 Structural Module

(A) The Aspect of Friction Torque. The bearings' Coulomb friction is dominantly a function of the co-tangent of the load contact angle and the magnitude of the axial or thrust load. (Radial loads were not considered inasmuch as their amplitudes are small in the despun condition.) The load contact angle itself varies directly at the bearing's elastic deflection and inversely as the algebraic sum of the bearings' initial diametral clearance and the shaft's and the housings diametral changes. The latter are induced by initial bearing fits onto the housing and the shaft and the temperature variations of these elements. The functional relationships of the bearing friction torque imply that its increase is affected by either (1) diametral changes of the housing and the bearings in a direction that reduces the contact angle; or (2) an increase of the thrust load; or (3) simultaneous occurrences of both factors.

(B) Temperature Effects on the Bearing Suspension System

- Radial motion of Bearing Suspension Elements

  Radial temperature variation of the suspension components was taken as the dominant forcing function that causes diametral changes of the housing, the shaft, and the bearing races. The latter consisted of three diametral variation components, namely:

  (1) Changes of the housing's inside diameter and the bearing's outside diameter with respect to the initial interference or clearance values between them, existing at a reference installation temperature of 72°F

  (2) Changes of the bearing's inside diameter and the shaft's outside diameter with respect to their initial interference or clearance values, existing at a reference installation temperature of 72°F.

  (3) Changes of the bearing outer race inside diameter and the bearing inner race outside diameter as a function of their temperature variations.

The major assumptions were:

(1) The bearing ball diameter was not considered thermally dependent by virtue of the small diameter that renders insignificant diametral changes when compared with the effects of the DMA's structural elements and the bearing races

(2) Unless otherwise specified, the steady-state temperature of the housing was assumed to approach the temperature of the outer race outside diameter.

To develop an understanding of the sensitivities involving the geometric changes in the bearing suspension system, the upper and the lower temperature bounds for specific mechanical events associated with the bearing friction variations were determined. These are presented in Table 5.2-1 together with remarks of plausibility. Unless otherwise noted, the calculated temperatures of elements were constrained by the assumption that except for the bearing suspension element considered, all others were retained at the reference temperature of 72°F.

The immediate effect of the mechanism of the thermal diametral component expansion is to increase the bearing friction by a reduction of the load contact angle value in the presence of a constant bearing preload. Large bearing friction increases can be only induced by closing the existing clearances between the OD of the shaft and the ID of the bearings and by forcing the bearings internal clearance to approach zero value. As indicated in Table 5.2-1, the bearing suspension components temperature conditions required to create the geometrics required for large friction development are not plausible in view of the orbital and the thermal simulation data.

- Axial Motion of the Bearing Suspension Elements

The operational success of the bearing suspension design depends on the maintenance of the free floating inner race of the "top" bearing (90 MM) in both radial and axial directions in order to retain the nominal condition of the bearing preload mechanism

Table 5.2-1. Diametric Dimensional Variation of Bearing Suspension Components – a Function of Temperature

Mechanical Event	Temperature @ Bottom Brg.	Temperature @ Top Brg.	Remarks
• The temperature of the housing at which loose fit will occur between ID of housing and OD of bearing	(1) 241°F	(1) 275°F	(1) Temperature not plausible in view of the orbital and thermal simulation data.
• The temperature of the housing at which diametral clearance will no longer exist	(1) -162°F	(1) -220°F	(2) Possible event.
• Inner race temperature at which tight fit will occur between inside diameter of bearing and the outside diameter of shaft	(2) 70°F	(1) 49°F	(3) Considered because lubrication depletion factor external to the bearing elements will cause an increase of both the outer race and the inner race temperature levels. Lubrication depletion, both external and internal to the bearings, will cause larger gradients.
• Shaft temperature at which tight fit will occur	(2) 86°F	(1) 168°F	
• Shaft temperature at which the bearings' diametral clearance no longer exists [for assumed inner race to shaft temperature difference of 4°F]	(1) 118°F	(1) 130°F	
• Outer race temperature at which the bearings' diametral clearance does no longer exist [for assumed inner race to shaft temperature difference of 4°F]	(1) 340°F	(1) 260°F	
• Inner race temperature gradient (inner race less shaft temperature at which the bearing's diametral clearance no longer exists	(3) 50°F	(3) 62°F	

(see paragraph 5.2.2). The latter introduces a weak spring in series with the shaft's, the bearing's and the housing's axial stiffnesses. This affords axial thermal expansion of the housing with respect to the shaft without inducing large thrust loads. This thermally-induced relative displacement is a function of the product of the bearing center-to-center distance, the coefficient of thermal expansion of the materials envolved, and the difference of the average temperatures of the housing and the shaft. This displacement is dominant in considering the suspension performance. Other displacements (i.e., those which are a function of the axial temperature gradients along the housing and the shaft) appear to be insignificant in comparison.

Of interest is to note that a relative displacement of 0.003 inch will saturate the preload mechanism (refer to paragraph 5.2.2). This means that any further axial displacements will produce increases of bearing thrust load and thus the bearing friction. The temperature gradient (average temperature of the housing less the average temperature of the shaft) necessary to achieve such a condition approaches 67°F. The magnitude of such a gradient is not consistent with either the orbital data or test and thermal simulation data. Note also, that to develop the saturation of the preload mechanism, the average housing temperature must be greater than the average shaft temperature. This, of course, leads to the conclusion that the higher the shaft temperature with respect to the housing, the smaller is the possibility of saturating the preload mechanism. The last statement is somewhat mitigated by the discussions of the previous topic from which it may be deduced that the axial motion of the inner races of the bearings can be produced in the direction that also cause the saturation of the preload mechanism. The latter occurs as a direct consequence while accommodating the changes of the contact angle caused by the thermally-induced diametral variations of the pertinent suspension components. Exemplifying, small bearing contact angles require the inner race of the DMA's top bearing to be displaced towards the preload mechanism (see paragraph 5.2.2). These two aspects, as well as the increases of the thrust load, is further discussed in the subsequent paragraphs.

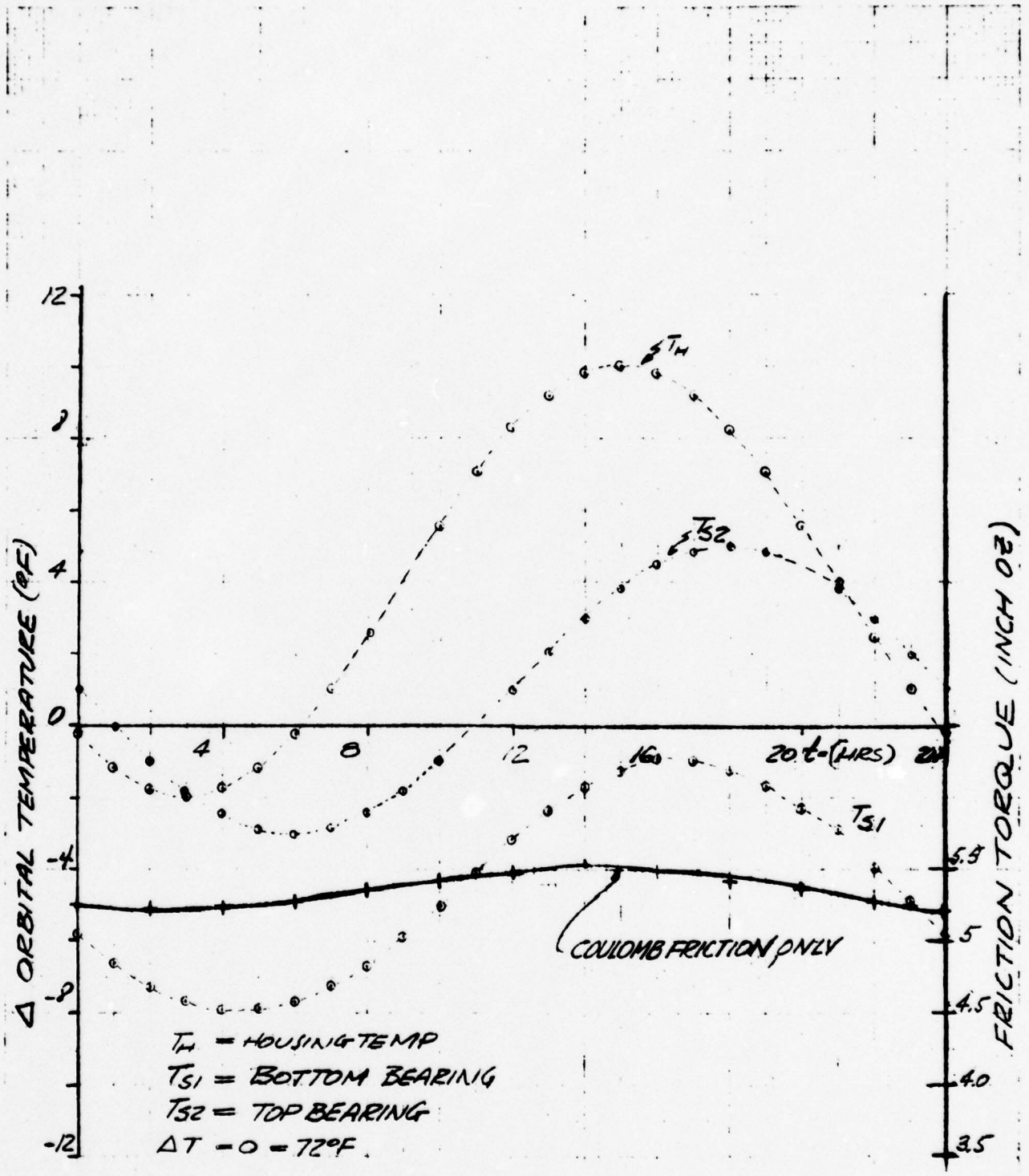


Figure 5.2-1. Normal Bearing Friction for Orbital Environment

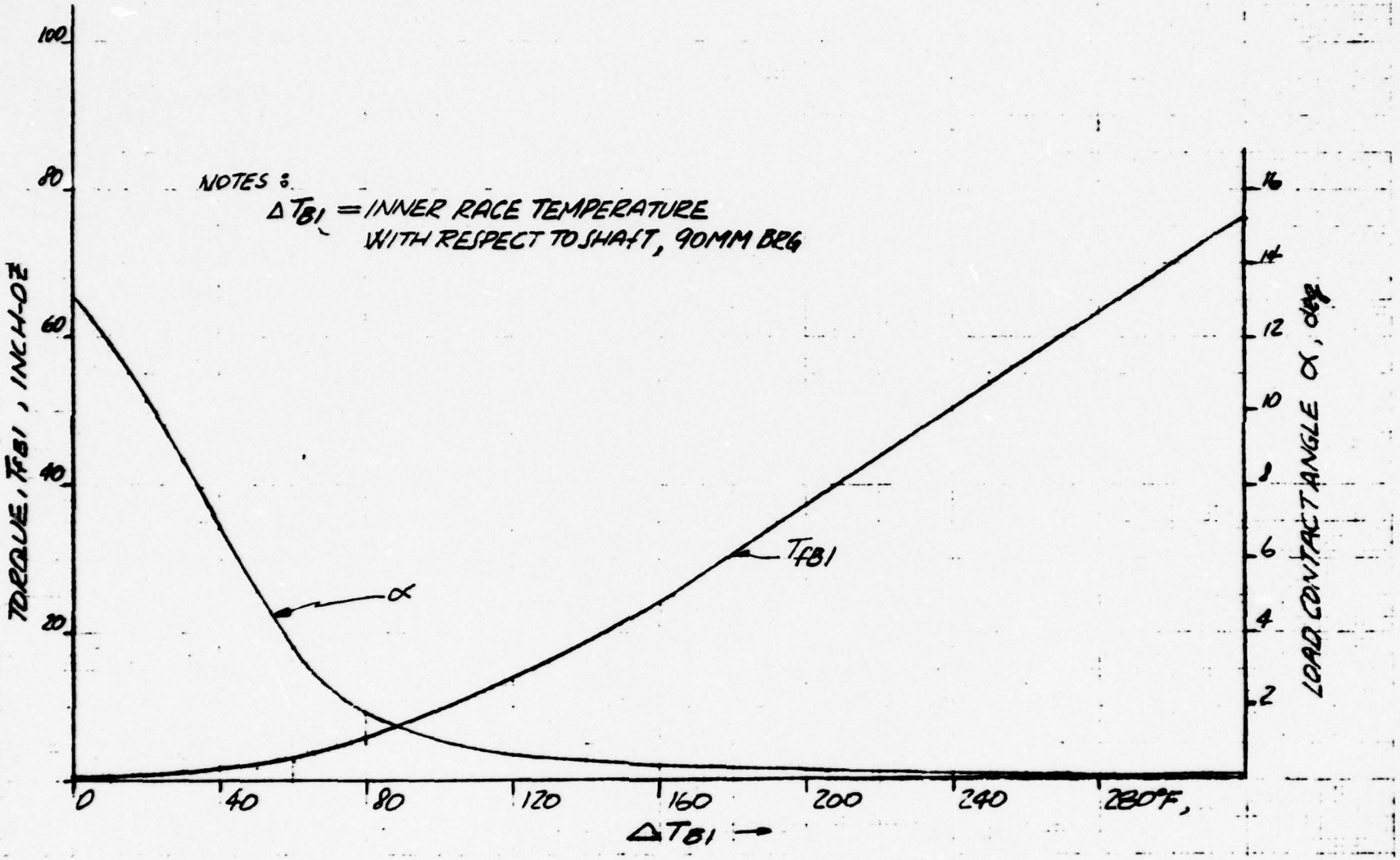


Figure 5.2-2. Friction Torque and Load Contact Angle as Funtions of the Inner Race Temperature Gradient, 90 mm BRG

(C) Detail Considerations of the Bearing's Friction Torque

- Orbital Performance

  To determine the effect of temperature variations on the amplitude of the bearing Coulomb friction, pertinent diurnal orbital temperatures occurring on 8 September 1975 were selected. These, together with the calculated friction for both bearings, are shown on Figure 5.2-1. The plots reflect the effects of the normal preload of 64 pounds and the geometric variations of the bearing suspension components by the temperature environment. Notice the insignificant torque variation of about 0.6 inch-oz during one diurnal period.

- Performance as a Function of Stipulated Temperature Gradients

  Since the telemetered thermal data for the DMA obviously did not provide the mechanism explaining the observed anomaly, various temperature gradients between the pertinent bearing suspension components were considered and their effects on the bearing friction was estimated.

  (1) Aspect of Lubrication Depletion - It appeared reasonable to assume that depletion of lubricant in the neighborhood of the top (90 MM) bearing will cause an increase of its inner race temperature. To determine this effect on performance, a 37°F temperature gradient between the shaft and the inside diameter of the bearing was considered The latter was based on an order of magnitude increase of the existing heat flow coefficient of conduction. The temperature environment of the other DMA elements was retained at levels shown on Figure 5.2-1. The imposed conditions resulted in a maximum friction torque increase of 1.5 in-oz.

  (2) Friction Torque as a Function of Inner Race to Shaft Gradient - The analysis of the hypothesized temperature gradient of item (1) was extended to the variations of the friction torque as a function of the discussed gradient

with all other temperatures retained at levels defined by the thirteenth hour of the diurnal DMA's temperature profile shown on Figure 5.2-1. The results of this work (Figure 5.2-2) indicate that to obtain the anomaly's nominal torque increase of 60-in-oz, the temperature gradient must approach 270°F.

The necessity of such a large gradient is caused by a relatively low rate of change of the load contact in the region of the bearing's zero diametral clearance. It follows that the sensitivity of the friction torque to the subject temperature gradient would be much higher should the bearing's preload be reduced.

- Friction Torque as a Function of Preload Mechanism Saturation

The saturation or closure of the preload mechanism was in part discussed in paragraph (B). Here the subject is extended to the quantitative summary of the preload saturation effect on the bearing friction torque. There are at least three factors that influence the closure of the preload mechanism:

- the radial temperature gradients between the bearing suspension components
- the angular misalignment of the inner race of the 90 MM bearing
- jamming of the clearance between the inner race of the 90 MM bearing and the shaft.

(1) Temperature Gradients Effect - The axial closure motion is a function of the bearing's reduction of its diametral clearance by the thermal gradients and the relative displacement of the housing with respect to the shaft due to the difference between the average temperatures of the housing and the shaft. This motion is in part mitigated by the elastic displacement of the bearings produced by the bearing's thrust load. Using the DMA's thermal conditions of Figure 5.2-1 and stipulating a

37°F temperature gradient between the inner race of the 90 MM bearing and the shaft, the closure situation depicted in Figure 5.2-3 was developed. Should the temperature gradient (average temperature of housing less average temperature of shaft) reach a value of 149°F, the anomaly's Δ torque results. Notice that for a nominal temperature gradient of 3.7°F between the 90 MM bearing inner race and the shaft (rather than the 37°F stipulated above), the necessary total gradient ΔT (average temperature of housing less shaft) to result in 60 in-oz bearing friction torque is 216°F.

The bearing friction torque values due to the gradient (ΔT) are shown on Figure 5.2-4. In order to recognize the magnitude of the thrust load, associated with the gradient ΔT, the relationship of these two quantities is also given on Figure 5.2-4. Figure 5.2-5 depicts the bearing friction torque as a function of the thrust load. Notice that the calculated correspondence with the experimental data is sufficiently good for acceptance with reasonable confidence the analytical relationships given on Figure 5.2-4.

(2) Angular Misalignment of Bearing - Geometrically, by virtue of the pertinent radial and axial clearances (associated with the top bearing and the preload mechanism, respectively), it is possible to produce an angular misalignment that saturates the preload mechanism. The maximum angular quantity about an axis perpendicular to the rotational axis of the DMA associated with the misalignment, approaches 0.0485 degree of arc. This angle produces (refer to Figure 5.2-6) an increase of the bearing friction by 16 in-oz. Hence, to achieve the anomaly-associated torque increase in accordance to Figure 5.2-4, the required temperature gradient is 128°F.

(3) Jammed Top Bearing's Inner Race - A hypothesis of the following conditions

(a) the radial clearance of the top bearing, between the inside diameter of its inner race and the outside diameter of the shaft is jammed by debris

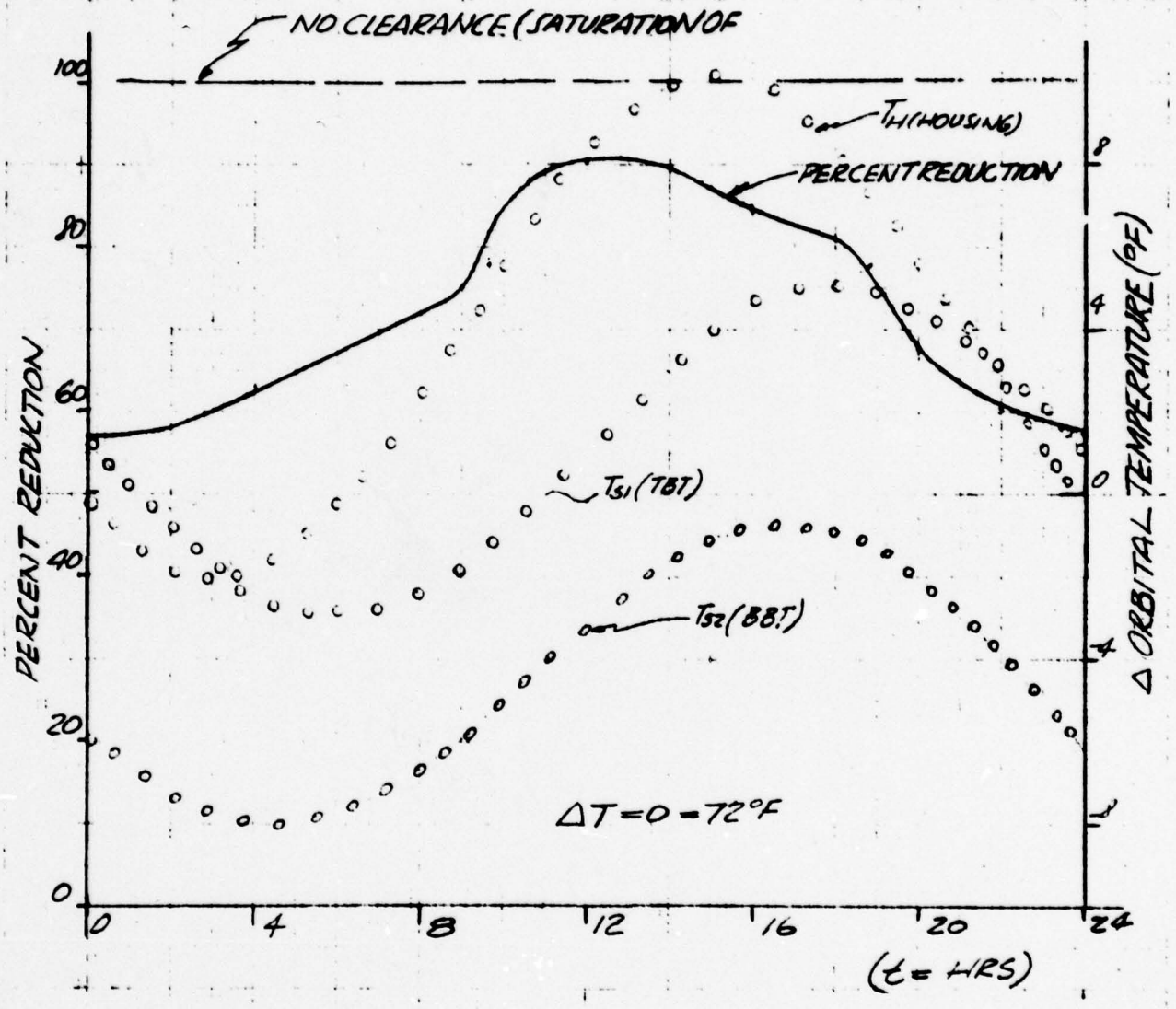


Figure 5.2-3. Percent Reduction of Axial Clearance (Between Race Shoulder and the Preload Mechanism)

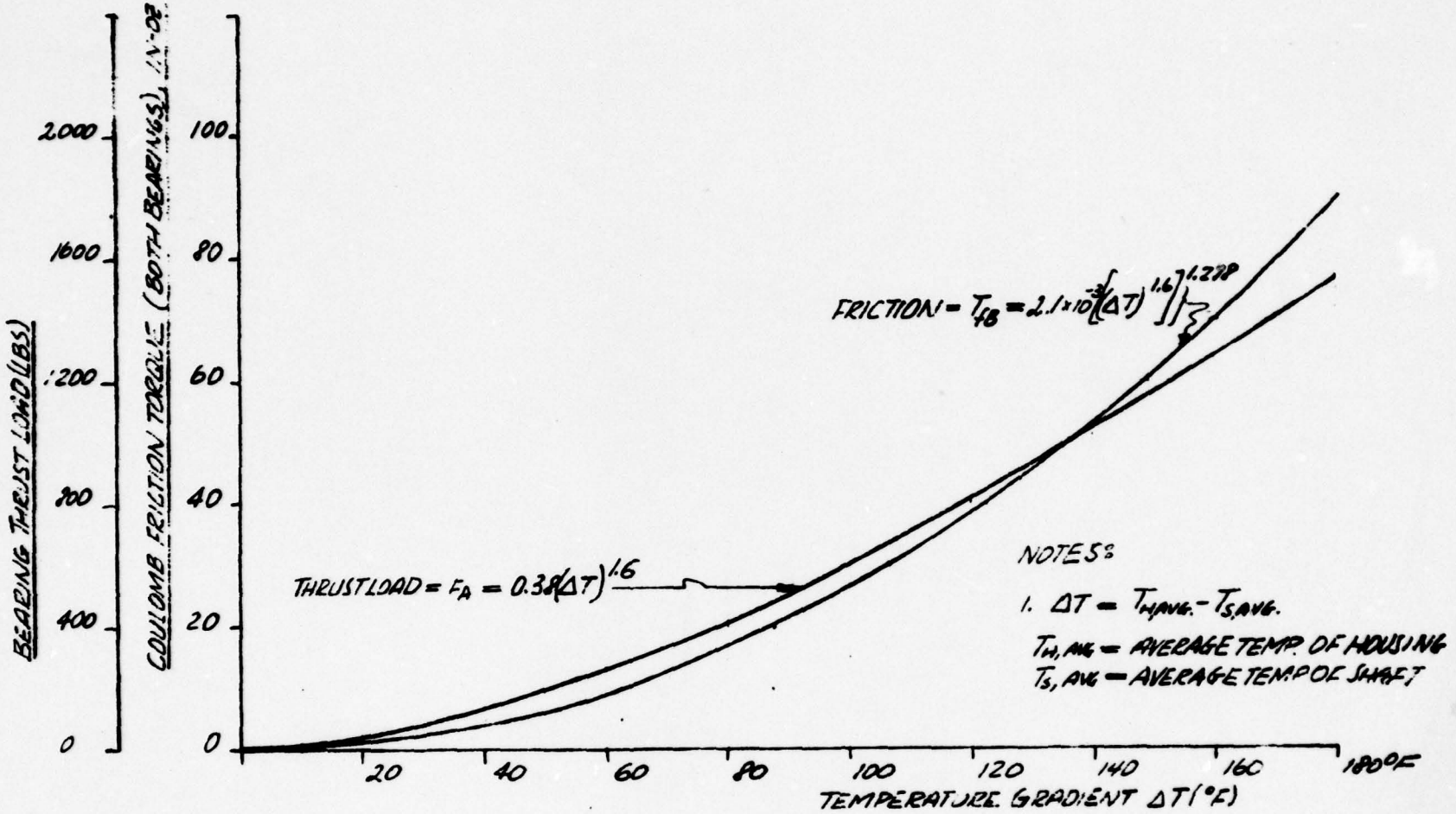


Figure 5.2-4. Bearing Δ Friction Torque and Thrust Load Versus Temperature Gradients (for Saturated Condition of Preload Mechanism)

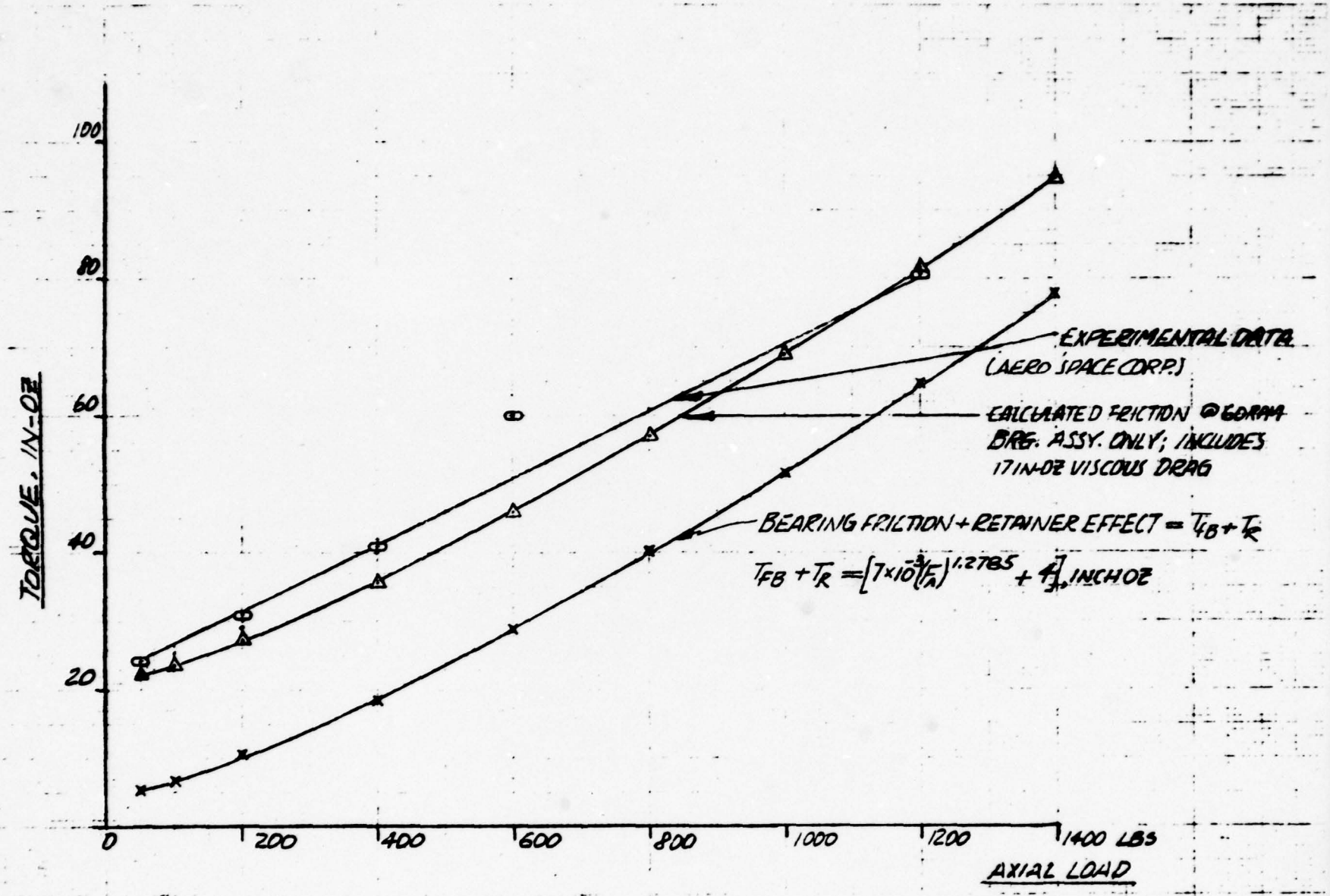


Figure 5.2-5. BRG Assembly Friction Torque Versus Axial Load

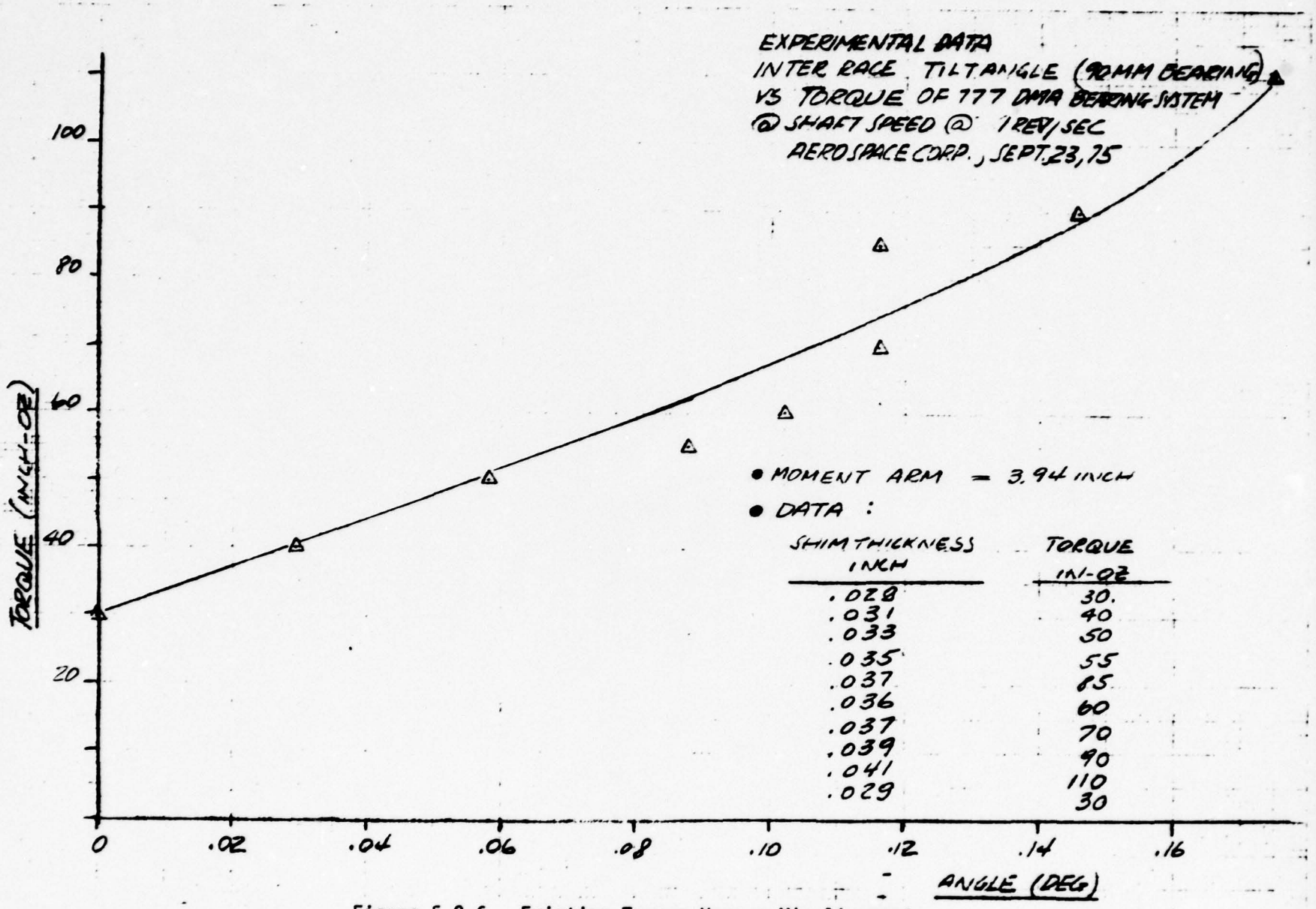


Figure 5.2-6. Friction Torque Versus Misalignment

(b) the intensity of jamming is sufficient to retain the nominal (0.003 inch) relative position of the bearing with respect to the preload mechanism under load,

(c) the axial load is produced by a thermal gradient which is defined as the difference between the average housing and shaft temperatures,

requires a thermal gradient (Figure 5.2-4) of 169°F to satisfy the anomaly's observed Δ torque increase of 60 in-oz.

- Feasibility of Anomaly DMA Torques as a Function of Thermal Environment

  Reference to Table 5.2-2, which summarizes the aspects of the bearing friction torque induced completely or partially by the thermal gradients, indicates that the pertinent temperature gradients required to produce the steady-state friction characteristics of the DMA's orbital anomaly are inconsistent with either the orbital or the thermal simulation data.

(D) Dimensional Analyses of Bearing Ball's Separators. A worst case analysis envolving a review of dimensional sufficiency of the ball bearing retainers was performed. Considered were the separators associated with the structural assembly's bottom bearing (110 MM), top bearing (90 MM) and the 30 MM slip ring's assembly bearing.

The separator's geometric sufficiency criterion used in the presented analyses were defined as:

- the distance (ε) between a point (P_2) at the outboard edge of the separator's thickness dimension and belonging to the locus of points defining the outside diameter of the separator, and the point of tangency (P_1), associated with the separator's pocket and its companion ball, must have a positive value. In other words, the outside of the ball pockets must intersect the balls above their equators.

- There must exist a clearance (c) between the 90 MM bearing separator's width dimension and the washer, of the preload mechanism, for the worst case of dimensional considerations.

TABLE 5.2-2

Temperature Required for Anomaly's
Δ Friction Torque Increase

Hypothesized Conditions	Gradient Required to Produce 60 in-oz Friction (°F)
• Temperature effects of local lubrication depletion in the neighborhood of the top bearing are superimposed over the typical orbital temperature environment of the DMA. The gradient between the inner race and the shaft caused by depletion is	. . . 270°F
• Preload mechanism is saturated by a 40°F gradient between the inner race (top bearing) and shaft; superimposed over the DMA's orbital environment a gradient, ΔT, (average housing less average shaft temperatures) is	. . . 147°F
• Nominal orbit, DMA's temperature conditions exist. Gradient ΔT is necessary to saturate the preload mechanism and produce anomaly friction is.	. . . 216°F
• Nominal orbit, DMA's temperature conditions exist. Top bearing is misaligned; the gradient ΔT is	. . . 128°F
• Nominal orbit, DMA's temperature conditions exist. Preload mechanism's axial clearance of 0.003 inch exists. 90 MM bearing race is jammed on the shaft by debries; the gradient ΔT is	. . . 149°F

Note: Nominal bearing friction variation for normal orbital operation is 0.4 in-oz. If bearing misalignment is assumed to cause saturation of the preload mechanism, 17.5 in-oz torque increase would be expected.

The magnitude and the direction of the defined edge distance (ε) were of interest because increases of bearing friction can occur should ε become less than zero, since the retainer might tend to be over-ridden (jammed) by the balls.

All the computed edge distance values, as shown below, were positive

Bearing	Edge Distance (ε)
110 MM	0.026 inch
90 MM	0.017 inch
30 MM	0.011 inch

quantities and appeared to be large enough for satisfactory bearing performance, provided the edges of the separator have either sharp corners or their chamfer's dimension is limited to small values, say 0.005 inch.

However, since the deburring radius or chamfer is not controlled by the fabrication drawing, possibility exists that "ε" can become less than 0.015 inch, the separator's edge distances (ε) for the bearings of interest become:

Bearing	Edge Distance (ε)
110 MM	0.011 inch
90 MM	0.002 inch
30 MM	-0.004 inch

The determination of the bearing friction torque increase as a function of a negative edge distance value was not within the scope of these analyses. However, for the retainer's steady-state conditions, a coarse approximation of the bearing torque increase is the product of the nominal friction torque and the ratio of the negative edge distance to the bearing ball radius. Utilization of the latter indicates that small negative values of ε insignificantly affect the bearing performance.

The worst-case value estimate of the retainer-washer clearance (c) resulted in a value of -0.0030 inch. The consequence is a possibility that the retainer can on occasion ride against the preload washer, much as it can on occasion ride on the bearing inner race land. The effect should not be a major one; however, the design can and should be altered to eliminate this possibility.

(E) Relative Inner Race Rotation. To satisfy the concern that a relative motion of a loose fitted inner race with respect to the shaft may be a mechanism of increased friction torque, an analysis was conducted. The following conclusions become evident:

- The friction between the spring-loaded washer and the shoulder of the inner race (90 MM bearing) is sufficient to prevent the subject relative motion for the operational modes except the launch vibration environment.
- No source of driving torque amplification due to potential "creep" of the race about the shaft was found. Internal gear set type operation requires extremely high radial loading, far in excess of what appears possible in any DMA under normal conditions.

The analysis was conducted under the following conservative assumptions:

(a) Elements of the DMA are treated as rigid. Thus, there is no mechanical filtering of motor-applied torques. This approach is conservative unless the motor torques are applied at the shaft natural frequency, an impossible condition since the motor bandwidth falls far below this value.

(b) The spacecraft rotor is treated as being decoupled from the motor due to high motor-to-rotor shaft compliance. This is conservative as finite coupling would only tend to reduce the preload necessary to "lock" the inner race to the shaft.

(c) The shaft is not in contact with the inner race, and the bearing located near the platform flange experiences no frictional/mechanical hysteresis-type losses. These conditions again require the most of the preload mechanism.

5.2.4 Structural and Power Modules

(A) Aspect of Gap Closures

In both the platform despun and spun-up cases, conditions exist that will induce relative dimensional changes between the housing and the shaft mounted elements of the power module. The magnitude of the elemental approachment (closure) is of interest because it establishes design sufficiency, or should complete and sustained closure exist, explains the anomaly. The highest tendency to closure, because of its geometric location with respect to the structural module, is the resolver snubber radial gap. Hence, the estimate of its dimensional changes became the principal objective of the subject analyses for both modes of the spacecraft operation. The motor and the labyrinth seal in the neighborhood of the top bearing were also considered for the spun-up mode.

(B) Resolver Snubber Closure in the Normal (Despun) Operational Mode

Since the magnitudes of external forces acting on the DMA while despun are insufficient to cause significant relative displacements of the shaft and housing mounted elements, they were neglected. The principal sources considered were: (1) the motors' magnetic radial unbalance force, (2) material creep, and (3) thermal expansion. Their effects are delineated.

Source	Worst Case Gap Reduction
(1) Motor loads on shaft take up any radial clearances between shaft and inner races of bearings	.0016"
(2) Snubber grows in diameter due to dimensional instability of material, accelerated by elevated temperature from motor heating	.0023"

Source	Worst Case Gap Reduction
(3) Bracket grows in diameter due to dimensional instability but not as much as spacer because of lower temperature. (Bracket may go out of round because of unsymmetrical grain orientation since it is fabricated from plate)	.0010"
(4) Spacer grows in diameter more than the bracket, due to coefficient of thermal expansion, as motor temperature rises. (Spacer 178°, bracket 111°, motor dissipation = 20 watts - see Table 5.1-3)	.0016"
(5) The ΔT across the diameter of the motor shaft, due to location of the windings on one side, causes bending (for 12.6 watt power dissipation)	.0002"
RSS	.0034"

Notice that although the manufacturing controls allow the minimum radial gap of 0.002 inch, the nominal gap is 0.0085 inch, and actual gap measurement of typical units is 0.005 inch minimum. Comparing these facts with the 0.0034 inch gap reduction, it is unlikely that the DMA's high friction is caused by the snubber interference. Moreover, the thermal simulation data for the high torque periods does not support this as the friction-producing mechanism (see Section 5.1).

(c) Gap Closures in the Spun-up Mode

Spin-up of the platform introduces loads not present in the despun state due to product of inertia and the center of mass offsets. The vehicle spin velocity produces moments and lateral forces (primary centrifugal) that act on the DMA's platform flange. The consequence of the flange loads is a change in the dimensional clearances between the housing and the

shaft elements of the DMA. The determination of the magnitude of closure as a function of the platform's spin speed was the dominant purpose of an analysis. The analysis considered two loading conditions: (1) antennas inboard; and (2) antennas outboard. The "antennas outboard" condition was taken to be the nominal state for the standby mode of operation. In this mode, the spun-up forces will cause the antennas to move outward and away from the mass center of the spacecraft. The "antennas inboard" condition nominally exists while despun, and can be maintained up to platform inertial speeds of about 20 rpm.

The analysis was conducted under the following assumptions:

- Only centrifugal forces were considered
- The resulting structural forces were taken to be point loads. The shaft was considered to have continuous securement along its interface periphery with the spacecraft. The latter is contrary to the actual four-point flexible mount situation.
- The bottom bearing (110 MM) by itself is not capable of sustaining any moments applied to the housing.
- Line-to-line bottom bearing fit-up with shaft, and maximum clearance (0.001 inch) between the inner race of the top bearing (90 MM) and the shaft were adopted for the analyses. It was also assumed that misalignment due to the bearings' clearance geometry will take place at the application of small magnitude loads.
- The magnetic unbalance forces of the motor were neglected
- Thermal effects were not considered.

The analysis considered the total relative approachment to be the function of three effects (refer to Figure 5.2-7).

(1) The bearing looseness (clearance between inside diameter of bearing [90 MM]and the shaft) causes relative rotation of the housing with respect to the shaft. The direct consequence is the misalignment of the bearings' outer race with respect to the inner races. For the bearing looseness effect, the housing and the shafts of the structural and the power modules are considered to be of infinite stiffness (in bending). The housing rotates with respect to the shaft about an apparent pivot point, a function of the radial stiffness of the structural module's housing, shaft, and the bearings.

(2) The second effect is attributed to the radial deflections of the bearings. This tends to increase the angular rotation of the housings with respect to the shafts.

(3) The third effect considers the pertinent structural deflections. Notice from Figure 5.2-7 that the slopes of the structural curvatures of the structural module's shaft and housing are opposite in sense and, therefore, tends to mitigate the summed effect of the first two aspects.

The results of this analyses for the two loading cases are presented in Table 5.2-3 and Figures 5.2-8 and 5.2-9.*

Inspection of the table and the snubber closure plots reveal the following:

- The reaction forces are larger for the bottom bearing than for the top bearing in the "antennas inboard" case and conversely in the "antennas outboard" case. The reason for this phenomena is the polarity reversal of the despun lateral force acting on the DMA flange.

* It is of interest to note that (at the snubber) the closure due to side loads can be combined with the closures due to dimensional changes (thermal and material stability) by replacing item (1) of 5.2.4(B) by the values from Figures 5.2-8 and 5.2-9.

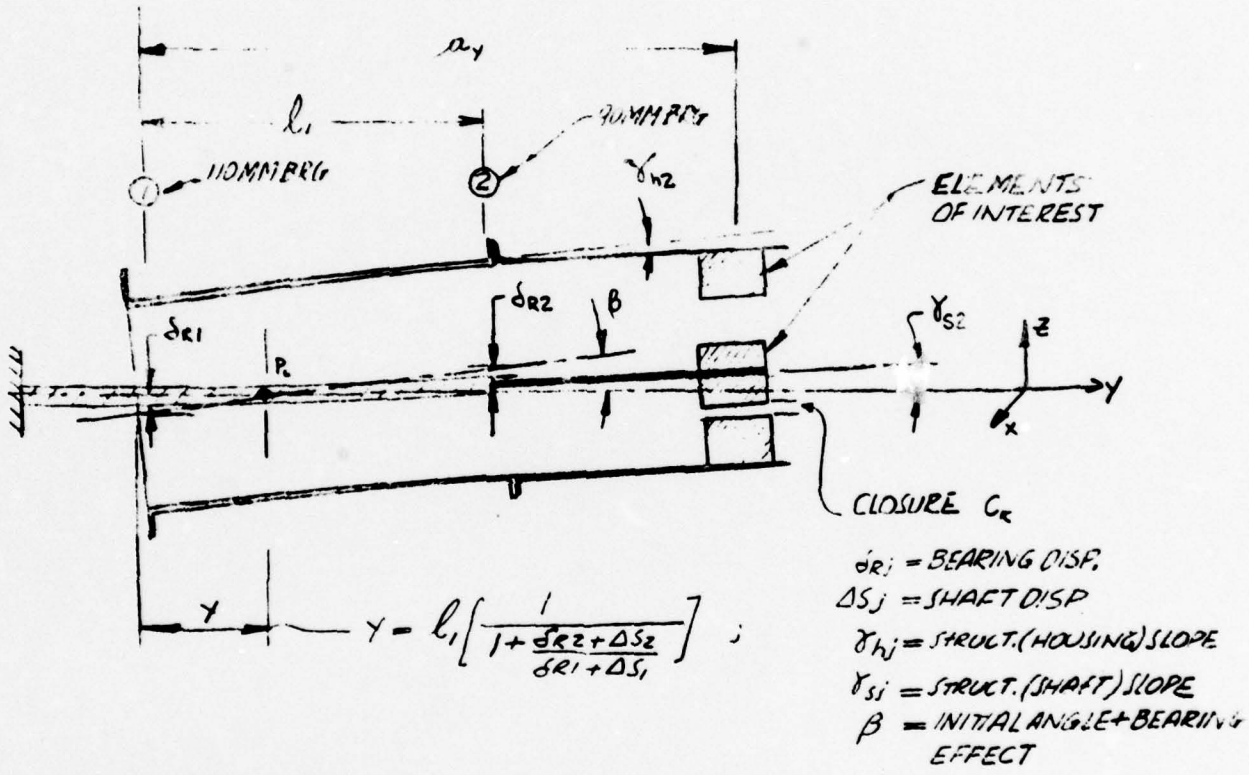


Figure 5.2-7. Relative Motion Between Housing and Shaft

TABLE 5.2.3

CRITICAL GAPS CLOSURE AS A FUNCTION OF PLATFORM SPIN-UP SPEEDS

Quantities	Units	Symbols	SPIN SPEED (RPM)							
			20		40		60		80	
			110MM Brg	90MM Brg	110MM Brg	90MM Brg	110MM Brg	90MM Brg	110MM Brg	90MM Brg
• Antennas Inboard Case										
Bearing Reactions	lbs	R_j	19.	15.	78.	62.	176.	140.	311.	247.
Resolver Snubber Gap Closure	inch	C_R	1.55×10^{-3}		1.44×10^{-3}		1.26×10^{-3}		1.40×10^{-3}	
Motor Gap Closure	inch	C_M	1.35×10^{-3}		1.28×10^{-3}		1.17×10^{-3}		1.32×10^{-3}	
Labyrinth Gap Closure	inch	C_L	1.11×10^{-3}		1.09×10^{-3}		1.06×10^{-3}		1.22×10^{-3}	
• Antennas Outboard Case										
Bearing Reactions	lbs	R_j	53	58	212	230	477	518	848	922
Resolver Snubber Gap Closure	inch	C_R	1.44×10^{-3}		1.39×10^{-3}		0.99×10^{-3}		0.31×10^{-3}	
Motor Gap Closure	inch	C_M	1.28×10^{-3}		1.28×10^{-3}		1.07×10^{-3}		0.67×10^{-3}	
Labyrinth Gap Closure	inch	C_L	1.09×10^{-3}		1.16×10^{-3}		1.16×10^{-3}		1.10×10^{-3}	

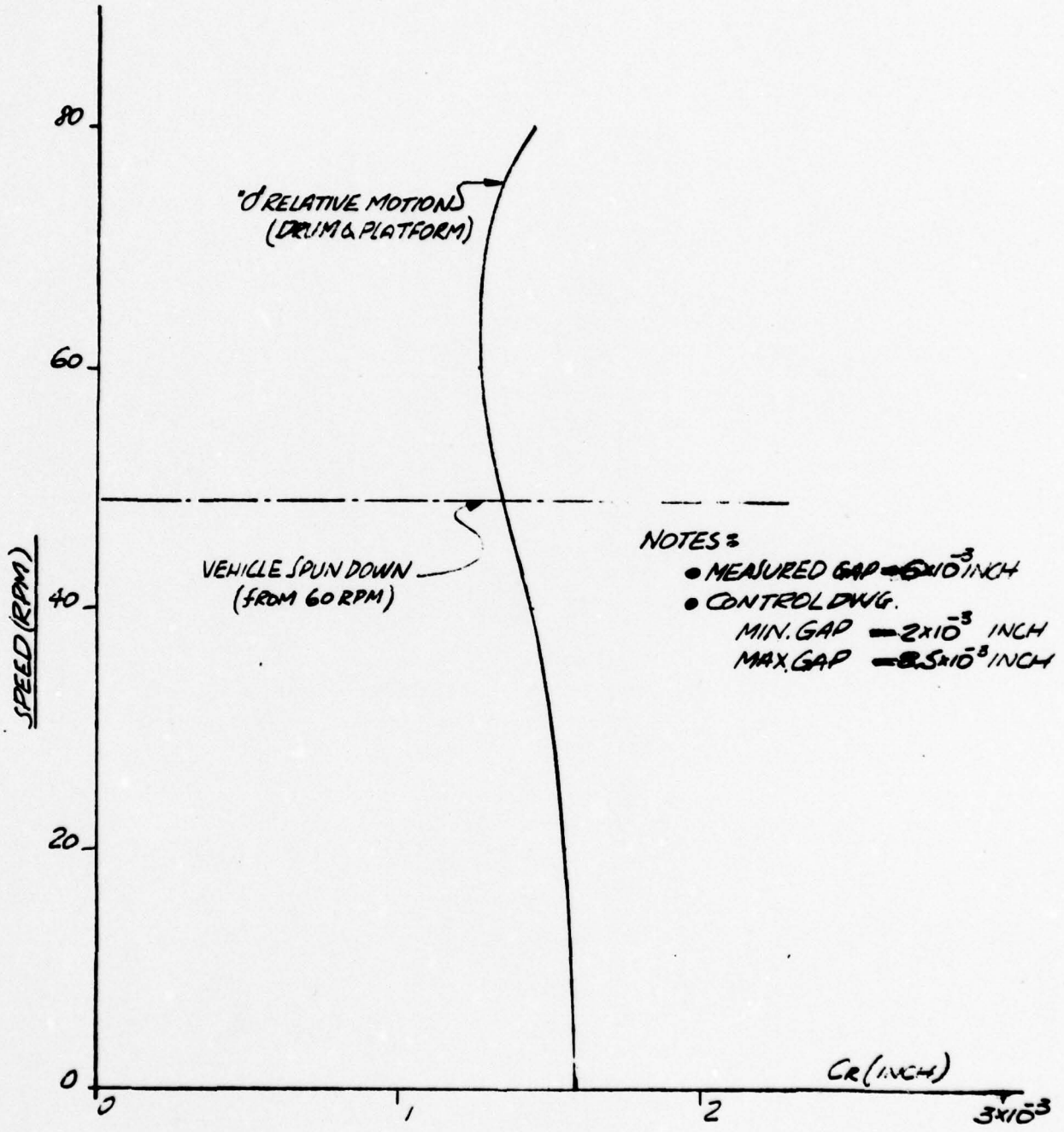


FIG 5.2-8 RESOLVER SNUBBER ELEMENTAL APPROACHMENT (CR)
VS
PLATFORM SPIN UP SPEED
(ANTENNAS INBOARD CASE)

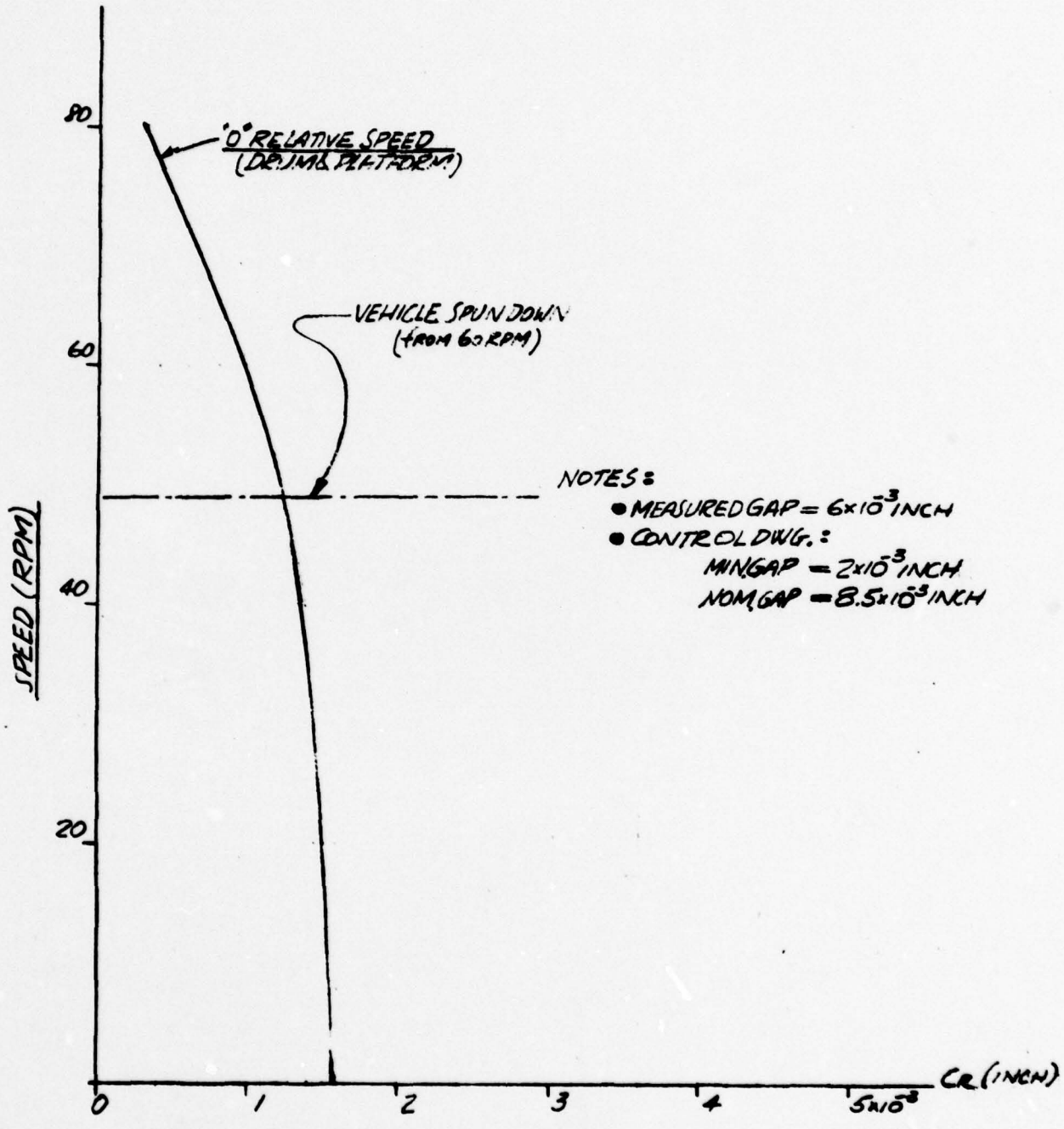


FIG. 5.29 RESOLVER SNUBBER ELEMENTAL APPROACHMENT (CR)
VS
PLATFORM SPIN UP SPEED
(ANTENNAS OUTBOARD CASE)

- The resolver snubber closure development vs. speed is not a function of the square of the spin-up velocity. There are several effects that force this lack of correspondence. These are:

  (1) The geometric loosness of the top bearing causes almost instantaneous misalignment of the housing with respect to the shaft, upon application of small radial forces to the bearings.

  (2) The bearings' elastic axial deflections, due to preload, tend to stiffen the bearings with respect to radial forces until the latter are sufficiently high in magnitude. This occurs at bearing reactions approaching 250 lbs.

  (3) The initial geometric looseness noted in item (1) also influences the bearings' races misalignment angle. Analysis indicates that the rate of change of the bearings' radial deflection is lower for relatively high values of misalignment. In general, the DMA's bearing misalignment angle decreases with application of radial load.

  (4) The bearing's radial deflection effect, excluding items (1), (2), and (3), is not dominant in establishing the value of the snubber closure. Analyses indicate that the structural curvatures of the shaft and the housing (due to external loads) are opposite in sense. Therefore, the initial value of closure will tend to decrease with increasing spin speed. Notice that, eventually, when the shaft's curvature slope becomes completely dominant, the value of the snubber closure will start to increase.

(5) Of some interest is the snubber closure characteristic vs spin-up speed for the "antennas inboard" case. Here, at approximately 60 rpm, the value of C_R begins to increase, whereas for lower speeds, it was a decreasing function. The reason for this occurrence is the fast rate of decrease of the bearings' axial deflection which renders more compliant bearing to radial load.

(6) Notice from Table 5.2-3 that the bearing radial deflection effect is more dominant for relatively short distances (a_y) to the elements of interest (refer to Figure 5.2-7). This is exemplified by the labyrinth seal closure (C_L), in which case the closure values appear to decrease very closely with the spin-up speed and thus the bearing loads. The influence of the structural curvatures is not as significant.

(D) Conclusions

The most critical clearance in the DMA is at the power module (resolver) snubber. Analyses indicate that for both the despun and the spun-up platform conditions, closure of the resolver snubber gap is unlikely, but (in the despun case) possible with the Phase I DMA assembly procedures.

5.2.5 Summary of Conclusions

The analyses performed led to the conclusion that the DMA's dimensional configuration is sufficient and will not cause the observed anomaly. This statement excludes the effects of the lubricant deterioration, the slip ring assembly, and the motor performance

At most, a 17.5 in-oz friction torque increase from nominal is predicted for conditions observed in 9433 orbital data. This torque is the consequence of hypothesized top bearing misalignment causing a locked preload mechanism condition. There is also the possibility of intensification of the vehicle pointing disturbances due to marginality of the bearing ball separators. The possibility of interference of resolver snubber gap exists; however, analyses above (as well as evaluations of orbital data and tests) indicate this to be an unlikely source of the observed orbital anomaly.

Analyses have indicated questionable dimensionery of the bearing retainer, an area which should be addressed for the Phase II DMA.

6. SYSTEM, ASSEMBLY, AND COMPONENT TESTS

In support of the 9433 anomaly investigation, a variety of laboratory tests have been conducted, including:

- Closed loop system tests using flight configured hardware
- Assembly-level DMA tests
- DMA component tests (bearings, slip ring assembly, motor, and power-module snubber)

A portion of the component tests were performed at Aerospace Corporation and witnessed by (or reported to) TRW personnel; these Aerospace tests are reported here to the extent permitted by available information.

6.1 System Tests

The closed-loop system tests were motivated by the unexpected results of the on-orbit friction tests (Section 3.4). The primary objective was to attempt a duplication of the friction test data (i.e., the torque saturation phenomenon). A secondary goal was to study motor-electronics operation in the saturated regime.*

Laboratory system tests were conducted using the qualification model DMA (S/N3-2) with its rotor interface (shaft) flange mounted on a pier and an inertia fixture (the "orange slice") mounted on the platform (housing) flange. Thus, in this test configuration (which is the one normally used for laboratory despin tests), the rotor is stationary while the platform rotates. In order to simulate the abnormally high level of friction observed in 9433, a spring-loaded Teflon rod was pressed against the orange slice near its periphery, with the contact pressure adjustable to provide varying friction levels.

In several respects, this test set-up is not representative of the orbital situation:

- The weight of the orange slice (approximately 400 lbs) is supported by the lower main bearing of the DMA, thus adding to the preload of this bearing and increasing the friction torque.

---

* Subsequent motor tests were more fully instrumented in order to provide definitive motor-electronics test data (Section 6.5).

- The motion of the orange slice produces additional deceleration torques due to windage.
- Convective effects due to orange slice motion produce cooling not present in the orbital situation.
- No attempt was made to duplicate orbital thermal interfaces (i.e., the tests were conducted at room temperature in air).

Figure 6.1-1 summarizes the results of five test runs. Run (1) is a run-down (equivalent to a platform spin-up in orbit) with the motor unpowered by turning off the DEA power amplifier and no external friction load. The friction level at 60 rpm was estimated at 57 in-oz from the rate data; moreover, a noticeable speed dependence was observed (i.e., an average friction torque of 49 in-oz in the 40-50 rpm range, compared to an average of 69 in-oz in the 70-80 rpm range). The overall increase in friction level can be attributed to the increased load on the lower main bearing and windage, with the speed-dependence primarily due to the latter effect.

Runs (2) through (4) represent performance with varying levels of friction applied via the Teflon rod mentioned above. In Run (5), the friction load was removed and the redundant motor winding was fully shorted to evaluate the braking effect thus produced. These runs showed a definite reduction in motor torque capability with increased speed (later verified by motor tests), but did not exhibit the apparent increase in DMA friction torque seen during the 9433 on-orbit friction tests.

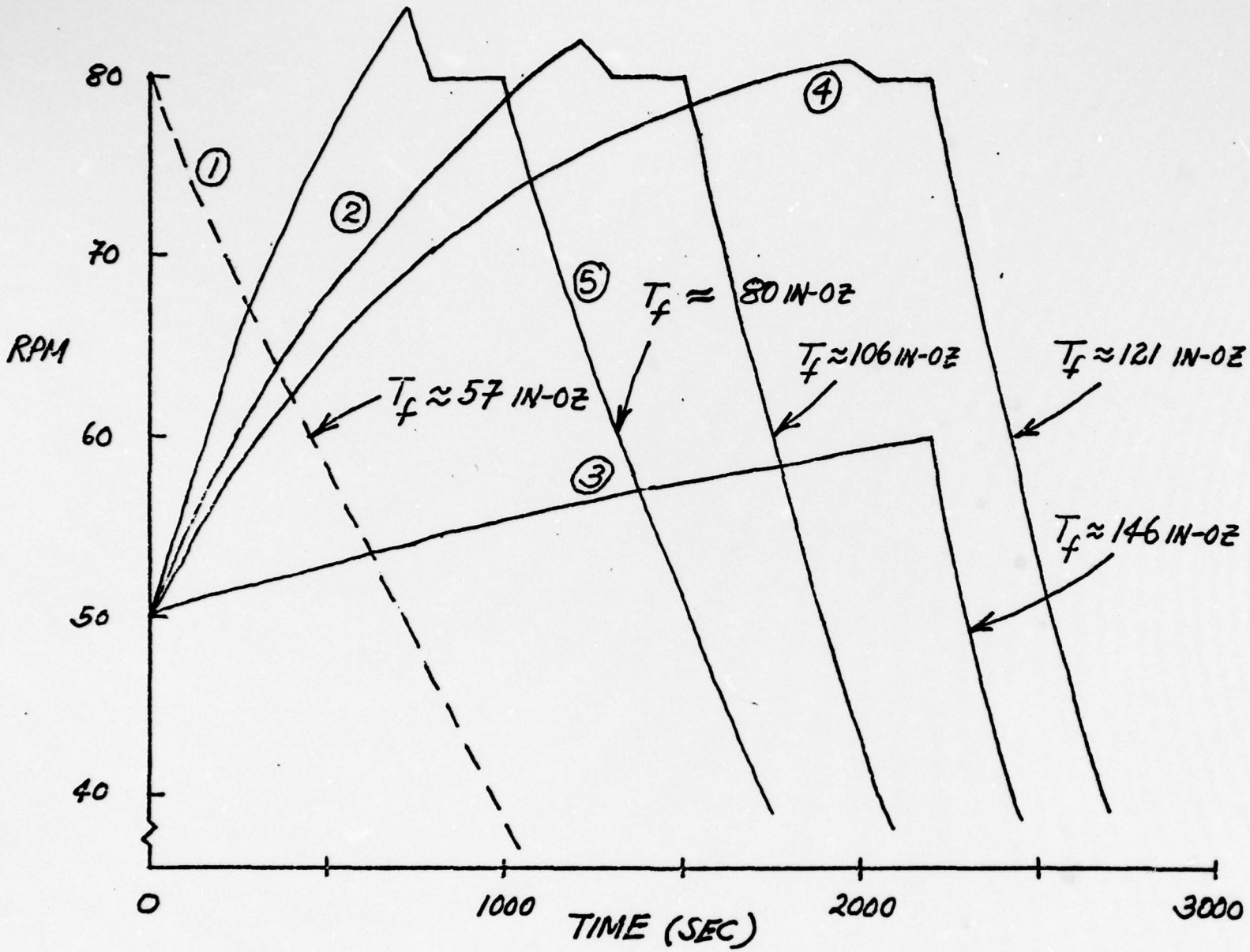


Figure 6.1-1. Laboratory System Test Results (9 October 1975)

6.2 DMA Assembly Level Tests

In addition to the system tests described above and the component tests reported in subsequent sections, assembly-level DMA tests were conducted on the life test unit (S/N 3-5), the flight spare unit (S/N 3-1), and the qual unit (S/N 3-2). In these tests, bearing friction was measured (with no load) by monitoring motor current. Performance of the life test unit was sampled throughout the period of the life test; this unit and the others were tested as part of the 9433 anomaly investigation, with various spin speeds considered. Figure 6.2-1 summarizes the torque history for the DMA life tests; Table 6.2-1 presents the data from testing each of these units during November. None of these tests show results which are noticeably abnormal; all data is similar and within the regime anticipated from a normal DMA. It is particularly notewrothy that the friction data from the life test DMA, which disassembly showed to have abnormal lead deposits in the retainer of the lower main bearing (Section 7), is not remarkable.

During testing of the life test DMA in air, a clearly audible sound was noticed to emanate from the DMA. This sound was recorded via a microphone on tape and later analyzed. Unfortunately, the quality of the recording arrangement and the relatively short period of recording prevents a definitive conclusion regarding the source of this sound. Spectral analysis, using a repeating continuous loop technique to provide low frequency data, showed the peak value of the low-frequency spectrum to occur just below 0.5 Hz; this particular peak, shown in Figure 6.2-2, appeared consistently in a number of data samples while none of the other peaks shown in the spectrum seemed to be repeated. Since the retainer frequencies (at 60 rpm) of the upper and lower main bearings are, respectively, 0.4.46 Hz and 0.453 Hz, this spectral data suggests that a major low-frequency component of the noise was related in some manner to retainer motion.

This data was also assessed in the high frequency regime, without using the repeating loop approach. The spectral data is shown in Figure 6.2-3. Note that much of the characteristic (e.g., roll off at high and low frequencies) can be attributed to the recording setup (microphone and recorder). The peak at 60 Hz is simply line ripple, as are probably those at 120 Hz and 180 Hz. However, there are other peaks at approximately 460 Hz and 920 Hz (repeated in a number of data samples)

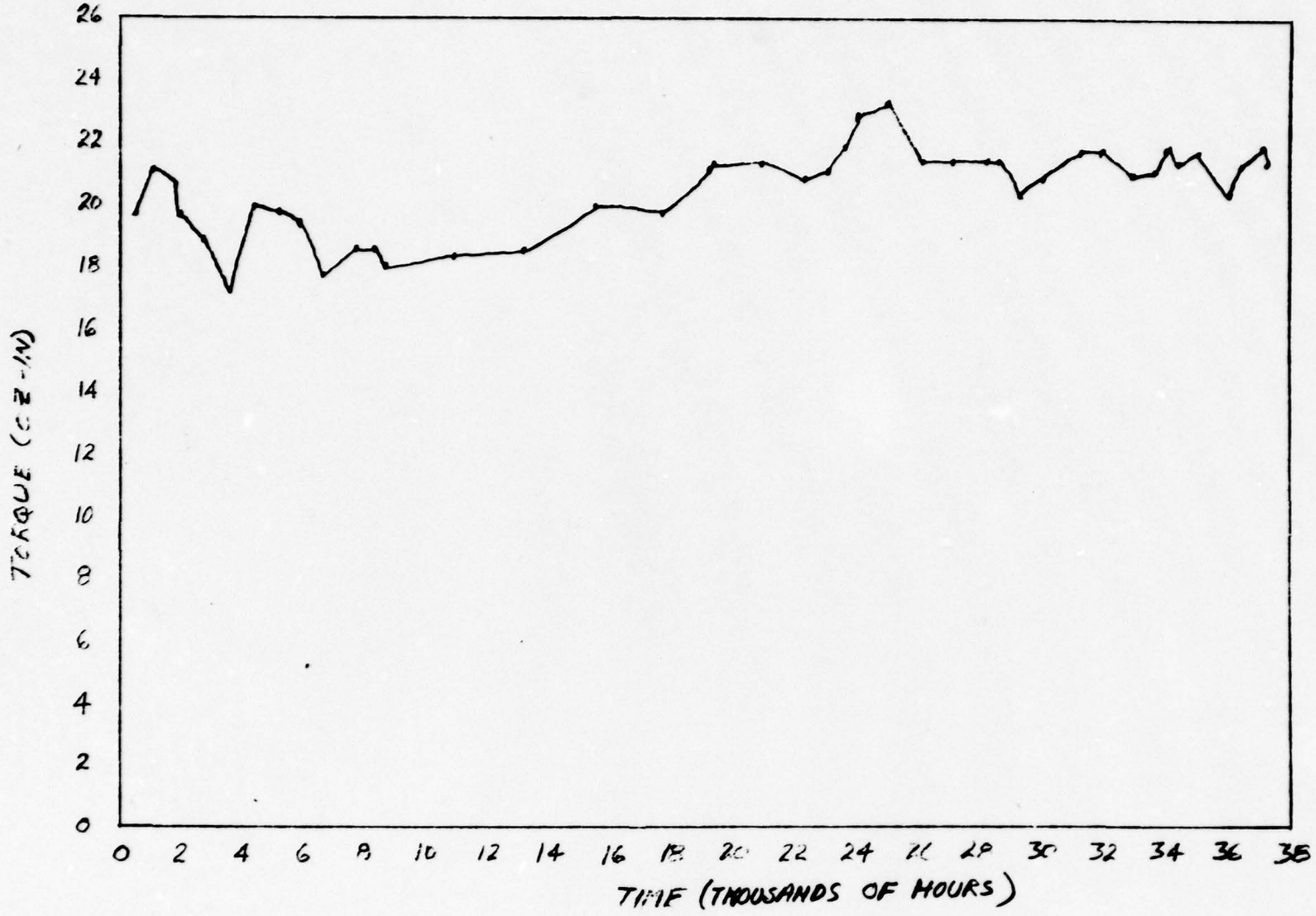


Figure 6.2-1. Torque History From DMA Life Test

Table 6.2-1. DMA Assembly-Level Torque Test Data

TEST ENVIRONMENT	SPEED (RPM)	LIFE TEST DMA (S/N 3-5)		FLIGHT SPARE DMA (S/N 3-1)		QUAL MODEL (S/N 2-1)	
		MOTOR 1	MOTOR 2	MOTOR 1	MOTOR 2	MOTOR 1	MOTOR 2
VACUUM	20	17.5	16.2	22.7	23.8	UNIT NOT TESTED IN VACUUM	
	40	19.7	18.3	27.5	28.3		
	60	20.3	20.8	30.2	30.2		
	80	23.8	23.1	32.7	33.8		
	100	28.3	25.6	35.7	36.0		
AIR	20	17.7	16.2	24.2	23.4	21.2	20.9
	40	20.3	18.7	29.3	27.9	24.1	23.6
	60	20.7	20.5	32.2	29.8	24.7	24.4
	80	24.1	23.4	34.9	33.3	22.4	22.5
	100	28.7	26.0	38.1	35.4	22.2	23.7

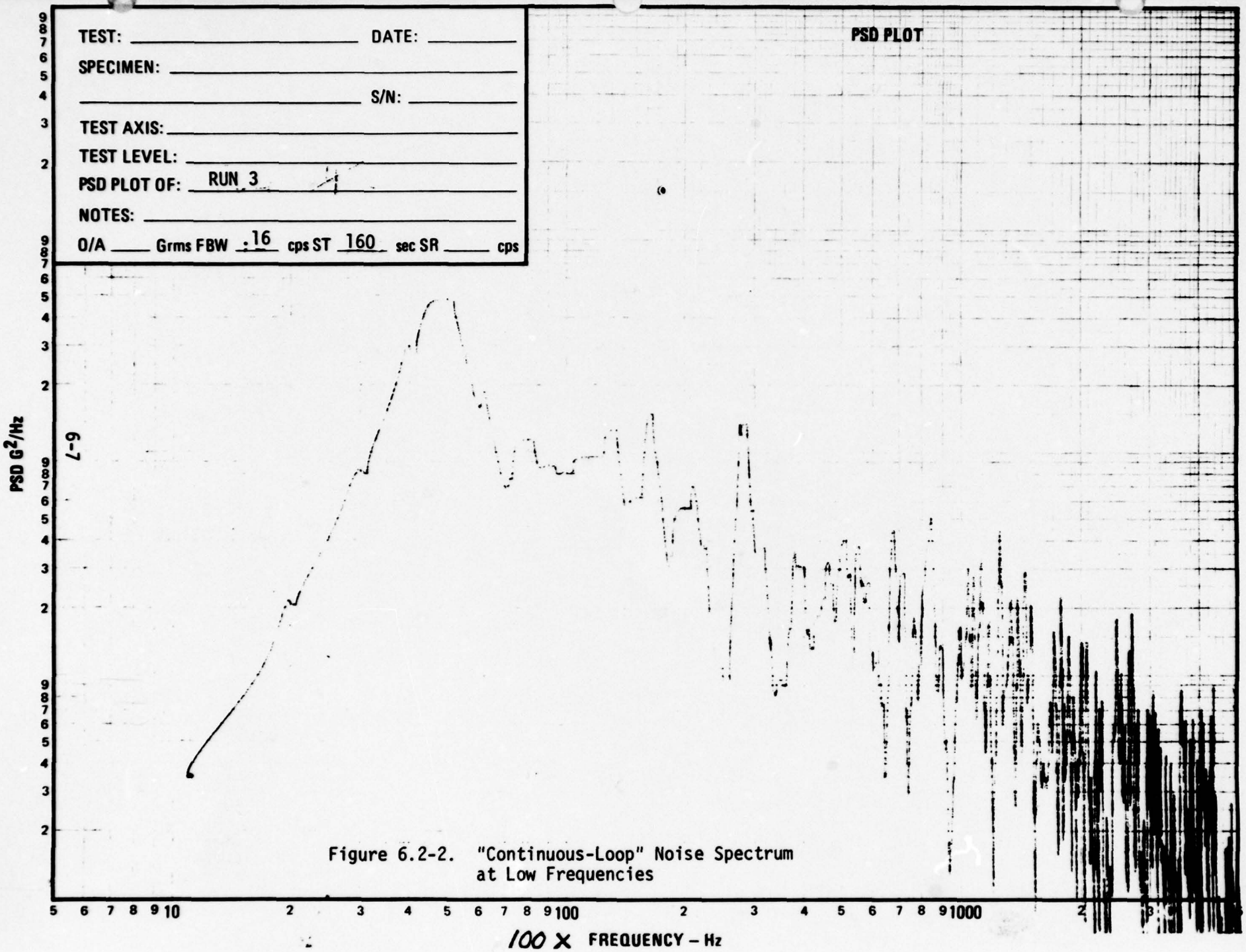


Figure 6.2-2. "Continuous-Loop" Noise Spectrum at Low Frequencies

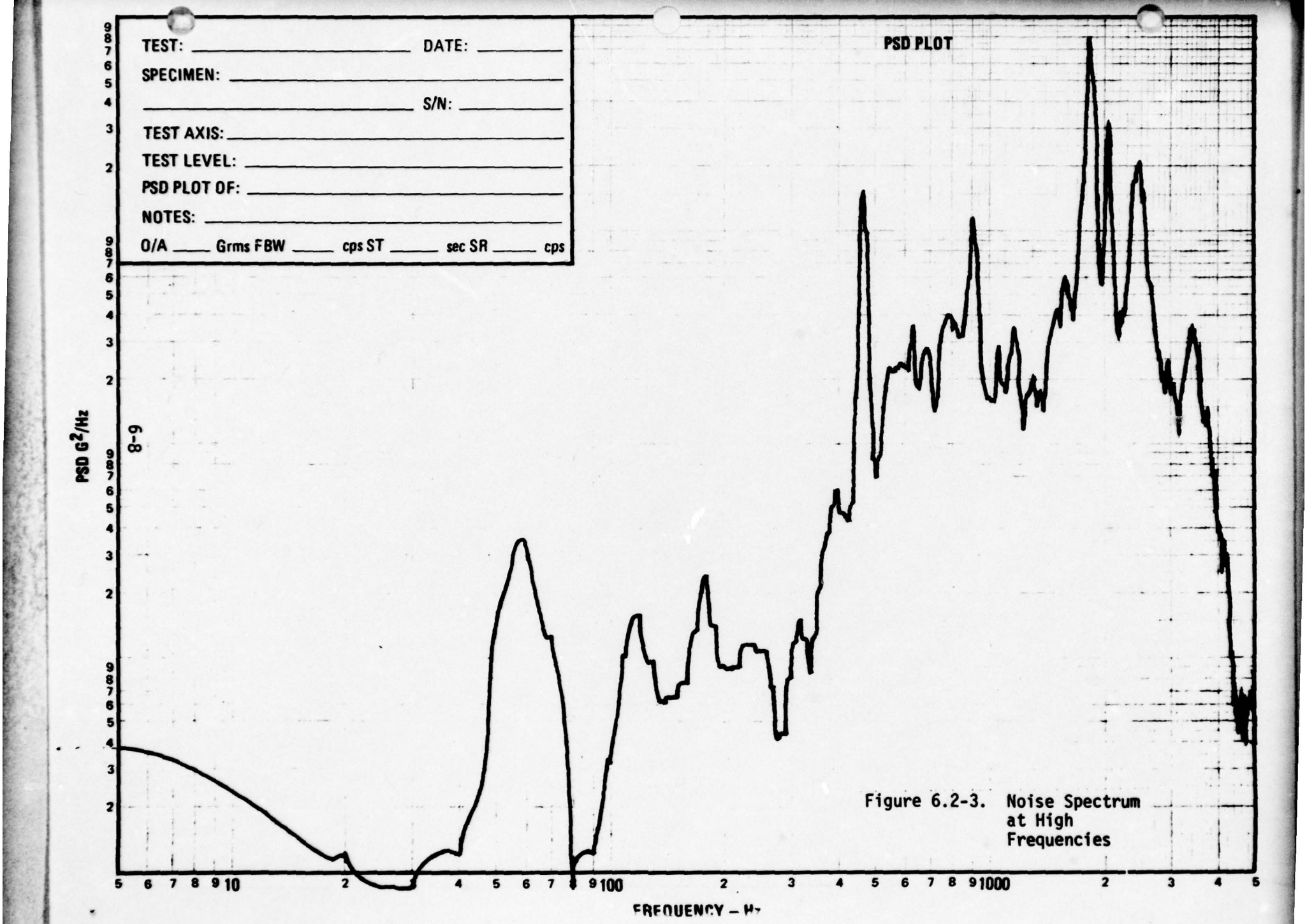


Figure 6.2-3. Noise Spectrum at High Frequencies

which appear to be too high in frequency to be attributed to line effects. These peaks may be from ambient (room) noise, since no background noise tape was made at the time or they may be due to retainer whirl or sequeal, since they are characteristic of those frequencies found in ComSat Labs' data.* However, this identification of the noise as related in a retainer must be regarded as possible rather than probable, since no additional confiriming data (such as visual observations or *in situ* bearing torque measurements) are available.

6.3 Bearing and Slip Ring Tests

6.3.1 Tests at Aerospace Corporation

During the early phase of the 9433 anomaly investigation, a number of bearing and slip ring assembly tests were conducted by Aerospace Corporation personnel. Table 6.3-1 is a summary of these results as supplied to TRW. The following paragraphs further summarize these tests and their results.

* C. J. Pentlicki, "Investigations of the Intelsat IV Bearing and Power Transfer Assembly," ComSat Technical Review, Vol. 13 No. 1, Spring 1973.

Table 6.3-1. TORQUE SIGNATURES OF POTENTIAL BEARING FAILURE MECHANISMS AS DETERMINED FROM AEROSPACE CORPORATION TEST DATA

Source of Torque Disturbance	Test Results (Torque Characteristics)
1. (a) Increased axial loading of despin bearings due to differential thermal expansion	Torque under normal 60 lb preload - 30 oz-in Torque under maximum 1200 lb preload - 82 oz-in
(b) Raceway misalignment due to debris in sliding fit or preload spring hang-up.	Torque due to eccentric axial load >1000 lb tilting raceway (90 mm brg) - 110 oz-in
2. Despin bearing(s) balls sliding in raceways and/or bearing(s) rotating as journals.	Despin bearings rejected debris inserted during rotation. Debris jammed under balls while stationary increased torque from 50 oz-in to >800 oz-in. Torque due to locked retainer (90 mm brg) - 320 oz-in.
3. Higher average torque due to increasing metal to metal contact	Thermally polymerized lubricant (Apiezon C) inserted in 90 mm brg increased torque to 30 oz-in; polymerized lubricant inserted in both despin bearings increased torque to 65-70 oz-in. Polymerized lubricant inserted into both slip rings bearings increased torque from 3 oz-in to 10 oz-in.
4. Slip ring bearing(s) balls sliding in raceway(s) and/or bearings rotating as journals.	Debris jammed under balls while stationary (8 mm brg). Torque initially varied between 5 to 60 oz-in. After 6 hours of continuous rotation, torque increased to 140 oz-in.

6.3.1.1 Bearing Tests

The first group of tests involved DMA main bearing behavior for the conditions of jamming and the introduction of debris between balls and the bearing races. These tests were not witnessed by TRW personnel, but the reported results (by Aerospace) can be reduced to the following:

- The jamming of the races to force journal effects produces torque values, which are much higher than the steady state torque characterizing the DMA's anomaly behavior.
- The impact of metallic debris on the bearing torque, for the test time period, was insignificant. The debris were either coined or thrown away from the ball track.
- Polymerized lubricant (Apiezon C) resulted in a torque increase of about 30-40 in-oz above the nominal value of 30 in-oz.

Quantitative tests were conducted on the main bearing subassembly, in order to characterize bearing friction torques as a function of axial loads and bearing misalignment.

- Bearing Friction as a Function of Thrust Load

  The DMA was mounted to an air bearing's null seeking dynamometer. A special axial loading spring assembly was mounted in-line with the DMA shaft to afford relatively accurate application of various value thrust loads. An extension of the shaft passing concentrically through the loading mechanism was driven by a rate control servo motor. The bearing friction torque, reacting against the null servo, was measured directly by the dynamometer system, and the value of the applied load was a function of the calibrated spring deflection. The test data was taken at 60 RPM and the results are given on Figure 6.3-1. The data suggests that lock-up of the preload mechanism will not produce steady torques of the magnitude seen in orbit.

- Bearing Friction as a Function of Bearing Misalignment

  Using the same test facility, and a nominal bearing preload condition of 64 lbs, top bearing misalignment was induced by installing shims of various thicknesses between the bearing race and a plate fixed to the shaft. The resulting data obtained at 60 RPM shaft speed is given on Figure 6.3-2. This data shows inconsistencies with the observed orbital data, inasmuch as the maximum bearing misalignment geometrically possible is 0.04 degree, and at this value, the bearing friction increase from nominal is less than 15 in-oz.

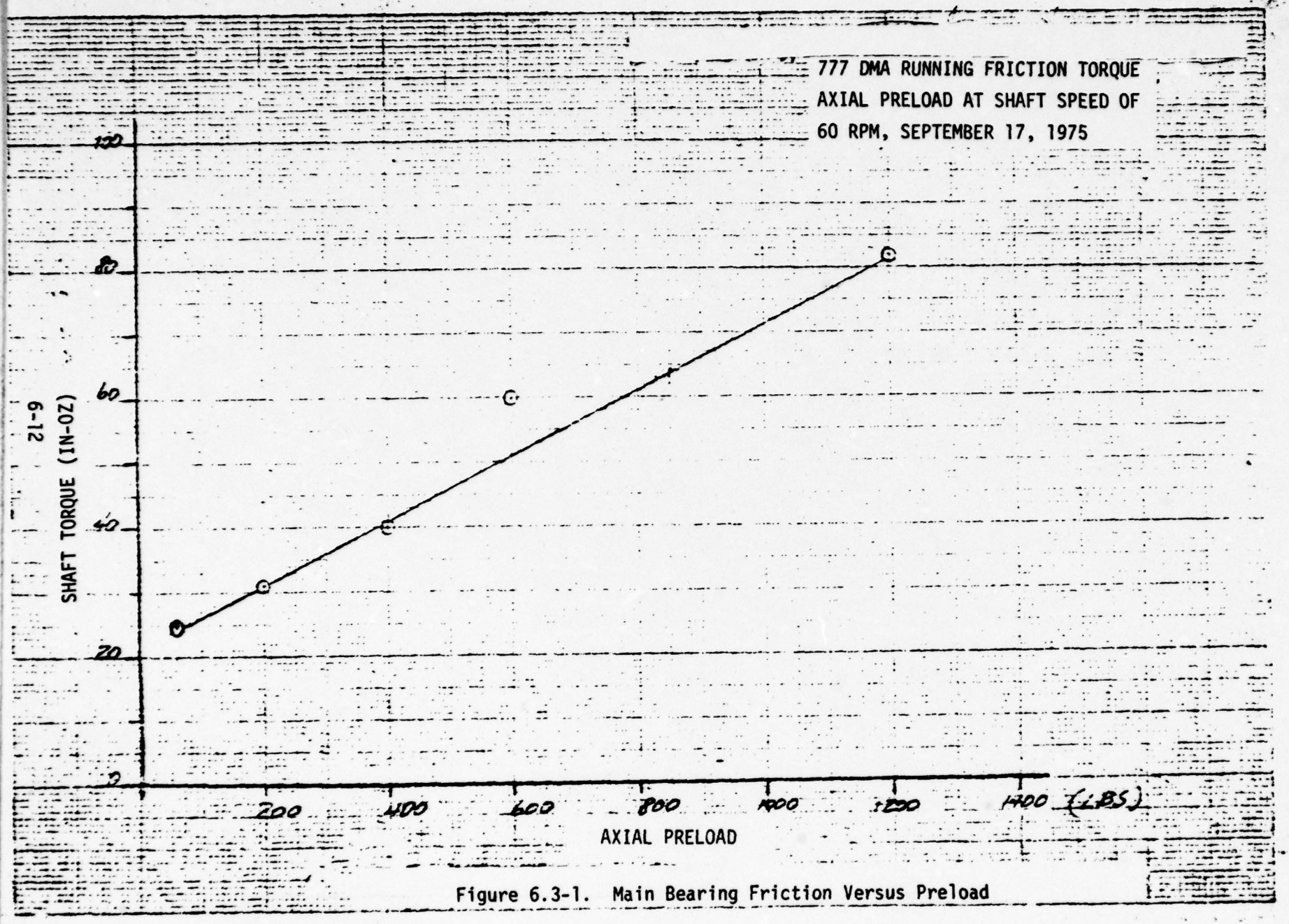


Figure 6.3-1. Main Bearing Friction Versus Preload

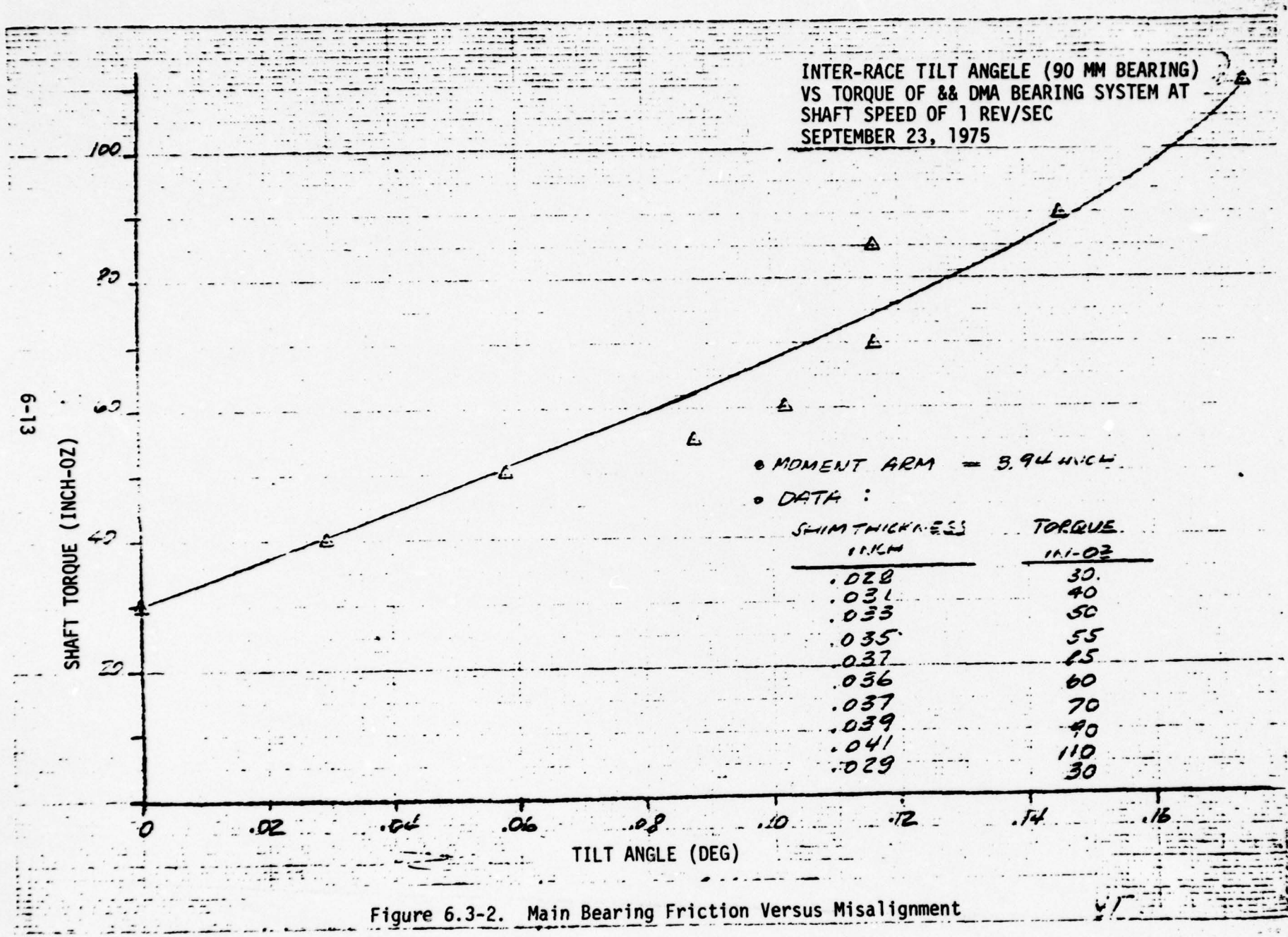


Figure 6.3-2. Main Bearing Friction Versus Misalignment

6.3.1.2 Slip Ring Assembly Tests

The slip ring assembly bearing tests were conducted by Aerospace Corporation with the test facility described in Section 6.3.1. The significant results were:

- The slip ring assembly bearings nominally exhibit approximately 3 in-oz torque
- When debris is introduced, the torque increases, but eventually tends to return to the nominal friction torque value
- When subjected to jamming that forces a bearing journal effect (small diameter bearing), the system friction increased monotonically for the period of the test; for example, six hours of operation produced 140 in-oz torque.

6.3.2 Tests at TRW

A number of bearing and slip ring tests have been run at TRW in the course of the DSCS-II program. However, from a functional point-of-view, most recent testing has focussed on the assembly tests, system tests, and motor/electronics tests reported elsewhere in this section. Specific bearing cartridge functional tests have been run in support of the life test anomaly investigation and will be reported when those studies are complete.

Much component-level life testing has been completed and documented, as summarized in Table 6.3-2.

Table 6.3-2.

List of Reports Documenting 777 DMA Bearing and

Slipring Assembly Life Test Results and Analyses

Life Tests/Lubricant	Krytox 143AB	Vac Kote
Three Month Drive Bearings	7521-381	7521-148
Twelve Month Drive Bearings	7511-733/73 7511-786/73	7511-733/73 7511-913/73
Thirty-Six Month Drive Bearings	7511-2610/75	7511-2218/74(2) 7511-2422/75
Life Test DMA Bearings	None Tested	(4)
Twenty-Four Month Slipring Assembly Bearings	See below	See below
Three Month Inspection	7521-440	7521-440
Twelve Month Inspection	7511-214/72 7511-394/72 7511-411/72	7511-410/72
Twenty-Four Month Inspection	7511-2414/75	7511-646/73
Thirty-Six Month Slipring Assembly Bearings	7511-2414/75(1)	(3)
Six Month Storage Bearings	7511-182-72	7511-182-72

(1) The Krytox 142 AB slipring assemblies were terminated prior to completion of the testing

(2) Two bearings were examined and replaced after three years operation. The remaining bearings were tested for an additional year and have not yet been examined.

(3) The 36 month Slip ring Assembly was run for a total of 4 years and has not been examined yet.

(4) The Life Test DMA bearings are being examined.

6.4 Snubber Tests

A nominal .00825 inch radial gap separates the snubber stator from the opposing rotor. A failure mechanism was posed in which this gap would somehow close, causing metal-to-metal rubbing. The purpose of this test was to determine what would happen if the snubber surfaces contacted while rotating. Would they seize up, would they stabilize at some intermediate friction torque condition, or would they wear away, causing the friction to diminish?

A thermal gradient between rotor and stator could theoretically close the entire nominal gap. This situation was unlikely, however, since it would require (under nominal conditions) a gradient in excess of 330°F, far greater than possible (see Appendix A). A more plausible situation would be partial closure of the gap due to faulty assembly and completion of the closure by subsequent mechanical distortion such as material instability and/or more reasonable thermal gradients.

In order to evaluate the effects of snubber interference and estimate the trends in performance which might occur, the laboratory test set-up is shown in Figure 6.4-1 was conceived and implemented. A simulated snubber rotor element was mounted above the DMA as shown while a simulated snubber stator was suspended via a fixed overhead frame. Both the rotor and stator were machined to provide flight-type dimensions, material, and surface treatment. The stator was mounted via a pivot so that contact with the rotor could be maintained via an adjustable spring load (which was monitored using a load cell). During tests, the loading was adjusted to maintain a constant total friction of approximately 110 in-oz, as indicated by motor current on an oscilloscope; approximately 50 in-oz of this total friction was due to the snubber contact.

The test procedure was to run for a period of time and then to shut down and measure the total decrease (wear) or increase in dimensions along the contact radius. Figure 6.4-2 shows the radial wear resulting from a two hour test in which a constant snubber friction of approximately 50 in-oz has been maintained. The normal force was initially 5.9 lbs and was steadily reduced during the first 11 minutes to 3 pounds. During this period, the snubber was producing a black debris as the anodize coating was being worn

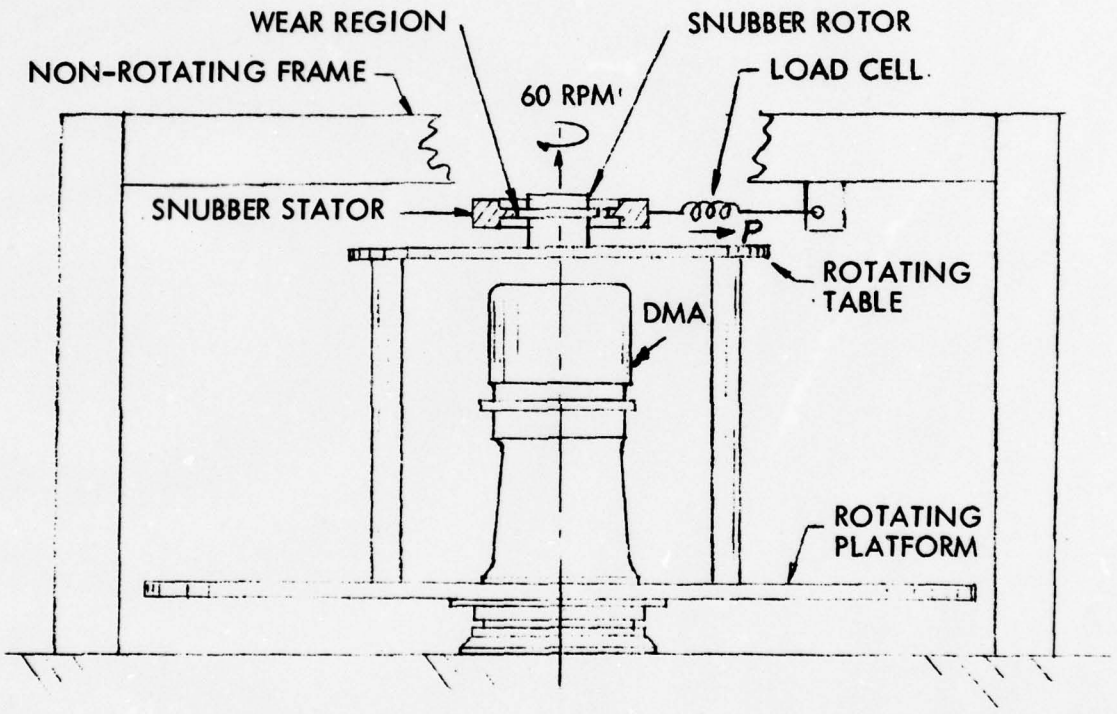


Figure 6.4-1. Snubber Test Set-Up

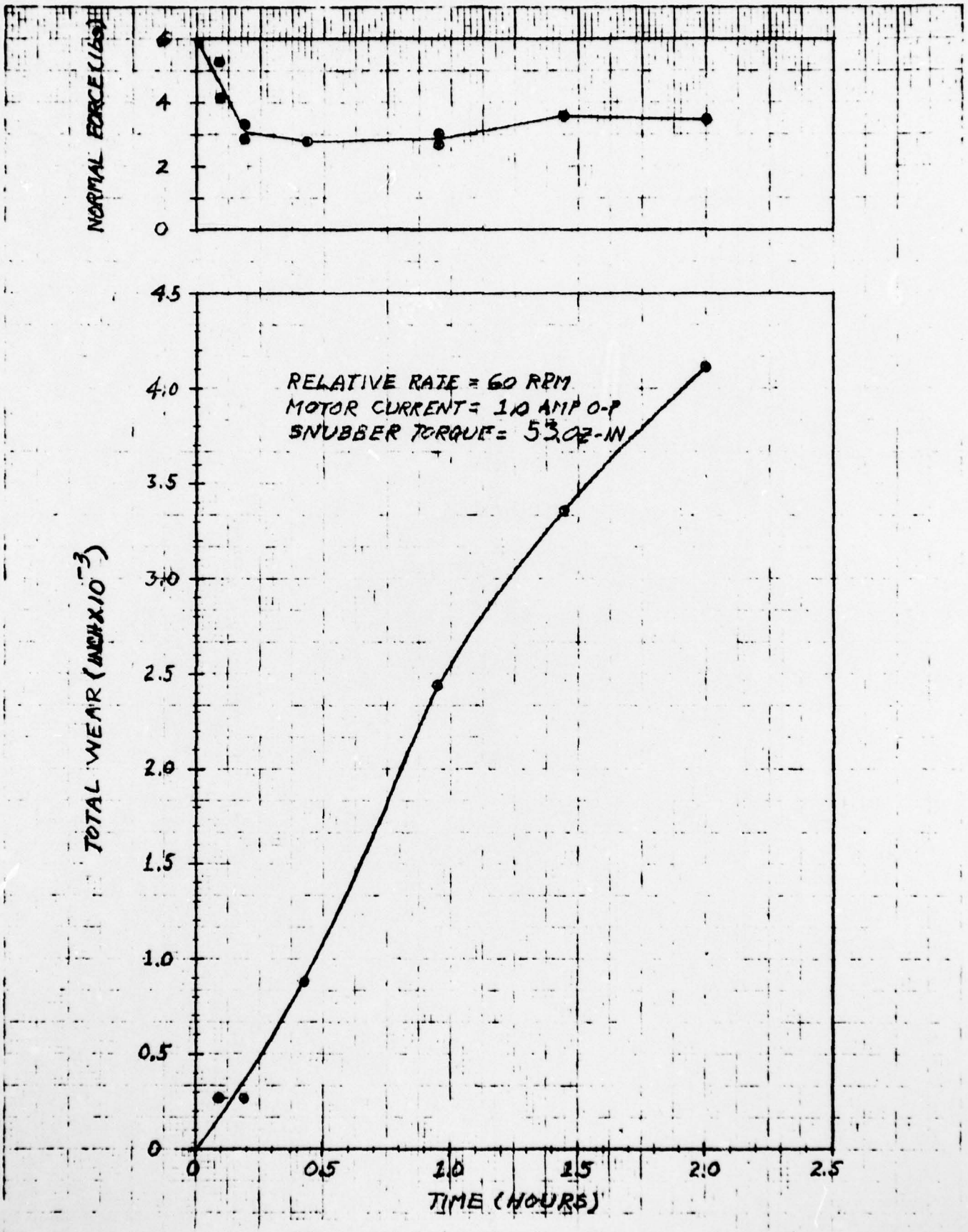


Figure 6.4-2. Snubber Wear Test Data

off. The reduction in normal force at constant torque indicated an increased shearing force. The shearing force stabilized after 11 minutes at a value of approximately 1.41 lbs. This was representative of a coefficient of friction of 0.47 between the snubber rotor and stator. Figure 6.4-2 indicates that the total radial wear increased steadily at a rate of approximately .002 inch per hour. The wear debris after 11 minutes consisted of galled powder, flakes, and rolled strands of aluminum.

The wear rates shown by these tests argue against the possibility of sustained rubbing at the snubber, since contact pressures of the magnitude required to develop significant frictional effects also cause wear rates which, in less than two hours, would eliminate any interference possible due to assembly tolerances, material creep, or thermal effects (Section 5.2). However, in employing the results of these tests, it should be remembered that they were performed in a laboratory under ambient thermal conditions. Thus, neither the vacuum of space nor the thermal conditions of a DMA snubber in orbit were accurately simulated.

6.5 Motor Tests

The DMA motor tests included three tasks:

- establish general performance characteristics of the DMA motors.
- investigate the effects of broken hypernik ring in the motor.
- evaluate the performance characteristics of the redesigned (Phase II) DMA motor.

6.5.1 DMA Motor Performance

The purpose of this test was to determine the performance characteristics of the DMA and its drive electronics under certain controlled conditions so that their behavior and capabilities are better understood. To accomplish this task, a dynamometer table was set up as shown in Figures 6.5-1, 6.5-2 and 6.5-3. In includes an air-bearing table which provides a nearly frictionless support for the DMA. With the DMA housing mounted to air-bearing table and the shaft attached to a fixed structure through a torsional strain gauge and flexible coupling, the output torque of the motor is measured by the pre-calibrated strain gauge. The table speed is measured with a photo-electric detector and counter. Two small control motors, one AC and one DC, are engaged to the air-bearing table through a thin mylar belt. For each error (voltage compensated error signal) setting, the DMA is allowed to spin at its no-load speed; then the control motor is energized with increasing potential so that its opposing torque slowly brings the DMA/air bearing table to a stall. The output torque and speed (strain gauge and photodetector outputs) are simultaneously recorded on an X-Y plotter, thus creating the torque/speed curve.

A DMA motor was supplied by BBRC for this evaluation. In order to ascertain the accuracy of test data, both the engineering model DEA and the flight spare DEA were used to generate a family of torque/speed curves as a function of error (bias) voltages. These test results are presented in Figures 6.5-4 and -5.

A peculiar phenomena revealed by the test data is that the speed curves do not converge to a peak torque as the error voltage is increased linearly to a maximum value of 5 volts. Instead, they assume declining slopes (Figures 6.5-3 and 6.5-4) at error voltages over 3 volts. Moreover, the torque reduction appears to be speed-dependent - greater reduction with increasing speed. This characteristic can partially explain the net torque decrease near 80 rpm during the initial friction test on 30 September 1975 (Figure 3.4-2).

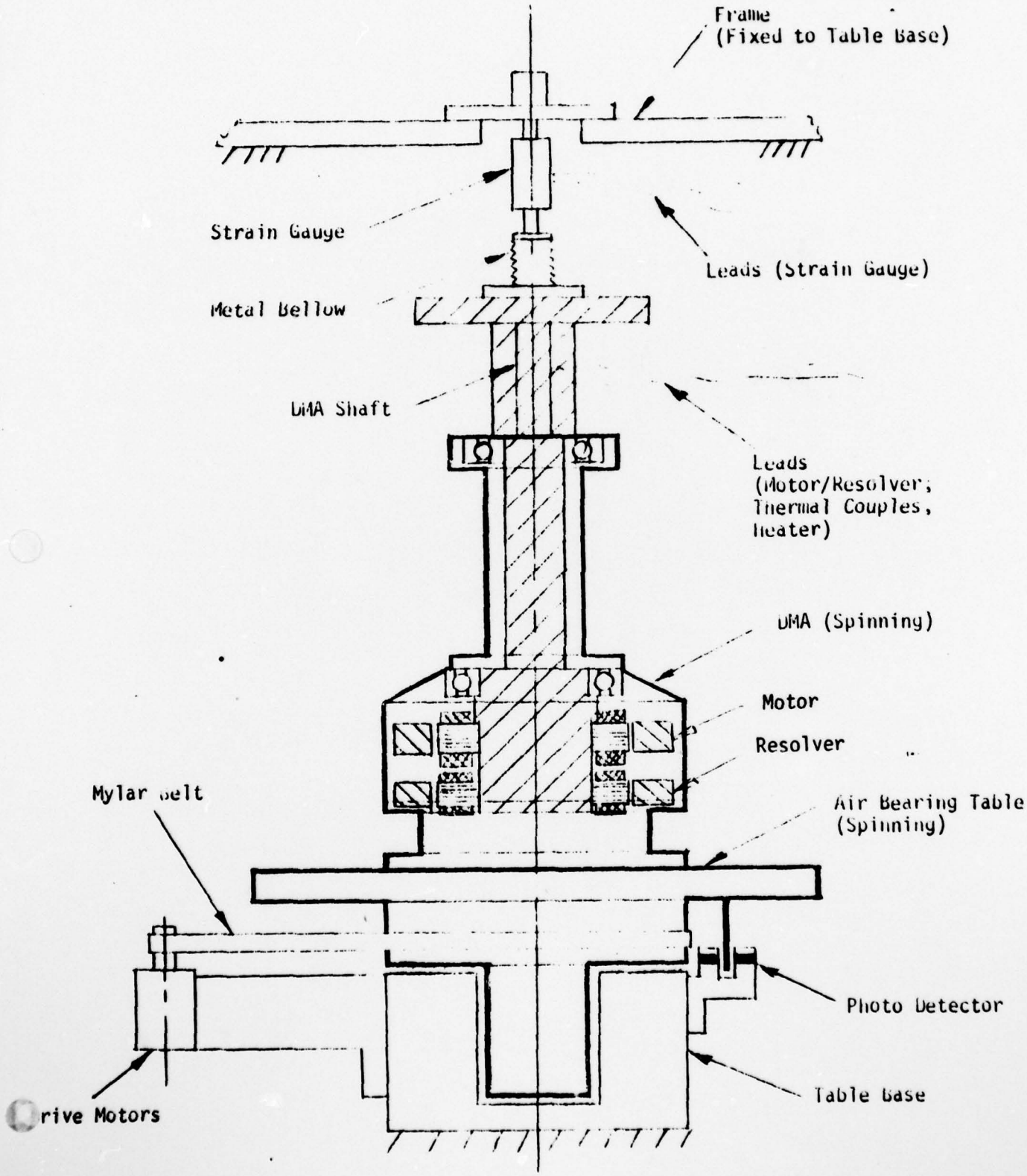


Figure 6.5-1. Mechanical Setup - 777 DMA Motor Test

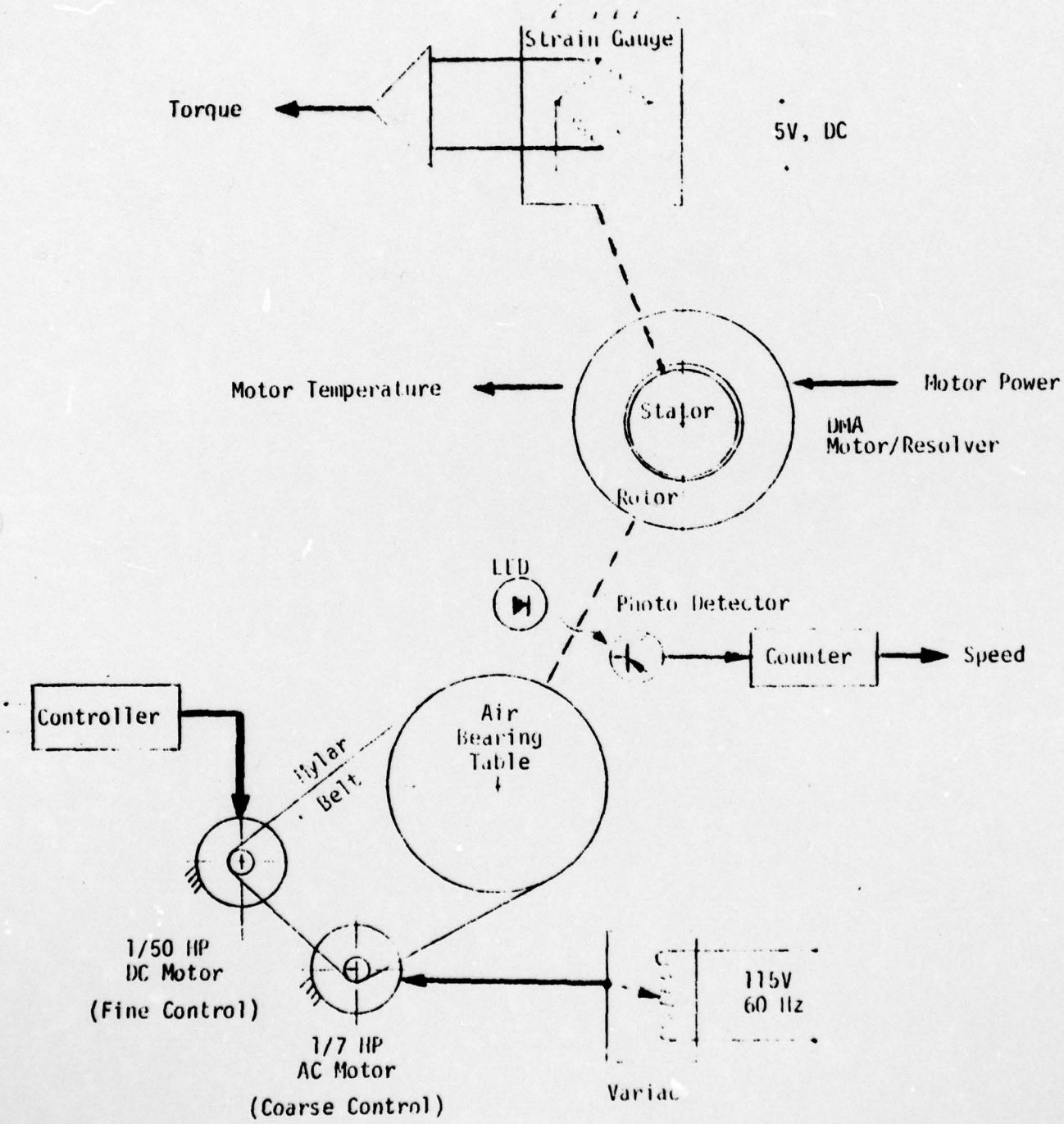


Figure 6.5-2. Schematic Diagram - 777 DMA Motor Test Setup

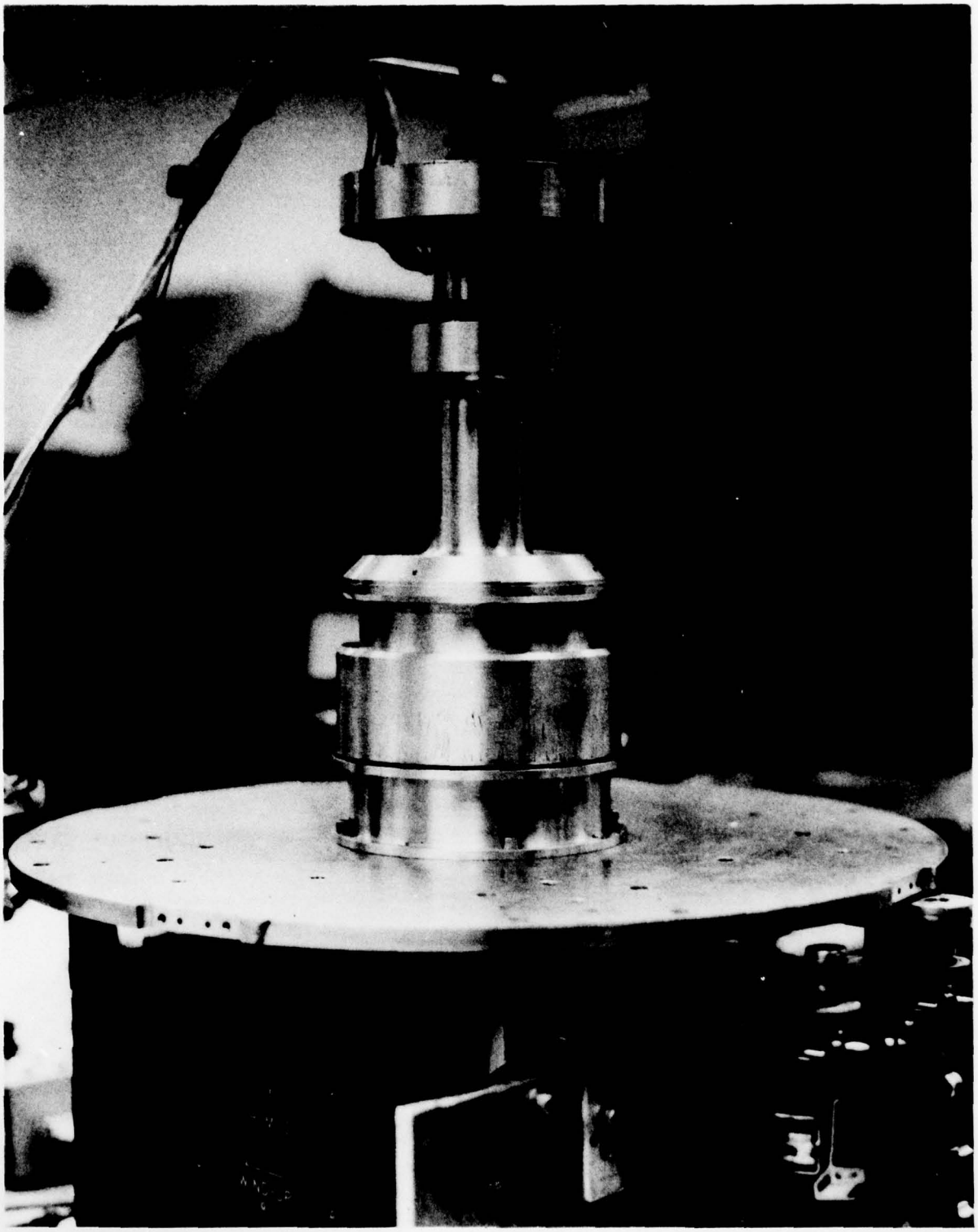


Figure 6.5-3. Motor Test Setup

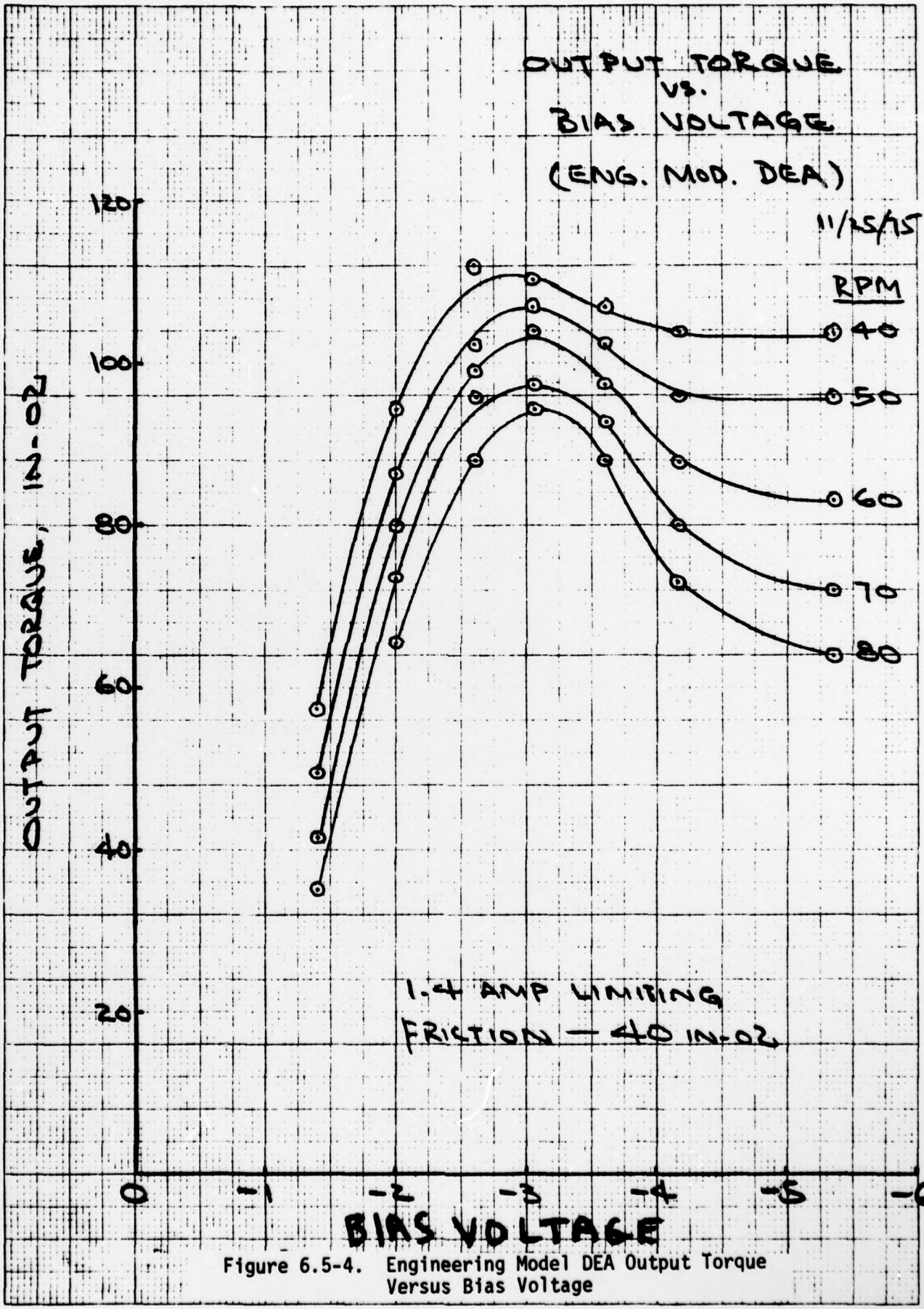


Figure 6.5-4. Engineering Model DEA Output Torque Versus Bias Voltage

EUGENE DIETZGEN CO.
MADE IN U. S. A.
NO 340-20 DIETZGEN GRAPH PAPER
20 X 20 PER INCH

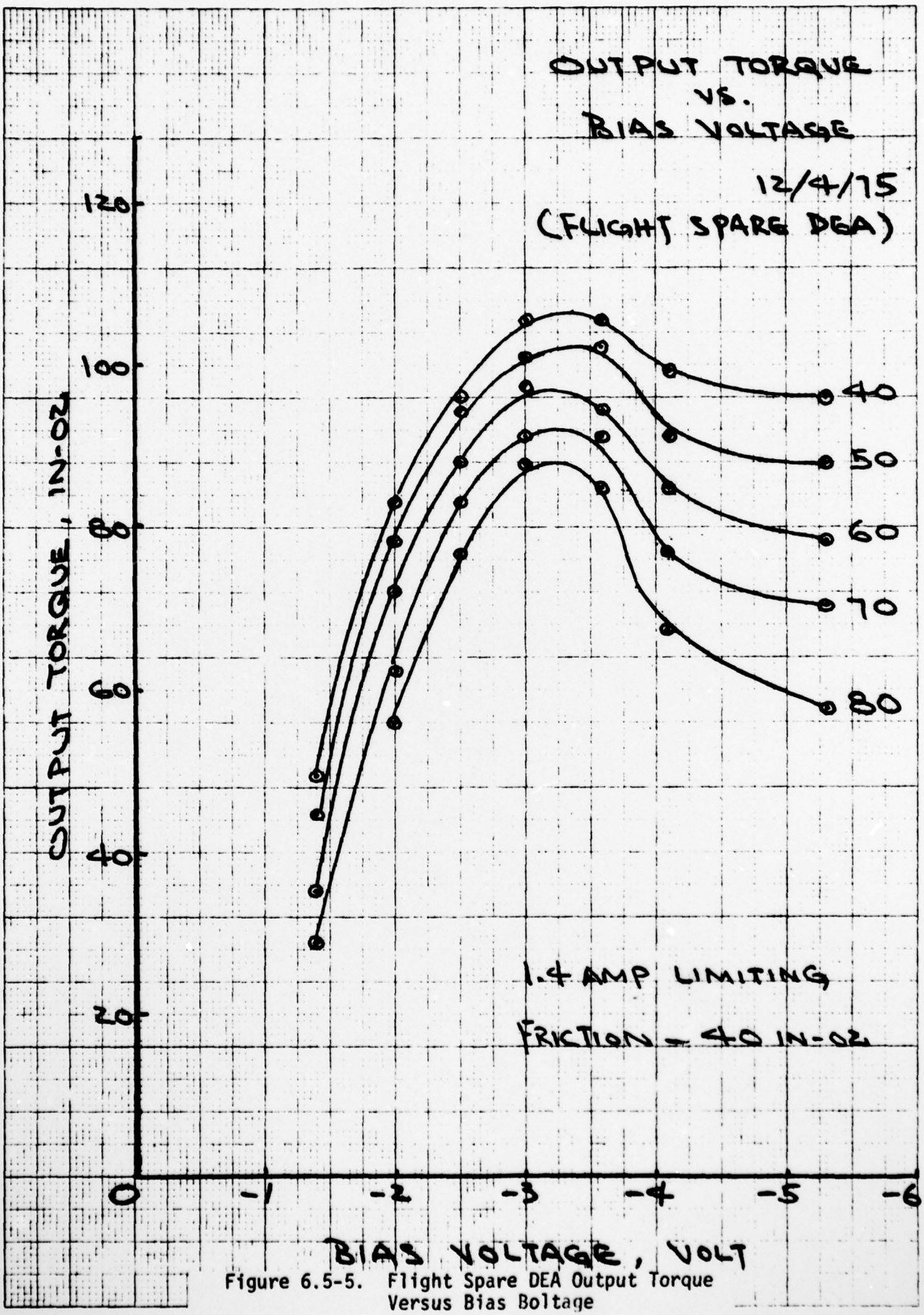


Figure 6.5-5. Flight Spare DEA Output Torque Versus Bias Boltage

Test Data indicates that this torque decrease is due to a phase shift between the resolver signal and the drive current to the motor. Referring to Figure 1-4, this phase shift occurs due to the switching regulator being duty-cycled by the current detector to maintain a limited motor current in the saturated regime. This is equivalent to a reduction in the forward-loop gain of the feedback loop consisting of the summing amplifier, the pulse-width modulator, the switching regulator, and the power bridge. Such a decrease in the open-loop gain results in a decrease in the bandwidth of the closed-loop characteristic, with an attendant increase in phase shift between the resolver demodulator output and motor input.

6.5.2 Effect of Broken Hypernik Ring

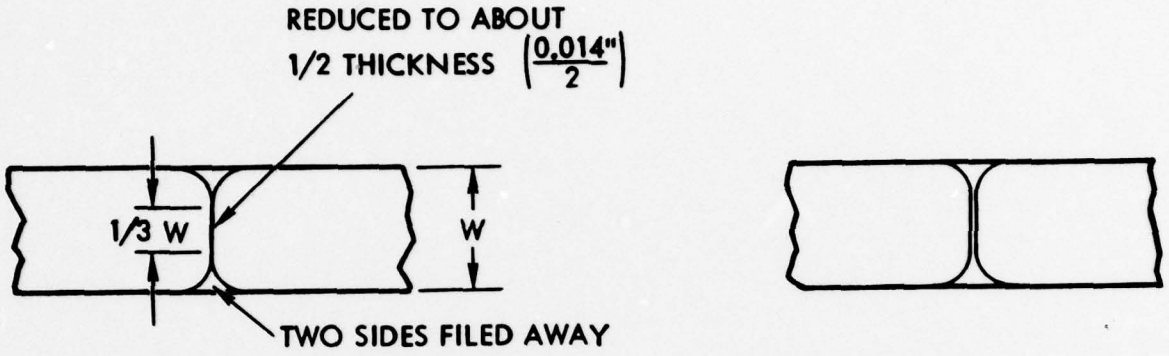
For the purpose of evaluating the possibility of a broken hypernik ring as a contributor to the apparent friction increase in the 9433 DMA, the hypernik ring of the test motor was severed in four progressing steps, and the DMA friction and performance were measured at each stage:

(i) The hypernik ring was partially broken as shown in sketch "a" below. It exhibited no increase in friction, nor any change in performance.

(ii) The hypernik ring was completely severed at one location, sketch "b," but the ring retained its original contour even though the two broken ends lost adhesion to the lamination stack for about two slot widths. Maximum breakaway torque (mechanical) increased from 40 in-oz to 60 in-oz, because each time the broken ends passed by a magnet in the rotor, they were pulled and rubbed. However, running friction and performance showed no noticeable change, even after 8 hours of rotation at 60 rpm in both directions.

(iii) The hypernik ring was manually separated from the stack for about 1/2 of the circumference (witnessed by Aerospace personnel). The breakaway friction varied between 140 and 200 in-oz. The maximum motor output torque could hardly overcome the friction.

(iv) When the hypernik ring was completely separated from the stack, the friction jumped up to 30.5 in-lb. After some forced rotation at 60 rpm for about 5 minutes, the friction stabilized around 20 in-lb, well in excess of the motor capability.



a. PARTIALLY BROKEN

b. COMPLETELY SEVERED

In conclusion, results from the four cases investigated above do not correlate to the friction level and DMA behavior observed. Considering the good adhesion and conformity of the ring to the stack, even after complete severence, it is unlikely that the high friction can be attributed to a broken hypernik ring.

6.5.3 Performance of Phase II DMA Motor

A test model incorporating the newly-designed DMA torque motor was fabricated for comparative purposes (see Figure 6.5-6). The performance curves are plotted in Figures 6.5-7 and -8, for 1.4 amp and 2.0 amp current limiting, respectively. It is apparent that this new motor has a higher torque sensitivity than the minimum specified (130 in-oz/amp versus 102 in-oz/amp minimum specified). In the case of 2.0 amp limiting, however, the maximum output voltage of 28 volts was reached before current saturation. Therefore, the droop in output torque at higher speeds was due to back emf instead of phase shift in the current limiting circuit. These results show that the earlier motor test, using a Phase I motor, yielded results which were not unit dependent. In addition, an increase of the current limit to 2.0 amps significantly ameliorates the torque droop seen in Figure 6.5-4.

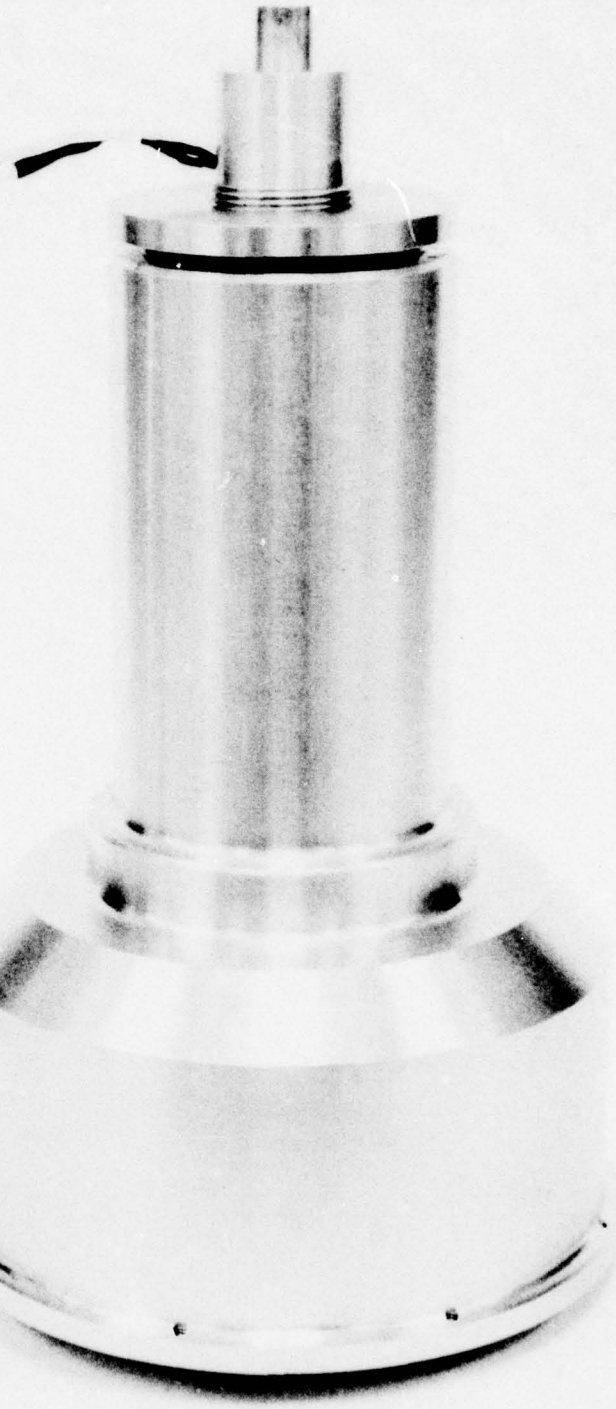


Figure 6.5-6. Test Fixture for Phase II Motor

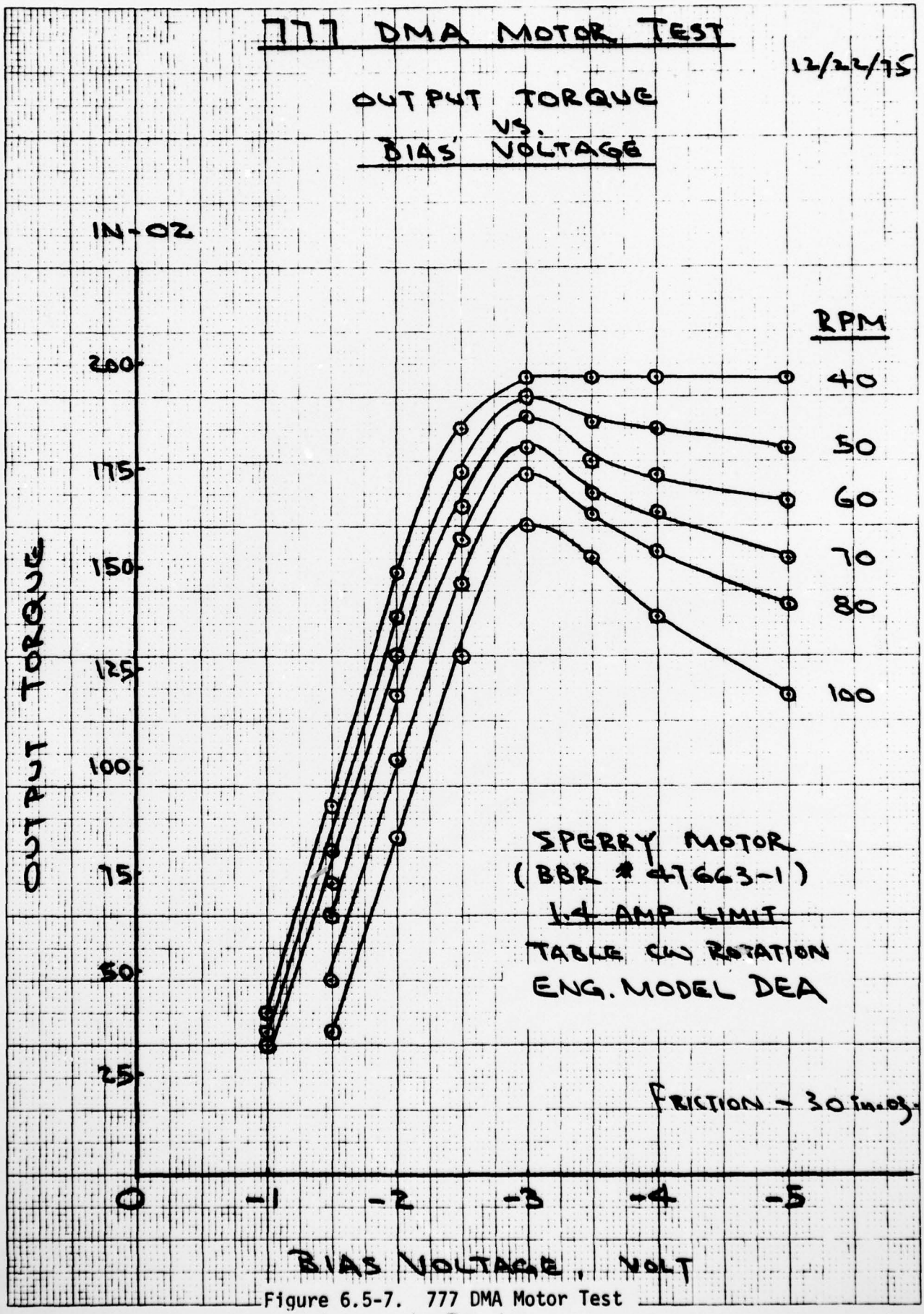


Figure 6.5-7. 777 DMA Motor Test

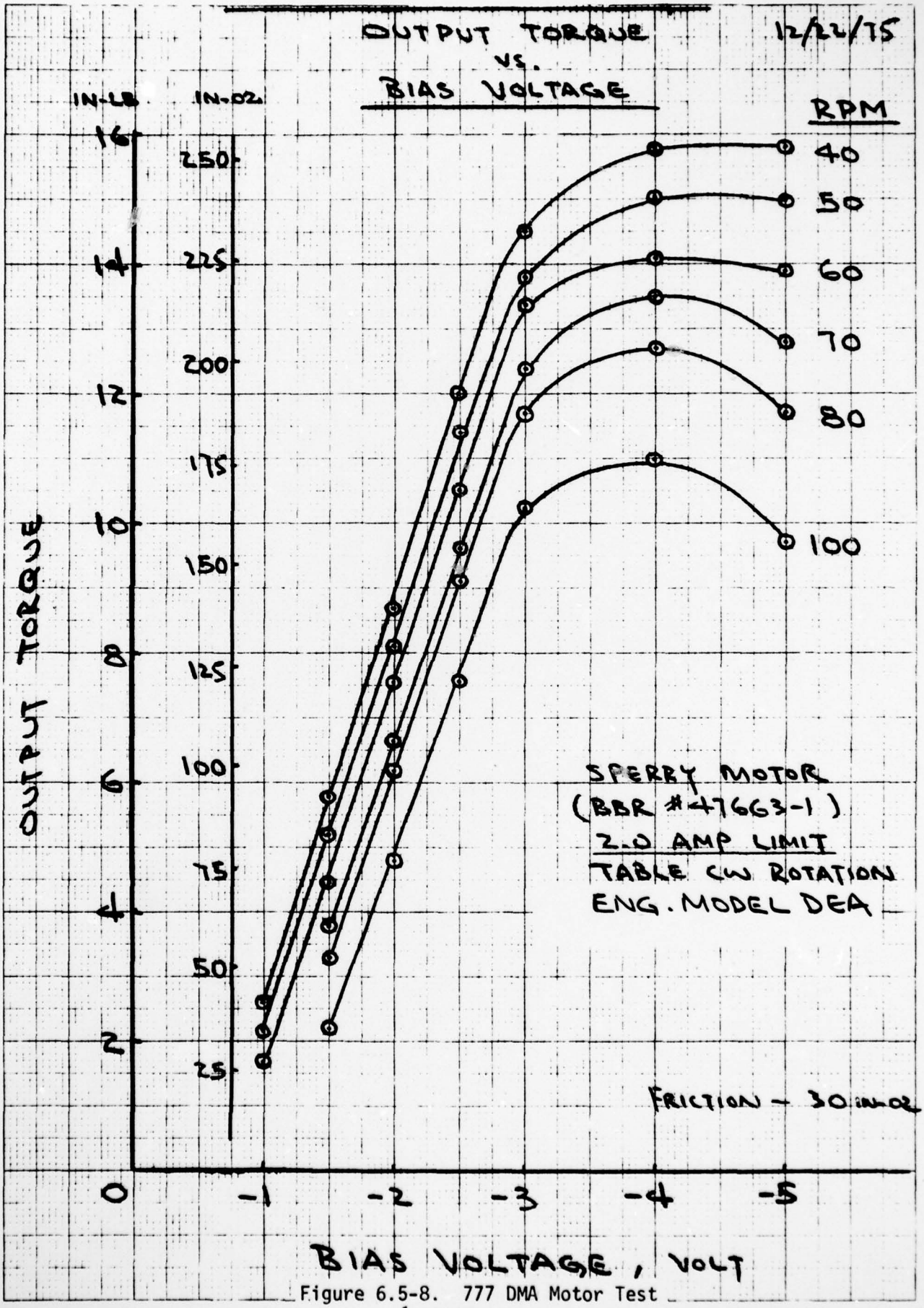


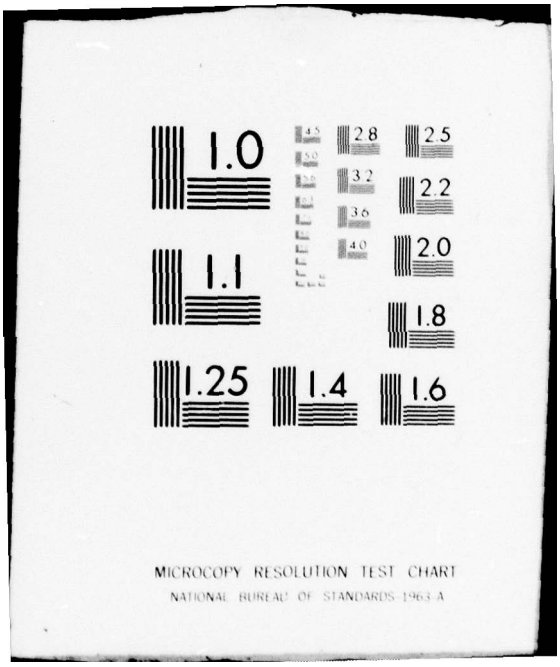
Figure 6.5-8. 777 DMA Motor Test

AD-A073 437 TRW DEFENSE AND SPACE SYSTEMS GROUP REDONDO BEACH CA F/G 22/1
9433 DESIGN POINTING ANOMALY. VOLUME I. TECHNICAL REPORT.(U)
JAN 76 P C WHEELER F04701-75-C-0257
UNCLASSIFIED TRW-28600-AR-010-01-VOL-1 SAMSO-TR-79-13-VOL-1 NL

3 OF 3
AD A073437



END
DATE FILMED
10-79
DDC


1.0
1.1
1.25
1.4
1.6
2.0
2.2
2.5
2.8
3.2
3.6
4.0
4.5
5.0
5.6
MICROCOPY RESOLUTION TEST CHART
NATIONAL BUREAU OF STANDARDS-1963-A

7. DMA DISASSEMBLY AND INSPECTION

In conjunction with the 9433 anomaly investigation, both the life test unit (S/N 3-5) and the flight spare (S/N 3-1) were disassembled and inspected.* In the first case, primary interest focussed on the effects of four-year operation in a vacuum environment. Examination of the flight spare was particularly concerned with any deterioration or contamination which might have occurred due to storage or handling. (It is noteworthy that the storage and handling history of the flight spare unit closely approximates that of the 9433 DMA prior to launch - see Section 8.)

Evaluation of these units (in particular of the several abnormalities found in the life test unit) is still in progress. Presented here is a summary of the preliminary results of DMA disassembly and inspection.

7.1 Approach

In order to insure a successful disassembly, a detailed disassembly procedure was developed (Table 7-1) and employed systematically with each unit. Prior to disassembly, each unit was tested functionally, as reported in Section 6. Following transportation to the disassembly area (a clean room), each unit was disassembled according to Table 7-1. This operation was performed at TRW by a BBRC technician experienced in the assembly and disassembly of this unit, and witnessed by TRW and BBRC engineers. Extensive photography was employed to assure a record of each step of the process.** In addition, a disassembly notebook was maintained.

The procedure of Table 7-1 is based on (and incorporates by reference) the BBRC DMA.assembly procedure. Appendix C presents the complete disassembly procedure (i.e., including the referenced documents).

---

* Note that disassembly and inspection was already planned as part of the life test program. However, the tests and examinations (still in progress) have been far more extensive than originally planned.

** These color photographs are in the possession of A. H. Rosenberg of TRW and can be reviewed upon request.

Table 7-1. Disassembly and Inspection Procedure — 777 DMA Life Test Unit S/N 3-5

ITEM NUMBER	DESCRIPTION OF OPERATION	APPLICABLE DOCUMENT	REMARKS
1	PERFORM FUNCTIONAL TESTS WITH UNIT IN VACUUM TEST CHAMBER AS FOLLOWS: (a) Measure resistance of all motor windings at ambient temperature. (b) Measure DMA running torque at 20, 40, 60, 80, and 100 RPM using method specified in life test procedure, DA-032, Para.5.4.9 & 5.4.10, using motor/resolver set #1. (NOTE: Calculate torques after Kv measurement.) (c) Measure Kv (BEMF Constant) of Motor #2. Use to calculate K_T (motor torque constant). Measure during 1b at 60 RPM only. (d) Repeat (1a) using motor-resolver set #2 (e) Repeat (1b) using motor #1 (f) Measure all MPU signals at 40 and 80 RPM	TRW DA-032 Para 5.4.9 & 5.4.10 TRW DA-032 Para 5.4.12 & 5.4.13	Document Results on Data Sheets
2	SLOWLY BACK FLUSH VACUUM CHAMBER WITH DRY NITROGEN. REMOVE BELL JAR. REPEAT FUNCTIONAL TEST OF 1b, 1c, 1d, 1e, and 1f.		Document Results on Data Sheets

Table 7-1. Disassembly and Inspection Procedure — 777 DMA Life Test Unit S/N 3-5 (Continued)

ITEM NUMBER	DESCRIPTION OF OPERATION	APPLICABLE DOCUMENT	REMARKS
3	MEASURE RADIAL AND AXIAL DISPLACEMENTS OF HOUSING FLANGE WITH DIAL INDICATOR. REFERENCE TO ALIGNMENT MARK ON FLANGE.		Document Results on Data Sheets
4	MEASURE MPU GAPS FOR MPU'S 1 & 2	BBRC 32701	Document Results on Data Sheets
5	DMA SHALL BE REMOVED FROM VACUUM CHAMBER AND DELIVERED TO M2/1313 FOR DISASSEMBLY. CAUTION: DMA SHALL BE COVERED WITH CLEAN NYLON BAG, FOR TRANSPORTING. DMA MUST BE HANDLED WITH CLEAN, LINT-FREE GLOVES.		
6	DMA DISASSEMBLY SHALL BE CONDUCTED IN A CLASS 100,000 CLEAN AREA PER FED-STD-209. DISASSEMBLED PARTS SHALL BE VISUALLY INSPECTED AND MAINTAINED IN A CLASS 100 BENCH AREA. CLEAN GLOVES SHALL ALWAYS BE USED WHEN HANDLING DMA AND ITS PARTS. ALL PARTS REMOVED SHALL BE STORED IN CLEAN NYLON BAGS AND SEALED WHERE POSSIBLE, AND IDENTIFIED.		

Table 7-1. Disassembly and Inspection Procedure – 777 DMA Life Test Unit S/N 3-5 (Continued)

ITEM NUMBER	DESCRIPTION OF OPERATION	APPLICABLE DOCUMENT	REMARKS
6 (cont'd)	ALL LOOSE CONTAMINENTS OBSERVED SHALL BE STORED ON CLEAN FILTER PAPER IN HOLDERS AND IDENTIFIED THE FOLLOWING OPERATIONS ARE THE DISASSEMBLY AND INSPECTION SEQUENCE: NOTE: PHOTOGRAPHS SHALL BE TAKEN AT EACH INSPECTION POINT AND OF ALL QUESTIONABLE OBSERVATIONS		
7	REMOVE BELL PLATE (34451), END BELL (32719), AND CABLE CLAMP (84971).	BBRC 32701 ITEMS 8,12,64, P 110330, Para 5.14	
8	VISUALLY INSPECT BELL END FOR EVIDENCE OF CONTAMINANTS. MEASURE RESOLVER SNUBBER CLEARANCE AND REFERENCE TO ALIGMENT MARK ON SHAFT.	BBRC 32701	Remove sample of any observed contaminant.
9	DISASSEMBLE AND REMOVE SLIP RING ASSEMBLY. NOTE: CABLE BUNDLES J1, J2, AND J3 MUST BE UNLACED AND LOOSENED AT BOTTOM OF SHAFT. UNLACE J7 AND REMOVE MPU'S.	BBRC 32701 P 110330 Para 5.1	Store slip ring for further disassembly

Table 7-1. Disassembly and Inspection Procedure – 777 DMA Life Test Unit S/N 3-5 (Continued)

ITEM NUMBER	DESCRIPTION OF OPERATION	APPLICABLE DOCUMENT	REMARKS
10	REMOVE RESOLVER STATORS EXAMINE FOR EVIDENCE OF DEBRIS AND/OR RUBBING. PAY SPECIAL ATTENTION TO SNUBBER PARTS	BERC 32701 P 110330 Para 5.10a & 5.11 a	Document Observations
11	MEASURE MOTOR GAP CLEARANCE. REFERENCE TO ALIGNMENT MARK ON SHAFTS	BBRC 32701	Documents Observations
12	DISASSEMBLE MOTOR HOUSING FROM BERYLLIUM HOUSING INSPECT MOTOR ROTOR FOR DEBRIS AND /OR RUBBING. INSPECT OUTER RING FOR EVIDENCE OF CRACK OR DEFORMATION. INSPECT RESERVOIR IN HOUSING - DO NOT REMOVE.	BBRC 32701 P 110330 Para 5.9 & 5.7	Document Observations Store with reservoir up for later inspection.
13	CUT THERMISTOR #1 AND #2 LEADS NEAR J7, REMOVE MOTOR SHAFT HARDWARE. NOTE: WIRE RETAINER (33279) ITEM 31 ON 32701 MUST BE BROKEN TO ALLOW MOTOR CABLE TO BE DRAWN THRU SHAFT. REMOVE MOTOR/ RESOLVER SHAFT.	BBRC 32701	Exercise caution so not to disturb bearings.
14	VISUALLY INSPECT PRELOAD MECHANISM AND TOP BEARING FOR EVIDENCE OF DEBRIS, CONTAMINANTS & LUBRICATION		Document Observations

Table 7-1. Disassembly and Inspection Procedure – 777 DMA Life Test Unit S/N 3-5 (Continued)

ITEM NUMBER	DESCRITPION OF OPERATION	APPLICABLE DOCUMENT	REMARKS
15	MEASURE PRELOAD GAP CLEARANCE	P 110330 Para 5.3	Document Results
16	REMOVE PRELOAD MECHANISM. EXAMINE ALL PARTS FOR DEBRIS, CONTAMINANTS AND LUBRICATION. INSPECT FOR VISUAL EVIDENCE OF WASHER ROTATION. INSPECT INNER RACE JOURNAL FOR ROTATION AND AXIAL MOTION.	P 110330 Para 5.3	Document Results
17	SEPARATE SHAFT FROM BEARINGS EXERCIZING CARE NOT TO DISTURB LUBRICATION AND DEBRIS	BBRC 32701 P 110330 para 5.2	
18	INSPECT SHAFT FOR EVIDENCE OF LUBRICATION ON SURFACE AND CONDITION OF BOTH BEARING JOURNALS		Document Results. Store for further inspection and analysis
19	INSPECT HOUSING FOR EVIDENCE OF LUBRICATION. INSPECT BEARINGS FOR EVIDENCE OF DEBRIS, CONTAMINANTS AND LUBRICATION. NOTE: AT THIS POINT THE DECISION WILL BE MADE TO MAKE BEARING MEASUREMENTS PRIOR TO REMOVAL FROM HOUSING.		Document Results. Store for further inspection and analysis

Table 7-1. Disassembly and Inspection Procedure – 777 DMA Life Test Unit S/N 3-5 (Continued)

ITEM NUMBER	DESCRIPTION OF OPERATION	APPLICABLE DOCUMENT	REMARKS
20	REMOVE RESERVOIRS FROM BOTH HOUSING AND SHAFTS AND INSPECT.		Document Results. Store for further inspection and analysis.
21	REMOVE BEARINGS FROM HOUSING AND PERFORM A DETAILED INSPECTION AS REQUIRED BY LIFE TEST PLAN. A DETAILED PLAN WILL BE ISSUED PRIOR TO INSPECTION		Document results.
22	SLIP RING ASSEMBLY SHALL BE DISASSEMBLED, EXAMINED AND ANALYSES PERFORMED AS REQUIRED BY LIFE TEST PLAN. THIS WILL FIRST INCLUDE SLIP RING AND BRUSHES, FOLLOWED BY SLIP RING BEARING INSPECTION. A DETAILED PLAN WILL BE ISSUED PRIOR TO INSPECTION.		Document results

7.2 Disassembly and Inspection Results

7.2.1 Life Test DMA (S/N 3-5)

Disassembly was initiated on 3 November 1975. Prior to disassembly, oil spots were noted around the housing reservoir screw holes, indicating a slight oil migration due to capillary action. Black light examination indicated that no significant quantity of oil was present in these spots.

During the initial stages of disassembly, the minimum clearances in various areas of the power modules were measured:

- Upper resolver - >0.0085 in.
- Snubber - >0.006 in.
- Lower resolver - not measured
- Motor - >0.010 in.

Following removal of the power module elements and the slip ring module, the structural module was rotated manually, resulting in a noise similar to that recorded during pre-disassembly functional tests (see Section 6.) No source of this noise was visually apparent in the assembled module.

Further disassembly allowed viewing the balls of the main bearings and their inner races as well as the shaft. A relatively large concentration of lubricant in the lower (110 MM bearing) end of the structural module was apparent. Inspection of the inner races and the shaft journals indicated the possibility of limited ($\leq 45°$) motion of the main bearing inner races. The balls of the upper bearing were quite shiny in appearance, while those of the lower bearing exhibited a buffed texture with heavy banding.

Disassembly of the bearings led to discovery of a large (visually apparent) quantity of metallic lead in the ball pockets of the lower bearing retainer. Tables 7-2 through 7-5 summarizes the results of inspection for each of the life test DMA bearings. Microscopic examinations later showed pits and dent patterns ("bear claws") in the 90 MM main bearing races and poor surface finish on the balls of the 110 MM main bearing.

Owing to the significant unexpected results found in testing and inspection of the life test DMA (i.e.: audible sound while rotating at operational speeds; metallic lead deposits in the 110 MM bearing retainer

Table 7-2. Inspection of 90 MM Main Bearing of Life Test DMA

	Inner Ring	Outer Ring	Retainer	Balls
Surface finish	Smooth and polished	Smooth and polished	N/A	Smooth and polished ball banding on all balls - partially frosted.
Wear debris	Very small, whitish along ball path; white spot or flaky material in race thrust face**	Very small; whitish along ball path.	Very small amount in ball pockets.	Very small amount.
Fretting, Galling	Possible galling on bore of inner race*	None	N/A	None
Dewetting	None	None	None	None
Pits, dents	None	Several pits or spall marks in ball path, approx 4-6; "bear claw" marks in ball path	N/A	None
Delamination	N/A	N/A	No delamination retainer appears to have had different quan of phenolic impregnation of the outer layers.	
Retainer ball pocket rub marks	N/A	N/A	Very little rubbing at bore.	N/A
Lubricant appearance	Very small amount of lubricant; a few greaselike droplets	Very small amount of lubricant.	Very small amount of lubricant	Very small amount; greaselike.

* Race does not appear to have rotated more than one inch and a half, measuring from rub marks and possible galling on open face. Analysis required to determine possibility of chemical reaction between MoS_2, VacKote, and 440C of contact points of bore with a shaft.

** MoS_2 is adhering in inner ring bore.

N/A - Not Applicable.

Table 7-3. Inspection of 110 MM Main Bearing of Life Test DMA

	Inner Ring	Outer Ring	Retainer	Balls
Surface finish	Smoky or hazy appearance from debris mask surface; some evidence of grind machine marks	Smooth and honed** with little evidence of abnormal machine marks; only slight evidence of grind marks in ball path	N/A	Frosted; many ball marks.
Wear debris***	Large particles, all flakelike; black, large; quantity mostly along ball path	See inner ring description	Heavy black particles on all ball pockets	Large black or possibly translucent particles
Fretting, galling	Bore and closed face clean; open face has small amount of rubbing	OD and faces clean	N/A	None
Dewetting	None	None	None	None
Pits, dents	None	None	N/A	None
Delamination	N/A	N/A	None	N/A
Retainer ball pocket rub marks	N/A	N/A	Rub marks, thrust face of bore; debris in ball pockets deposited on closed face	N/A
Lubricant appearance*	Difficult to assess.	Difficult to assess*; copius amount of lubricant.	Difficult to assess*; copius amount of lubricant.	Difficult to access*

* Analyses required of debris and lubricant to access.

** In ball path, there is a location where it is raised and may possibly be redeposited, compacted debris.

*** All large particles are flakelike and have a metallic luster.

N/A - Not applicable.

TABLE 7-4. INSPECTION OF LARGE SLIP RING BEARING OF LIFE TEST DMA

	Inner Ring	Outer Ring	Retainer	Balls
Race surface finish	smooth; polished	smooth, polished	N/A	very polished; a slight frosting; one or two balls with single band
Wear debris	along both sides of ball path	along both sides of ball path	bore and ball pockets	very small amount
Fretting, galling	none	none	N/A	none
Dewetting	none	none	none	none
Pits, dents	none	none	N/A	none
Delamination	N/A	N/A	bore; first lamination, thrust and closed face, several locations	N/A
Retainer ball pocket rub marks	N/A	N/A	closed face, several locations	N/A
Lubricant appearance*	difficult to assess	difficult to assess	difficult to assess	difficult to assess

* Analysis required of debris and lubricant to assess.

N/A - Not applicable.

TABLE 7-5. INSPECTION OF SMALL SLIP RING BEARING OF LIFE TEST DMA

	Inner Ring	Outer Ring	Retainer	Balls
Race surface finish	smooth; polished	smooth; polished	N/A	frosted balls
Wear debris	along ball path closed face; black; significant amount	along ball path; open face; black; significant amount	shiny, metallic material on ball pockets; bore; black, significant amount	very small amount
Fretting, galling	none	none	N/A	none
Dewetting	none	none	none	none
Pits, dents	machine marks on closed face; source unidentified.	none	N/A	slight scuff marks
Delamination	N/A	N/A	none	N/A
Retainer ball pocket rub marks	N/A	N/A	bore and ball pockets	N/A
Lubricant appearance*	copius amount; slightly darkened	copius amount; slightly darkened	copius amount	difficult to a assess

* Analysis required of debris and lubricant to assess.

N/A - Not Applicable.

ball pockets; migration of lubricant toward lower end of structural module), an extensive life-test anomaly investigation was initiated, including

- physical-chemical tests
- metallurgical examinations
- thermal simulation
- lubricant transfer analyses
- bearing dimensional measurements
- bearing torque tests
- review of bearing module tests and inspection.

These activities are still in progress and will be reported in a separate document.

With reference to the 9433 anomaly, it should be noted that the life test DMA - despite the obvious abnormalities observed - showed no significant change in running torque as indicated by motor current drain. Perhaps the result of primary note is the lubricant degradation (i.e., departure from expected state) shown by the lead deposits. This tends to support consultant conclusions that the lubrication system is marginal and that the 9433 anomaly is likely to have been initiated by degraded lubrication. No further inferences should be made until evaluation of the life test results is completed.

7.2.2 Flight Spare DMA (S/N 3-1)

Disassembly was initiated on 6 November 1975. Prior to disassembly, the following noteworthy abnormalities were noted:

- One alignment mirror was chipped
- The threads of MPU No. 3 were damaged
- An accelerometer was found to be cemented to the shaft at the rotor (lower) end
- Oil spots were noted around the housing reservoir screw holes
- MPU No. 3 and MPU No. 5 had extremely small gaps (<<0.0005 inch)

During the early stages of disassembly, the minimum clearances in critical power module gaps were measured:

- Upper resolver- >0.008 in.
- Snubber - >0.0055 in.
- Lower resolver- not measured
- Motor - >0.010 in.

These results are very similar to values measured in the life test DMA and noted above.

Upon further disassembly, the shaft and bearings became visible. No major migration of lubricant (such as seen on the life test unit) was apparent. However, there was a dark band below the shaft reservoir, suggesting a heavier concentration of oil than in other shaft and housing areas.

Tables 7-6 and 7-7 summarize the results of inspecting the main bearings after their disassembly.

Evaluation of these results is continuing (although with less priority than the life test anomaly investigation).

No specific differences which relate to the 9433 anomaly are apparent.* However, the abnormalities noted prior to disassembly suggest that a review of assembly and handling procedures is in order.

7.3 Conclusions

At this stage, no direct link can be assumed between the 9433 anomaly and the results of DMA disassembly and inspection; indeed, no such result was expected. However, from this exercise came the following conclusions, alerts, and recommendations:

- A recommendation must be made to have better handling of the DMA's during assembly, transport, and integration at BBRC and TRW. A plan should be established by Quality Assurance to accomplish this.

---

* The extreme closure of the MPU gaps is a potential cause of interference; however, torques from this area would have a specific signature and would be seen early in operation (e.g., at some point during the first yearly thermal cycle).

TABLE 7-6. INSPECTION OF 90 MM MAIN BEARING OF FLIGHT SPARE DMA

	Balls	Inner Ring	Outer Ring	Retainer
Surface finish	banded	polished; some grind marks in race	polished	more fuzzy Jeburring required
Wear debris	small amount	small amount; grey along ball path	small amount, grey along ball path	small amount
Fretting, galling	none	slight rubbing,open face surface - possibly one turn	none	N/A
Dewetting	none	none	none	none
Pits and dents	none	none	none	N/A
Delamination	N/A	N/A	N/A	none
Retainer rub marks	N/A	N/A	N/A	slight,ball pockets and bore
Lubricant appearance*	no degradation film	no degradation-film	no degradation-film	no degradation-film

* Sample flake-like particle taken from inner ring was submitted for X-ray diffraction analysis.

N/A - Not Applicable.

TABLE 7-7. INSPECTION OF 110 MM MAIN BEARING OF FLIGHT SPARE DMA

	Balls	Inner Ring	Outer Ring	Retainer*
Surface finish	polished; one ball scratched	polished	polished	More fuzzy deburring required
Wear debris	small amount	MoS_2 transferred from journal; small, grey along ball path	small, grey along ball path	small amount
Fretting, galling	none	none	none	N/A
Dewetting	none	none	none	none
Pits, dents	none	none	several; small approx 0.005 in in ball path	N/A
Delamination	N/A	N/A	N/A	none
Retainer rub marks	N/A	N/A	N/A	Slight - ball pockets and bore
Lubricant appearance	no degradation-film	no degradation-film	no degradation-film	no degradation-film

* Flake-like particle submitted for X-ray diffraction analysis.

N/A - Not Applicable.

- Workmanship and Inspection must be upgraded to eliminate the misapplication of processing materials and damage to parts. On S/N 3-1, epoxy spot bonding was positioned in the wrong locations and scuffing of a cable handle occurred.
- Because of the large amounts of oil observed in the vicinity of the S/N 3-5 110 MM bearing and very small amount in the vicinity of the upper (90 MM)bearing, the design should be assessed, considering all transport mechanisms to reduce this potential problem on flight DMA's.
- The amount of molybdenum disulfide burnished onto the flame spray aluminum oxide should be more closely controlled (i.e., the thickness, total quantity,or process should be specified to reduce the possibility of MoS_2 particles sloughing and building up on the journals).
- The mechanism for lead formation in the life test DMA 110 MM bearing must be understood, and the significance of the lead upon performance and life test evaluated.
- The metallic defects (e.g., in the balls of the lower main bearing) are cause for concern and must be understood.
- Oil creep to the outer DMA housing surfaces through the housing reservoir screw holes should be eliminated.

8. DMA ASSEMBLY, TEST AND STORAGE HISTORY

8.1 General Data

Eight flight despin mechanical assemblies (DMA) were delivered to TRW in the period of August 1970 through March 1971 for usage on six satellites, one spare unit, and one life test unit. In addition, 20 sets of bearings were furnished for various life tests; history of each bearing by serial number is presented in Table 8-1. In November 1970 it was discovered that problems of bearing surface finish and possible retainer delamination existed that might adversely affect bearing life. This led to the return of all delivered units to BBRC and a complete disassembly of all bearings for inspection and disposition.

Each DMA was assembled and tested to BBRC controlled and approved drawings, specifications, and process and test procedures. When descrepencies occurred they were documented on Nonconforming Materials Report (NMR) and dispositioned through a Materials Review Board (MRB), or a TRW Supplier Information Request (SIR) was sent to TRW for approval. Copies of all NMR's are included in each DMA end-item documentation (see Appendix D). Once a unit is received by TRW it is controlled in Integration Stores and the spacecraft integration and test area. A history of each DMA at TRW is presented in Table 8-2.

8.2 9433 DMA (S/N 3-2)

Spacecraft 9433 was flown with DMA S/N 3-2. During the assembly and acceptance test period at BBRC any discrepancy was formally handled through the Materials Review Board. A history of the discrepancies is presented in Table 8-3.

Referring to Table 8-3, the only discrepancy that might be related to higher running torques is item 2. The dent to the Hypernick band referred to was approximately .010 inches diameter and 0.005 inches deep. The ring is bonded circumferentially to the motor laminations and is 4.490 inches in diameter and 0.44-inch high. There, it can be seen

	003		004		005		006		007		008		009		010		011		
SERIAL NUMBER	(-1)	(-3)	(-1)	(-3)	(-1)	(-3)	(-1)	(-3)	(-1)	(-3)	(-1)	(-3)	(-1)	(-3)	(-1)	(-3)	(-1)	(-3)	(-1)
DELIVERY DATE	2/21	2/21	2/21	2/21	4/9	4/9	4/9	4/8	4/9	4/9	4/8	4/9	7/22	5/14	5/14	5/14	7/22	5/14	5/14
LUBRICATION STATUS (1)	V	V	V	V	V	V	V	V	V	V	V	V	K	K	K	V	K	K	V
CONDITION OF SEPARATORS (2)	S	S	S	S	S	NI	O	No separator	O (quite porous)	NI	NI	NI	S	S	S	-	S	-	S
SURFACE FINISH (MAXIMUM READING) (3)	4/6	4/6	3/5	6/8	32 (I)	NI	6/8	6/8	NI	4/6	4/6	4	4/6	6/8	6/8	6/8	6/8	4/6	14/16
USEAGE (4)	QS	2-1	2-1	QS	BTM1	BTM1	NA	NA	BTM1	BTM1	3-1	3-1	K	K	K	K	K	K	3-4
CONDITION OF SEPARATOR (2) (PER QAD #57, REV. A)	U	19	New	U*	U	NI	U	U Burned	U	NI	U position 22	A 8	New	A 9	A 10	A 10	New	A 11	new
FINAL USEAGE (4)	EV	SLT	SLT	EV	NUFS	NUFS	RTV	BTM1 (V)	-	-	3-5 (Life test Unit)	3-5	BTM1 (K)	BTM1 (K)	BTM1 (K)	BTM1 (V)	BTM1 (K)	BTM1 (K)	BTM1 (V)

	022		023		024		025		026		027		028		029		030		
SERIAL NUMBER	(-1)	(-3)	(-1)	(-3)	(-1)	(-3)	(-1)	(-3)	(-1)	(-3)	(-1)	(-3)	(-1)	(-3)	(-1)	(-3)	(-1)	(-3)	(-1)
DELIVERY DATE	5/14	5/14	7/22	5/14	5/14	5/14	5/14	5/14	7/22	5/14	5/14	5/14	7/22	5/14	-	5/14	5/14	5/14	9/1
LUBRICATION STATUS (1)	V	V	V	V	V	V	K	K	V	V	N	V	V	V	-	N	N	V	K
CONDITION OF SEPARATOR (2)	NI	NI	0	0	NI	NI	S	0	S	0	S	0	NI	NI	-	0	S	0	S
SURFACE FINISH (MAXIMUM READING) (3)	8/10	6/8	NI	NI	4/6	4/6	8/10	6/8	6/8	6/8	4/6	8	4	4/6	-	6/8	14/16	8/10	6/8
USEAGE (4)	BTM2	BTM2	2-1	2-1	BTM2	BTM2	K	K	FS 1.5cc	FS	K	K	3-6	3-6	-	FS	K	K	K
CONDITION OF SEPARATOR (2) (PER QAD #57, REV. A)	A 22	A 22	A 23	A 23	A	A	A new	A 25	36	A 26	A new	A 27	A 28	A 28	-	A 29	A	A 30	new
FINAL USEAGE (4)	BTM1 (V)	BTM1 (V)	2-1	2-1	-	-	BTM3 (K)	BTM1 (K)	3-2	3-2	SLT	BTM2 (V)	3-6	3-6	-	SLT	RTV	BTM2 (V)	BTM1 (K)

*Contaminated - Pencil mark

CODES: (1) V = VACKOTED, N = NOT LUBRICATED, K = KRYTOX

(2) S = SEPARATION, O = NO SEPARATION, NI = NOT INSPECTED, A = ACCEPTABLE PER QAD #57, U = UNACCEPTABLE

(3) 6/8 = 6/ to 8/, NI = NOT INSPECTED

(4) 3-1, 3-2, ETC; BTM1, BTM2, ETC; NA - NOT ASSIGNED; QS = QUAL SPARE; FS = FLIGHT SPARE; K = TO BE LUBE
NUFS = NON UNIFORM FILM STUDY; S = SCRAP; T RTV = RETURN TO VENDOR; EV = ENGR EVALUATION ONLY

Table 8-1. DMA Bearing Status

011		012		013		014		015		016		017		018		019		020		021	
(-1)	(-3)	(-1)	(-3)	(-1)	(-3)	(-1)	(-3)	(-1)	(-3)	(-1)	(-3)	(-1)	(-3)	(-1)	(-3)	(-1)	(-3)	(-1)	(-3)	(-1)	(-3)
7/22	5/14	5/14	5/14	5/14	5/14	7/22	5/14	-	5/14	5/14	5/14	5/14	5/14	5/14	5/14	5/14	5/14	5/14	5/14		5/14
K	K	V	V	V	V	K	K	-	V	V	V	V	V	V	V	V	V	V	V		K
S	-	S	0	S	S	S	0	-	0	NI	NI	NI	NI	S	0	S	NI	NI	NI	Rejected at ITI	NI
6/8	4/6	14/16	6/8	8/10	6/8	6/8	6/8	-	6/8	4/6	4/6	4/6	6/8	6/8	6/8	4/6	16/32	4/6	4/6		6/8
K	K	3-4	3-4	3-3	3-3	K	K	-	FS	3-5	3-5	3-2	3-2	3-7	3-7	BTM1	BTM1	BTM2	BTM2		FS
New	A 11	new	A 12	A 13	A 13	new	A 14		39	A 16	A 16	U 20	A 17	12	A 18	U	A	A new	NI		A 21
BTM1 (K)	BTM1 (K)	BTM1 (V)	3-4	3-3	3-3	BTM3 (K)	BTM3 (K)	BTM2 (V)		3-8	3-8	3-7	3-7	3-1	3-1		NUFS	BTM1 (V)			BTM3 (K)

030		031		032		033		034		035		036		037		038		039		040	
(-1)	(-3)	(-1)	(-3)	(-1)	(-3)	(-1)	(-3)	(-1)	(-3)	(-1)	(-3)	(-1)	(-3)	(-1)	(-3)	(-1)	(-3)	(-1)	(-3)	(-1)	(-3)
5/14	5/14	9/17	5/14	9/17	5/14	9/17	5/14	9/17	5/14	9/17	5/14	9/17	5/14	9/17	5/14	9/17	5/14	9/17	5/14		
N	V	K	K	K	K	K	K	K	K	V	V	V	V	V	K	V	V	V	V	K	
S	0	S	0	S	0	S	0	S	0	S	0	S	0	S	0	S	0	S	0		
14/16	8/10	6/8	6/8	4/6	6/8	4/6	28/30	4/6	6/8	4/6	4/6	6/8	6/8	4/6	14/16	6/8	12/14	4/6	6/8		
K	K	K	K	K	K	K	K	K	K	V	V	V	V	V	V	V	V	V	V		
A	A 30	new	A 31	A 32	A 32	new	A 33	U new	dirty 34	011	037	A 25	A	30	A 35	U	? disco -lered	A 39	A		new
RTV	BTM2 (V)	BTM4 (K)	BTM4 (K)	BTM4 (K)	BTM4 (K)	BTM4 (K)	BTM4 (K)	SLT	SLT	SLT	SLT	BTM2 (V)	NUFS	BTM2 (V)	BTM3 (K)	BTM2 (V)	RTV	3-4	NUFS	BTM3 (K)	

= UNACCEPTABLE PER QAD #57

K = TO BE LUBED WITH KRYTOX; V = TO BE LUBED WITH VACKOTE; SLT = STORAGE LIFE TEST·
ON ONLY

Table 8-2. DMA Installation History

S/N 3-1	S/N 3-2	S/N 3-3	S/N 3-4
19 Aug 70 - Installed Flt 1 6 Nov 70 - Removed for bearing inspection 28 Dec 70 - Installed Flt 4 9 Feb 73 - Removed to storage as spare	18 Sep 70 - Installed Flt 2 3 Nov 70 - Removed for bearing inspection 21 Dec 70 - Installed Flt 3 9 Apl 73 - Removed for heater installation 25 Apl 73 - Installed Flt 3 13 Dec 73 - Launch (forward satellite)	4 Dec 70 - Installed Flt 1 2 Nov 71 - Launch (forward satellite)	17 Dec 70 - Installed Flt 2 2 Nov 71 - Launch (aft satellite)
S/N 3-5	**S/N 3-6**	**S/N 3-7**	**S/N 3-8**
Jun 71 - Initiate Life Test Jun 75 - Complete 4yr test Nov 75 - Dissassemble & Inspect	15 Feb 71 - Installed Flt 5 9 Apl 71 - Removed for Eng. Eval. test on DMA S/N 3-8 13 Apl 71 - Reinstall Flt 5 9 Mar 73 - Remove from Flt 5 9 Mar 73 - Installed Flt 4 13 Dec 73 - Launch (aft satellite)	5 Mar 71 - Installed Flt 6 May 75 - Launch (Booster failure)	10 Apl 71 - Installed Flt 5 for special test 13 Apl 71 - Remove Flt 5 to stores 9 May 73 - Installed Flt 5 May 75 - Launch (Booster failure)

Table 8-3. Unit Discrepancy History at BBRC (DMA S/N 3-2)

	DATE	REPORT	DISCREPANCY	DISPOSITION
1)	5-21-70	SIR 11089	Slip Ring Assembly	
			Leads from rings 4, 42, 64, 68, 83, and 85 had nicked insulation.	All leads covered with shrink tubing.
			Lead from ring 45 damaged insulation and shield.	Cut off ring and brushblock leads to ring 45. Used leads from spare ring 57.
2)	7-13-70	NMR 24063	Dent in band around torque motor 4.490 dia.	Use as is.
			Small metal slivers along edge torque motor.	Removed during pre-assy cleaning.
3)	7-29-70	NMR 24306	Slip ring Assembly	
			Wire #9 shaft end abraded	Repaired per TRW SRP 7-1
			Wire #85 shaft end insulation cut 16" from end of bellows housing	
4)	8-14-70	NMR 24425	Slip Ring Assembly	
			Following wires abraded, cut & abraded: 50, 75, 77, 84, 86; 72, 74, 80, 82	Reworked to drawing spec

Table 8-3. Unit Discrepancy History at BBRC (DMA S/N 3-2) (Continued)

	DATE	REPORT	DISCREPANCY	DISPOSITION
7)	12-7-70	NMR 25905	P/N 32708-1 S/N 017 retainer unacceptable	Scraped & replaced with S/N 020
			P/N 32702-1 S/N 017 races & balls were acceptable however, due to reprocess time span to restore lubrication to flight status, these parts were not reinstalled in DMA 3-2.	Replaced with S/N 026
			P/N 32708-3 S/N 017 races, balls and retainer were also acceptable however due to reprocess time span to restore lubrication to flight status these parts were not reinstalled in DMA 3-2.	Replaced wtih S/N 026

NOTE: Reassembly of DMA 3-2 was per procedure except the thermistor in-line connections were made per special rework procedure.

Acceptance test per modified ATP 26469 (exceptions per TRW TWX 777-S1-3081, 3064, & 3090)

NOTE: DMA 3-2 when returned to TRW was installed on S/C 3-3 (12-21-70)

Table 8-3. Unit Discrepancy History at BBRC (DMA S/N 3-2) (Continued)

	DATE	REPORT	DISCREPANCY	DISPOSITION
5)	8-17-70	NMR 24573	Magnetic Pickup	
			Dim. or S/N B09 is 0.421, S/B .400/.398	Returned to vendor
			Strain relief extended 1 1/4", S/B 0.125	Use as is.
			S/N B02 & B09 had cracked insulation at shrink tube & pickup potting.	Rework at BBRC
			S/N B12 had potting void at tube & pickup	
6)	8-24-70	NMR 24716 SIR 11721	During Y axis vibration no current on motor #1 due to operator error (failed to place switch on test equip, to correct position).	Use as is.

NOTE: DMA was installed on S/C 3-2 on 9-18-70
DMA was removed from S/C 3-2 on 11-3-70 to return to BBRC for suspect bearings
No TRW rejection document initiated at this time

that this dent could not possibly cause separation of the ring. All the remaining descrepancies except for item 7 were mostly minor damage to wire leads which required detailed corrective action that did not impact the reliability of the unit. Item 7 covered the bearing inspection and retest discussed in paragraph 8.1; a similar NMR exists for each DMA.

A handling history of the DMA S/N 3-2 at TRW is presented below. After mating of the platform or inertia simulator, the DMA carried this load (approximately 450 pounds) until a demating occurred.

S/N 3-2 HANDLING HISTORY

18 Sept 70	Install DMA
3 Nov 70	Removed for braing inspection
21 Dec 70	Installed DMA
21 Dec 70	Installed inertia simulator
22 Dec 70	Back EMF test
8 Feb 71	Spin/despin test complete
12 Feb 71	Remove inertia simulator
16 Sept 71	Mate platform
23 Feb 72	Demate platform
19 Sept 72	Mate platform
9 Jan 73	Demate platform
6 Feb 73	Mate (flight 6 despin)
15 Feb 73	Demate
9 Apr 73	Remove DMA (apply strip heaters)
25 Apr 73	Install DMA
28 Apr 73	Install inertia simulator
8 May 73	Remove inertia simulator
10 May 73	Mate platform
20 Jul 73	Demate (mixer failure)
26 Jul 73	Mate platform
13 Dec 73	Launch (forward satellite)

9. SYSTEM SIMULATION AND ANALYSIS

9.1 Simulation Results

In an effort to better understand the nature of the bearing friction changes in the S/C 9433, several different types of disturbances torques were simulated using the computer program SIM777 described in Appendix E. The resulting pointing error excursions were then analyzed and compared to flight data, in order to characterize the disturbance torques.

In particular, it was desired to know the amplitude and duration of the disturbances that were occurring on S/C 9433. Data used in this investigation consisted of the normal mode pointing error, which was recorded once every second, and the torque voltage, which was recorded approximately once every 2 minutes. The torque voltage is important because it gives a rough indication of the steady-state friction level (See Appendix F).*

The simulation effort was directed toward "backing out" the size of the disturbance torques by simulating disturbances, and comparing the resulting simulated error with the flight pointing error. Basically, three forms of disturbance torques and their resulting effect on the pointing error were studied:

- Sudden shift in bearing friction level
- Impulsive disturbances (both amplitude and width of torque pulses were varied)
- Multiple friction pulses.

---

*Data from rate mode operation which gives a more direct measure of friction torque has been discussed in Section 3.0.

9.1.1 Step Change in Bearing Friction Level

The first case studied was the effect of a step change in the running friction level (drag torque). In this case, step changes of various amplitudes were simulated in order to determine the peak errors that would result. In all cases, it was assumed that at the time prior to the disturbance, the integrator voltage had reached its steady-state value (i.e., that value necessary to offset the running friction level and the motor back emf).

Figure 9-1 is a plot of the peak excursion error due to various size step changes in the bearing friction*. These curves are parameterized as a function of the drag torque at the time of the disturbance, with the maximum motor torque available assumed to be 170 in-oz. It can be seen that as long as the motor torque is not saturated, the expected peak error is a linear function of the size of the step change and is independent of the drag torque. However, in regions where, due to high drag torque, the commanded control torque exceeds the motor capability, the peak error increases steeply.

Figure 9-1 can thus be used to estimate the magnitude of the disturbance torque by knowing the peak error (obtainable from flight data) and by knowing the drag torque (a rough estimate is obtainable from the motor voltage readings, which are recorded about once every 2 minutes).

*Later results will show that these peak errors result whenever the friction level changes for a duration of 10 sec or more.

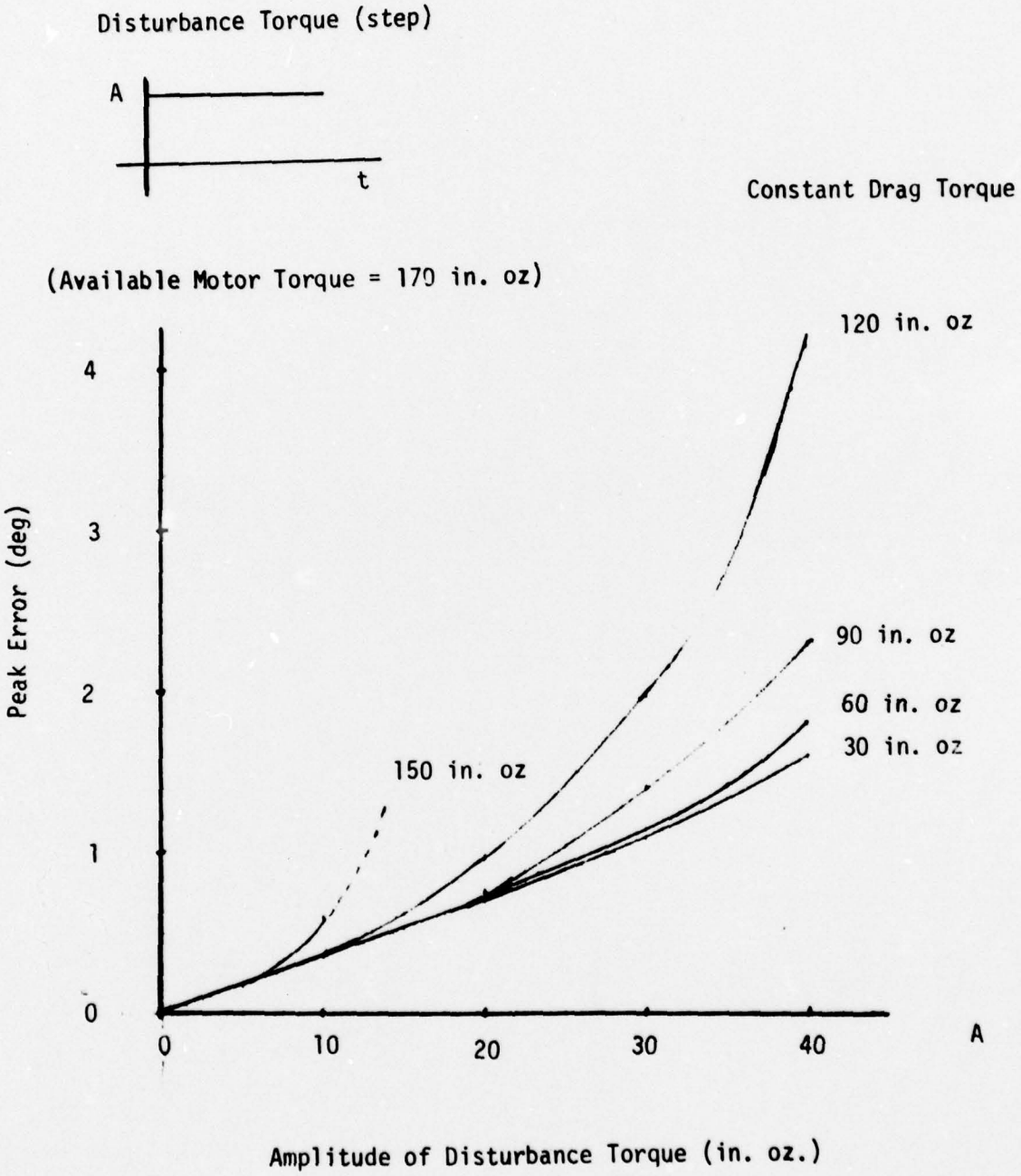


Figure 9-1. Pointing Error as a Function of Step Change in Friction Level (Gain State 8)

9.1.2 Friction Pulses

The second level of investigation was concerned with the effect of sudden short disturbance torques on the pointing error. In Figures 9-2 and 9-3 the peak errors resulting from disturbance pulses of various widths are plotted. The amplitudes of the disturbance torques are parameterized. Figure 9-2 assumes a drag torque of 60 in-oz and Figure 9-3 assumes a drag torque of 120 in-oz. In both cases, it can be seen that for large amplitude disturbances, the error increases as a function of pulse width up to about a pulse width of ten to fifteen seconds; further increase in pulse width of the disturbance torque has no effect on the peak pointing error. This is due to the integrator time constant (15 sec).

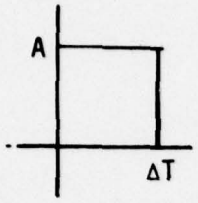
9.1.3 Simulation of Observed 1.5 Degree Pointing Excursion

An effort was made to match the simulated results with observed flight data. Figure 9-4 is a typical pulse plotted from flight data from September 10, 1975 when peak errors of approximately 1.5 deg were observed. For simulation, a constant friction level of 120 in-oz was assumed.* If the maximum available torque were 170 in-oz, then from Figure 9-3 it can be seen that a torque disturbance of a minimum of 25 in-oz was necessary to cause the pointing error. This is a significantly larger pulse than the 5 in-oz that was hypothesized to be the result of retainer whirl.

---

* Later analyses of orbital data, employing the results of an in-depth thermal simulation of the DMA, show the -2.1 volt compensated error signal to be equivalent to a friction level of approximately 100 in-oz (see Appendix F).

Disturbance Torque



Constant drag torque - 60 in. oz.

Pulse Amplitude - A

(Available motor torque = 170 in. oz.)

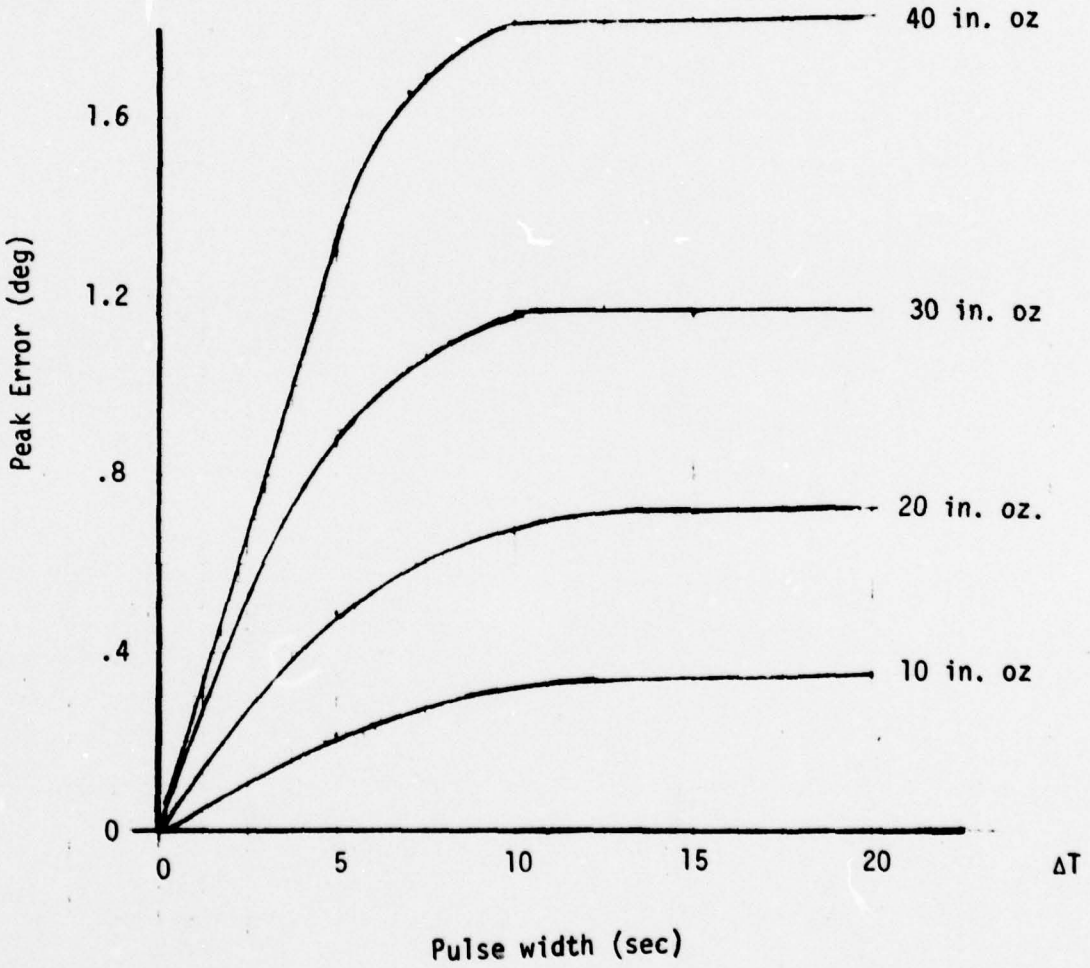


Figure 9-2. Peak Pointing Error as a Function of Disturbance Torque Pulses (Gain State 8)

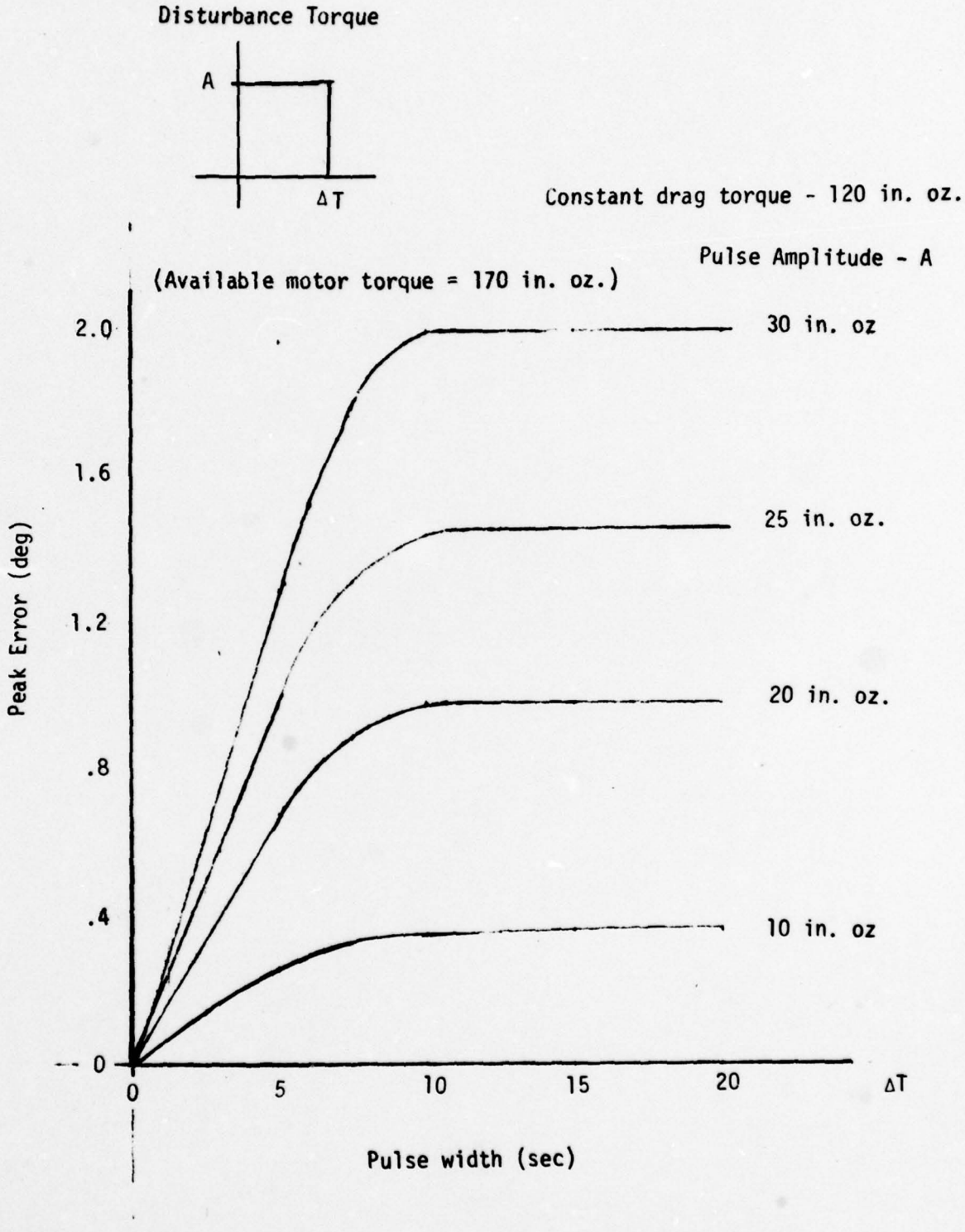


Figure 9-3. Peak Pointing Error as a Function of Disturbance Torque Pulses (Gain State 8)

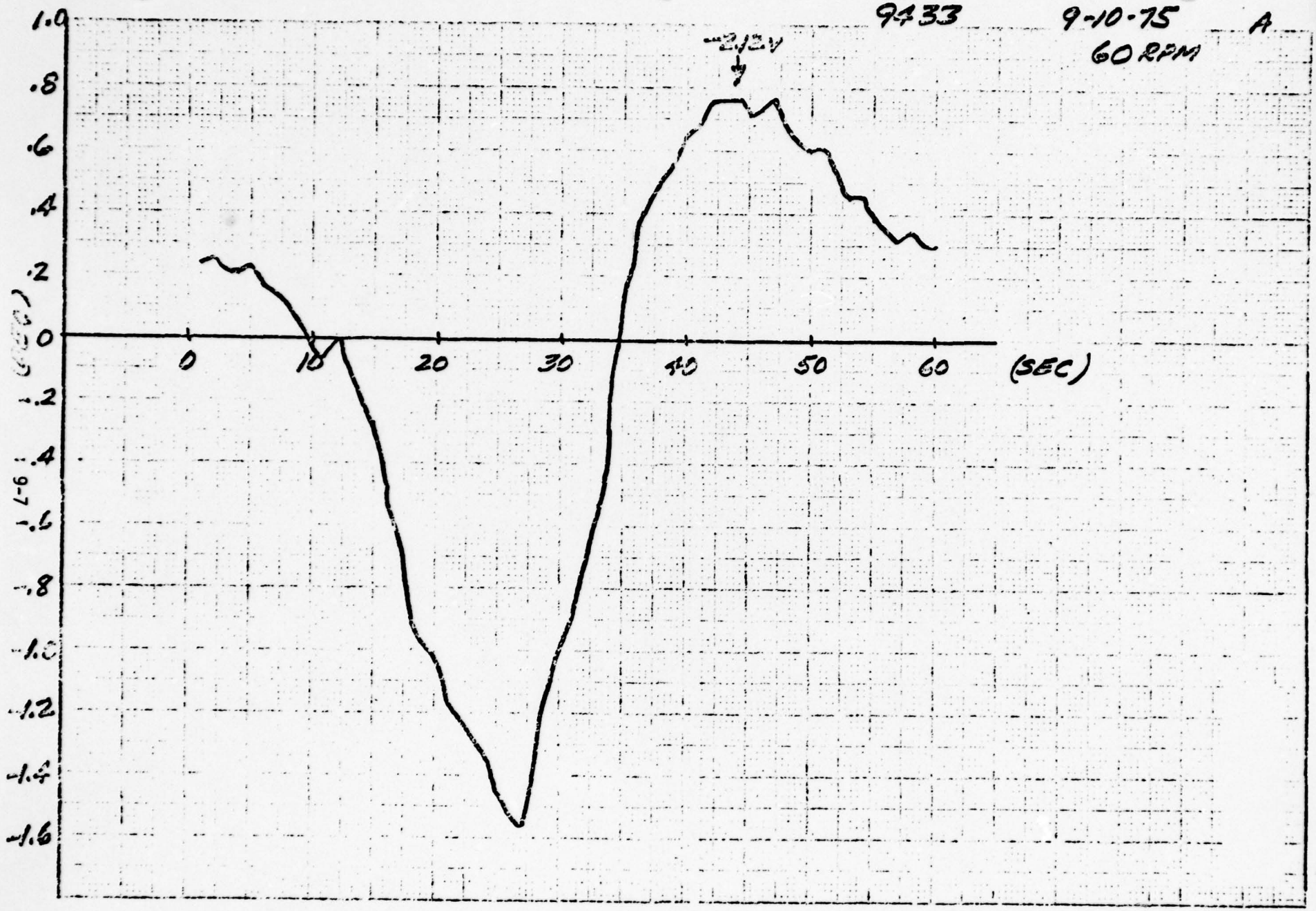


Figure 9-4. Pointing Error plotted from Flight data, Sept. 10, 1975

In order to duplicate the shape of the observed pointing error pulse, (i.e., width, rise time, overshoot) torque pulses of various amplitudes and widths that resulted in the same peak-error ($\approx 1.5^{\circ}$) were synthesized. These pulses are shown in Figures 9-5 through 9-9. The results are summarized in Table 9-1.

When the rise time and error pulse width are compared as well, it is apparent that the disturbance torque pulse of about 25 in. oz. amplitude and 15 sec width gives the best agreement between the simulated and observed pointing error excursion.

It was noted in the above cases that the overshoot after the torque disturbance was removed was not as high in the simulated case as was observed in the flight data. It was then hypothesized that the sudden increase is friction level was followed by "negative" pulses, somewhat smaller in magnitude. This is shown in Figure 9-9.

After having studied the effect of a single torque pulse on the pointing error, the effect of multiple friction pulses was considered. Figure 9-10 shows the response of the system to a train of friction pulses of 20 in. oz. amplitude, or 40 in. oz. peak-to-peak.

9.1.4 Configuration C Comparison

A question came up as to how well an improved controller (Configuration C) which uses a rate loop in addition to the platform position loop in Normal Mode, would perform in the presence of the disturbance pulse that caused an observed pointing error of about 5 degrees. To simulate this case, a running friction torque of 120 in-oz was assumed (maximum torque capability = 170 in-oz), and a disturbance pulse of 42 in-oz for 15 seconds was simulated. The results for both controllers are shown in Figure 9-11. The configuration C results show a peak error of .065 deg; thus the rate loop virtually desensitizes the despin control system to the effects of torque pulses.

---

* These simulation results were obtained prior to the significant rate mode transients. Torque pulses of varying amplitudes and durations have been observed in this data.

** See 74.7531.9-07, "A Comparative Study of Three Despin Controller Designs for Dual Spin Spacecraft", H. Scheichel, 12 February 1974.

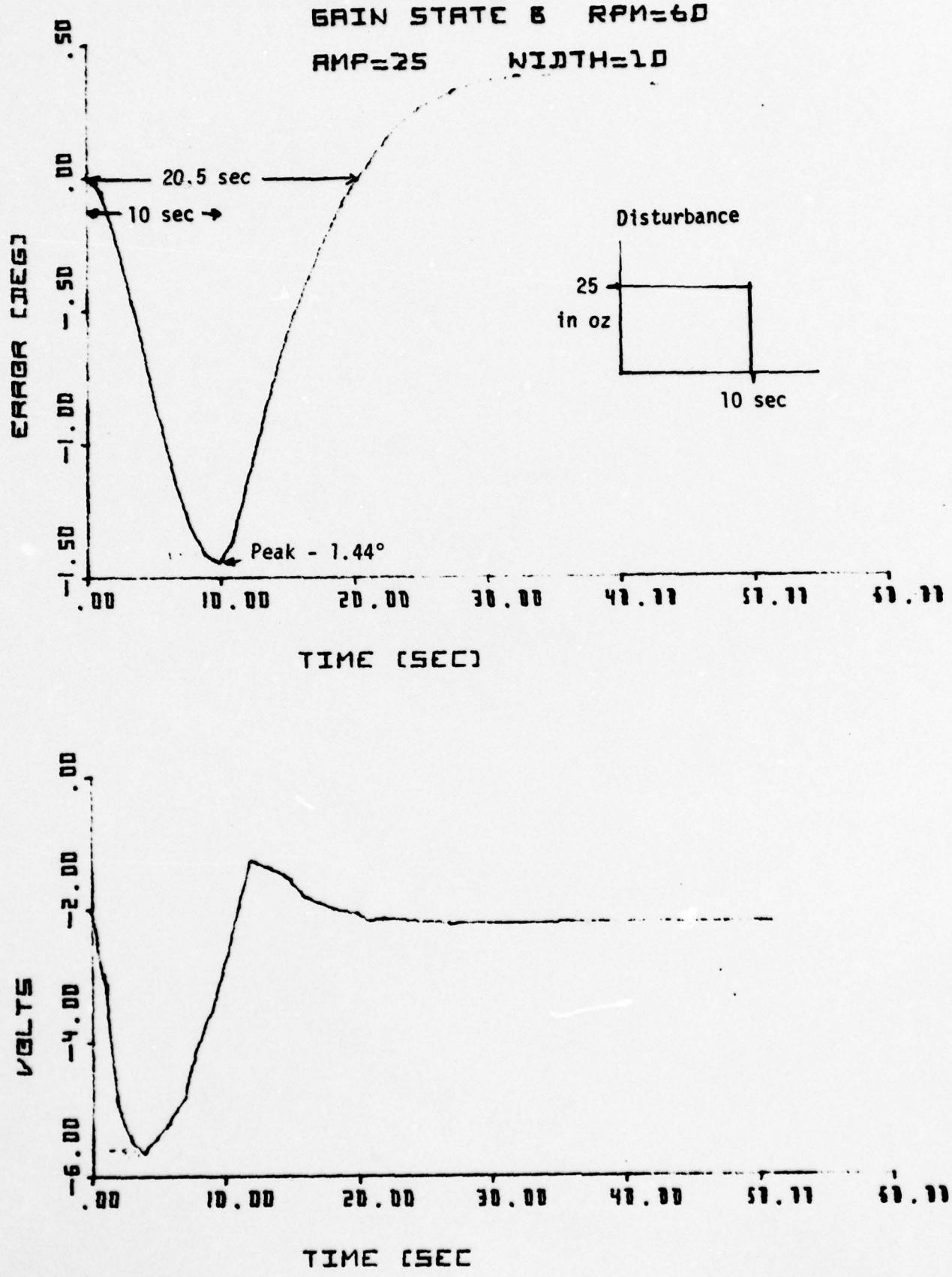
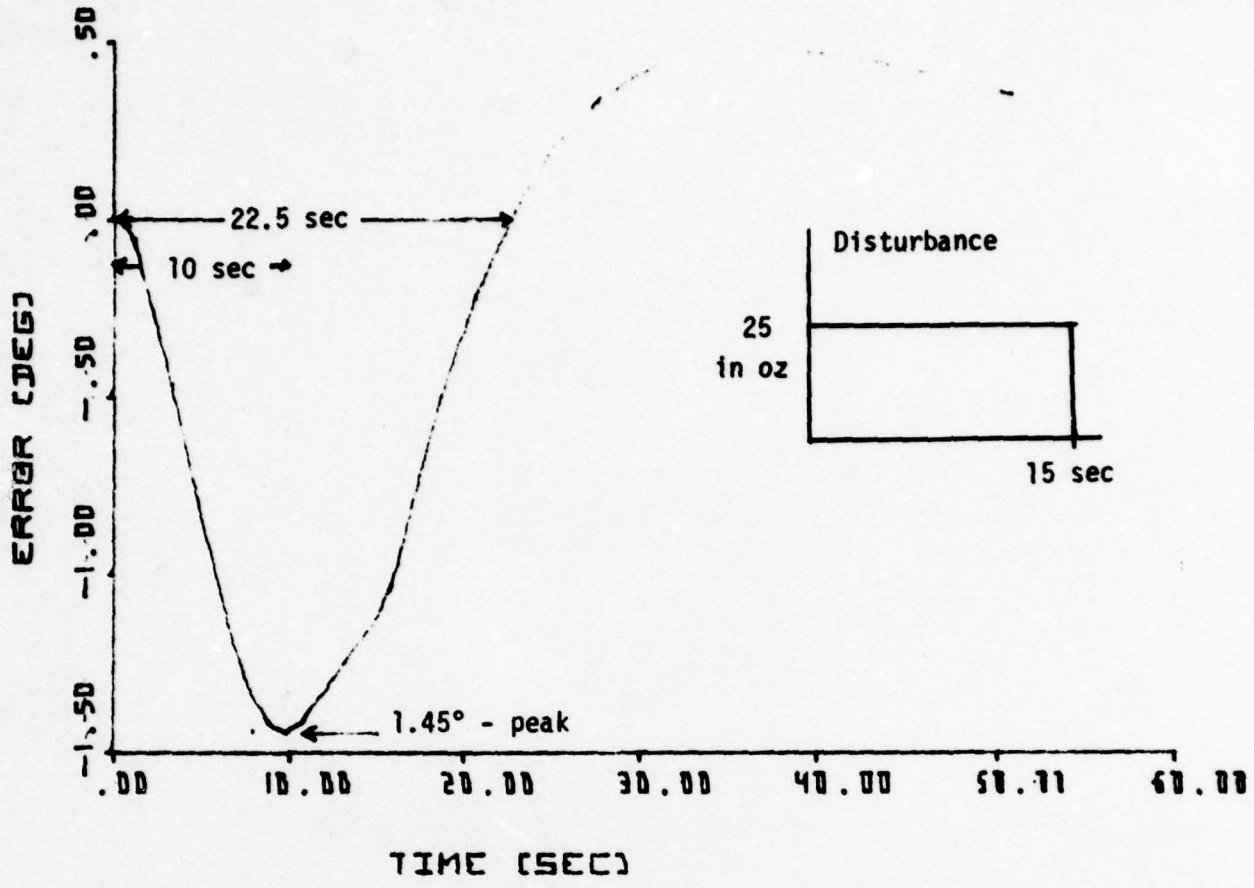

DRAG TORQUE=120 IN OZ
AVAIL TORQUE =170 IN OZ
GAIN STATE 6 RPM=60
AMP=25 WIDTH=10
20.5 sec
10 sec
Peak - 1.44°
Disturbance
25
in oz
10 sec
ERROR (DEG)
.50
.00
-.50
-1.00
-1.50
.00
10.00
20.00
30.00
40.00
50.00
60.00
TIME (SEC)
VOLTS
.00
-2.00
-4.00
-6.00
.00
10.00
20.00
30.00
40.00
50.00
60.00
TIME (SEC

Figure 9-5.


.50
.00
-.50
-1.00
-1.50
ERROR (DEG)
22.5 sec
10 sec
1.45° - peak
Disturbance
25
in oz
15 sec
.00
10.00
20.00
30.00
40.00
50.00
60.00
TIME (SEC)

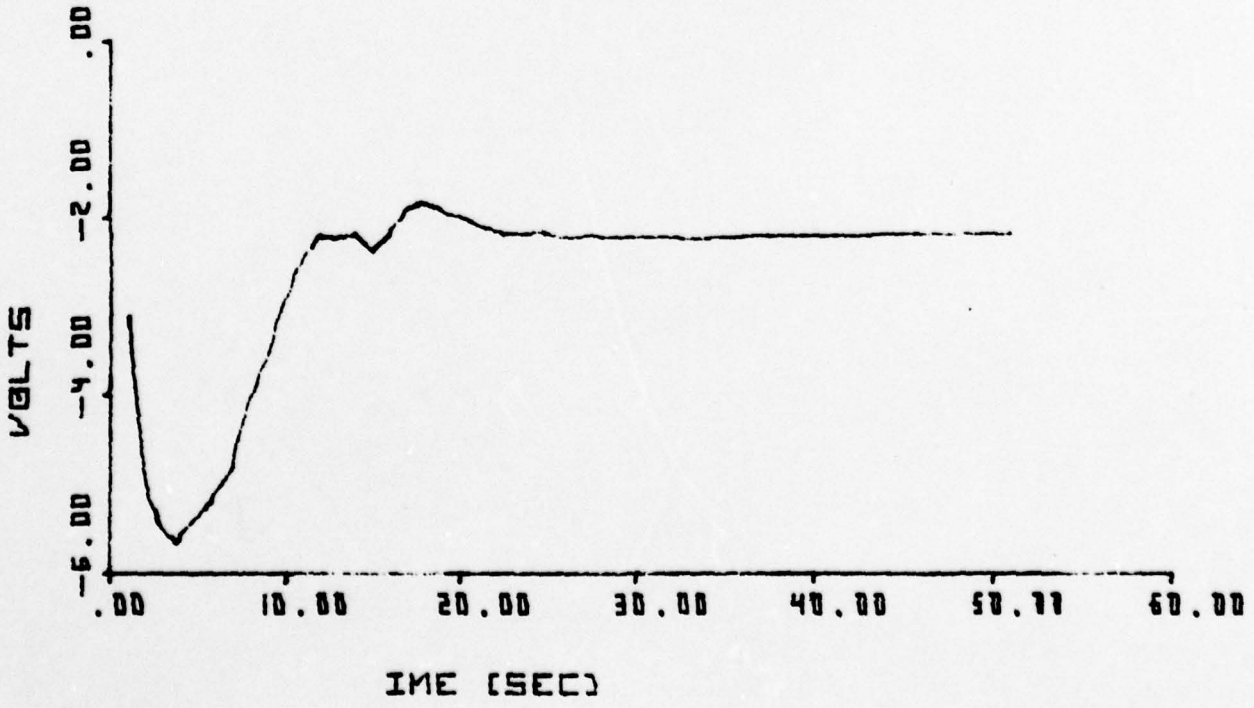

.00
-2.00
-4.00
-6.00
VOLTS
.00
10.00
20.00
30.00
40.00
50.00
60.00
IME (SEC)

Figure 9-6.

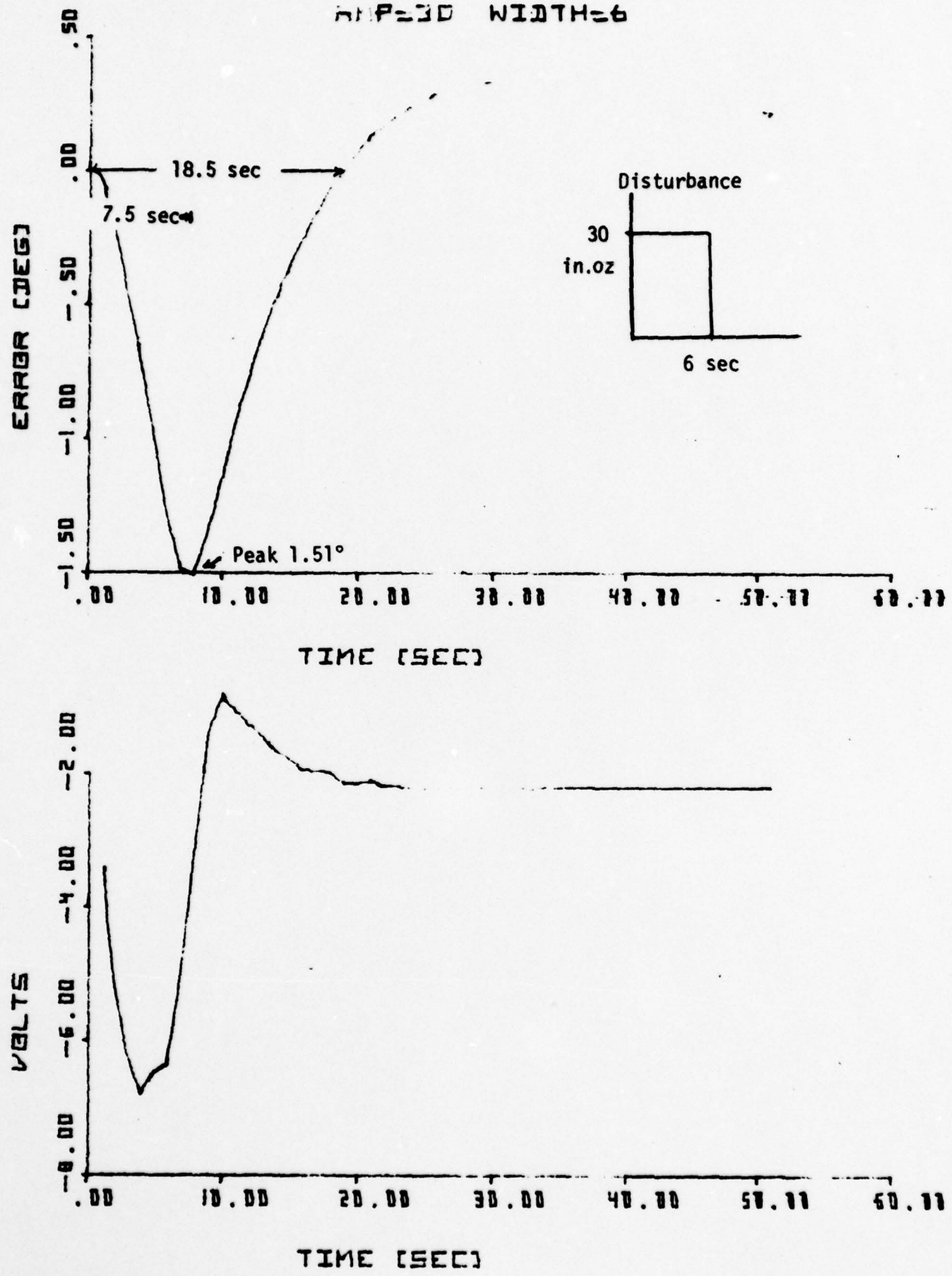

AMP=30 WIDTH=6
.50
.00
-.50
-1.00
-1.50
ERROR [DEG]
18.5 sec
7.5 sec
Peak 1.51°
Disturbance
30
in.oz
6 sec
.00
10.00
20.00
30.00
40.00
50.00
60.00
TIME [SEC]
-2.00
-4.00
-6.00
-8.00
VOLTS
.00
10.00
20.00
30.00
40.00
50.00
60.00
TIME [SEC]

Figure 9-7.

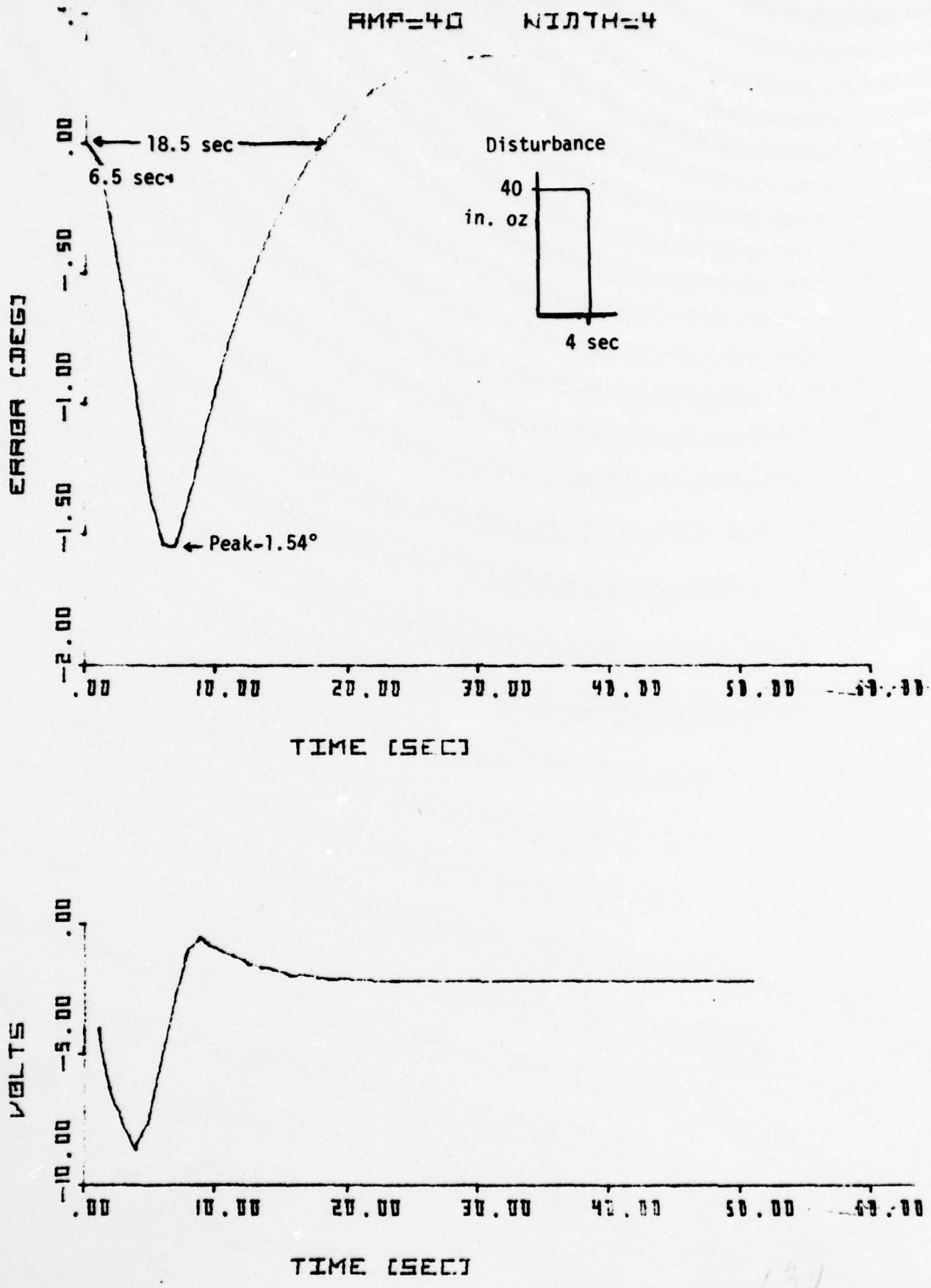

AMP=40 WIDTH=4
18.5 sec
6.5 sec
Disturbance
40
in. oz
4 sec
Peak-1.54°
ERROR [DEG]
.00
-.50
-1.00
-1.50
-2.00
.00
10.00
20.00
30.00
40.00
50.00
TIME [SEC]
VOLTS
.00
-5.00
-10.00
.00
10.00
20.00
30.00
40.00
50.00
TIME [SEC]

Figure 9-8.

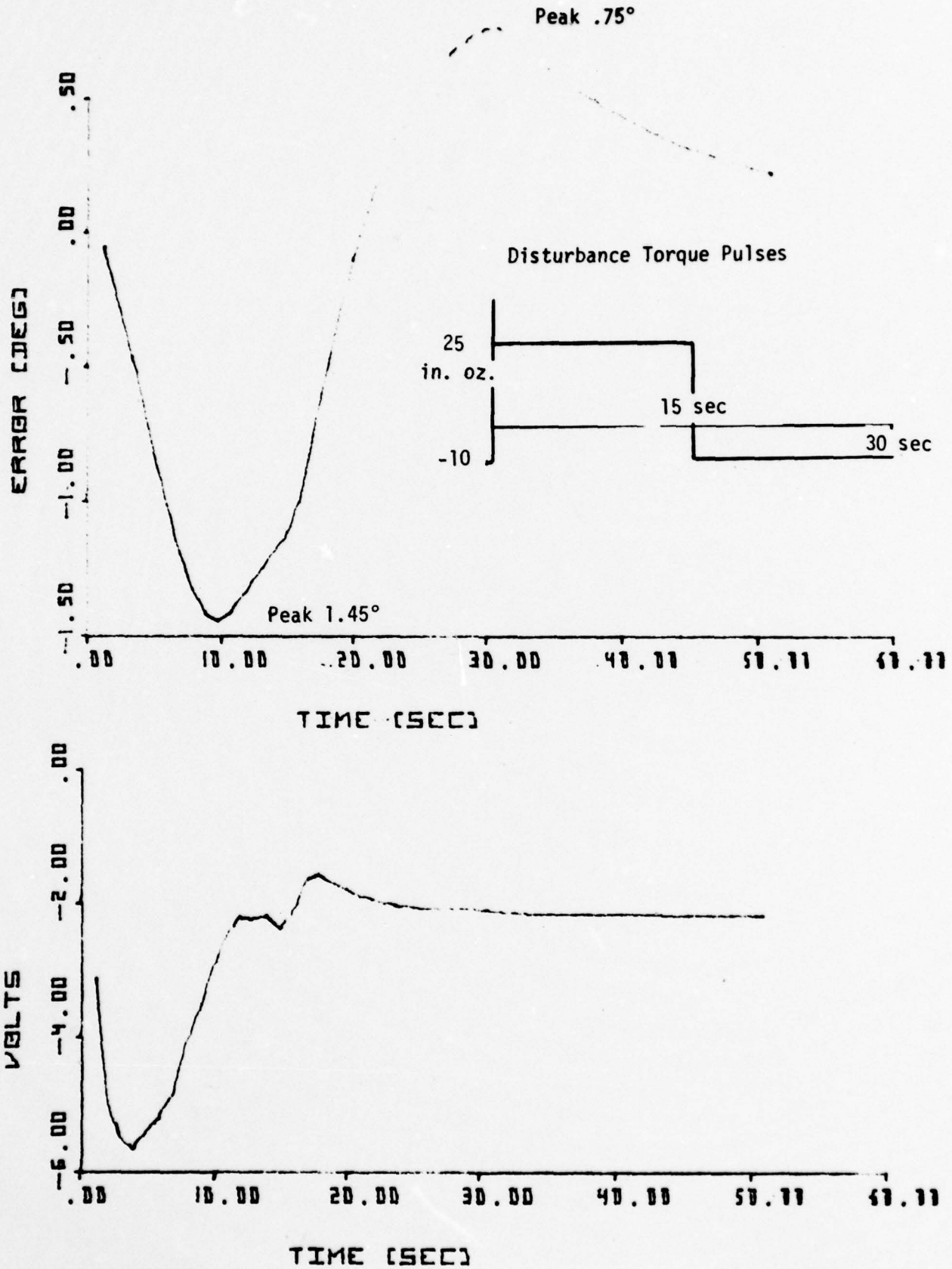
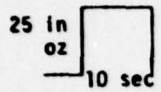
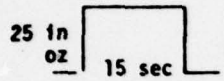
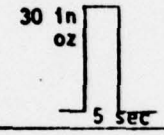
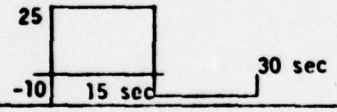
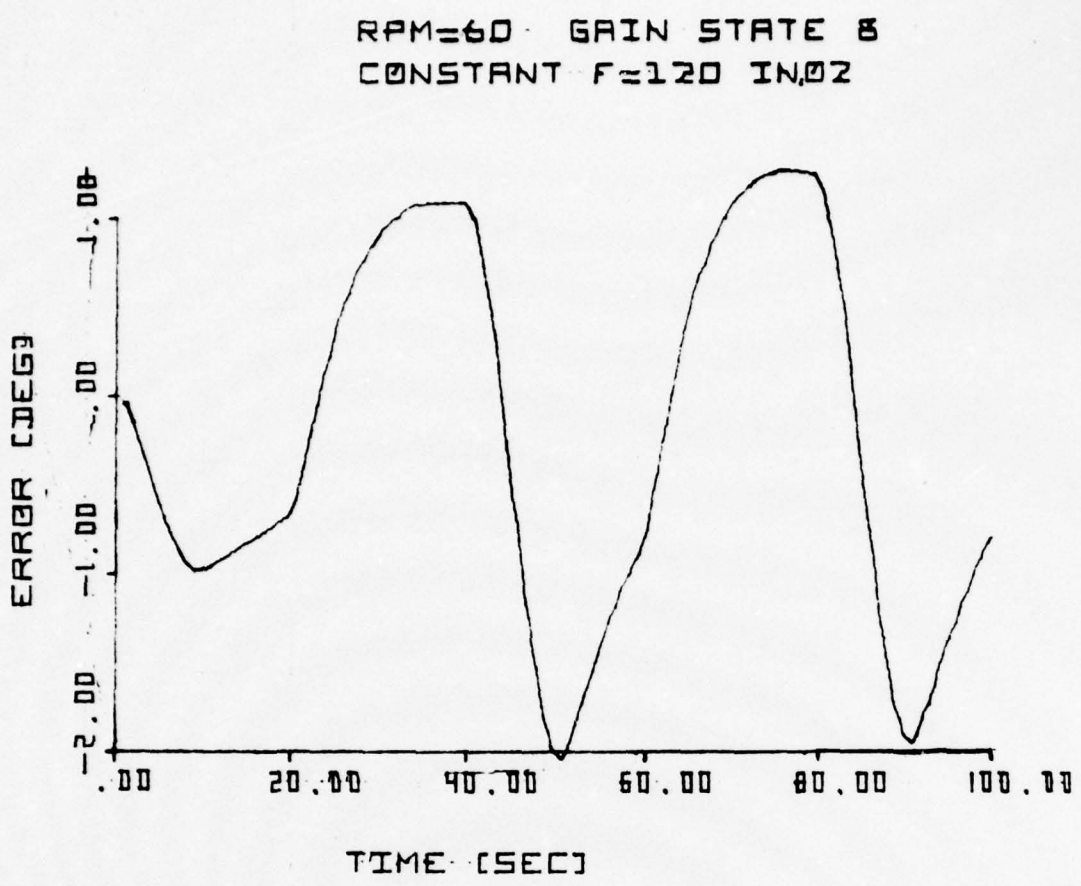

Peak .75°
Disturbance Torque Pulses
25
in. oz.
-10
15 sec
30 sec
ERROR (DEG)
.50
.00
-.50
-1.00
-1.50
Peak 1.45°
.00
10.00
20.00
30.00
40.00
50.00
60.00
TIME (SEC)
VOLTS
.00
-2.00
-4.00
-6.00
.00
10.00
20.00
30.00
40.00
50.00
60.00
TIME (SEC)

Figure 9-9.

Table 9-1. Summary of Simulated Responses for Various Torque Pulses

DISTURBANCE TORQUE (Fig.) (SIMULATED)		PEAK ERROR REPONSE (DEG)	RISE TIME (SEC)	PULSE WIDTH (SEC)	OVERSHOOT (%)
		1.44	10	20.5	26%
		1.45	10	22.5	33%
		1.51	7.5	18.5	22%
		1.54	6.5	18.5	21%
		1.45	10	20.5	52%
Flight Data	Sept. 10	1.55	13	25.0	49%
	Sept. 12	1.4	10	20	
		1.4	10	18	
		1.6	8	14	NOT AVAILABLE
		1.3	10	20	



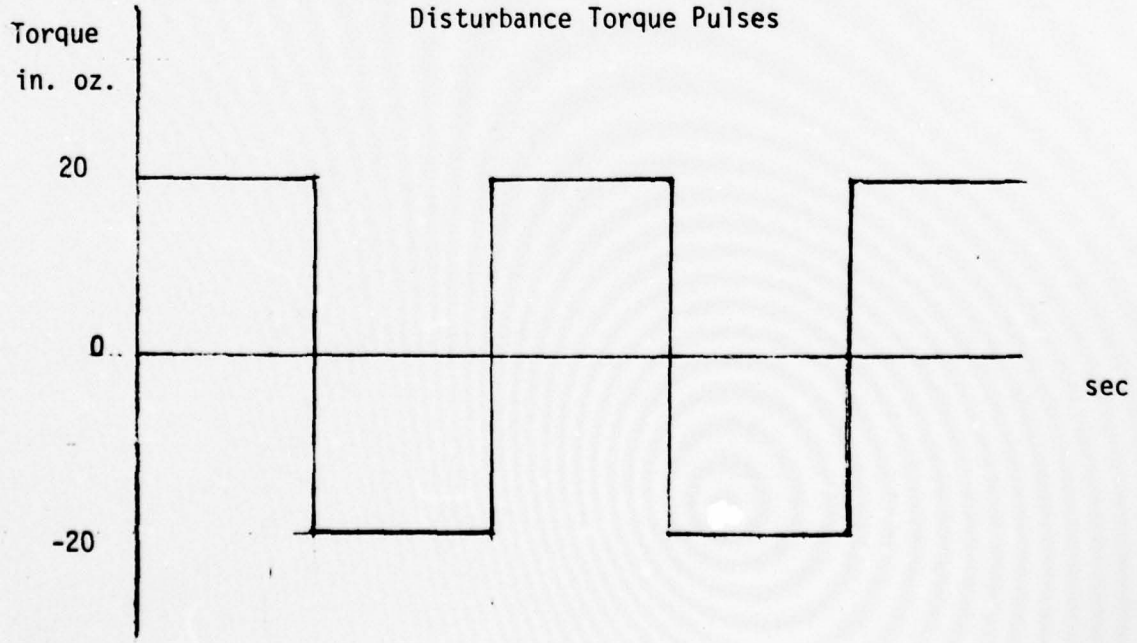
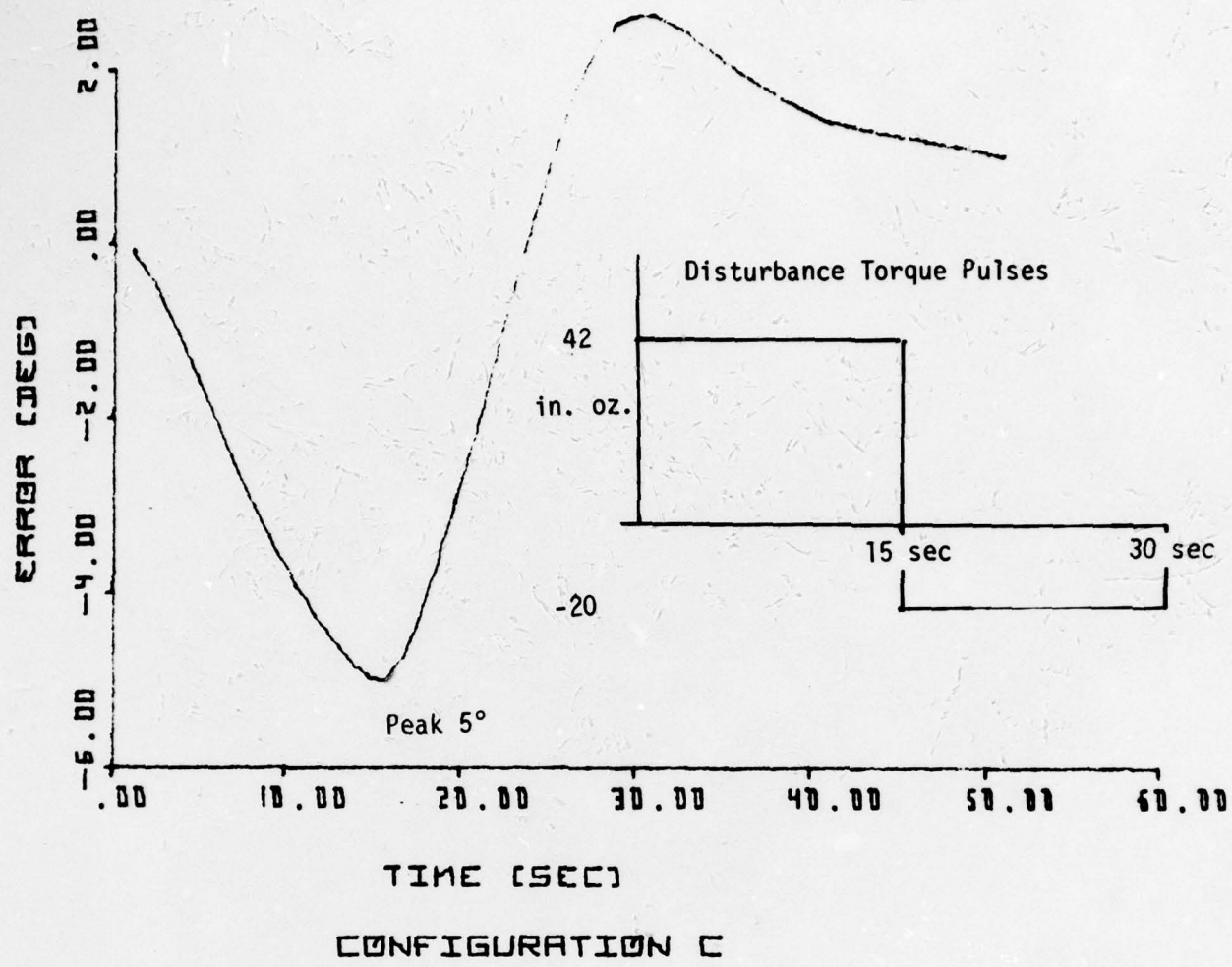


Figure 9-10. Error Response Due to Multiple Pulses



CONFIGURATION C

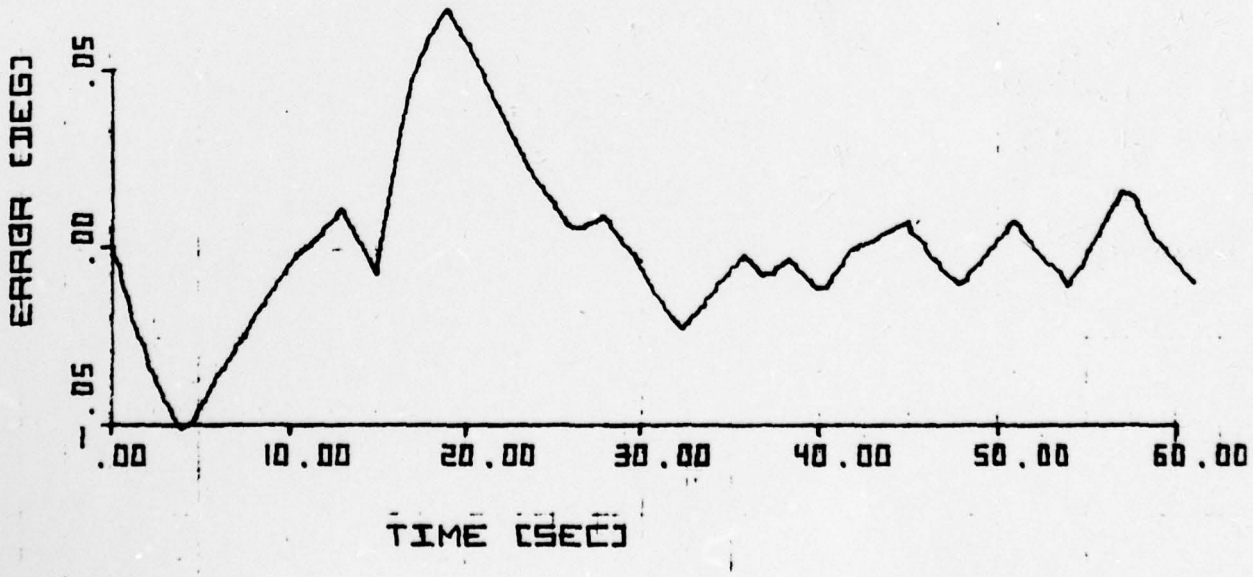


Figure 9-11. Comparison Between 777 Controller and Configuration C

9.2 Spectral Analysis

Selected pieces of Power Spectral Density (PSD) data of platform pointing error performance covering a four month time period (June to September 1975), up to the time of the first total spin-up are evaluated in this section. The data was furnished by Aerospace Corporation in the form of plots and data listings and was calculated from platform pointing error data taken over operating time intervals lasting several hours.

The objectives of the analysis were to: (1) analyze the characteristics and trends of the given PDS pointing error data base; (2) transform the pointing error PSD data back to an equivalent torque disturbance PSD; (3) compare the calculated disturbance torque PDS to one case of ground test torque PSD data and; (4) relate the peaks and trends of the disturbance torque PSD data to possible bearing disturbance harmonics.

9.2.1 Data Analysis

The overall expected trends for the pointing error data base PSD and the calculated disturbance torques PSD are summarized in Table 9.2-1 for the data shown in Figures 9.2-1 through 9.2-4. The discussion of these trends is divided into (1) a discussion of overall chronological PSD trends for the pointing error data base; (2) a discussion of disturbance torque trends in low frequency control band (less than 0.038 Hz), and; (3) high frequency trends in the band out to 0.5 Hz or one half the sampling frequency. The correlation of the PSD peaks with bearing frequencies and test data is also summarized after these discussions. Additional details of the analysis are presented in Appendix I.

9.2.1.1 Overall Chronological Pointing Error PSD Trends

(a) 6/27/75 to 9/01/75 Pointing Error Performance

The performance summary Table 9.2-1 shows that during the three month interval from 6/27/75 to 9/12/75 the peak pointing error PSD at low frequencies increases by a factor of 40:1, where a 6 times increase occurs within the last half month, (with in the first 12 days of September up to the time of the first anomaly)

Table 9.2-1. Summary of Performance 9433

Gain State	7	7	7	8	
Date	6/27/75	8/12/75	9/01/75	9/12/75	
Day	178	224	244	255	
Opr.Start Time~Sec Zulu	53680	44531	42484	31746	
Opr.Stop Time ~ Sec Zulu	55995	49206	44675	33992	
Pointing Error PSD (D^2/Hz)					
Control Band (f < .038 Hz)					
Maximum	0.260	1.02	1.7	10.0	
Minimum	0.012	0.03	0.15	1.0	
High Freq. Band (f>0.038 Hz)					
Average @ f≃0.09 Hz	0.002	0.003	0.003	1.0	
Peak @ f≃0.1 Hz	0.05@.10Hz	0.07@.11Hz	0.006@.11Hz	9.0@.17Hz	
Average @ f≃0.5 Hz	0.0015	0.001	0.0015	0.06	
Δ Torque PSD (In oz^2/Hz)					Ground Test Data
Control Band (f<0.38 Hz)					
Maximum	140	1100	800	101,000	94
Minimum	4.2	9.0	12.0	800	1.0
High Freq. Band (f>0.38 Hz)					
Average @ f≃0.09 Hz	2.0	6.0	20.0	8000	<1.0
Peak @ f≃0.1 Hz	440*	950*	90*	900,000*	11@0.2Hz *
Average @ f≃0.5 Hz	550	1100	3000	220,000	8@0.42Hz *
					45@0.92Hz **
Δ Mean Square Torque $(in/oz)^2$ x 0.5					
End of Control Band f = 0.038 Hz	1.2	5.0	6.6	310	
High Freq Band f≃0.09 Hz	1.4	5.5	8.0	600	
Before Jump f≃0.1 Hz	1.4	5.5	8.5	1200	
At Jump f≃0.1 Hz	7.2*	16.0*	8.5*	7000*	
f =0.5 Hz	1000	260	500	50 000	
In oz (RMS) f = 0.5 Hz	44.5	22.8	31.5	315	

* Peaks occur at frequencies listed in Pointing Error PSD Data

** Test Data Peaks

Δ Sensor Noise Including Quantization Uncertainty = 0.03σ Degrees

Although the platform pointing error PSD amplitude is increasing with time, certain similarities in the data are noticeable during the time interval or 6/27/75 to 9/01/75. For example, the cutoff of the PSD pointing error data occurs asymptotically at a rate of 80 DB per decade out to 0.1 Hz, and thereafter at about 10 DB per decade to 0.5 Hz. The high asymptolic rate is due to the inertia load effects which dominate performance at frequencies higher than the control bandpass frequency (approximately 0.038 Hz). This asymptote represents a constant disturbance torque band line. The lower asymptotic rate at the low PSD amplitude-high frequency position of the spectrum is due to a combination of the effects of sensor noise, pointing error quantization, and sampling effects or folding occurring at these frequencies. For example, if the PSD of broadband sensor noise is considered equal to the noise variance divided by the sampling period or approximately 10^{-3} degrees squared per second, it appears that the pointing error PSD asymptotically approaches this value. This indicates that pointing error is down to within the sensor noise range at frequencies near 0.5 Hz.

At low frequencies, however, the high pointing error trend could be caused by high frequency 1 Hz disturbances folded about 0.5 Hz or one half the sampling frequency. Since the platform rotates at 1 Hz, there is a strong likelihood of bearing disturbances occurring at this frequency. Since pointing error data is also sampled near this frequency, large pointing error amplitudes occurring near 1.0 Hz could be folded back and added to the low frequency pointing error. However, the torque disturbances causing these large amplitude high frequency pointing error excursions would have to be significant because of the 80 DB per decade attenuation contributed by the load inertia at high frequencies. These assumptions appear valid for the data in the 6/27/75 to 9/01/75 time period range. The preanomaly data taken on 9/12/75 does show strong effects of folding over the high frequency range

(b) 09/12/75 Pointing Error Performance

The 09/12/75 pointing error data shows approximately a 40 DB per decade attenuation for frequencies greater than the control bandpass frequency of 0.038 Hz or approximately half the rate of shown in the earlier cases. Furthermore, an amplitude shift upwards of 20 DB is noted for the low frequency end and 40 DB shift at the high frequency end (near 0.5 Hz). The decrease in slope to one half the normal constant torque inertia load line 80 DB/decade can be explained by an increase in the torque in the high frequency range. The departure from the 80 DB/decade trend noted in the earlier cases is also significant since this indicates the additive effects of folding at higher frequencies on the pointing error PSD. The folding effect probably strongly influences the pointing error PSD across the spectral band.

9.2.1.2 Calculated Torque PSD Trends

The torque PSD was calculated using the pointing error PSD data and an effective broadband sensor noise of σ degrees as inputs to the square of the real parts transfer functions relating these inputs to the output torque PSD. Three forms of control transfer relationships were developed in the analysis. These include: (1) linear control model; (2) linear model with the addition of a zero order hold in the pointing error output channel; (3) sampled data model which uses an impulse transfer function representation of the control system. The latter two models were used primarily to study performance in the high frequency band to separate noise and folding effect from possible PSD peaking due to retainer disturbances. The first two models provided substantially the same torque PSD data in the control band or frequencies below 0.038 Hz. This appeared reasonable since the sampling frequency is over 40 times the control system band, so torque values within the control band appear accurate if aliasing effects are considered small (This appears valid for the first 3 cases up to 09/01/75). At high frequencies, the unexpected rise in the calculated torque PSD required a re-examination of the pointing error data at these frequencies and sources of error which include sensor noise estimation, quantization effects and sampling, where these effects could bias the torque PSD to higher values. Higher frequency performance is

governed chiefly by the platform load inertia and is therefore outside the response of the control system. The significant conclusions covering the modeling assumptions and the resultant torque trends in the high and low bands, are listed as follows:

(a) Effective Sensor Noise Estimation

A good estimate of the broadband sensor noise is required to study high frequency performance since the pointing error PSD is low in this frequency range. Sensor noise input PSD is subtracted from the pointing error PSD data to obtain data with minimum noise for torque PSD calculation. The sensor noise of 0.03 deg (1 σ) was selected as the best compromise which would provide non-negative torque PSD calculations at the high frequencies. This noise is considered to represent the difference between true sensor noise and the quantization uncertainty or one half the quantization interval of 0.0137 deg/count.

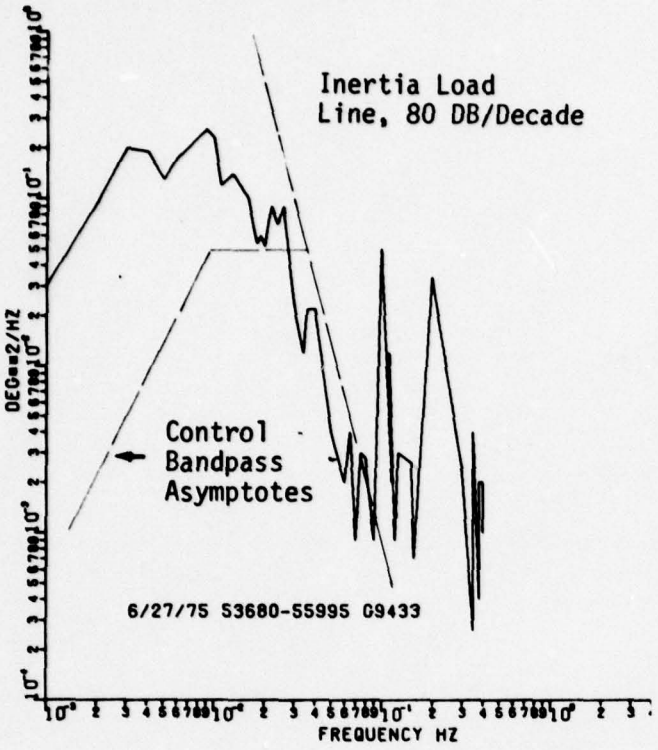
(b) Linear Model Torque Trends

The torque trends are summarized in Table 9.2-1 and are shown in Figures 9.2-1 B and C through 9.2-4 B and C. Both linear models show substantially the same result. For example, the linear model with the zero-order hold shows slightly higher torques at low frequencies and higher torques at high frequencies.

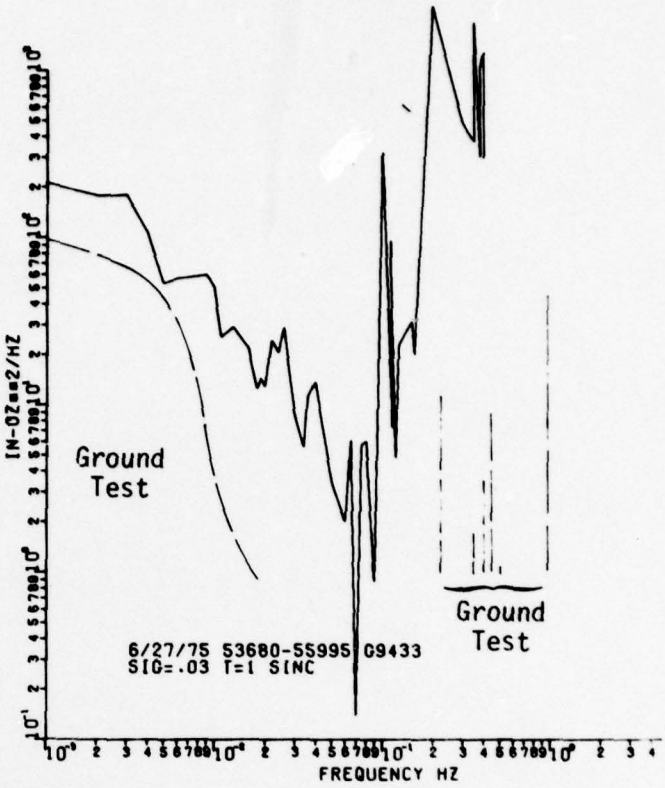
- Low Frequency Trends

The calculated torque within the control band of 0.038 deg was compared to a single piece of ground test PSD data which is shown superimposed on the above figures. A similarity in curve shape is noted. The calculated torque curves appear higher in amplitude and the cutoff appears to be shifted to higher frequencies from 0.01 to 0.04 deg. The closest fit appears to occur with the early 6/27/75 data where, for example, at the low frequency end (at 0.001 Hz) a peak of 140 $(\text{in oz})^2$ per Hz was obtained as compared to the ground test data of 94 $(\text{in oz})^2$ per Hz. As time increases, the torque PSD values shift upward, but the shape is generally preserved in the low frequency band. At 9/12/75, before the first anomaly, torque

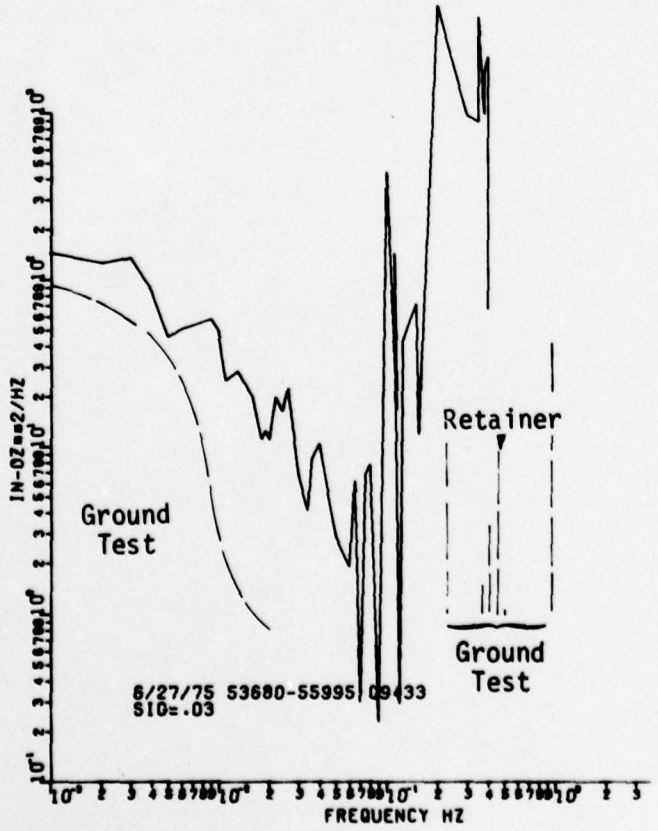
A. Pointing Error PSD Data



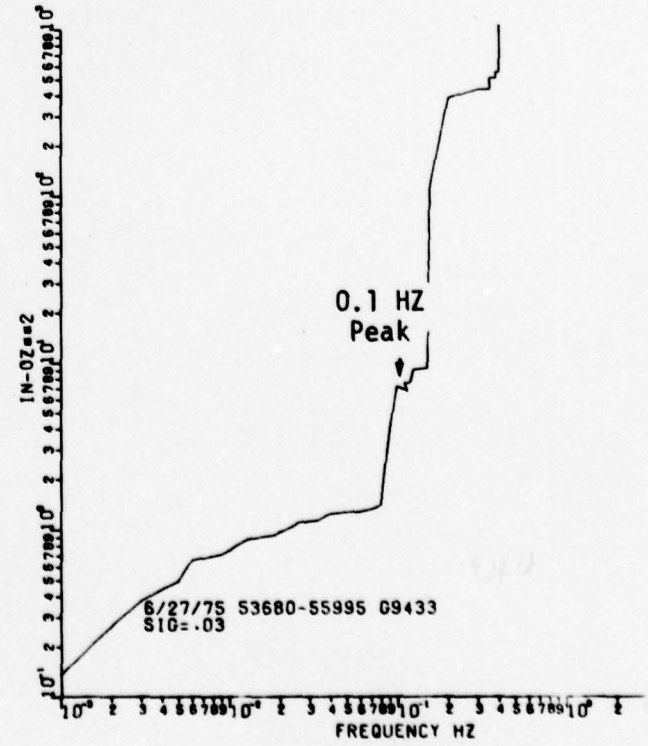
C. Linear (ZOH) Corrected Torque P



B. Linear Torque PSD



D. Mean Square Torque Error x .5



Figure, 9.2-1. 9433 Pointing Error Data and Torque PSD 6/27/75 (Gain State 7)

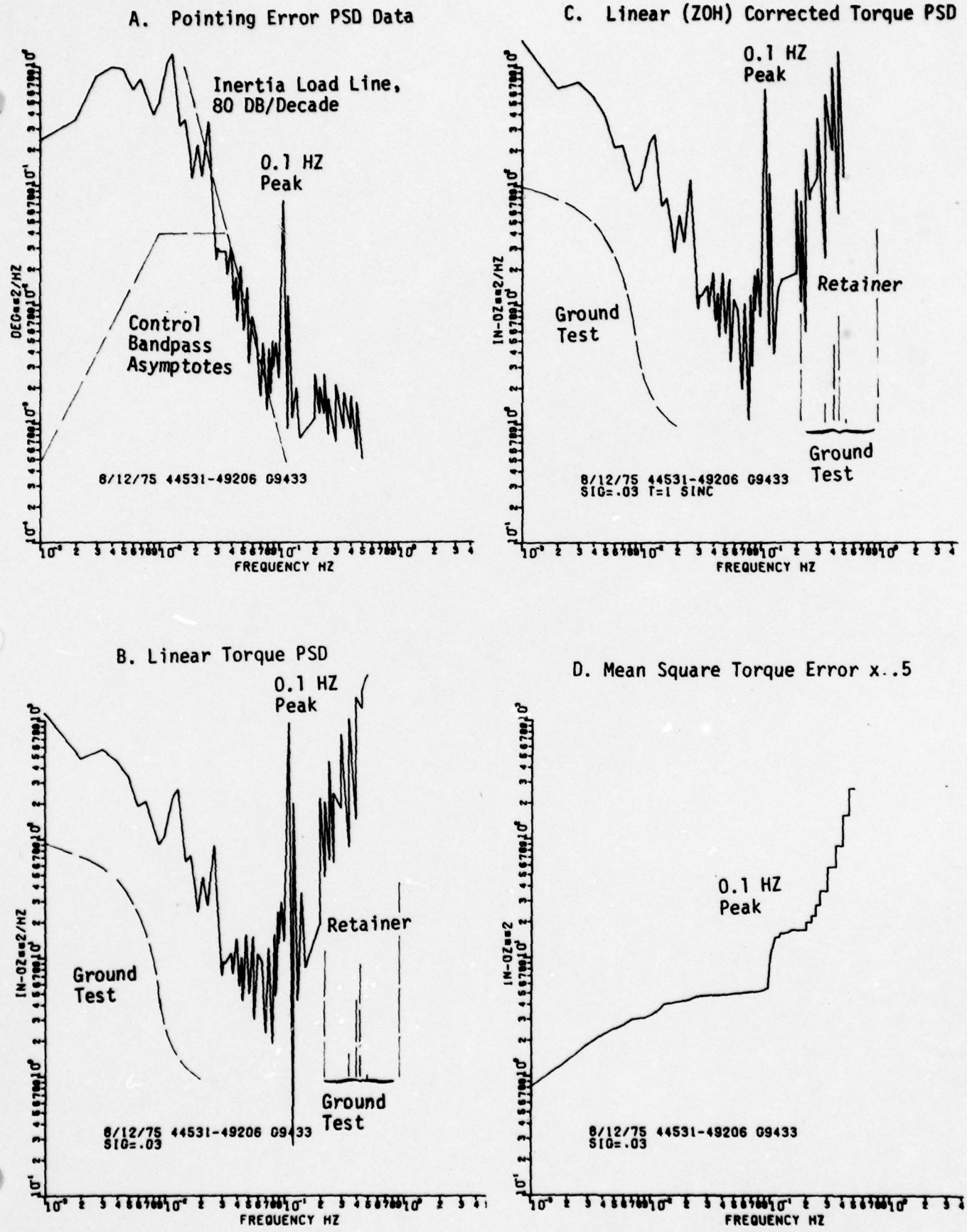


Figure 9.2-2. 9433 Pointing Error Data and Torque PSD 8/12/75 (Gain State 7)

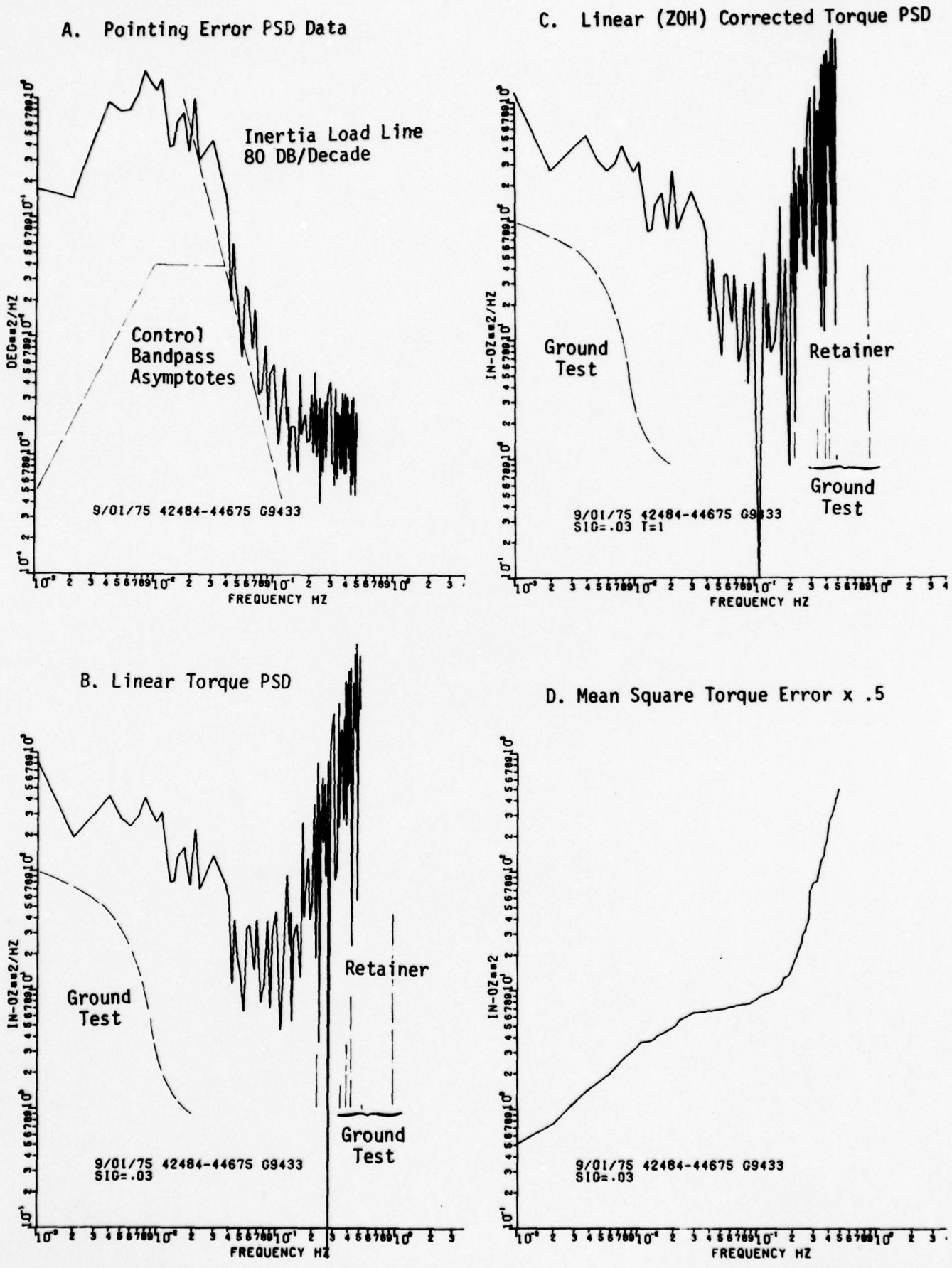
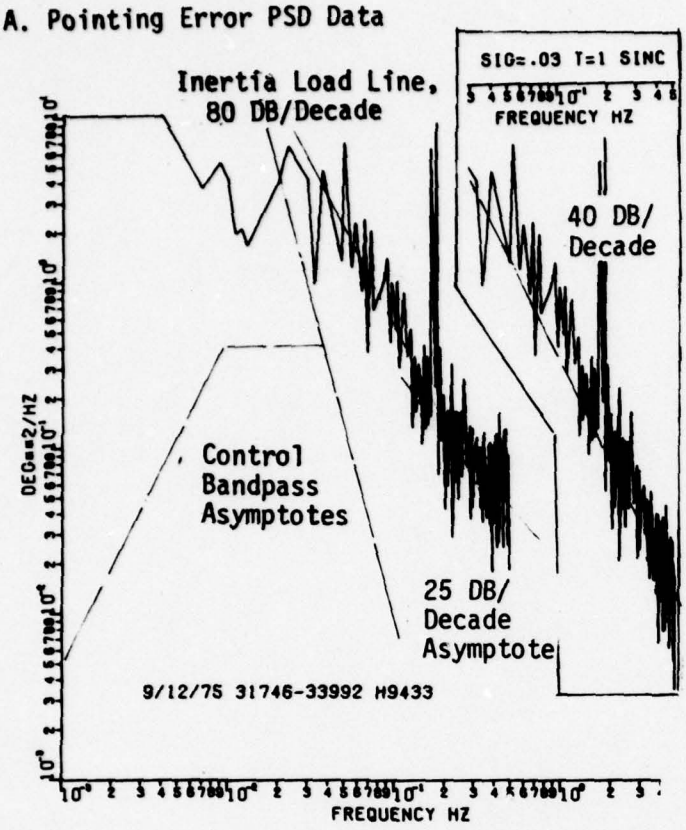
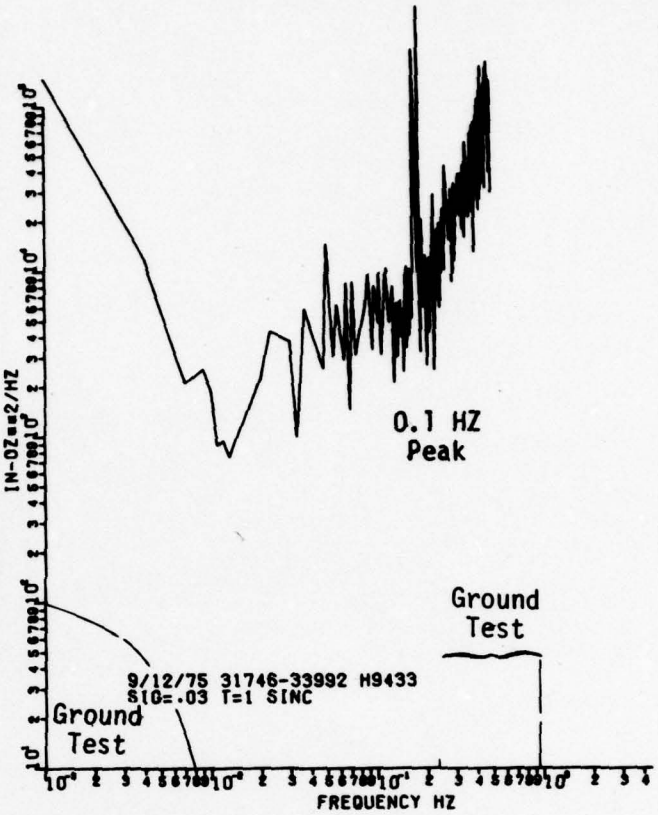


Figure 9.2-3. 9433 Pointing Error Data and Torque PSD 9/01/75 (Gain State 7)

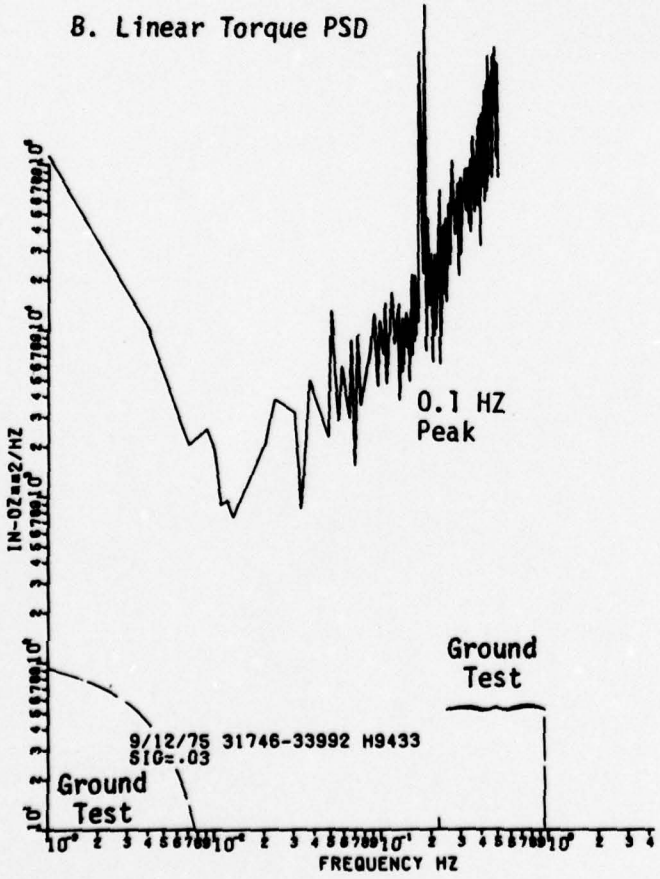
A. Pointing Error PSD Data



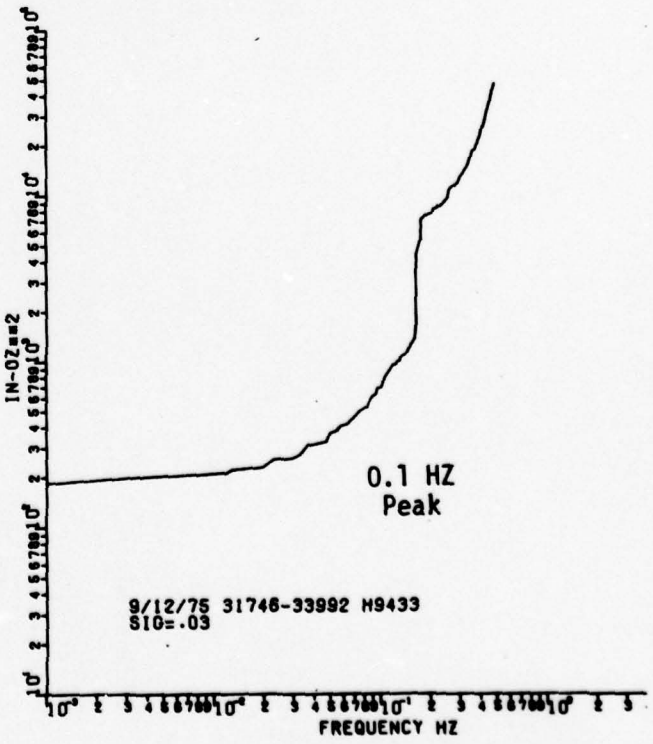
C. Linear (ZOH) Corrected Torque PSD



B. Linear Torque PSD



D. Mean Square Torque Error x .5



9.2-4. 9433 Pointing Error Data and Torque PSD 9/12/75 (Gain State 8)

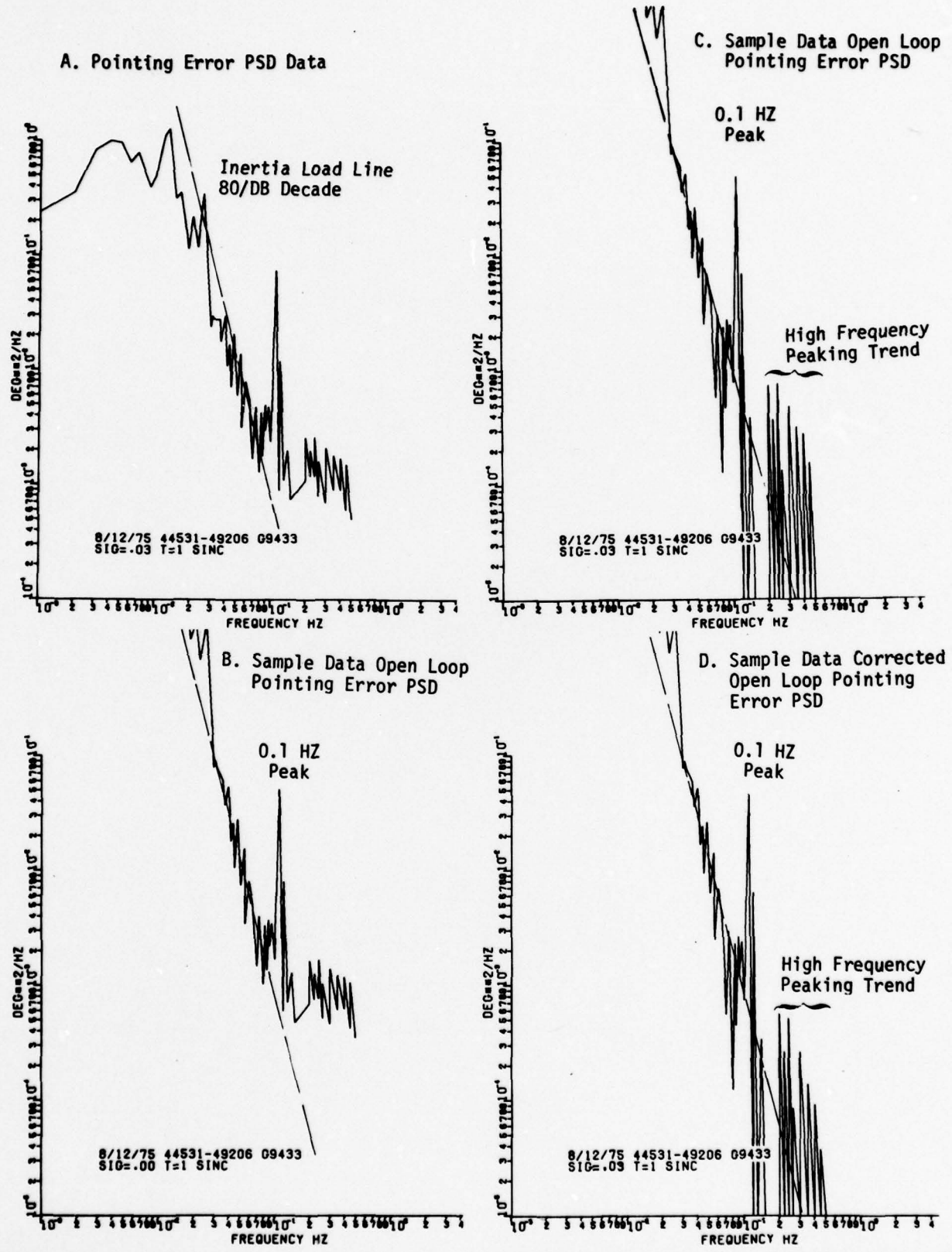


Figure 9.2-5. Pointing Error Data and Sample Data Open Loop Pointing Error PSD (Gain State 7)

PSD has increased to 10^5 (in oz)^2/Hz.

- High Frequency Trends

The most noticeable high frequency trend is the broadband increase of torque PSD at a rate varying from 20 to 40 DB per decade. The question is whether this trend is real or as a result of data reduction roundoff, nonlinear effects of quantization not included in the model, or the effects of sampling. Sensor noise was removed from the pointing error date up to the point of calculating negative torque PSD at these frequencies. The effect of sampling on the pointing error PSD for a simple system with load inertia having a constant torque, PSD input verified the following fact: with no sampling, and with a constant torque band input, pointing error PSD should decrease at 80 DB per decade. The effect of sampling results in decreasing this rate by 80 log $[\text{sinc}(\pi f/f_s)]/\sqrt{f_s}$ DB. Where f equals 0.5 Hz or one half the sampling frequency f, 15.5 DB (factor of 6) must be added to 80 DB/decade curve to correct the inertia load for sampling. The effect of sampling can be applied to the ghigh frequency end of the torque curves and results in at most a 15.5 DB wighted reduction in the torque PSD values shown. Figures 9.2-1D through 9.2-4D show the four cases where the input data was corrected using a sample hold model by the sampling factor. The resulting torque trend still rises in the high frequency band. Within this band are the retainer frequencies (0.45 Hz) and this rise could be caused by large torque inputs associated with retainer torque disturbances.

(c) Sampled Data High Frequency Trends

The impulse transfer functions of the control system were developed for the control system. These transfer functions relate the sensor and pointing error PSD inputs to open loop pointing error output. In this case, with the control system sampler in the feedback loop relative to the torque disturbance,

the torque PSD cannot be calculated explicitly; however the open loop pointing error output PSD or the open loop effect of the disturbance torque input PSD acting on the platform inertia load dynamics can be calculated. These calculations were performed with variations of the sensor noise removed from the pointing error PSD data. (see Figure 9.2-5 for details).

At high frequencies (above the control band frequency of 0.038 Hz) both the pointing error and calculated open loop pointing error PSD show good agreement, the differences being the removal of the higher order control dynamics, sensor noise and sampling effects in the transformation. The pointing error PSD calculation shows that the PSD rises above the 80 DB per decade control line for both the low and high frequency ranges with the noise and sampling effects removed. This substantially backs up the torque PSD calculation and indicates that large PSD amplitudes exist at both the low and high frequency ends of the spectrum.

9.2.1.3 Peak Trend Analysis

An attempt was made to correlate the peaks shown in the pointing error data and transformed torque PSD's with the bearing component frequencies thought to cause these disturbances. However, no definite correlation trends were found. For example, the theoretical bearing component frequency differences and shaft to component frequency differences range from 0.44 to 0.619 Hz for the DMA retainers and zero and 1 Hz for the inner race and shaft. The ball frequencies are in the 5 Hz range with frequency differences about 0.006 Hz. However, no definite trend in sharp peaks was found in the high frequency end (0.4 to 0.5 Hz) or at the low frequency end of the spectrum. A consistent peak in the data, however, was found around 0.1 Hz. It is noted that in the single piece ground test data available, a peak in torque PSD (45 $(in\text{-}oz)^2/Hz$ occurred at 0.9 Hz. The peak noted at 0.1 Hz, could be a result of difference between the sampling frequency (Carrier) at 1.0 Hz and the 0.9 Hz disturbance noted in the ground test data.

Figures 9.2-1E through 9.2-4E show the results of integrating the calculated torque PSD over the spectrum. The resultant output at any frequency is equal to one half the mean square torque error. The mean square torque error is also useful for picking out the peaks because they show up as sudden jumps in mean square error. The most pronounced jump is noted to consistently occur at about 0.1 Hz and an overall steep slope trend occurring at the high frequency end, also reflects the large torque inputs at these frequencies.

9.2.2 Conclusions

The conclusions of this analysis are briefly summarized as follows:

(1) Overall Pointing Error PSD Trends

Of the four pieces of pointing error PSD data examined, the first three taken at 6/27/75, 8/12/75, and 9/1/75 have similar band pass characteristics and show an increasing pointing error PSD with increasing calendar time. (The maximum peak PSD increases from 0.26 to 1.7 deg^2/Hz during this time). At the high frequency (0.5 Hz) end of the spectrum the pointing error PSD appears to approach the expected sensor noise PSD level of 10^{-3} deg^2/Hz. Folding or aliasing effects beyond the Nyquist frequency (0.5 Hz) should also appear small due to the low bandpass of the plant i.e., and 80 DB per decade cutoff in the PSD provided by the platform load inertia for torque disturbances.

The 9/12/75 pointing error PSD however exhibits different trends. Peak pointing error increases to 10 deg^2/Hz, about double the previous increase. At high frequencies, attenuation is less and the level at least 40 DB above the sensor noise level. These effects demonstrate that frequencies higher than 0.5 Hz are folded back, and these effects are inseparable in the pointing error PSD data.

(2) Overall Calculated Disturbance Torque PSD Trends

The disturbance torque PSD evaluation is divided into low frequency trends within the control bandpass (approximately 0.038 Hz) and high frequency trends out to 0.5 Hz.

At low frequencies, the torque was compared to ground test data which showed similar shape characteristics in this frequency range. For the 06/27/75 data peak torque PSD was 140 $(\text{in oz})^2/\text{Hz}$, while ground test data was 94 $(\text{in oz})^2/\text{Hz}$. As time increased, both the torque and bandpass frequency increased. By 09/01/75, the torque PSD was over 8 times the ground test level and at 09/12/75 over 1000 times the 06/27/75 level.

At high frequencies, the torque showed an unexpected rise, sometimes exceeding the low frequency peak. The torque PSD at high frequencies was calculated from pointing error PSD data near the sensor noise level so these values are suspect from the standpoint of nonlinear errors, true sensor noise, and sampling effects. In correcting the calculation for sampling effects, this higher torque trend was reduced somewhat but still remained near the low frequency peak. The broadband rise in torque within this frequency range could be significant because the DMA retainer disturbance frequencies are at 0.44 Hz. For the 09/12/75 data, well out of the noise effects, but subject to aliasing effects, the torque trend is the same, i.e., a broadband peaking near the high frequency end of the spectrum.

(3) Peaking Trends

No sharp peaking trends were noted in the data that would be comparable to calculated bearing or retainer frequency data A sharp peak occurred consistently in the data at 0.1 Hz. Also noted in the ground test data was a peak occurring at 0.90 Hz. The peak noted in the flight data could be caused by the same source, i.e., the 0.90 Hz peak folded back to the 0.1 Hz range.

10. CONSULTANT EVALUATIONS

During the course of the 9433 anomaly investigation, several consultants were engaged by TRW. Each of these has submitted a written report. This section summarizes the conclusions of these reports (each of which is presented in Appendix G).

10.1 Donald H. Buckley (NASA/LeRC)

Mr. Buckley, who is Head of the Lubrication Fundamentals Section of the Lewis Research Center, met with TRW personnel for one day during October. His conclusion, based on the data presented that day, is that the orbital anomaly was caused by inadequate bearing lubrication. He feels that all torque transients (including the drops in torque observed subsequent to his report) as well as the rise in average torque can be so explained. His report is presented in Appendix G.1.

His recommendations include:

- As short-term "fixes," provide for greater lubricant retention in the bearings and a change in lubricant type to one with lower volatility
- As a long-term improvement, use solid-film lubricants.

10.2 Delco Electronics

Personnel from Delco Electronics attended several meetings at TRW. Their representatives were Robert Breneman, George Campbell, and Ed Loper. Based on extensive review of orbital data, evaluation of the DMA design, and inspection of various life-test bearing sets, they have concluded that the most likely cause of the orbital anomaly is a bearing failure due to inadequate lubrication. Their report is enclosed in Appendix G.2.

Their recommendations for DMA improvement include:

- Provide more lubricant at the bearings by one or more of the following measures: more initial lubricant; heating the lubricant reservoirs; increase oil capacity of retainers; add a command-operated "oiler;" design a "real reservoir" for the bearings

- Improve bearing quality by requiring better surface finish and geometry and by instituting improved bearing screening procedures
- Review DMA assembly procedures to eliminate potential for surface contamination and debris generation
- Consider eliminating potential for bearing inner race rotation to reduce the possibility of self-generated debris.

10.3 Draper Labs

Representatives of CSDL who have participated in the 9433 anomaly investigation include R. J. Schiesser, H. B. Singer, and E. P. Kingsbury. As reported in Appendix G.3, they conclude that the 9433 despin control anomaly is due to lubricant breakdown within at least one of the DMA bearings.

CSDL has recommended several design and process changes; they continue to support TRW in process evaluation and improvement. Suggested design changes include:

- Remove dams from bearing outer races to eliminate the possibility of damage to balls during assembly
- Change ball-to-race (inner) conformity to promote EHD film formation
- Design a positive lubrication system
- Use a full ball complement (retainerless) bearing to eliminate retainer instability problems (in conjunction with positive lubrication system).

Recommended process changes relate to metal parts processing and improved bearing screening procedures.

10.4 Thomas Barish (Independent Consultant)

Mr. Thomas Barish, an independent consultant in the Los Angeles area, reviewed the DMA design and inspected life test bearings. In his report (Appendix 6.4), he concludes all fits and tolerances to be excellent and that the effects of probable thermal gradients should be insignificant. He does express the following concern: due to their races, the bearing raceway roundness will conform to that of the housing (and potentially the shaft at the lower main bearing). Mr. Barish indicates the following candidate failure modes:

- loss of lubricant
- cage failure to ball speed variation

and (less likely):

- broken parts (debris) momentarily lodged in the bearing
- failure in the slip ring assembly.

He suggests that lubricant failure would be unlikely to produce sudden jumps in friction, but could lead to a retainer failure. He concludes that some sort of scraping or rubbing (including the possibility of a failed retainer) is most consistent with the orbital data.

10.5 Chet Pentlicki (ComSat Labs)

Mr. Chet Pentlicki, Assistant Manager of the Structural/Mechanical Design Department of ComSat Laboratories, attended a series of meetings at Aerospace and TRW during three days in October 1975. During this time, he examined typical telemetry data, reviewed the DMA design, and inspected Aerospace test facilities.

In his report, he indicates a preference for the "bearing failure" theory (Appendix G.5). He draws a relationship between the retainer instability phenomenon observed on other 777 spacecraft (as well as 9433) and marginal lubrication, and presents a scenario of resulting retainer wear and debris production. He attributes the high DC running torque to a debris coating on the balls and cites test data supporting this hypothesis.

Mr. Pentlicki recommends more generous lubrication and an improved preload design.

11. CORRELATION OF FAILURE MODES WITH DATA

Table 4-1 presents a delineation of candidate 9433 failure modes and, for each, an estimate of the resulting performance signature. Other sections of this report, and the accompanying appendices present orbital data as well as analyses, test results, consultant opinions, etc. which bear upon these candidate failure modes. This section relates the various data to the failure modes defined in Section 4.

11.1 Review of Data

Much data arising from the anomaly investigation has been presented in the preceeding sections and the appendices. Before considering consistency with each of the failure modes, the major anomaly investigation results will be summarized.

11.1.1 Orbital Data (Sections 2, 3)

Available orbital data includes: operational data (while in Normal Mode control); unplanned events (transients which drop the spacecraft out of Normal Mode); friction/dynamic tests (systematic tests conducted in order to characterize the friction torques); recovery data (obtained during attempted and successful despin of the platform from the fully spun-up state). The most notable characteristic of this data is its lack of consistency and repeatability. However, it is, based on the evaluations of Section 3, possible to summarize the orbital performance related to the 9433 despin control anomaly.

- Prior to mid-August 1975, there were several periods showing a slight (but abnormal) temporary increase in running friction.
- Starting in mid-August, there was a rise in running friction, from a normal level of 30 in-oz to a level of about 95 in-oz, just prior to loss of operational status on 13 September 1975.
- Running friction has, during periods of normal operation remained in the neighborhood of 90-100 in-oz at most times since 13 September 1975.
- There have been occasional periods (observed since 28 November 1975) when the running friction has dropped to a relatively low level (e.g., 40 in-oz). On 28 November, this condition persisted for about 2.5 hours.

- Large torque transients have been observed at various times (e.g, on 11 December, a bistable friction characteristic occurred, with steps of approximately 200 in-oz).

- At one time (13 October), a transient torque of approximately 600 in-oz was observed.

- On several occasions, firing axial thrusters during periods of high torque has appeared to reduce the friction dramatically, suggesting that sideloading is a beneficial effect.*

- Recovery from the fully spun-up condition (i.e., platform despin) has only been successful after lowering the spin rate to approximately 20 rpm and pulling in the narrow coverage antennas to reduce the platform mass unbalance.

- A recovery attempt at 31 rpm showed a friction torque level which was high, but which varied insignificantly over a total platform revolution (i.e., there were no torque "high spots").

- Data from the orbital dynamic tests indicates that introducing sideloads by overspinning the platform by 10-20 rpm improves the smoothness of rate control.

- Data from various periods shows large variations in friction level over short periods.

- There appears to be no significant dependence of torque upon bearing temperatures.

- Runup/rundown data from the orbital dynamic tests suggest highest running friction when the platform is at zero inertial rate.

- Rundown data shows the torque not to have a significant viscous drag component.

- Platform stopping positions while fully spun-up show no repeating pattern.

Using these observations as a point of departure, it is possible to develop a hypothetical model for the 9433 anomaly:

(i) Some mechansim (call it Mechanism A) has caused the running friction to increase, over a period of about one month, from a level of 30 in-oz to nearly 100 in-oz. This higher level has been sustained almost continuously, since 12 September 1975.

---

* More limited data suggests that firing the thrusters during lower torque periods can increase the friction torque.

(ii) Mechanism B causes occasional large torque increases above the 100 in-oz level noted in (i). Mechanism B may be related or unrelated to Mechanism A.

This dual-mechanism model appears to fit much of the data above. For example, Mechanism A could produce a constant running friction while B provides, in some "on-off" fashion, the torque perturbations. Mechanism B can be sensitive to rocking and sideloads (accounting for recovery dynamics as well as the results of orbital tests) while A is not. The decrease in running torque to a near-nominal level would be explained by a temporary cessation of Mechanism A, with B inactive. In summary, Mechanism A is viewed in this characterization as a (more or less) sustained effect, insensitive to sideloads and producing a torque of 90-100 in-oz; Mechanism B is a mechanical phenomenon which produces high torques and which can be established (or eliminated) by sideloads and/or "jiggling."

11.1.2 Thermal/Dimensional Analyses (Section 5; Appendices A, B)

Thermal simulations and dimensional analyses have been conducted in order to evaluate certain possible failure modes. Results can be summarized as follows:

- No correlation was found between periods of high transient torques and thermal data (e.g., gradients at snubber and bearings).
- Dimensional and thermal analysis revealed no plausible source of the increased running friction (60-70 in-oz above nominal).
- Under extreme and unlikely conditions, interference can occur at the snubber gap while despun; full spin-up conditions decrease the likelihood of interference.
- The bearing retainers as dimensioned may, for some bearings, underride the balls; the 90 MM bearing retainers can ride against the preload washer. No significant torque increase would be expected.
- The motor power dissipation is the main factor in determining key DMA thermal conditions (motor temperature, snubber temperature, top bearing temperatures, gradient from top to bottom bearing).
- Analysis indicates that rotation of the 90 MM bearing inner race relative to the shaft is improbable.

11.1.3 System, Assembly, and Component Tests (Section 6)

A variety of tests have been conducted and reported in Section 6. These tests have considered the total despin control system, the DMA, bearings and slip ring assemblies, motor, and the power module snubber. Major pertinent results are:

- System tests showed a roll-off in motor torque capability at high rates, but otherwise did not duplicate the orbital friction tests.
- Bearing tests showed extreme preloads and tilt angles are required to produce the observed friction torque increase (and agreed with analysis data).
- Polymerized lubricant in main bearing raceways can increase DMA torque by 40 in-oz.
- Debris jammed in main bearings produced very large torques (>800 in-oz).
- Snubber tests show that sustained torques of 50 in-oz will produce wear at a rate of approximately 0.002 inch per hour.
- Motor tests show a drop-off of torque capability at high rates, due to a phase shift in the DEA between the resolver signal and the motor drive current.

11.1.4 DMA Disassembly and Inspection (Section 7)

The life test and flight spare DMA's were disassembled and inspected. The detailed aspects of this work are still underway. The results at this time include:

- All critical gaps were close to nominal, indicating no potential for interference in these units.
- A significant lubricant degradation was found in the life test DMA, where significant quantities of metallic lead were noted in the ball pockets of the 110 MM bearing retainers.
- Lubrication migration to the lower end of the unit was found in the life test DMA.
- The flight spare DMA was seen to suffer from assembly and handling deficiencies.

11.1.5 Consultant Evaluations (Section 10; Appendix G)

Four consultant reports were received, two representing individuals and two from organizations with several participants. Major findings include:

- Three out of four reports identify inadequacy of lubrication as the most likely cause of the anomaly; the fourth includes it as a possible cause.
- Improved bearing screening processing measures were recommended.
- The mechanism for transfer of lubrication from the reservoirs to the balls and raceways (by evaporation/condensation) was considered to be questionable; a positive lubrication system ("oiler") has been recommended.
- One consultant feels that some sort of scraping or rubbing is most consistent with the orbital data.

11.1.6 Other Data

Other data is developed in appendices or in other report sections:

- Simulations have been able to match orbital data by the choise of appropriate torque characteristics (Section 9)
- Analyses have shown no likely source of friction external to the DMA (Appendix H)
- A new more realistic model for motor performance has been developed (Appendix F)
- A history of DMA assembly test and storage has been developed (Section 8).

11.2 Discussion of Failure Modes

Candidate failure modes are identified in Table 4-1. Each is discussed below, with reference to orbital data as well as analysis and test results.

11.2.1 Structural Module

11.2.1.1 Axial Restriction of Preload Mechanism

Analyses presented in Section 5.2 have shown that extreme thermal gradients (e.g., in excess of 150°F between the housing and the shaft) are required to produce a friction increase of 60 in-oz with the preload

mechanism axially restricted. Since thermal gradients this large do not exist in the 9433 structural module (Section 5.1), this mechanism is not the source of the high running friction nor of the large transient torques.

11.2.1.2 Degraded Lubrication

The effects of degraded lubricant are difficult to establish by analysis or by any single planned test. This is an area where a body of experience is essential. Consultants with such experience have generally supported this mechanism as the cause of the 9433 despin control anomaly (Appendix G). Evaluation of the design suggests the lubrication system and its transport mechanisms to be questionable. Moreover, the amount of lubricant initially in the main bearings was relatively small and the bearing surface finishes permitted significant boundary lubrication operation; these factors would tend to hasten deterioration of the lubricant.

The only tests related to these effects were conducted by Aerospace Corporation. These tests (Section 6.3) were run with thermally polymerized Apiezon C inserted into DSCS-II main bearings. The result, a 34-40 in-oz increase in the friction level, is not inconsistent with the 9433 anomaly. However, these tests can hardly be considered conclusive (in either sense), since the lubricant was artifically polymerized and the tests were run in air rather than in vacuum.

Degraded lubrication is a likely cause of the 9433 anomaly. This factor would, inevitably, lead to other types of bearing deterioration and accentuate the effects of other phenomena known to exist (e.g, retainer riding on land of inner race) upon friction.

11.2.1.3 Structural Distortions in Structural Module

Section 5.2 has dealt in depth with the effects of potential structural distortions in the DMA. Short of structural failures (which would have been apparent earlier in the orbital life of 9433), no structural distortions appear able to cause torques of the type observed.

11.2.1.4 Metallic Debris in Main Bearings

Metallic debris in the main bearings could occur due to a lubrication failure (i.e., a wear-related effect) or due to assembly deficiencies. It seems that effects not related to wear would appear early in flight; thus, if debris is the cause of the 9433 anomaly, it is likely to be wear-related. Debris could be a major cause of lubricant degradation (see 11.2.1.2), due to increased metal-to-metal contact in the DMA main bearings. Bearing tests at Aerospace Corporation indicate that metallic debris would be coined or thrown away from the ball track. However, these tests were run in air and without degraded lubricant (which would be likely to accompany and/or cause the debris), and so must be regarded as inconclusive.

11.2.1.5 Retainer Whirl

Retainer whirl (or instability) has been identified as the source of pointing perturbations on other DSCS-II satellites and on other spacecraft (e.g., Intelsat IV). The torques anticipated from this effect, with an otherwise normal bearing, are small (e.g., 5-15 in-oz). Tests have shown this phenomenon not to lead to any increase in the average running torque or any long-term degradation. It is possible that some of the large torque transients observed on 9433 are related to retainer dynamics, with a torque amplitude which has been increased by other factors (e.g., lubricant degradation).

11.2.1.6 Excessive Lubricant

Excessive lubricant in one area of the structural module could result in high levels of friction. However, this (viscous) friction would be expected to depend in no small way upon speed and temperature. No such trend is apparent in the 9433 orbital data; a systematic and monotonic speed dependence appears to be totally lacking.

11.2.1.7 Jammed Main Bearing

Tests and analyses indicate that a jammed main bearing is an unlikely cause of the increase in running friction. Intermittent jamming (e.g., by a retainer or debris) could explain the occasional high-amplitude torque transients as well as the sustained periods of transient torque activity.

11.2.1.8 Interference at Magnetic Pipper

Interference at the DMA magnetic pipper would result in a torque which occurs as a once-per-revolution pulse. In addition, such a torque: should occur early in the mission; should show a definitive dependence upon platform rotor relative position; and, should decrease in time due to wear. None of these characteristics have been observed, suggesting that interference at the pipper has not occurred in 9433.

11.2.2 Power Module

11.2.2.1 Mechanical Interference

Mechanical interference in the power module (i.e., at the motor, resolvers, or snubber) appears to be a failure mechanism which could cause large torques with a signature consistent with the orbital data. Dimensional analysis has shown the snubber gap to be the critical clearance within the power module and that (while nominal clearances are ample) under worst-case assembly conditions (in combination with extreme thermal gradients and/or material creep), closure can occur at the snubber in the despun condition. Further analysis showed that such interference would be relieved (rather than increased) by the sideloads due to platform spin-up.

In order to evaluate the long-term trends associated with snubber rubbing, snubber tests were performed. These showed that sustained snubber rubbing with the contact pressures necessary to produce a large friction increase (e.g., 50 in-oz) would wear away enough material to eliminate any possible interference within two hours. This suggests that production of a 60-70 in-oz friction increase, sustained for several months, is not likely to occur due to snubber rubbing. Finally, disassembly of the life test and flight spare DMA's showed gaps at the snubber in excess of 0.005 in.

11.2.2.2 Debris in Gaps

Debris in the above-mentioned gaps (or the labyrinth seals) could cause torque increases. However, due to clearing (or wearing away), only transient torques would be expected from such a mechanism. Debris could get into these gaps from metal-to-metal rubbing in the power module or from bearing/retainer wear debris. However, an increase in the running torque or sustained periods of transient torque activity would seem unlikely.

11.2.2.3 Fractured Hypernik Ring

Tests have shown the hypernik ring of the motor very difficult to fracture and loosen. Once loosened, it would tend to jam the mechanism entirely and irrevocably.

11.2.2.4 Shorted Motor Winding

Orbital data is inconsistent with this occurrence. Back emf data from both motors appears normal and both motors appear to operate similarly and normally while in use. There has been no noticeable increase in the speed-dependence of running torque. Moreover, such a mechanism would be unlikely to produce the extreme torques (e.g., 600 in-oz) seen on occasion.

11.2.2.5 Open Motor or Resolver Winding

This would cause a significant change in the performance of the affected drive channel. No such phenomenon has been observed in the orbital data.

11.2.3 Slip Ring Module

11.2.3.1 Bearing Related Effects

All bearing related effects discussed in Section 11.2.1.2, 11.2.1.3, 11.2.1.4, and 11.2.1.6 apply equally to the slip ring bearings. However, the torques produced would be much smaller. In view of the preceding remarks, these effects in the slip ring bearings would not cause the torques seen in 9433 orbital data. Moreover, any major deterioration in these bearings would certainly produce an effect (not seen) in the performance of some slip ring circuits.

11.2.3.2 Bearing Jammed

Complete jamming of a slip ring bearing would cause it to journal on its shaft interface surface. Tests run at Aerospace Corporation have shown that large torques would initially be produced, with an increase with time (e.g., 140 in-oz after 6 hours of running). However, with extended operation, weardown of the epoxy coating of the shaft would be expected, reducing the torques and resulting in noisy slip ring data. This does not appear to match the orbital data.

11.2.3.3 Deterioration of Brushes and/or Slip Rings

The slip ring performance would be noticeably affected while the torque increase would be slight. No correspondence with orbital data exists.

11.2.4 Non-DMA Effects

11.2.4.1 Interference Produced by Thermal Insulation

Orbital data does indicate a partial failure of the secondary radiation shield, which is mounted on the rotor, below the cross-beam on which the DMA is mounted. Due to differential contraction, this thermal shield would be expected to curl outward and (due to the Teflon on the lower surface) downward. No evidence of anomalous behavior exists for any other thermal blanket.

Interference of a thermal blanket could cause large torques. However, the result should be a wearing or clearing away due to the considerable forces involved. This is an unlikely source of the sustained increase in running friction.

11.2.4.2 Interference due to HLTWT Heater Harness

This event should cause a loss of operation in these heaters (not having occurred) and should not produce sustained torques due to clearing effects. In any case, this occurrence is very unlikely (see Appendix H).

11.2.4.3 Interference at Platform Pin Puller

This would produce a once-per-revolution torque pulse, inconsistent with data from the 31 rpm recovery attempt. Moreover, an interference from this source would have occured early in flight if at all.

11.3 Conclusions

The preceding sections have summarized the data resulting from the 9433 anomaly investigation and discussed each of the candidate failure modes. None of the analytically tractable or testable phenomena have shown any degree of consistency.

The most probable cause of the 9433 anomaly appears to be a main bearing deterioration due to degraded lubricant. It is easy to conceive of such an occurrence causing further bearing deterioration (e.g., debris generation, retainer rubbing, or wear) which could account for the large torque transients seen on numerous occasions since mid-September 1975. Moreover, the performance observed is consistentwith that predicted by several consultants (and with test data provided by one consultant). This conclusion seems to fit the dual-mechanism model discussed in Section 11.1, with the basic effects of lubricant degradation (e.g., formation of varnish in the ball paths as discussed in Appendix G) corresponding to Mechanism A and the subsequent accompanying effects (e.g., heightened torques due to the retainer) corresponding to Mechanism B.

The evidence for this identification of the anomaly is, and must remain, circumstantial and inconclusive. However, no other postulated failure mechanism appears consistent with the orbital data.

12. RECOMMENDED ACTION

Measures must be taken to guard against a recurrence of the 9433 anomaly. In the course of the anomaly investigations, a variety of actions have been given consideration. These have been defined in general terms, with the details dependent upon studies still in progress.

Decisions must be made from among a group of redesign options, some simple and others more extensive. Some clearly desirable changes in the DMA design may be impractical for F7 and F8 due to launch schedule constraints; these should be considered as product improvement for future incorporation. It is important to note that the design and process changes which can be incorporated for F7 and F8 should, when coupled with existing replenishment DMA design improvements, make improbable a repetition of the 9433 anomaly.

Before discussing potential changes growing out of the anomaly investigations, it is appropriate to summarize those which have already been incorporated into the replenishment DMA:

- The single drive motor with redundant windings has been replaced by a pair of motors of considerably higher torque capability. Note that these motors do not have hypernik rings.
- The power module snubber has been re-dimensioned, its material has been changed, and the minimum acceptable assembly clearance has been increased.
- The slip ring assembly has been modified to employ a larger bearing (identical to the upper slip ring bearing) at its lower end.
- All bearings are provided with an improved raceway surface finish (1.5 micro-inches vs 4 micro-inches in the earlier DMA's). This, coupled with the change in the lower slip ring bearing, should assure predominantly EHD operation of all bearings.
- Minor structural changes have been made to increase the load capacity of both the shaft and the housing.
- Additional bearing screening procedures have been instituted, including contact resistance measurements at normal operating speed.

These changes address a number of the identified weak points in the previous DMA and, with no further action, would decrease the possibility of a recurrence of the 9433 anomaly. In particular, the questions regarding the snubber and the motor hypernik ring are resolved, and the bearing integrity is improved.

General recommended action is identified below in two categories: design changes and process changes. Detailed study of these actions is currently in progress and will be reported in future documents.

12.1 Design Changes

Design changes can be grouped in two classes, those recommended for the next launch and those suggested for later incorporation. In the first category are

- retainer redesign
- increased DEA current limit

while the second includes

- positive lubrication system
- flexure preload mechanism
- controller rate loop.

Each of these recommendations, currently under study at TRW, is discussed below.

12.1.1 Retainer Design

The main bearing retainers are designed to ride near or on the inner race. As a result, they ride relatively low on the balls. Dimensional analyses (Section 5) have shown that the outer edge of the ball pockets can make contact with the balls very near their equators under worst case conditions. Although analysis shows the ball pocket edge to always be slightly above the equator, an increase in the outside diameter of the retainer is recommended as a measure to positively preclude the jamming which might occur if a ball made contact with the retainer below its equator. In addition, measures must be taken to avoid contact of the retainer with the preload washer. These changes will be made for the next launch (F7-F8).

12.1.2 Increased Drive Torque Margin

In the DMA's thus far employed in the DSCS-II program, the nominal maximum drive torque has been limited at approximately 140 in-oz, compared with a normal running friction (from all sources) in the neighborhood of 30 in-oz. This torque margin of slightly less than 5:1 was judged adequate and was considered so during operation, until the major 9433 anomaly.

The available torque in the F1-F6 despin control system was limited by two factors - the possibility of motor demagnetization and the current delivery capability of the DEA. The new motors of the replenishment DMA overcome the first limitation; however, the second still remains and is addressed below.

On various occasions, an extreme increase in torque margin, attainable only by using a motor much larger than the one now present in the replenishment DMA design, has been suggested. This issue, also, is discussed in a subsequent paragraph.

12.1.2.1 Increased DEA Drive Current

The primary reason for limiting the drive current in earlier DMA's was the possibility of motor demagnetization. In the replenishment DMA, much higher currents (i.e., 5 amps versus the existing 1.4 amp current limit) can be tolerated by the motor. However, the DEA current limit is still set at 1.4 amps. An increase in this current limit, to more fully utilize the increased motor capability, is recommended.* Studies in this area have been initiated.

Factors which constrain the DMA drive current limit include:

- The thermal design of the DMA, in which the heat dissipated in the motor is a primary factor
- The current handling capability of the ten existing power transistors in the power amplifiers and the switching regulator
- Other aspects of the DEA circuitry (e.g., the effect of higher current levels upon inductors in the drive circuitry).

---

* Tests with the new DMA motor and the engineering model DEA with the current limit raised to 2.0 amps, show that the torque roll-off phenomenon revealed by motor tests is significantly alleviated.

These factors are under study, with an increase in the current to the neighborhood of 2.0 amps anticipated. However, an increase of even this modest amount will require replacement of the existing power transistors with stud-mounted units, due to thermal considerations. It should be noted that the launch of F7-F8 with the present DEA current limit is completely acceptable, even with the increase in running friction anticipated from added bearing lubricant.

12.1.2.2 Change in DMA Motor

Incorporation of a larger motor into the DSCS-II DMA has been suggested, in order to provide a much larger torque margin than is now available. An increase in motor torque, beyond that now available in the replenishment DMA would have several implications:

- The power module structural design would require modification to accommodate the new mechanical interfaces; the DMA size and weight constraints now in existence would probably be exceeded.
- Increased power dissipation in the motor would require review and probable revision of the DMA thermal design, perhaps affecting the structural module as well as the power module.
- Modification of the DEA would be implied, particularly since the present DEA design is unable to fully utilize the torque capability of the new replenishment DMA motors.
- Other spacecraft elements would possibly be affected including the structural interfaces with the DMA and the power subsystem.

For these reasons, a further increase in the DMA motor torque should not be given serious consideration without detailed study of the effect upon the DMA, the DEA, and other spacecraft subsystems.

12.1.3 Positive Lubrication System

The existing lubrication system depends upon transport mechanisms which are, at best, not well understood. Improvements in the present system, such as defined above, will not alter this dependence. Until these mechanisms are well defined and understood, the effectiveness of such changes in the existing design will be difficult to establish.

The alternative is a change in the basic lubrication supply system concept - to one which does not depend upon poorly understood transport mechanisms. In concept, a positive lubrication system is one which injects a metered quality of lubricant directly into the area requiring lubrication (e.g., onto a bearing raceway). Such systems have been employed in at least two instances - the Skylab control moment gyros and the Intelsat IV-A BAPTA (DMA); in the latter case, the "oiler" is a backup to the conventional reservoir supply system.

The development required to incorporate a lubricant injector into an existing DMA design may be considerable. Moreover, other changes may be indicated to take full advantage of such a system (e.g., removal of the bearing retainers and addition of balls to the bearings, as recommended by Draper Labs personnel).

It is certain that a positive lubrication system cannot be added to the DMA for F7-F8 with the present launch schedule; nor can any significant change be made in the present lubricant supply system. However, development of a positive lubrication system is strongly recommended for future incorporation. The alternative of improvements in the existing system (for example, the addition of reservoir heaters) is less appealing, because dependence upon questionable lubricant transfer mechanisms (evaporation/condensation, surface creep, etc) would be retained.

12.1.4 Preload Mechanism

The preload mechanism of the DSCS-II DMA, employing a sliding interface between the shaft and the main bearing inner races, has long been considered a less than optimum aspect of its mechanical design. Potential problems with this design include debris generation due to rotation of the inner races and, axial binding, leading either to excessive bearing loading or loss of preload. These occurrences, however unlikely, should be dealt with in any consideration of DMA re-design.

A preload mechanism which employs flexure suspension of the bearing race having axial freedom has long been considered by TRW personnel as the ideal approach. The Intelsat IV BAPTA design employs this scheme and BBRC is in agreement with this philosophy. However, incorporation of this approach within the DSCS-II DMA is inconsistent with the F7-F8 launch schedule.

Considering F7-F8 schedule factors, are there improvements which can be made in the preload mechanism and/or related mechanical interfaces? Focussing on the potential for inner race rotation with resultant metallic debris generation, techniques of restraining rotation without introducing a flexure suspension have been suggested:

(i) A spline or keyway interface between the main bearing inner races and the DMA shaft

(ii) Pinning the clutch plate to the top main bearing thrust face and the preload mechanism pressure pads.

The first technique would restrain rotational motion but would increase the risk of axial binding; moreover, remanufacture of all shafts and bearings would be required. The pinning technique appears safer (i.e., no increase in the probability of axial binding); however, the drilling of holes into the thrust faces of the bearings could be deleterious and would require remanufacture of all upper main bearings. In either case, detailed engineering design followed by full requalification would be required.

A structural change in the main bearing preload mechanism is not recommended at this time. However, consideration should be given to coating the clutch plate (e.g., with aluminum oxide) to reduce the possibility of debris generation in the event of inner race motion. Finally, a development program leading to eventual incorporation of a flexure preload mechanism is strongly recommended.

12.1.5 Controller Rate Loop

Transient pointing perturbations, with amplitudes in the 0.2-0.4 degree range, were observed on 9433 prior to the major anomaly and on other DSCS-II spacecraft. With regard to these anomalies, the following conjectures can be made:

- This anomaly appears unrelated to the increase in running friction exhibited by 9433
- It appears that no wear phenomenon is involved, since such perturbations were observed in the initial weeks of 9433 operation.
- The amplitude and signature of these perturbations are consistent with the retainer whirl identified in 1973 for 9432 and observed on Intelsat IV spacecraft.

We can conclude that these perturbations are due to a different cause than the 9433 major anomaly and that, if they must be eliminated, totally different measures may be required.

During 1973, these short-term perturbations were studied and concluded to arise from retainer instability. Studies at TRW, Hughes, and Combat have addressed this problem. The overall conclusion is that retainer whirl is difficult to eliminate by design, short of eliminating the retainer altogether. The available options appear to be:

(i) Tolerate occasional perturbations in the 0.2-0.4 degree range

(ii) Redesign the despin controller to make the system insensitive to these torque perturbations (i.e., the rate loop modification identified during the 1973 studies).

Option (i) is acceptable in the near-term. Incorporation of the rate loop is recommended as a long-term product improvement.

12.2 Process Changes

The issue of changes in the processes whereby the DMA and its components are manufactured is a complex one, and is beyond the scope of this report. A number of possible process changes are now under intensive study with participation by personnel from TRW, BBRC, Draper Labs, and Fafnir. The following discussion summarizes the major areas under consideration. Final recommendations await completion of these ongoing studies and will be documented in a separate report.

As mentioned above, the F7-F8 launch schedule is a prime driver in making process-change decisions. However, the option of phased incorporation of process modifications exists, just as it does in the area of design changes. Attractive process changes which are inconsistent with the existing F7-F8 launch schedule should be considered for possible application for manufacture (or retrofit) of DMA's for later satellites.

The question of procedural modifications concerns the total span of DMA-related activity, ranging from component manufacturing and selection to storage and handling of the DMA prior to launch. Focussing on the issues related to bearing quality and performance, the following process categories are considered:

- Metal Parts Processing
- Non-Metal Parts Processing
- Bearing Screening
- Lubrication Process
- Assembly and Test Procedures
- DMA Storage and Handling

It is generally agreed that the methods by which the bearing (and related) components are manufactured and processed, is crucial to the performance and endurance of the DMA. A number of detailed changes are under study including: techniques for cleaning metal bearing components; bearing component inspection approaches; extraction procedures for the bearing retainers; extraction procedures for the lubricant reservoirs; and passivation techniques.

The replenishment DMA program now includes contact resistance measurements at operating speed as a bearing screening procedure. The addition of low-speed (e.g., one rpm) dynomometer tests, recommended by Draper Labs and Delco, is likely, both for individual bearings and for the assembled structural module.

The procedures for DMA lubrication are currently under detailed review. At the very least, the amount of lubricant initially present in the main bearings will be increased significantly. Additional aspects of the lubrication process being studied include:

- the technique for impregnating the lubricant reservoirs
- the amount and distribution of the boundary lubrication additive (lead naphanate) - for example, the possibility of impregnating the reservoirs with only Apiezon-C is under consideration
- the techniques used in reprocessing bearings
- tests of lubricant quality to verify adequacy and provide better controls.

The DMA assembly, test, handling, and storage procedures are also under review. Assembly and test issues include: possible use of handling fixtures during certain critical assembly steps (e.g., to handle bearing

components); measurement and recording of certain key dimensions during assembly; and additional dynamic tests during and after assembly. The procedural requirements for DMA handling (during spacecraft integration and test) and for storage are also being given attention; changes in this area are expected to be minor.

In summary, a number of potential process changes are under intensive consideration at this time. Final recommendations will be made at the conclusion of these process investigations and will be documented at that time.